# Phase Change Materials for Non-volatile Electronic Memories

#### Von der Fakultät für

Mathematik, Informatik und Naturwissenschaften der Rheinisch-Westfälischen Technischen Hochschule Aachen zur Erlangung des akademischen Grades eines Doktors der Naturwissenschaften genehmigte Dissertation

# vorgelegt von Diplom-Physiker Martin Stefan Salinga aus Herten in Westfalen

Berichter: Universitätsprofessor Dr. Matthias Wuttig Dr. Simone Raoux

Tag der mündlichen Prüfung: 4. Juni 2008

Diese Dissertation ist auf den Internetseiten der Hochschulbibliothek online verfügbar.

# Abstract

Starting from a brief introduction into the physics of phase change materials their applications in the field of data storage are reviewed. Without the latter there would certainly be less attention paid to the topic today, even in basic research. For years now, optical data storage media based on phase change materials have been successfully produced for the mass market. Despite its maturity there are still new ideas on how to further improve this technology in order to stay competible with other storage media in the future. In contrast, for the application of phase change materials in electronic memories the situation is completely different. Although proposed decades ago, today it is still a rather young and promising technology.

In this work both applications are analyzed with respect to their requirements to the incorporated phase change material, with an emphasis on the second one. For optical storage and especially in the case of electronic memories the author arrives at the conclusion, that the crystallization kinetics of phase change materials is the most urgent and fundamental problem that needs to be solved. The emphasis on a deep and quantitative understanding of this phenomenon implicitely criticizes the popular approach of studying the switching of electronic cells for phase change based memories without an in-depth research of the crystallization kinetics.

After this identification of the research objective, the result of a thorough review of the literature on the theory of crystallization is presented. The understanding of glass formation turns out to be extremely important, since it deals with the stability of an amorphous solid or undercooled liquid against structural reconfiguration. Consequently, a separate chapter is dedicated to the theory of glass formation.

Based on the knowledge of the theoretical connections between glass transition and crystallization it is investigated how meaningful a calculation of the enthalpy of atomization is for a prediction of stoichiometric trends not only of glass transition, but also of crystallization. The sparce experimental evidence on the glass transition temperature of phase change materials is compared to the calculated enthalpies. The same is done for a series of measurements of crystallization. These comparisons show that the proposed strategy works well for predicting the influence of a stoichiometric

variation of a phase change material on its stability against crystallization.

The author's critical review of the literature on crystallization kinetics reveals that the widely used classical crystallization theory still lacks a rigorous experimental prove of its validity. The latter is difficult, because the multitude of quasi-free parameters generally ensures a good mathematical agreement between theory and the often very limited experimental data.

Such a check of validity of the theory is especially challenging for phase change materials: In a wide range of high temperatures crystallization proceeds so fast, that until now an experimental quantification of nucleation rate and crystal growth velocity was only possible in a rather limited regime of low temperatures. The extrapolation of such data over the whole temperature range up to the melting temperature by application of the equations provided by the classical theory is assessed to be too uncertain to be trusted.

To close that gap with experimental evidence and to advance therewith towards a disentanglement of electronic and thermal effects involved in the switching of an electrical cell, a new experimental setup has been designed and realized. It combines laser induced annealing experiments with the capability to apply and measure fast electrical pulses. The implementation of a control of the sample's base temperature is an additional, valuable component. Each of the sections of the new setup on its own is already a sophisticated tool, that enables its user to investigate phase change materials on very short time scales. Examples for this are unprecedented laser experiments that have been performed by the author. Some of those innovatively separate crystal nucleation and growth. Others demonstrate a path towards a quantitative measurement of crystallization kinetics in the melt-quenched amorphous state. The latter is highly relevant for technology, since it is that amorphous phase, that is realized in applications.

But the new setup is more than just the sum of its parts. The combination of optical, electrical and thermal experiments opens up a wide field of new possibilities. This is indicated by the demonstration of an electrical experiment for the investigation of the threshold-switching effect, the phenomenon describing an abrupt breakdown of the resistivity of the amorphous phase upon application of a critical electric field. The initialization of the sample by laser annealing allows for a "clean" experiment in which the starting conditions are not dependent on the property of interest itself, in this case the electrical behaviour. Such a successive approach from purely thermal experiments towards the testing of the realistic but complex cells of a phase change based electronic memory is necessary to stepwise synchronize the numerical simulations. This strategy is essential for achieving a deep understanding of the physical processes involved in the switching of such cells.

Beyond these technologically important measurements the new setup is pioneering for a multitude of further optical and electrical experiments that are likely to make valuable contributions to the research of the physical properties of phase change materials. Examples for such experiments are proposed at the end of this work.



# Kurzfassung

Übersetzung des englischen Originaltitels: Phasenwechselmaterialien für nichtflüchtige elektronische Datenspeicher

Ausgehend von einer kurzen Einführung in die grundlegenden physikalischen Eigenschaften von Phasenwechselmaterialien werden zunächst die Anwendungen solcher Materialien auf dem Gebiet der Datenspeicherung betrachtet, ohne welche das Thema heute sicherlich auch auf Seiten der Grundlagenforschung weitaus weniger Beachtung fände. Optische Datenspeicher, die Phasenwechselmaterialien verwenden, werden schon seit vielen Jahren erfolgreich für den Massenmarkt hergestellt. Hier liegt also eine ausgereifte Technologie vor, bei der allerdings neue Ideen für nochmalige Verbesserungen vorliegen, mit denen für weitere Jahre Konkurrenzfähigkeit gegenüber anderen Speichermedien erreicht werden könnte. Ganz anders sieht es für die Verwendung von Phasenwechselmaterialien in elektronischen Datenspeichern aus. Obgleich schon vor Jahrzehnten vorgeschlagen, ist sie in ihrer heutigen Form eine recht junge, dabei aber überaus vielversprechende Technologie.

Beide Anwendungen werden in dieser Arbeit hinsichtlich ihrer Anforderungen an die verwendeten Phasenwechselmaterialien analysiert, wobei der Schwerpunkt auf den elektronischen Speichern liegt. Dabei wird herausgearbeitet, dass sowohl für optische, aber gerade auch für elektronische Datenspeicher, das tiefe und damit auch quantitative Verständnis der Kristallisationskinetik von Phasenwechselmaterialien die dringendste und fundamentalste Fragestellung ist, die es in diesem Zusammenhang zu bearbeiten gilt. Damit wird implizit der verbreitete Ansatz kritisiert, gerade bei elektronischen Phasenwechselspeichern ohne eine entsprechend sorgfältige Studie der Kristallisationskinetik das Schaltverhalten zu erforschen.

Nach der Identifizierung dieses Forschungsziels wird das Ergebnis einer ausgiebigen Literaturrecherche zur Theorie der Kristallisation präsentiert. Als überaus wichtig stellt sich dabei das Verständnis der Glasbildung heraus, da hierin die Stabilität eines amorphen Festkörpers bzw. einer unterkühlten Flüssigkeit gegen strukturelle Umordnung behandelt wird. Aus diesem Grund wird der Theorie der Glasbildung ein eigenes Kapitel gewidmet.

Basierend auf dem Wissen um die theoretischen Zusammenhänge zwischen Glasübergang und Kristallisation wird untersucht, inwieweit von einer berechneten Atomisierungsenthalpie von Phasenwechselmaterialien ausgehend Aussagen über stöchiometrische Trends in deren Glasübergangstemperatur oder sogar über Veränderung in der Kristallisation getroffen werden können. Der Vergleich der berechneten Enthalpien mit den raren experimentellen Ergebnissen für die Glasübergangstemperatur von Phasenwechselmaterialien sowie mit Messungen zur Kristallisation zeigt, dass diese Strategie in der Tat eine Vorhersage über den Einfluss von Stöchiometrievariationen auf die Stabilität eines amorphen Phasenwechselmaterials gegen Kristallisation erlaubt.

Bei der kritischen Behandlung der Literatur zur Kristallisationskinetik stellt sich heraus, dass die weit verbreitete klassische Kristallisationstheorie bislang noch nicht rigoros experimentell bestätigt werden konnte. Dies erweist sich deshalb als schwierig, weil die Vielzahl von quasi-freien Parametern in der Regel dafür sorgt, dass eine mathematische Übereinstimmung der Theorie mit den meist sehr begrenzten experimentellen Daten erreicht werden kann, ohne dass daraus unbedingt auf die Richtigkeit der Theorie geschlossen werden müsste.

Bei Phasenwechselmaterialien stellt sich eine solche Überprüfung der Gültigkeit der Theorie als besonders schwierig heraus, da die Kristallisation in einem weiten Bereich hoher Temperaturen so schnell fortschreitet, dass eine experimentelle Quantifizierung von Nukleationsrate und Wachstumsgeschwindigkeit bisher nur in einem sehr begrenzten Regime niedriger Temperaturen möglich war. Eine Extrapolation solcher Daten über den gesamten Temperaturbereich hinweg bis hin zur Schmelztemperatur mittels der Formeln aus der klassischen Theorie wird darum als zu unsicher beurteilt.

Um diese Lücke mit belastbaren Daten zu schließen und um damit den Weg für eine Entflechtung der elektronischen und der thermischen Effekte beim Schalten einer elektrischen Zelle zu bereiten, wurde ein neuer experimenteller Aufbau entworfen und realisiert. Er verbindet laserinduzierte thermische Experimente mit der Möglichkeit, elektrisch zu schalten und zu messen. Ergänzt werden diese beiden Zweige durch die Implementierung einer Steuerung für die Basistemperatur der Probe. Jeder dieser Kernbestandteile des neuen Messplatzes ist für sich genommen bereits ein technisch hoch entwickeltes Gerät, das seinen Benutzer in die Lage versetzt, Phasenwechselmaterialien auf schnellen Zeitskalen zu untersuchen. So werden etwa noch nie da gewesene Laserexperimente durchgeführt, die eine Entkopplung von Nukleation und Wachstum erlauben oder einen Weg zur quantitativen Bestimmung der Kristallisationskinetik in aus der Flüssigkeit abgeschreckten amorphen Phasen darstellen. Die letztgenannte Sorte amorpher Zustände ist von hoher technologischer Relevanz, da sie es sind, die beim Schalten in den Anwendungen erzeugt werden.

Der neue Messplatz ist aber mehr als die bloße Summe seiner Teile. Die Kombination von optischen, elektrischen und thermischen Experimenten erschließt völlig neue Möglichkeiten. Dieses Potential wird in der Vorstellung von elektrischen Experimenten angedeutet, die zur Untersuchung des Phänomens des abrupten Einbruchs des Widerstands der amorphen Phase unter Anlegen eines elektrischen Feldes kritischer Stärke dient. Die Initialisierung einer ensprechenden Probe mittels gepulster Laserstrahlung erlaubt ein "sauberes" Experiment, dessen Randbedingungen, in diesem Fall sein Anfangszustand, nicht bereits durch die zu erforschende Eigenschaft selbst, nämlich das elektrische Verhalten, bestimmt ist. Eine solche schrittweise Vorgehensweise auf dem Weg von rein thermischen Experimenten hin zum Testen einer realistischen, aber komplexen Zelle eines phasenwechselbasierten elektronischen Datenspeichers ist notwendig, um die numerischen Simulationen sukzessive anzupassen. Diese Strategie ist essentiell, um ein wirkliches Verständnis der Schaltprozesse innerhalb einer solchen Zelle zu erreichen.

Über diese technologisch wichtigen Messungen hinaus schafft der neue Aufbau die Voraussetzungen für eine Vielzahl weiterer optischer und elektrischer Experimente, die zur Erforschung der Eigenschaften von Phasenwechselmaterialien wichtige Beiträge liefern können. Einige solcher Experimente werden beispielhaft am Ende dieser Arbeit vorgeschlagen.



# Contents

	1 1110	e page		]								
	Abs	tract .		iii								
	Kur	zfassung	g	vii								
	Con	tents.		xi								
	List	of Figu	res	XV								
	List	of Tabl	les	xix								
I			Change Materials:	-1								
Р	nysı	cs an	d Applications	1								
1	Intr	oducti	ion	3								
	1.1	Princi	ple of phase change materials	3								
	1.2	Struct	ure of this study	5								
2	App	Applications of Phase Change Materials										
	2.1	Optica	al data storage	7								
		2.1.1	Concepts of optical storage	7								
		2.1.2	Development of new materials for optical storage	S								
		2.1.3	Future of optical data storage	12								
	2.2	Electr	onic memory	14								
		2.2.1	Flash memory	14								
		2.2.2	Dynamic and static random access memory	16								
		2.2.3	Phase Change RAM	16								
3	The	eory of	Glassformation	29								
	3.1	Freezi	ng a liquid	29								
	3.2	Tempe	erature dependence of the viscosity	31								
	3.3	Therm	nodynamics	34								

## CONTENTS

4	$Th\epsilon$	eory of Crystallization	39								
	4.1	1 The driving force									
	4.2	Crystal nucleation	44								
		4.2.1 Basic classical nucleation theory	46								
		4.2.2 Heterogeneous nucleation	54								
		4.2.3 Transient nucleation	56								
	4.3	Crystal growth	58								
	4.4	.4 Beyond classical theory									
	4.5	General models on transformation	65								
II	P	rediction of Glass Transition Temperatures	69								
$\mathbf{M}$	otiva	ation	71								
5	Mo	dels of Glass Transition in Literature	74								
	5.1	Constraint theory	74								
	5.2	Segmental motions	75								
	5.3	Gibbs DiMarzio equation	76								
	5.4	Modified Gibbs DiMarzio equation	77								
	5.5	Stochastic agglomeration theory	77								
	5.6	Glass transition and bond energy	79								
6	The	e Model Used	81								
7	Cor	nparison with Glass Transition Temperatures	85								
8	Cor	nparison with Crystallization Temperatures	95								
II	I I	Measurements of Crystallization Kinetics	107								
M	otiva	ation	109								
9	Exi	sting Techniques	112								
	9.1	Slow crystallization at low temperatures	112								
	9.2	Slow crystallization at high temperatures	116								
	9.3	Fast crystallization at intermediate temperatures	116								
10	Cor	ncept for a New Experimental Setup: POET	119								

11 Realization of <i>POET</i>	122
11.1 Overview	122
11.2 Laserlight: generation, shaping and combination	124
11.3 Intensity measurement of incoming light	126
11.4 Visual monitoring	129
11.5 Sample positioning	130
11.6 Sample heating	130
11.7 Laser beam movement	133
11.8 Outcoupling of reflected light	134
11.9 Intensity measurement of reflected light	136
11.10Autofocus	137
11.11Electrical testing	139
11.12Control software	141
12 Experiments Using <i>POET</i>	145
12.1 Power-time-effect measurements	145
12.2 Incubation time experiments	150
12.3 Dual-spot experiments	155
12.4 Amorphization and recrystallization	163
12.5 Optically assisted electrical measurements	168
12.6 Proposal of new experiments	174
12.6.1 Fast and isothermal measurements of crystal growth velocity	174
12.6.2 Resistance versus temperature measurements for the melt-	
quenched amorphous state	176
12.6.3 Influence of capping layers	176
12.6.4 Electronic properties of phase change materials	177
12.7 Conclusion	177
	150
Acknowledgements	179
Bibliography	183
Curriculum Vitae	201

## CONTENTS

# List of Figures

1.1	Switching principle of phase change materials	4
2.1	Progress of phase change based re-writable optical storage media	10
2.2	Phase change materials suitable for optical storage	11
2.3	Mushroom cell for Phase Change RAM	20
2.4	Line cell for Phase Change RAM	21
2.5	Bridge cell for Phase Change RAM	27
3.1	Viscosity in liquids and glasses	30
3.2	Temperature dependence of viscosity for varying fragility	33
3.3	Relation between relaxation time, entropy, and potential energy landscape	36
4.1	Gibbs free energy for crystalline, liquid and amorphous phase	42
4.2	Approximations for the difference in Gibbs free energy between liquid	
	and crystal	45
4.3	Gibbs free energy for formation of crystalline clusters	47
4.4	Steady state nucleation rate versus temperature	53
4.5	Heterogeneous cluster formation on a flat surface	54
4.6	Gibbs free energy difference for crystal growth	59
4.7	Crystal growth velocity versus temperature	63
7.1	Schematic of the heat flow into a sample while heating with a constant	
	rate	87
7.2	Heat flow results of $Ge_2Sb_2Te_5$ from Kalb	89
7.3	Viscosity plot explaining relaxation, glass transition and crystallization	
	measurements in DSC	90
7.4	Ternary diagram of calculated glass transition temperatures for the	
	GeSbTe system	91
7.5	Comparison between predicted and measured glass transition tempera-	
	tures for GeSbTe	93

#### LIST OF FIGURES

8.1 Calculated glass transition temperatures for AlGeSb	96
8.2 Calculated glass transition temperatures for CuGeSb	96
8.3 Calculated glass transition temperatures for AlSbTe	97
8.4 Calculated glass transition temperatures for CuSbTe	97
8.5 Resistivity versus temperature for Al doped $Sb_2Te$	102
8.6 Resistivity versus temperature for Cu doped $Sb_2Te$	103
8.7 Resistivity versus temperature for Al doped $Ge_{18}Sb_{82}$	104
8.8 Resistivity versus temperature for Cu doped $Ge_{18}Sb_{82}$	105
10.1 Concept of <i>POET</i>	120
11.1 Overview of $POET$	123
11.2 Laserlight creation and combination in reality	125
11.3 Laser beam profile on sample	127
11.4 Heated sample holder	132
11.5 Faraday isolator	135
11.6 Autofocus	138
11.7 Electrical testing concept	140
12.1 Power-time-effect diagrams for as-deposited GeSbTe	146
12.2 Power-time-effect diagram for as-deposited SbTe	148
12.3 Power-time-effect diagram for as-deposited GeSb	149
12.4 Analysis of reflectivity traces	151
12.5 Incubation time for varying laser power	152
12.6 Incubation time for varying heat barrier thickness	154
12.7 Incubation time for varying phase change layer thickness	154
12.8 AFM image of dual-spot laser experiments	156
12.9 SEM images of dual-spot laser experiments	157
12.10Image processing of dual-spot experiments I	158
$12.11 \mathrm{Image}$ processing of dual-spot experiments II - circle correlation and	lysis 160
$12.12 \mathrm{Image}$ processing of dual-spot experiments III - histograms of surface.	ace
height	161
12.13Image processing of dual-spot experiments IV - results	162
$12.14 \mathrm{AFM}$ image of dual-spot experiments with improved shift precision	164
12.15Reflectivity change upon amorphization	165
12.16Reflectivity change upon recrystallization	166
12.17 AFM image of amorphization and recrystallization marks	167
12.18AFM image of electrical line cell	169
12 19Threshold switching in GeSb line cell	179

### LIST OF FIGURES

12.20Threshold	voltage d	ependence	on initial	resistance					173

# List of Tables

2.1	Industrial engagement in Phase Change RAM	18
6.1	Enthalpy of atomization for groups IVB, VB and VIB	83
6.2	Homo-nuclear bond enthalpy for groups IB, IIB and IIIB	83
7.1	Calculated glass transition temperature, bond enthalpy and number of bonds for GeSbTe alloys	92
8.1	Calculated glass transition temperature and total bond enthalpy for Al and Cu doped SbTe and GeSb	100

## LIST OF TABLES

# Part I

Phase Change Materials: Physics and Applications

# Chapter 1

# Introduction

When it is not necessary to change, it is necessary not to change.

LUCIUS CARY, VISCOUNT FALKLAND

## 1.1 Principle of phase change materials

Before this text will dwell on the subject of various physical effects in so-called phase change materials and their versatile applications in information technology, the term "phase change material" itself needs to be defined first. Aware of the presence of multiple types of phase transitions in the wide fields of physics, this work focuses on the transitions between crystalline, liquid and amorphous states. What distinguishes phase change materials from all others is not the sheer existence of both a crystalline and an amorphous solid state. Provided with deliberately fast or slow cooling rates one could, at least theoretically, prepare every material in these two kinds of condensed matter. The uniqueness of this class of materials consists in the combination of high structural stability of both states up to moderate temperatures and extremely fast phase transitions at high tempertures.

While this peculiarity alone has caused persistent interest on the side of basic research, the reason for the area of phase change materials receiving much attention from application oriented research is the occurrence of a strong property contrast between the different solid states in many phase change materials. The most prominent and at the same time most easily accessible properties are the electrical resistivity and the optical reflectivity. Thus both are used to store information, either in electronic or in optical data storage. Fig 1.1 illustrates how the state of a phase change material can be switched by heating it, e. g. using a voltage or a laser light pulse, respectively. To let the material crystallize a temperature below the melting temperature has to be realized for a sufficiently long period of time, which depends on the inherent properties of the

#### 1.1. PRINCIPLE OF PHASE CHANGE MATERIALS

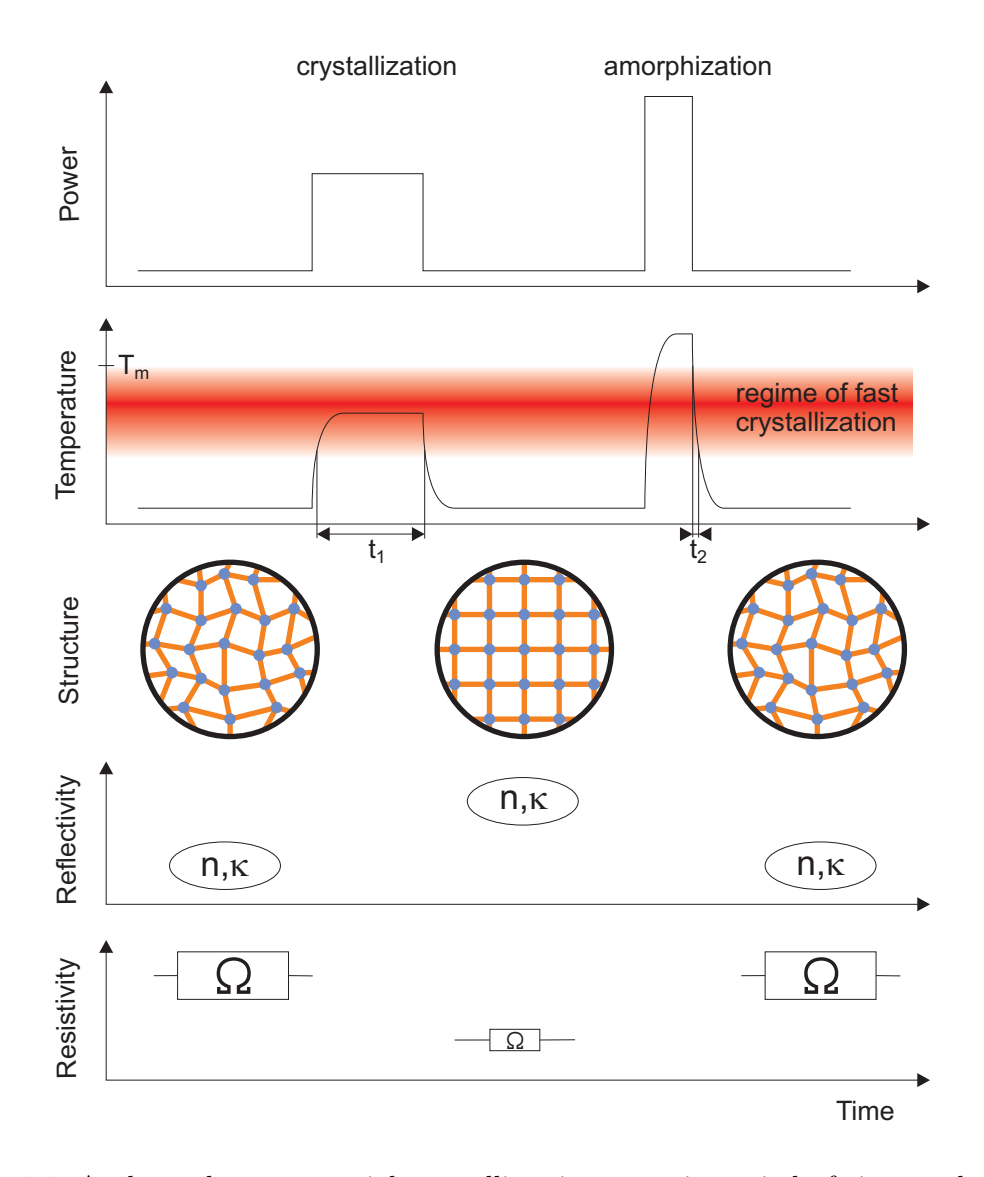


Figure 1.1: A phase change material crystallizes in a certain period of time  $t_1$  depending on the temperature it is kept at. The amorphization of a previously crystalline volume is obtained by melting, i. e. heating above  $T_m$ , and subsequently rapid cooling of the material minimizing the time  $t_2$  at temperatures that cause fast crystallization. The property contrast in reflectivity (symbolized by the optical constants n and  $\kappa$ ) or resistivity (symbolized by resistors marked with an  $\Omega$  of varying size) can be detected with probe powers that are reduced as far as possible avoiding modifications of the structural state. Heating and probing can be accomplished with laser light or with electrical current as it is realized in optical or electronic data storage media, respectively.

chosen material. Whereas for amorphization the material has to be molten and subsequently cooled down so rapidly that the temperature regime with high crystallization speeds is present only for a very short period of time circumventing crystallization of most of the previously molten volume. The latter is accomplished by designing the thermal surrounding of the phase change material accordingly, so that it extracts the heat from the melt quickly enough. The state of the switchable region is determined again using either laser light to measure the reflectivity or an electrical current pulse to check the resistivity. In both cases the probe power is sufficiently low to minimize modifications of the structural state of the material by the read-out process.

## 1.2 Structure of this study

The goal of this work is to contribute to a deeper understanding of the physics of phase change materials. This is considered not only to fulfill a scientist's obligation to satisfy man's curiosity to understand nature, but also to be the best way to find new materials with superior properties for applications. Thus part I of this text provides the reader with an analysis of function and requirements of state-of-the-art memory technologies employing phase change materials (chapter 2). As will become clear from this analysis, the kinetics of crystallization is surely one of the most important, if not the single most important, property one needs to have precise knowledge about when dealing with the application of these materials. The following review of the theory of glass formation (chapter 3) and crystallization (chapter 4) on the other hand will reveal that crystallization kinetics is indeed an already extensively researched subject, yet still with open questions especially with respect to the experimental examination of theoretical predictions. So science and application are strongly pointing towards an investigation of crystallization kinetics. Thus it should not take the reader by surprise that part II with a more theoretical and part III with a predominantly experimental approach both address this problem.

Part II focuses on the glass transition. After a description of different models for the glass transition (chapter 5) an algorithm is introduced which predicts the glass transition temperature of an alloy based on its composition (chapter 6). It is applied to a selection of phase change materials and the results are compared to experimental values (chapter 7). Finally, in chapter 8, the connection between glass transition and crystallization is discussed closing with predictions of stoichiometric trends for the crystallization temperature and their experimental verification.

Part III starts with a review of existing techniques for the measurement of crystallization kinetics (chapter 9). Against the background of the shortcomings of these

#### 1.2. STRUCTURE OF THIS STUDY

methods the idea of a new optical and electrical experiment, named  $POET^1$ , overcoming these limitations is developed in chapter 10. In chapter 11 then the implementation of the experimental setup is described in detail.

Measurements of the influence of heating power and duration on crystallization (sec. 12.1), measurements of incubation times of crystal nuclei (sec. 12.2), experiments decoupling crystal growth from nucleation (sec. 12.3) and the investigation of laser induced amorphization and recrystallization (sec. 12.4), all established with the new setup in the scope of this work, show the diversity of possibilities *POET* offers.

The versatility of the new setup becomes even more evident, when in section 12.5 electrical measurements are presented and finally in section 12.6 further novel experiments are proposed for future studies employing POET.

<sup>&</sup>lt;sup>1</sup>acronym for Phase change Optical Electrical Tester

# Chapter 2

# Applications of Phase Change Materials

Ich halte dafür, dass das einzige Ziel der Wissenschaft darin besteht, die Mühseligkeiten der menschlichen Existenz zu erleichtern.

Bertolt Brecht: Leben des Galilei

As already mentioned in the introductory chapter 1 phase change materials show a pronounced property contrast between their crystalline and their amorphous phase. This contrast allows to read out the state of a finite volume of material. The ability to selectively prepare either of these phases combined with the fact that even the amorphous phase shows structural stability over very long periods of time enables to write, store and read information. So far two conceptually different approaches have been followed in the application of phase change materials in the field of data storage, i.e. optical data storage (Sec. 2.1) and electronic memory (Sec. 2.2).

## 2.1 Optical data storage

## 2.1.1 Concepts of optical storage

In optical data storage information is read from a rotating disc that contains the stored data by detecting the change of reflection of a laser beam focused on the disc. Having this in common three major classes of optical data storage have been developed over the years: read-only, recordable and re-writable memory.

In the first class, the read-only memory (ROM), data is stored as a spiral-shaped series of indentations on the back side of a 1.2mm thick disc of polycarbonate which is covered with a reflecting metal layer, usually aluminum. The intensity of the reflected light on the photo detector varies between the laser hitting an indentation (pit) or

#### 2.1. OPTICAL DATA STORAGE

a not indented region (land). The indentations are stamped into the polycarbonate during the manufacturing process of the disc, so a later controlled change of the stored information is impossible. This technology started out with the development of the compact disc (CD) by Philips and Sony in 1979 resulting in the first commercial release of a compact disc in 1982. Though at first the CD was meant solely as a medium for music content, it was soon realized that it could serve as a storage medium for other data, too. Using basically the same storage concept as the CD the CD-ROM was commercially available in 1985 being the first generation optical disc for general digital data. While the data capacity of a disc increased in the second generation, Digital Versatile Disc (DVD), and again in the third generation of optical discs, High Definition Digital Versatile Disc (HD DVD) and Blu-ray disc (BD-RE), the class of read-only memory discs is still the most common format for the commercial distribution of music, video and software contents today.

In contrast to this the second class of optical storage media, the recordable memory, has for years become the most popular medium for storage of all kinds of digital data which is not meant for large quantity reproduction and distribution. The CD-Recordable, introduced in 1990, like its successors, the recordable versions of DVD and HD DVD, is based on the non-reversible change of the optical properties of a thin dye layer under high intensity laser irradiation. So in a recordable disc the data are not stamped into the polycarbonate during production, but are burned into the dye layer later by the end user. The reading process, however, is very similar to the read-only discs. A low power laser beam propagates through the polycarbonate and the dye layer, before it is reflected by a silver or gold film. The detected intensity of the reflected light obviously depends on the transmittivity of the irradiated area of the dye layer and is thus an indicator of the stored information.

Also since 1990 the third class of optical storage, re-writable media, has been on the market. Its characteristic advantage, i. e. the possibility of repeatedly writing and erasing data, has been accomplished by the implementation of phase change materials. As already mentioned in section 1.1 many phase change materials show a pronounced difference in reflectivity between their amorphous and their crystalline state. In rewritable optical storage media this contrast is utilized to read out the information, which is stored in form of amorphous marks in a crystalline surrounding. The amorphization is achieved by a short, but high power laser pulse, that locally melts the phase change material. The following cooling proceeds so rapidly that crystallization is avoided and the material solidifies into a mechanically stable amorphous phase instead. To erase such an amorphous mark, a laser pulse of moderate intensity heats the material to a temperature at which the amorphous volume can completely recrystallize in

the span of time given by the duration of irradiation (see Fig. 1.1). The laser intensity for reading has to be minimized in order to keep the temperature in the phase change material significantly below a regime with noticable crystallization speeds. Only in this way data can be read out repeatedly without degradation.

For completeness it should be mentioned that besides the ones already explained above there is another optical storage concept based on phase change materials commercially available today. Plasmon, a company based in the United Kingdom, offers an archiving system called Ultra Density Optical (UDO) which is aiming for the professional market, where special standards for handling legal data have to be complied with. For that reason especially the Write Once Read Many (WORM) version of UDO with its guaranteed longevity of more than 50 years is of great interest to Plasmon's customers. The technology behind UDO can be described, only slightly simplified, as an optical disc like the ones above packed in a cartridge.

#### 2.1.2 Development of new materials for optical storage

Over the past decades in all areas of information technology industry, e.g. hard disc drives, flash memory (see 2.2.1), Random Access Memory (see 2.2.2), etc., there has been a strong increase of storage density. This is also true for re-writable optical storage. Since the introduction of first generation re-writable discs with around 0.5 Gigabyte, the capacity rose by a factor of seven to the second generation, the DVD, and by another factor of ten to the third generation, the dual layer Blu-ray disc. These advances in data density have been mainly accomplished by improving the optics in order to reduce the size of the focused laserbeam. The reduction of the wavelength from infra-red via red to blue laser light together with a steady increase of the numerical aperture from 0.5 to 0.85 and the corresponding decrease of the minimal mark size is illustrated in Fig. 2.1.

These changes in the optical and mechanical architecture of the storage technique have implications on the requirements on the phase change material used. [2] Both states, the amorphous and the crystalline phase, have to be stable in a much smaller volume than in earlier generations. The reflectivity contrast has to be detectable and for effective heating the absorption of the shorter wavelength has to be high enough. Also for higher data transfer rates the crystallization speed has to be higher, as the cross-section of the passing laser beam is smaller and thus the duration of illumination on a given area of phase change material is reduced at a constant disc rotation. At the same time the risk of cross erasing, i. e. the unintentional partial erasure of adjacent amorphous marks during recording, is increased due to the closer spatial proximity of the marks. The latter two requirements obviously are to some degree contrary

#### 2.1. OPTICAL DATA STORAGE

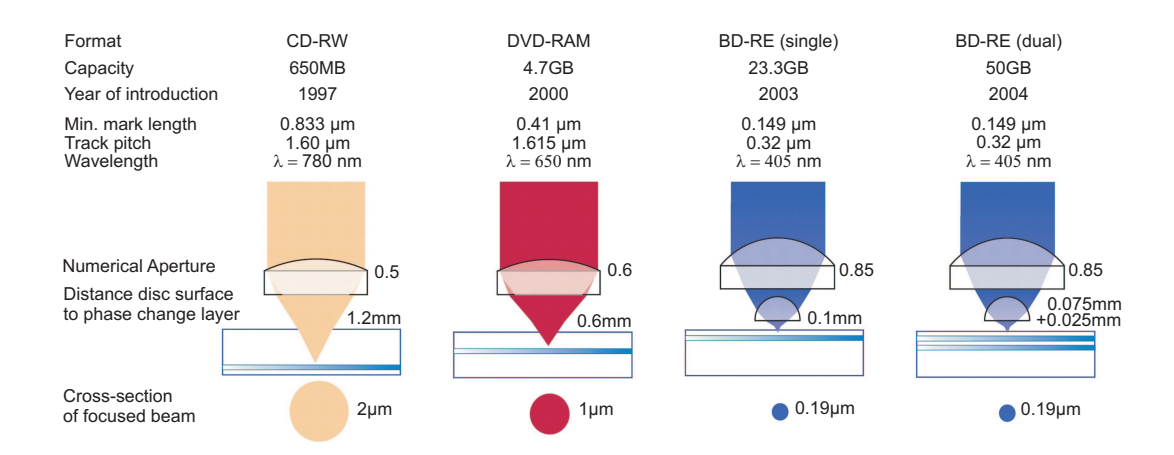


**Figure 2.1:** Progress of phase change based re-writable optical storage media: A redesign of the optics, i. e. usage of shorter wavelengths and higher Numerical Apertures, allowed for a reduction of the cross-section of the focused laser beam and thereby for a decrease of the minimal mark size and a corresponding increase in recording capacity. [1]

and thus a carefully chosen compromise between them regarding the crystallization speed is neccessary. These few examples already show clearly that the development of new materials with adapted properties is crucial whenever a step towards the next generation of an existing storage concept brings with it a new set of boundary conditions for the phase transitions.

It turns out that all materials that proved useful for optical data storage over the years are based on alloys from the Ge-Sb-Te ternary diagram as illustrated by Fig. 2.2. However, for an improvement of material properties researchers and developers have not limited themselves to the use of just these three elements, but instead have modified the compositions by doping with various other elements.

It is worth to mention, that in contrast to common semiconductor physics, doping in the context of phase change materials means an introduction of up to several percent of another element. Very small changes in stoichiometry, such as  $10^{-4}$  or less, so far have not been reported to produce any significant change in material properties. This robustness against slight variations in composition is one of the reasons why applications based on phase change materials are usually regarded to be comparably easy to manufacture and thus cost effective. On the other hand such a pronounced deviation from the behaviour of traditional semiconductors, such as Si or GaAs, that are dominating todays text books on semiconductor physics, add up to the list of peculiarities of phase change materials making them scientifically interesting.

Even though it was already in the 1960s when Stanford Ovshinsky first investigated the electrical properties of phase change alloys [3], it took around twenty years until

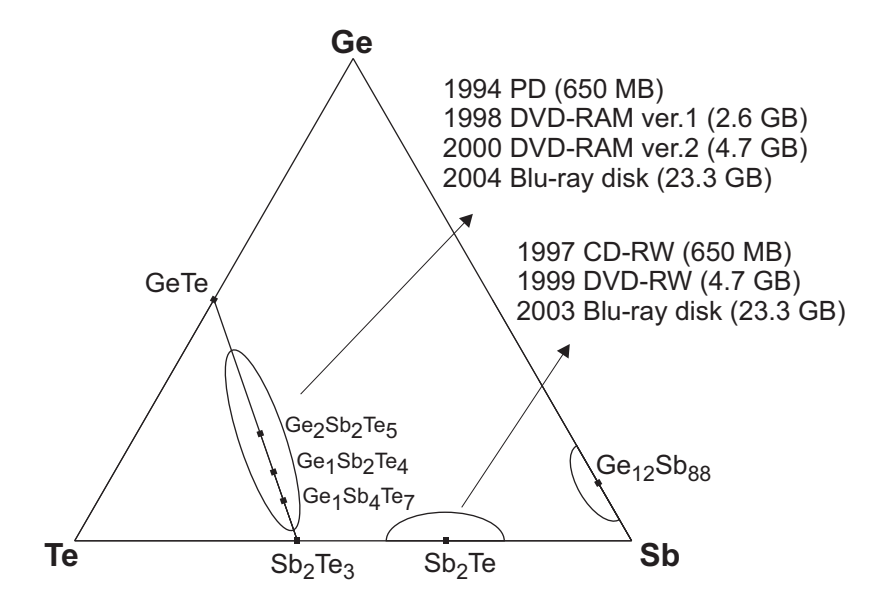


Figure 2.2: Phase change materials suitable for optical storage: So far all phase change materials that qualified for application in re-writable optical data storage are based on alloys from the Ge-Sb-Te ternary diagram. Besides the position indicating the composition, the years of discovery as a phase change alloy and the respective application in optical data storage is given. [1]

the usefulness of this class of materials for optical data storage became apparent<sup>1</sup>. One reason for this was the quite slow crystallization speed of the compounds Ovshinsky used in the beginning, which are rather good glass formers (see chapter 3 on glass formation). This actually allowed him to see purely electrical switching effects without structural phase transitions (see Section 2.2.3). The fact that for several years the scientific community mainly focused on the electrical properties [5, 6, 7, 8, 9, 10, 11, 12, 13, 14, 15, 16, 17, 18, 19, 20] might be another cause for the considerable delay until the first materials with fast recrystallization and good optical contrast were discovered in the 1980s, i.e. GeTe [21] and Ge<sub>11</sub>Te<sub>60</sub>Sn<sub>4</sub>Au<sub>25</sub> [22]. A clear goal of application in sight Yamada et al. explored other compositions on the so-called pseudo-binary tie line between GeTe and Sb<sub>2</sub>Te<sub>3</sub>, such as Ge<sub>1</sub>Sb<sub>4</sub>Te<sub>7</sub>, Ge<sub>1</sub>Sb<sub>2</sub>Te<sub>4</sub> and Ge<sub>2</sub>Sb<sub>2</sub>Te<sub>5</sub> [23, 24]. Compositional variations of the latter, such as NGeSbTe [25, 26], OGeSbTe [27], SnGeSbTe[28], BiGeSbTe [29, 30], GeBiTe [31] and PdGeSbTe[32], have been developed for better performance. Some of these alloys found their way into commercial products in recent years.

Fig. 2.2 gives an overview on phase change alloys that qualified for application in optical storage. Besides the compositions along the GeTe-Sb<sub>2</sub>Te<sub>3</sub> tie line mentioned

<sup>&</sup>lt;sup>1</sup>It is interesting to note that Ovshinsky and his coworkers themselves proposed the usefulness of chalcogenides for optical storage already in the beginning of the 1970s [4]. Their experimental study, however, remained rather rudimental.

#### 2.1. OPTICAL DATA STORAGE

above a second group of materials is located around Sb<sub>2</sub>Te. Ag, In and Ge have often been used as dopants of this binary compound. [33, 2, 34, 35] The best-known representative from this group is a composition close to Ag<sub>5</sub>In<sub>5</sub>Sb<sub>60</sub>Te<sub>30</sub>, often referred to as AIST, being frequently used in re-writeable media such as DVD-RW and DVD+RW [36].

A third group of fast crystallizing phase change materials is based around the Sbrich eutectic Ge<sub>12</sub>Sb<sub>88</sub>. The credit for the investigations of its fundamental properties regarding optically induced transitions is surely due to Afonso et al. [37, 38, 39, 40, 41, 42, 43, 44, 45, 46, 47]. Though this third group of materials undoubtly shows extremely fast crystallization and also significant optical contrast, it has so far not been implemented into an optical storage product by industry. Nevertheless it became a basis for the design of new phase change materials for electronic memory (see Section 2.2.3) [48].

The sum of the materials mentioned above shows nicely how in phase change materials the reflectivity contrast between the amorphous and the crystalline state, the crystallization speed or the temperature stability of the amorphous state can be changed by a modification of the composition. While in the past the finding of successful modifications often has been achieved by trial and error or at best based on intuition, in this work a systematic approach is persued towards a composition controlled modification of the temperature range that shows fast crystallization (part II).

#### 2.1.3 Future of optical data storage

While the third generation of optical discs just entered the United States and the European market in 2006 and as recently as in the beginning of 2008 the Blu-ray disc won the war of standards against the HD-DVD format thereby opening the door to real mass distribution of this technology, the fourth generation is already under development. The strategy of improving the optics, however, seems to have come to a limit. The feasibility of a further decrease of the laser wavelength into the ultra violett has to be regarded as very low. Not only due to the lack of suitable laser diodes but also because of the difficulty of achieving another increase in numerical aperture for this wavelength a significant reduction of the cross-section of the focused laser beam seems unrealistic, at least for the next years.

So instead of further working on reaching a lower value for Abbe's resolution limit, one idea is to go beyond Abbe's limit by utilizing near field effects. This could be accomplished by exploiting the non-linear optical behaviour observed in some phase change materials. A layer of such a material could serve as a mask for the recording layer underneath, transmitting most laser light only where the incident intensity is above a

certain threshold, i. e. only inside an inner circle of the focal spot of a Gaussian laser beam. This of course can then be smaller than what is given by Abbe's limit, i. e. the focal point itself. In 1998 Tominaga et al. proposed this so-called super resolution near field structure, abbreviated SuperRENS, as a concept for reaching higher data density in optical storage. [49, 50, 51] While the effect was first studied with Sb as masking material, in the following years various other compositions have been found to show a similar behaviour. However, its physical explanation is still controversial. Wether it is mainly an electronic effect, wether the temperature distribution plays a crucial role or wether even a spatially confined phase transition into the melt is the reason for the change in optical transmittance is not yet answered conclusively.

Whether a fourth generation optical disc, in case it is technically feasible, can be commercially successful or not will depend strongly on the development of competitive technologies, like holographic data storage or solid state memory.

The first, i. e. holographic data storage, approaches the market segment occupied by optical discs from the side of archival storage. For many years holography has been a scientific endeavour for research groups both in academia and industry [52]. Now InPhase Technologies (Colorado, USA), a Lucent Technologies venture spun out of Bell Labs research, is the first company that sells a commercial holographic data storage system named Tapestry. The pricing of the Tapestry drive of \$18,000 and the 300GByte Tapestry media of \$180.00 however lets the intrusion of holography into the consumer market seem unlikely<sup>2</sup>. At least in the near future its large data density, its long retention times and its fast data transfer rates make holographic storage only interesting for business archival systems, a field that has been dominated by magnetic tape storage for the last decades.

The second major future competition for optical discs, solid state memory, especially in form of flash memory (see 2.2.1), is already dominating the field of mobile applications, like cell phones and digital cameras, and has even entered the hard drive market. How far performance and especially cost of solid state memories will reach into the demand accommodated by optical storage, is difficult to predict. Though, as will be shown in Section 2.2.3, it might well be that at some point in time both technologies, optical storage and solid state memory, will be based on phase change materials.

 $<sup>^2</sup>$ US List Prices December 2007

## 2.2 Electronic memory

#### 2.2.1 Flash memory

Flash memory is a type of solid state memory, thus distinguishable from Floppy discs, optical discs, hard disc drives or tape drives, all of which of course are also made out of materials in their solid state, by the fact it contains no movable parts. Furthermore, flash is an electronic memory, i. e. electric fields are used for writing, erasing and reading out the bits. More specifically in flash memory an applied voltage moves electrons through a barrier of insulating material into a small volume, where the charge carriers are trapped as long as no voltage is applied to remove them. The latter fact already states that flash is a static memory, which implies that there is no need for refreshing the stored data after short periods of time, i. e. repeatedly reading out and storing it again. Moreover, flash memory is non-volatile, i. e. it retains the stored data without a power supply connected to it. This obviously is important especially for mobile applications, where battery power is limited and needs to be conserved, making non-volatility a big advantage over other electronic memories that are volatile, e. g. Dynamic Random Access Memory (2.2.2).

Besides this, another important feature of flash like of all other solid state memories is its variability in size. In cases where the spatial dimensions of the whole storage device are allowed to be large, usually the price per bit is the decisive argument for the choice of the storage technology often favouring hard disc drives or even tape storage. However, where a small package is needed, all technologies that include movable parts, like discs or tape, face the problem of needing space to realize the mechanics for accelerating the storage medium, which are not arbitrarily shrinkable. And even if these mechanics could fit into the given size of the package, the prize for the memory is kept up by the almost fixed costs of the read-head and the mechanics, respectively. Thus the reduction of the incorporated storage medium leads to a stronger decrease of data capacity than of the absolute costs of the package. One can conclude that for a variation of the total data capacity the cost per bit is more or less constant for solid state memories, while for storage concepts including movable parts the total cost of the package is rather constant due to the negligibility of the costs of the storage medium itself.

An interesting example for the regime of overlapping cost effectiveness of two different storage concepts is the market of digital audio players. The size of a first and second generation iPod by Apple was large enough to implement a small hard disc drive obtaining a minimum cost per bit in the given package. A couple of years later, however, the cost per bit in flash memory was more competible. So the new generations of the iPods, even those of roughly the same spatial size as the ones mentioned first, e.g. the iPod touch, incorporate flash memory for storing the music and video contents. In smaller mp3-players, e.g. Apple's iPod-nano, the implementation of a very small hard disc obviously made no sense from the beginning. It is worth to add, that for mass products like digital audio players besides the cost per bit there is another important parameter for the decision about which storage technology to incorporate into a product: the absolute available number of units. In times when a single company demands around a quarter of the worldwide production of flash memory <sup>3</sup> the steady supply of the storage device becomes a highly relevant business issue.

After for a short period of time hard disc drives had found a market even inside of rather small products, e. g. the digital audio players mentioned above, now despite the still higher costs Dell and Toshiba on the other hand are already selling laptop computers with solid state drives instead of hard disc drives as secondary storage because of its faster file handling, lower energy consumption and improved shock stability. This shows that in some, especially mobile applications, like PDAs, laptop computers, digital audio players, digital cameras and mobile phones, other properties of a storage concept can become important enough to outweigh a certain disadvantage in the cost per bit.

However, all advantages are worth nothing, if flash memory cannot keep up with the ever dropping prices per bit in the data storage market. For solid state memories the price of a bit is dominated by the area of the silicon wafer it occupies. So in order to reduce the price per bit of a solid state memory, the size of each bit has to be decreased.

For flash memory this task becomes increasingly difficult. Without going into too much detail, the core of the problem can be described as follows. As mentioned above, in flash technology electrons are stored in a volume that is confined by walls out of an electrically insulating material. Reducing this volume but keeping the number of injected electrons roughly equal leads to stronger repulsion among the electrons. Besides the need of higher voltages for writing such a bit, the driving force, that pushes the electrons out of the volume, increases. A tunneling of electrons through the insulating barriers becomes more probable making the stored data more volatile. As the spatial minimization of the structure also includes the thickness of the insulating walls, they are less capable of hindering the escape of the electrons, which is additionally increasing the volatility of the stored information. Without the invention of materials with significantly improved (di-)electric properties, this limitation of the scalability of flash must be assessed as a fundamental one.

<sup>&</sup>lt;sup>3</sup>http://www.electronista.com/articles/07/07/18/apple.quarter.of.all.flash/

#### 2.2.2 Dynamic and static random access memory

Dynamic random access memory (DRAM) is several orders of magnitude faster and can be switched also much more often than flash memory. These are the main reasons why it is used as primary storage being quickly accessed by a computer's processor. In DRAM each bit of data is stored in a separate capacitor within an integrated circuit. As the word *dynamic* in its name already indicates, due to the capacitors' loss of charge, the bits needs to be refreshed periodically to retain the stored information.

In contrast to DRAM Static Random Access Memory (SRAM) works without such a refreshment of the data. The bistable latching circuitry it uses to store a bit, however, can only be accomplished by a much more complicated cell structure. This structural simplicity of DRAM is its major advantage over SRAM: a single transistor and one capacitor are required per bit, while in SRAM six transistors are needed. So where ever very high bit densities are needed, either due to spatial limitations of the whole chip or simply to reduce the costly real estate on a silicon wafer per bit (2.2.1), DRAM is advantageous over SRAM.

In the ongoing efforts of scaling down the area per bit the challenges for DRAM are related to the problems flash memory faces, caused by the fact that both techniques try to transfer and store electric charges in very small volumes. A detailed analysis of the challenges for the scaling of DRAM and of the possible paths towards their solution is given by a research group at IBM <sup>4</sup>.

For this work, however, much more important than the scalability of DRAM is that Dynamic and Static Random Access Memory are both volatile in the sense that they lose the data when the power supply is removed. In the presence of limited battery resources this is a big disadvantage for mobile applications, opening a window for new memory solutions, that combine the speed and cyclability of DRAM with the non-volatility of flash memory. This technological gap is about to be filled by a Random Access Memory based on phase change materials, the so-called PCRAM, which will be described in detail in the next paragraph.

## 2.2.3 Phase Change RAM

As mentioned in the section on optical data storage (sec. 2.1.2) the interest in phase change materials began with the observation of their peculiar electrical behaviour in the 1960s [3], which already at that point in time gave reason to see a potential use of this kind of materials in electronic data storage applications. In his pioneering work Ovshinsky reports a breakdown of the electrical resistivity of the investigated materials

<sup>&</sup>lt;sup>4</sup>http://www.research.ibm.com/journal/rd/462/mandelman.html

upon applying voltages larger than a distinct threshold voltage. The highly conductive state remains as long as the applied voltage does not drop below a certain holding voltage. When it does, the material goes back into its original high resistivity state. Also already in this early work it is pointed out that in materials, which can undergo structural transitions easier than the alloys primarily described in the article, even a permanent but reversible change in conductivity could be induced by electrical pulses.

It was much later, though, that materials were found which showed both fast crystallization and high reflectivity contrast between the amorphous and crystalline state, two properties which were indispensable for the use in optical data storage. In consideration of this fact it is astonishing that the research activities towards an application of phase change materials in electronic memories were started only after they were already commercially successful in optical storage, if one disregards the activities of Ovshinsky and his companies for a moment.

This delay surely has to do with the generally lower expenses of pursueing the optimization of an existing technology compared to the development of a new one. Thus it was not until a couple of years ago when the end of progression of miniaturization of the structures in existing electronic memory technologies became foreseeable (see section on flash memory 2.2.1 and DRAM 2.2.2), that alternative concepts were looked for.

On this quest many semiconductor companies came to the conclusion that a memory based on phase change materials might be very promising as a future technology. The main advantages of a Phase Change Random Access Memory (PCRAM) are its very high switching speeds compared to flash, its non-volatility in contrast to DRAM and SRAM and of course its large potential for scalability towards extremely small cell sizes. These properties make PCRAM a universally applicable memory being particularly attractive for mobile electronics. Besides this, compared to technologies that store electric charges PCRAM stands out due to its radiation hardness [53], a property that is relevant for space and military applications. Table 2.1 gives an impression of the high interest of the semiconductor industry in PCRAM in recent years <sup>5</sup>.

After this brief excursion through the history of phase change materials with respect to electronic memories, now an explanation of the actual memory concept of PCRAM is due: A PCRAM cell basically consists of a small volume of phase change material that is electrically contacted from two sides. Like in phase change based optical discs the data are stored as the structural state of the alloy. Reading is based on the detection of the resistivity contrast between the amorphous and the crystalline phase. For that

<sup>&</sup>lt;sup>5</sup>based on information from http://ovonyx.com and http://en.wikipedia.org/wiki/Phase\_change\_memory

### 2.2. ELECTRONIC MEMORY

Table 2.1: Industrial engagement in Phase Change RAM

date	action
June 1999	Ovonyx joint venture is formed to commercialize PCRAM
	technology
November 1999	Lockheed Martin works with Ovonyx on PCRAM
	for space and military applications
February 2000	Intel invests in Ovonyx, licenses technology
December 2000	STMicroelectronics and Ovonyx sign Licensing
	and Joint Development Agreement
March 2002	Macronix files a patent application for transistor-less $\operatorname{PCRAM}$
July 2003	Samsung begins to work on PCRAM technology
August 2004	Ovonyx and Nanochip sign licensing agreement
	for high density, probe-based non-volatile memory
August 2004	Samsung announces successful 64 Mbit PCRAM array
February 2005	Ovonyx and Elpida sign technology licensing
	and support agreement for PCRAM
September 2005	Samsung announces successful $256\mathrm{Mbit}$ PCRAM array
October 2005	Intel increases investment in Ovonyx
December 2005	Hitachi and Renesas announce 1.5 Volt PCRAM
	with $100\mu\mathrm{A}$ programming current
December 2005	Ovonyx and Samsung sign licensing agreement for PCRAM
July 2006	BAE Systems (formerly Lockheed Martin) begins selling the
	first commercial PCRAM, a Radiation Hardened C-RAM
	512Kx8 Chip
September 2006	Samsung announces 512 Mbit PCRAM device
October 2006	Intel and STMicroelectronics show a 128Mbit PCRAM chip
December 2006	IBM Research Labs demonstrate a prototype with a cross sec-
	tion of 3 by $20\mathrm{nm}$ of the phase change material
January 2007	Ovonyx and Qimonda sign technology licensing agreement for
	PCRAM
October 2007	Ovonyx and Hynix sign technology licensing agreement for
	PCRAM

purpose a low voltage is applied and the resulting current containing the information about the cell's state is measured. For switching from amorphous to crystalline and backwards the material is heated by sending an electrical current through the finite resistance of the cell transforming electrical energy into heat, so-called Joule-heating. The current necessary to heat the amorphous cell to temperatures high enough for crystallization can be reached at voltages limited to a few volts, because in the so-called threshold switching effect the resistivity of the amorphous phase drops drastically upon the application of a critical electrical field.

Though the storing method is conceptually quite easy, in its details some difficulties show up. To overcome these, a precise knowledge about both, the crystallization behaviour and the non-linear electrical properties of phase change materials, is indispensable. It turns out that there are basically two approaches for developing a functioning PCRAM cell. The first starts from the properties of the chosen phase change material and adapts the architecture of the cell according to them. Especially the electrical and thermal conductivity of the direct surrounding of the switchable volume of the phase change material has to be adjusted.

To show how diverse the resulting structures can be, two cell designs from different research groups are presented. The first one, the so-called Ovonic Unified Memory (OUM), is illustrated in Fig. 2.3. Its name and development traces back to Ovshinsky himself. This vertical cell design is probably the most popular PCRAM architecture to-day. One of its advantages is that the phase change material does not need demanding lithographic structuring. Its deposition as a continuous film minimizes an unintended variation in material composition due to the fabrication process. The cylindrical bottom electrode serves not only as electrical contact but also as a heat source. It limits the volume of phase change material that is switched into the amorphous phase to the proximity of the bottom electrode, resulting in a shape similar to that of a mushroom cap. Despite the only partial amorphization there is a pronounced resistivity contrast compared to the completely crystalline cell, as long as the amorphous 'mushroom cap' completely covers the electrode.

The long experience with this kind of PCRAM cells, combined of course with the related intellectual property rights, surely is the main reason for the multiple collaborations of reknown semiconductor companies, like Intel or STMicroelectronics, with Ovonyx (see Table 2.1), a company that was formed in 1999 to commercialize the PCRAM technology originally developed by Energy Conversion Devices, founded by Ovshinsky.

So it is not surprising that the results the researchers around the group from STMicroelectronics published on the topic of PCRAM in recent years are based on this OUM

#### 2.2. ELECTRONIC MEMORY

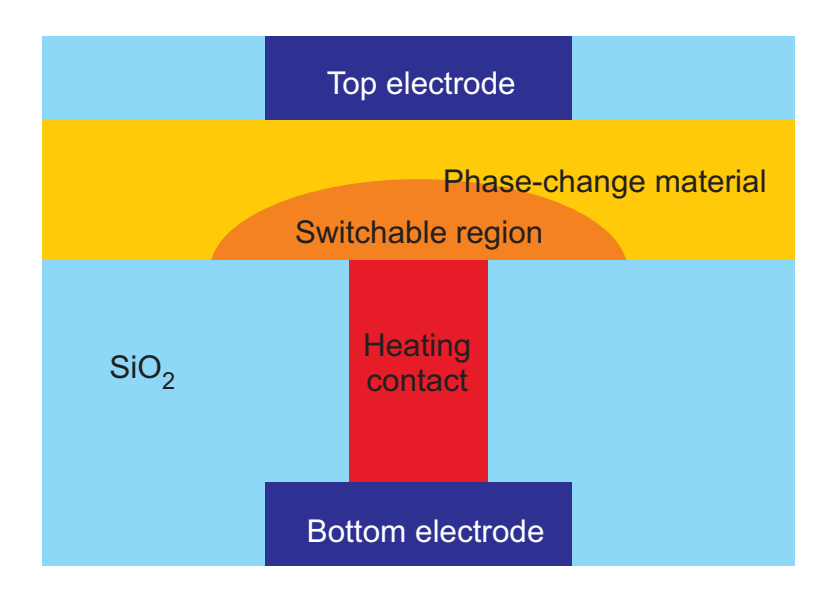


Figure 2.3: Architecture of a mushroom-like PCRAM cell, also referred to as Ovonic Unified Memory (OUM). The cross-sectional view shows that only the phase change material near the heating electrode is changing its structure between the amorphous and crystalline state. Its switching dynamics for the case of Ge<sub>2</sub>Sb<sub>2</sub>Te<sub>5</sub> are discussed in [54, 55, 56].

cell design [54, 55, 56]. The switching dynamics of this cell type have been intensively studied by that group, while they limited themselves, at least in their publications, to the use of the material Ge<sub>2</sub>Sb<sub>2</sub>Te<sub>5</sub>, which is known from optical storage and became the standard material for PCRAM.

The second example of a concept for PCRAM is the line cell, depicted in Fig. 2.4. It was proposed by Lankhorst and his colleagues at the Philips Research Laboratories in Eindhoven, Netherlands, in 2005 together with the use of a doped Sb<sub>2</sub>Te alloy, that they knew from their experience with phase change optical data storage, in this case DVD+RW [57]. The authors state that their main reason for investigating this lateral cell architecture is its conceptual simplicity. In OUM the requirements for the electrodes, especially for the heating bottom electrode, are multiple. The electrode materials have to have suitable resistivity, may not react with the phase change film and at the same time must keep suitable adhesion to it, even at high temperatures. Especially the last aspect is much less severe for the line concept, because there the highest temperatures do not occur next to the electrodes, which consequently stay cooler than in the OUM architecture.

Another advantage of the line concept over OUM is its lower programming power and current, for reasons that will be discussed later. This implies that the selection device (e.g. a MOS transistor) for each cell can be smaller saving valuable real estate on a silicon wafer. Strategies for the reduction of programming currents in OUM by decreasing the contact area between the heating electrode and the phase change

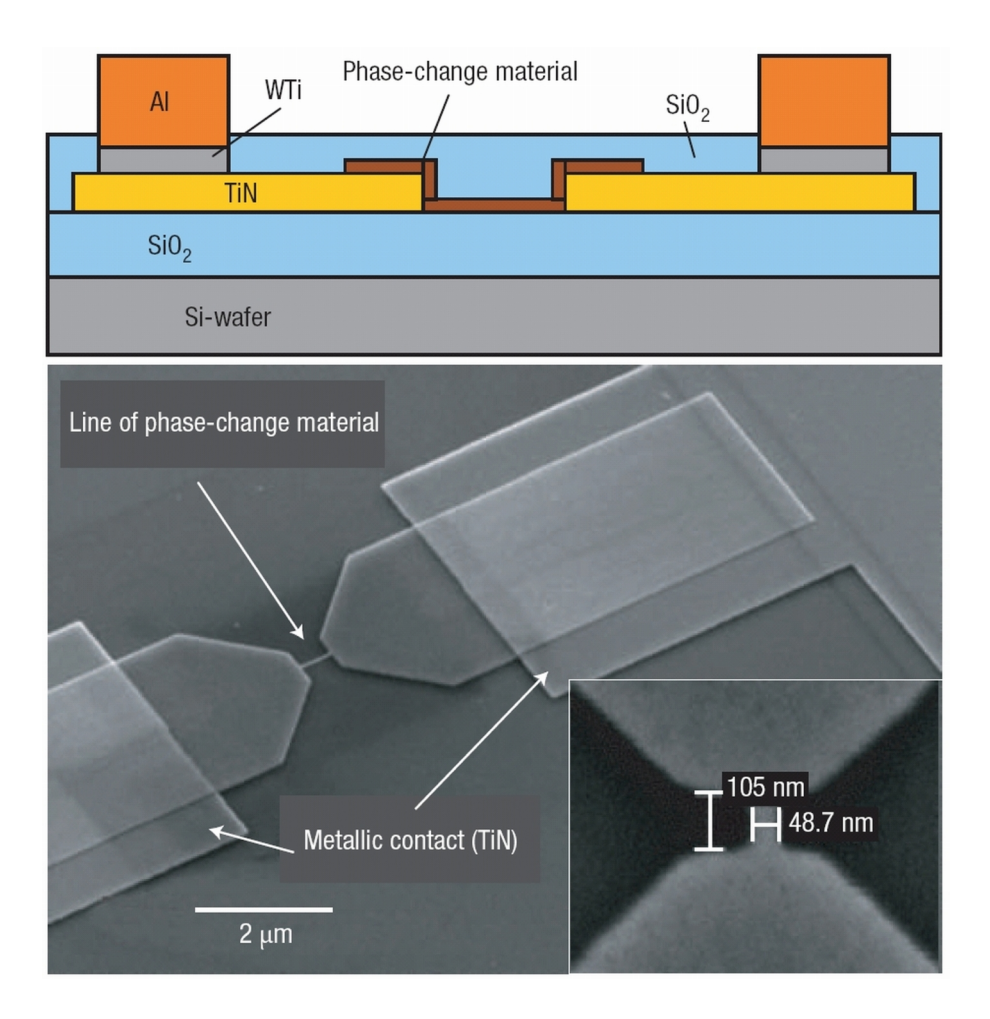


Figure 2.4: Architecture of a line cell for Phase Change RAM [57]: Schematic cross-section (top) and scanning electron micrograph (bottom) of a line-concept memory cell. The 500 nm long and 50 nm wide phase change line is prepared by electron-beam lithography. The inset shows an SEM of a similar, but shorter line cell.

#### 2.2. ELECTRONIC MEMORY

material typically require more additional lithographic processing steps for integration into logic CMOS process flows than the simplest realization of the line cell memory. Despite of the popularity of the OUM concept (Table 2.1) it is reasonable to say that the line cell approach is at least as promising for a successful realization of PCRAM as OUM is, although the area an OUM cell occupies is inherently smaller than that of a line cell.

After having revised two examples for the optimization of PCRAM by cell design, the second general strategy for the development of a functioning PCRAM cell will be described, which is quite opposite to the first one. In this approach starting from an existing cell architecture a material is searched for that has all properties required by the cell geometry. Actually to some degree this idea has been successfully used in the work of the group from Philips mentioned above, where the doped Sb<sub>2</sub>Te, an alloy with different crystallization kinetics than Ge<sub>2</sub>Sb<sub>2</sub>Te<sub>5</sub>, has been assessed to be more suitable for the line cell concept.

Yet, because the physical properties of a material are not independent of each other, but instead in some cases even strongly coupled, there is no direct path to a composition that provides exactly the ideal set of properties derived for a chosen cell structure. Optimizing a known material, which differs not too strongly from the catalog of requirements, with respect to a certain property by changing its stoichiometry or by alloying with new elements will usually lead to an unintended deterioration of other properties. For that reason it is not sensible to solely follow either the first or the second strategy. Instead a concerted development of cell architecture and the material promises the best chance to accomplish a PCRAM with highest performance. This means for example that when a material is found, which fulfills the most important requirements, especially those being rather independent from the choice of the cell design such as the long-time stability of the amorphous phase, but moderately fails to match other properties, an according adaption of the cell geometry to the new material is advisable.

In this procedure computer simulations turn out to be extremely helpful, as they can calculate the switching behaviour even of a complicated three-dimensional cell based on the electrical and thermal properties of the used materials. That way the expensive, because time-, machine- and personnel-intensive, lithographic fabrication of prototypes for an evaluation of the optimal cell geometry can be minimized. The significance of the computed predictions on the switching behaviour of a cell depends of course not only on the correctness of the assumed physical mechanisms, but at least as crucially on the precision of the material properties fed in.

In the case of phase change materials especially the temperature dependence of

the crystallization kinetics is essential. Its experimental determination, however, is extremely difficult, since the high crystal growth velocities at elevated temperatures are very difficult to detect. At this decisive point on the way to the realization of a PCRAM, the experimental setup *POET* proves to be very useful. That instrument has been designed, set up and put into operation in the scope of this work and thus is described in detail in Part III.

Even if computer simulation, provided that applied correctly, surely is the more precise tool to predict the performance of a cell, a good understanding of the physical processes during the switching persists to be important. In fact many deficiencies of a cell can be, at least qualitatively, traced back to its origins without a numerical calculation. As already pointed out above, it is extremely helpful to have the possibility to choose between different approaches for solving a problem. On this account the following considerations of different aspects of PCRAM cells will include both the role of the properties of the phase change materials and the thermal and electrical conditions of the structure.

The first issue to be addressed is the amorphization. Here the phase change material has to be heated above its melting temperature. As energy and thus power is a resource one likes to conserve, one goal is to hinder the heat from flowing out into the surrounding. The more heat stays inside the phase change material, the less electrical power is needed to melt it. It can be accomplished by surrounding the portion of the phase change material that undergoes the phase transition with a material of lower thermal conductivity. This is actually the case for the Philips concept compared to the OUM. In the line cells there is only a dielectric material like  $SiO_2$  with low thermal conductivity in the proximity of the melting phase change material, while in OUM the electrode is in direct contact with the molten region. The reduction in programming power does not only save energy, but allows also for a smaller transistor providing the current for the phase change cell, as was already mentioned as one of the advantages of the line cell earlier in this text. A secondary positive effect of using materials with low thermal conductivity in the surrounding of the phase change material is the reduction of the danger of thermal cross-erasure of neighboring cells.

However, after melting the phase change material must be cooled down so rapidly that the temperature regime of increased crystallization speed is passed fast enough to circumvent crystallization and instead reach amorphization. In the face of the limitation of this cooling rate by the thermal conductivity of the surrounding, the crystallization speed of the phase change material has to be chosen low enough. This in turn results in a longer re-crystallization time of the amorphous cell and thus in a decrease of the switching speed of the memory. Only a carefully chosen compromise between

#### 2.2. ELECTRONIC MEMORY

both requirements, minimization of the power consumption and maximization of the switching speed, can solve this dilemma.

Besides the reduction of the dissipating heat by lowering the thermal conductivity of the surrounding, there are at least two further approaches to decrease the need of power or current, respectively. First, a material with a lower melting temperature obviously needs to be heated only to a lower temperature, so less heat is neccessary. Second, a transistor has to provide the cell with maximum current, when the cell is in its completely crystalline state waiting for amorphization. Here an increase of the resistivity of the crystalline phase helps to reduce the necessary current.

The crystallization of a cell is not as demanding for the temperature profile as the amorphization is, because the maximum temperature is lower and the heating and cooling rates may be slower. In this switching process it is the initial electrical state, i. e. the resistivity of the amorphous phase, that is causing the difficulty. In order to bring enough current for heating through the phase change material, very high voltages would be necessary due to the very high resistivity of the amorphous phase; voltages that would exceed the maximum applicable voltage in most applications.

This problem, however, has in the past been solved by the nature of phase change materials itself, namely by its oldest, already by Ovshinsky in 1968 known characteristic: the breakdown of the resistivity of the amorphous phase in the presence of an applied electric field above a certain threshold voltage. This critical voltage turned out to be in the convenient range of a few volts for typical device structures and phase change materials used so far.

This fact must be estimated to be quite fortunate, since at first simply those materials have been chosen for an application in PCRAM which proved to be successful in optical data storage before, especially  $Ge_2Sb_2Te_5$  and its doped relatives. This choice must have happened without a deeper consideration of the non-linear electrical properties of the amorphous states of the chosen alloys, because the physical origin for this behaviour and of course also its connection with the composition of the material is not understood until today. A status that is due to be changed (see section 12.5), not only out of scientific curiosity, but also for a very practical reason: Without a clear idea about the dependence of the electrical non-linearity on the stoichiometry of a material the optimization of certain properties of the phase change material used might eventually not automatically lead to compositions with low threshold fields. This view seems to be shared by an increasing number of researchers, as becomes evident in the proposal of the doped  $Sb_2Te$  for PCRAM by the Philips group [57]. Besides its fast crystal growth velocity the doped  $Sb_2Te$  also shows a lower threshold field than the standard  $Ge_2Sb_2Te_5$  making it advantageous compared to other materials especially

for the use in a line cell concept.

Another challenge for the design of a PCRAM is the need to maximize the retention time. Nothing man made is forever, especially not in data storage. Thus also the duration information in a non-volatile memory staying intact is limited. To increase this period of time as far as possible is an obvious goal. Even if all electronic parts, transistors or diodes, contact electrodes and conduction channels, had an infinite life expectation, in a phase change based memory there is always an inherent limitation of the memory's retention time: the stability of the amorphous state of the phase change material.

As will be discussed in detail in the following chapters (chapters 3 and 4) an amorphous phase is not the energetically most favourable state, i. e. the transition into the crystalline phase is only hindered by a finite activation barrier. At temperatures low compared to the activation energy the chance of crystallization is very small. The higher the temperature the larger is the probability for crystallization. At first one might assume, that a phase change material that proved to stay amorphous for more than ten years in optical discs should lead to the same retention time inside an electronic memory. Yet this does not consider the temperature at which the device is kept: While optical discs are designed to withstand temperatures around 330 K for ten years, an electronic memory, especially if used on a computer's main board or applied in the automotive industry, has a significantly higher working temperature resulting in a requirement for long retention-times even at 420 K.

Clearly to fulfill this requirement, phase change materials have to be optimized. Of course there is always the option to simply try out a lot of compositions and test how stable their amorphous state is. However, the shear endless number of possible combinations of elements strongly demands a guideline for targeted experiments. Part II gives such a guideline by predicting stoichiometric trends in crystallization or glass transition temperatures, respectively.

Even though the retention time is a material issue in the first place and thus rather independent of the chosen cell architecture, at one point the structure of the memory might play a role: The scaling of the cell size towards extremely small volumes. Surely the danger of cross-erasing between neighboring cells has to be kept in mind when increasing the density of cells. This, however, is a rather technical problem that might loose a lot of its threat when one realizes that not only the heat barriers between adjacent cells will become thinner, but the amount of heat needed to write a bit will decrease with the volume of phase change material, too. The much more fundamental question is, how in smaller and smaller cells with the increasing influence of the boundaries the thermodynamics, the transition kinetics and the electrical properties of the

tiny volume of phase change material will change.

Actually, unlike for other memory concepts, e.g. Magnetic RAM, Ferro-electric RAM or flash, the physical mechanisms of switching a PCRAM cell predict an even improved performance with scaling the cell dimensions down to the nanosize<sup>6</sup>. The threshold voltage for a given material will be lower for shorter distances between the two electrodes. Smaller cells can be crystallized within the same or in the case of growth dominated crystallization within a shorter period of time leading to a faster programming speed. And finally, the smaller the cross-section of a cell the less material needs to be molten in order to block the charge carriers with a high-resistive amorphous plug. Less material to be molten again means less Joule-heating needed allowing for a lower programming current.

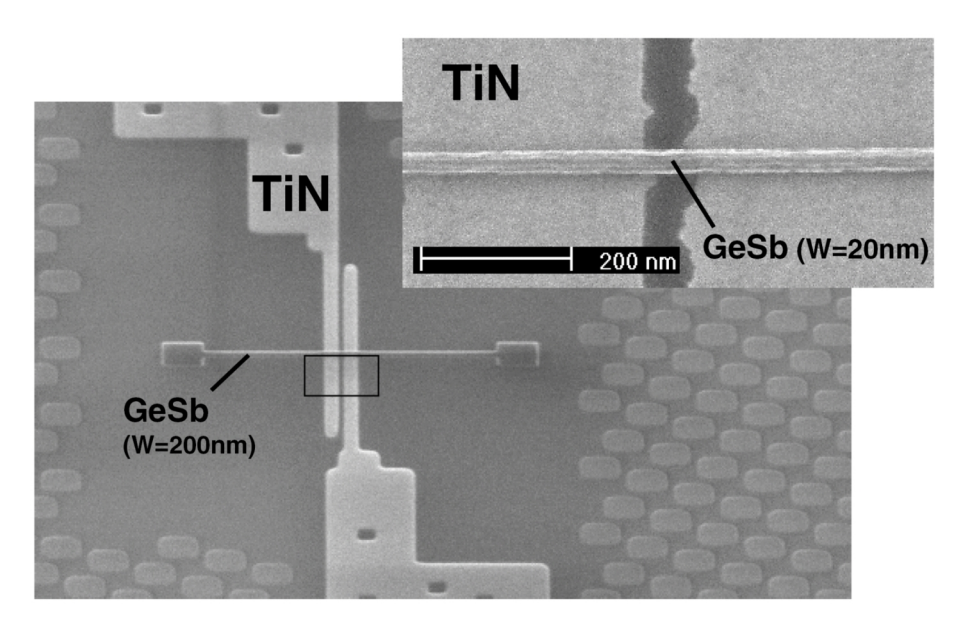
The reason why this good scalability is generally seen as one of the strategically most important advantages of PCRAM over competitive technologies is that the costly introduction of a new memory concept into the fabrication process is economically the more favourable the longer this memory can increase its bit density. Due to the paramount importance of the scalability it is worth not simply to trust in the correctness of the optimistic predictions but to actually prove at which small dimensions a PCRAM cell can work.

The accomplishments of a group of researchers at the IBM Almaden Research Center in this field is mentioned here, not only because the paper [48] represents the world record of the smallest working PCRAM device published, but also since the author of this thesis contributed to the work of this group in the course of his studies on phase change materials, as described in more detail later.

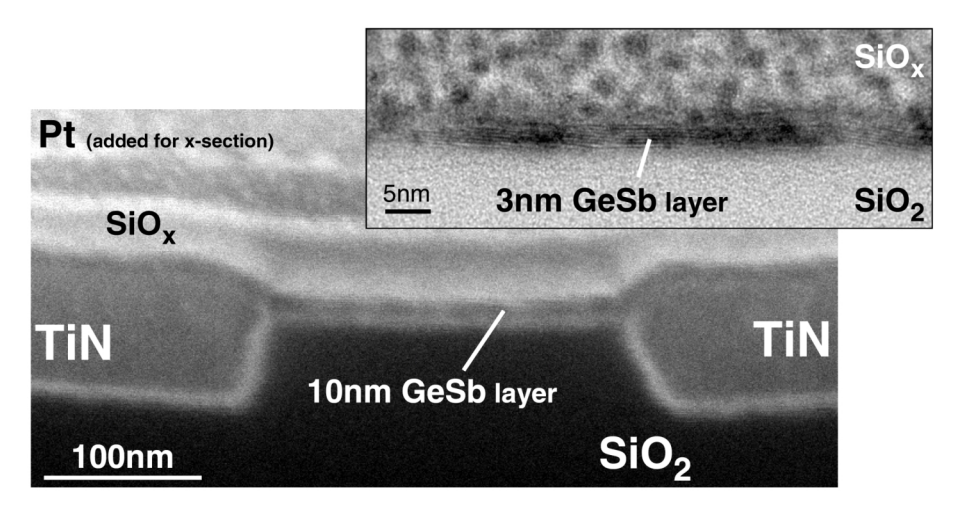
The article describes a bridge cell that is similar to the line cells fabricated by the Philips group. Fig. 2.5 shows both topview and cross sectional images of such cells. The lateral cell design has the advantage that the device's cross section is only linearly dependent on the lithographic patterning. It can thus be reduced effectively by the much easier reduction of thickness of the phase change material. This way devices with a cross section of only 3 nm x 20 nm have been realized and repeatedly switched.

Furthermore, the bridge cells were equipped with a new phase change material based on the known GeSb alloy. This material does not only show extremely fast switching speeds, but its amorphous phase is also stable up to much higher temperatures compared to the classic Ge<sub>2</sub>Sb<sub>2</sub>Te<sub>5</sub>. In Chapter 8 the effect of doping in GeSb is discussed in more detail for two dopants. There the temperature shift of the stability regime of the amorphous phase is both simulated based on a theoretical model and experi-

<sup>&</sup>lt;sup>6</sup>At least up to a point where the physics is not changing in a fundamental way such as in a decrease of the melting temperature upon volume reduction.



(a) topview



(b) cross section

**Figure 2.5:** Bridge cell for Phase Change RAM: Phase-change lines, in widths ranging from 20 to 200 nm, bridge the TiN electrodes. The SEM images in (a) give a topview on a bridge cell. The black rectangle indicates the location of the Focused Ion Beam cross section shown in (b). The bridge cells tested in [48] have been as thin as 3 nm.

#### 2.2. ELECTRONIC MEMORY

mentally determined. So [48] is a good example for a combined effort in innovative cell design and materials research towards the accomplishment of a PCRAM cell with better performance.

At the end of this section one more aspect of PCRAM should be mentioned for its importance for the future of this technology. As has already been discussed above, the bit density is extremely important with respect to the competibility of a solid state memory technology for its rather direct connection to the price of the memory. For that reason it is very appealing to store more than one logical bit into a single cell. This idea of "multi-level storage" could be realized in phase change cells by well defined degrees of partial crystallization leading to several distinct levels of resistance. To accomplish this goal it is extremely important to know the crystallization kinetics of phase change materials as well as the electrical and structural relaxation mechanisms, in particular in the amorphous phase. This thesis hence contributes to a better understanding of the underlying physics of both of these topics.

# Chapter 3

## Theory of Glassformation

Das tiefste und erhabenste Gefühl, dessen wir fähig sind, ist das Erlebnis des Mystischen. Aus ihm allein keimt wahre Wissenschaft. Wem dieses Gefühl fremd ist, wer sich nicht mehr wundern und in Ehrfurcht verlieren kann, der ist seelisch bereits tot.

Albert Einstein

### 3.1 Freezing a liquid

Upon cooling, a liquid becomes increasingly rigid against structural rearrangements of its molecules or atoms, respectively. A macroscopic measure for this rigidity is the viscosity  $\eta$ . It is defined as a resistance against deformation by an applied stress  $\tau$ 

$$\tau = \eta \cdot \dot{\gamma} \,, \tag{3.1}$$

wherein the strain rate  $\dot{\gamma}$  represents a deformation. As long as representatives of all possible thermodynamic microstates at a certain temperature can be sampled on the timescale of the experiment, the liquid phase can be regarded as being in *internal equilibrium*. When the structural dynamics is slowed down so much that the respective atomic rearrangements cannot be realized in the chosen time window, the system leaves internal equilibrium and freezes configurationally. The resulting state is called a *glass*.

<sup>&</sup>lt;sup>1</sup>It is not necessary to sample actually all microstates for a system to establish equilibrium. In most known systems this is actually impossible. In a Gedankenexperiment we look at a rather small system of  $N = 10 \cdot 10 \cdot 10 = 10^3$  particles each of which can be in one of two possible states. This system thus could be in  $2^N$  different configurations. As a conservative estimation one may assume that a single change of one particle's state takes place in  $\Delta t = 10^{-17} \, \text{s}$ . The mean time between two configurational changes of the total system is then  $\frac{\Delta t}{N}$ . This would result in a total time of at least  $\tau = 2^N \frac{\Delta t}{N} > 10^{270} \, \text{years}$  for sampling all microstates. Obviously this definition of sampling the microstates is neither meant when writing about configurational freezing nor is it necessary for

#### 3.1. FREEZING A LIQUID

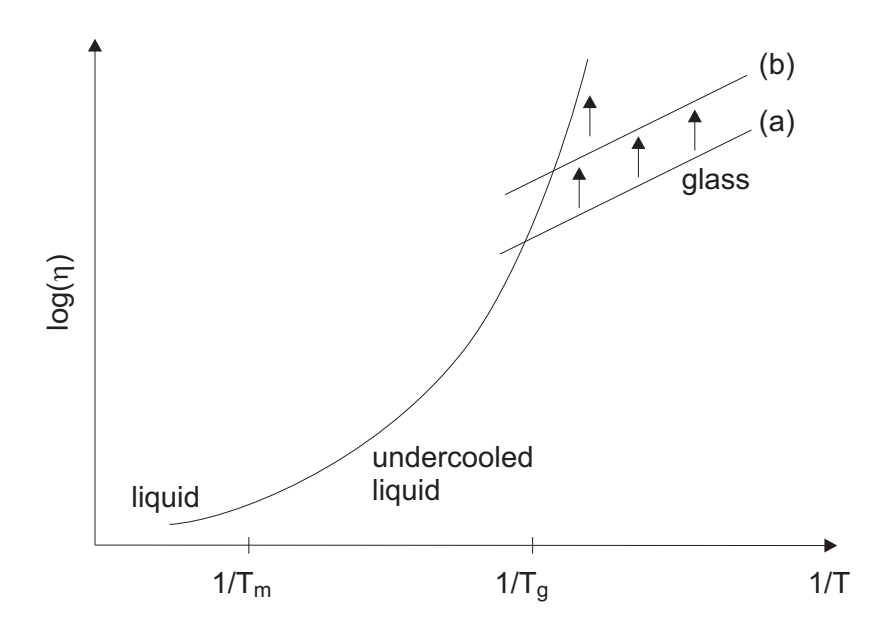


Figure 3.1: Viscosity  $\eta$  in liquids and glasses: Upon cooling down a liquid its viscosity rises continuously, i. e. the resistance against structural rearrangements increases, until at the glass transition temperature  $T_g$  the liquid falls out of internal equilibrium and forms a glass. This process depends on the time scale of the experiment: At slower cooling rates (b) the system remains longer in internal equilibrium than for faster coolings (a). The glass transition temperature is lower for slower cooling rates accordingly. The glass states experience structural relaxation towards the equilibrium curve (indicated by arrows). This relaxation is also hindered by a high viscosity. Thus for any given time scale there will be practically no relaxation observable in a glass after it reached a high enough viscosity.

Accordingly this effect is called *glass transition*. It follows directly from the given definition of the glass transition that the temperature at which it takes place depends on the chosen time window. Thus, e. g. the cooling rate codetermines the glass transition temperature. The slowing down of the structural dynamics in a liquid and its glasses is schematically illustrated in Fig. 3.1. Slower cooling rates give the system more time to maintain internal equilibrium shifting the glass transition to higher viscosities and lower temperatures. Glasses that freeze from different states of the liquid phase because of different cooling rates are distinct in their configuration and their viscosity [60].

As the falling out of internal equilibrium could only be defined with respect to a certain time scale, a glass does not stop to structurally rearrange on a longer time scale. Instead it relaxes towards the equilibrium state for the given temperature. So with respect to structural relaxation glasses are unstable. However, this instability again becomes marginal at any given time scale at high enough viscosities [61].

classifying a system to be in equilibrium. Instead a liquid falling out of equilibrium can be understood in the following way. As the system is cooled, certain correlated motions of the particles occur with less frequency. At the glass transition and below they are so rare that they are not measurable. [58, 59]

Nevertheless, structural relaxation in glasses is observed to have an effect on a physical property as strongly as the latter depends on the atomic configuration. The resulting influence of the thermal history on the properties of a material is thus not only important for their experimental investigation. It also turns out to be particularly problematic in applications that require a physical quantity of a glass to be reproducibly at a constant value <sup>2</sup>. Structural relaxation has been reported to increase the viscosity, for example, in some glasses by several orders of magnitude [61, 62].

Due to its structural rigidity the glass can be regarded as a solid state. Like the liquid phase it originates from, the glass shows no long range order that could be detected e.g. by x-ray diffraction experiments. Solids lacking long range order are called *amorphous*. Besides the quenching of a melt, there are other ways of preparing amorphous solids, such as sputter deposition, thermal evaporation, chemical vapour deposition, gel desiccation, electrolytic deposition, chemical reaction, shock-wave transformation, shear amorphization and others [63].

Expanding Elliott's definition stating that "a glass is an amorphous solid which exhibits a glass transition" [63], in the scope of this work it is sensible to also speak of a glass, when a material could exhibit a glass transition, if crystallization did not forestall a glass transition. This extended definition reverses the prediction of the universality of the glass transition by Cohen and Turnbull [64] postulating that all liquids would go through the glass transition if sufficiently undercooled <sup>3</sup> and provided that crystallization did not occur. The latter condition sensitizes to the fact that crystallization could interfere with the glass transition for some thermal conditions, but not for others. In the same sense an amorphous solid should be called a glass for its potential to undergo a glass transition irrespective of crystallization pre-empting its transition into a liquid phase or not.

## 3.2 Temperature dependence of the viscosity

In glasses the viscosity usually shows an Arrhenius-like temperature dependence [60], i.e. it is proportional to  $\exp(E/k_BT)$ , with an activation energy E, the Boltzmann constant  $k_B$  and the temperature T. Such a dependency can easily be identified as a straight line in a logarithmic plot of the viscosity against the reciprocal temperature (see Fig. 3.1). In the liquid phase a more or less pronounced deviation from an

<sup>&</sup>lt;sup>2</sup>For example in phase change materials especially the temporal drift of the resistivity of the glass is opposed to a successful realization of multi level electronic memory.

<sup>&</sup>lt;sup>3</sup>Undercooling or supercooling of a liquid refers to the realization of a temperature below the melting temperature, without crystallizing the material, although the crystal phase is energetically more favourable than the liquid one.

#### 3.2. TEMPERATURE DEPENDENCE OF THE VISCOSITY

Arrhenius-like behaviour is observed depending on the material. Liquids with approximately Arrhenius behavior are called *strong*. Those materials tend to be of tetrahedral network structure. A typical representative of this group is GeO<sub>2</sub>. Some Zr-rich Zr-Cu alloys, however, also proved to be strong liquids [65]. Liquids that show a pronounced deviation from Arrhenius behavior are called *fragile*. Fragile liquids tend to be more highly coordinated ionic liquids or aromatic hydrocarbons [65]. Interestingly elemental Selenium turns out to be a rather fragile liquid, too [66, 67].

To quantify this deviation from Arrhenius behavior, the kinetic fragility m is most commonly defined as the steepness of the temperature dependence of the viscosity  $\eta(T)$  in the undercooled liquid next to the glass transition temperature  $T_g$  [67]:

$$m = \left. \frac{\partial \log_{10} \eta(T)}{\partial \left( \frac{T_g}{T} \right)} \right|_{T = T_g} . \tag{3.2}$$

Or as Sastry nicely phrased [68]: "Fragility measures the rapidity with which a liquid's properties (such as viscosity) change as the glassy state is approached." Experimentally determined fragilities have been reported to range from around m = 20 (for  $\text{GeO}_2$ ) up to m = 145 (for cis-/trans-decalin) [67].

Over the years various equations have been proposed for a mathematical description of the temperature dependence of the viscosity in undercooled liquids [65]. While many of them are limited to a specific group of materials, the Vogel-Fulcher-Tammann equation has been generally applied to all types of materials:

$$\eta(T) = \eta_0 \cdot \exp\left(\frac{DT_{FV}}{T - T_{FV}}\right) \qquad (T > T_{FV}), \qquad (3.3)$$

where  $\eta_0$ , D, and  $T_{FV} < T_g$  are constants.

This equation is the most frequently applied one, particularly when the use of its equivalent, the Williams-Landel-Ferry equation, is taken into account [70]. The latter equation is applied to polymer liquids and rubbers concentrating on the term including the temperature dependence and therefore eliminating the pre-exponential term of Eq. 3.3. Like several of the other equations, the Vogel-Fulcher-Tammann equation is provocative because of its implication that a singularity exists for a non-zero temperature  $T_{FV}$ , where relaxation times diverge. This distinctive feature will be discussed from a thermodynamic point of view later in the context of the Kauzmann paradoxon.

The Vogel-Fulcher-Tammann equation shows best agreement with experimental data for liquids that show only small deviations from Arrhenius behavior, which include most of the common liquids of the geochemical and technological world. For most of

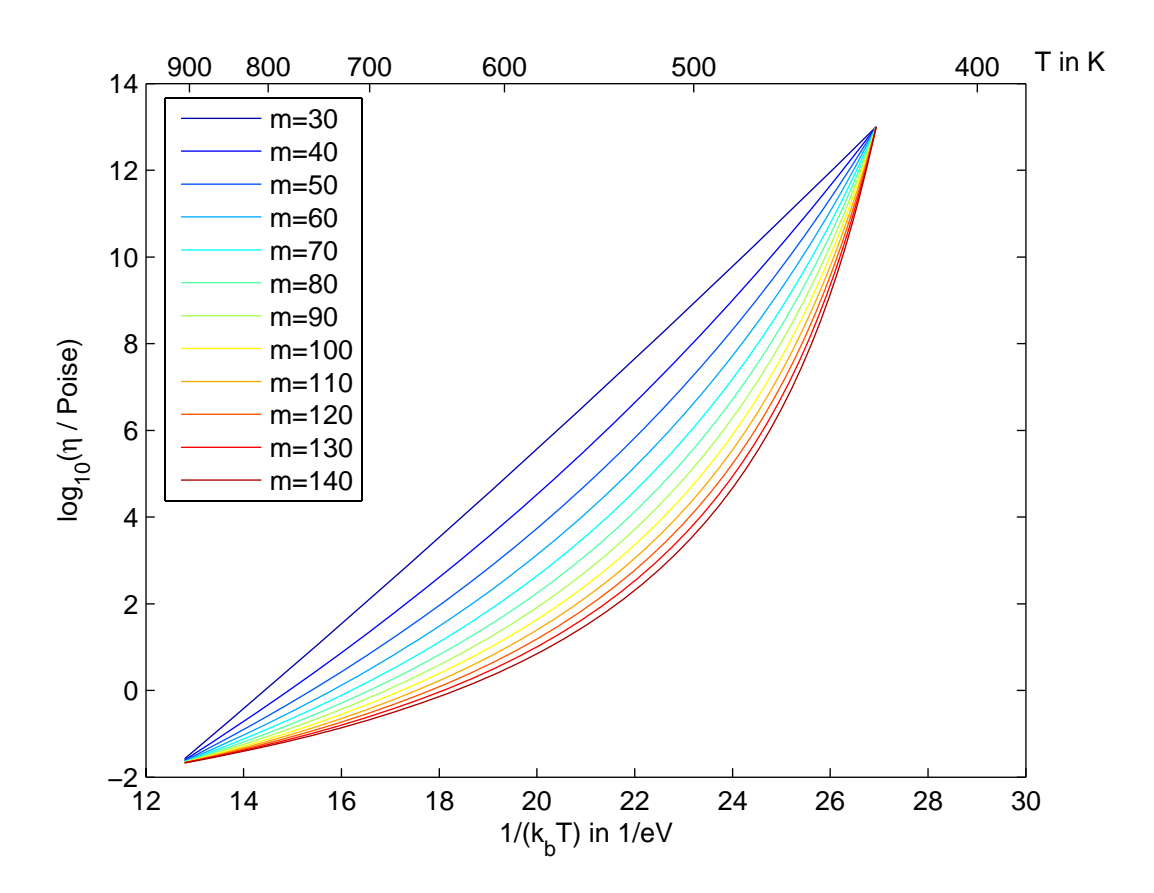


Figure 3.2: To illustrate the temperature dependence of the viscosity for varying fragility m, the following parameters have been used to apply the Vogel-Fulcher-Tammann equation, Eq. (3.3):  $\eta(T_m = 916 \text{ K}) = 10^{-2} \text{ poise} = 10^{-3} \text{ Pa s}$  and  $\eta(T_g = 428 \text{ K}) = 10^{13} \text{ poise} = 10^{12} \text{ Pa s}$ , which is commonly used for the viscosity at the glass transition temperature  $T_g$ .  $T_g$  and the melting temperature  $T_m$  are experimental values for  $\text{Ge}_2\text{Sb}_2\text{Te}_5$ , a typical phase change material, taken from [69]. The fragility m is used according to the definition in Eq. (3.2).

#### 3.3. THERMODYNAMICS

the more fragile molecular liquids the equation is not capable of following the experimental data over the complete temperature range. Besides, neither does any other simple three-parameter equation. In those materials systematic deviations are found with a tendency to smaller curvature both near the glass transition temperature and at high temperatures, compensated for by an excess curvature in between. In most cases, however, the equation has only been applied to data covering some two to four orders of magnitude in viscosity, where it usually performs well. [65]

For an illustration of how the temperature dependence of viscosity in the undercooled liquid of a phase change material looks like, assuming that it follows the Vogel-Fulcher-Tammann equation, Eq. 3.3, Fig. 3.2 plots the relation for a wide range of hypothetical fragilities.

## 3.3 Thermodynamics

One would expect intuitively that entropy has to play a role in the glass transition, since disordered systems are considered. In section 3.1 the glass transition was described as the freezing of a liquid, meaning that a system cannot realize representatives of all microstates that correspond to the internal thermodynamic equilibrium of the liquid phase in a given time.

Adam and Gibbs [71] identified the decrease in the number of configurations that the system is able to sample as the origin of viscous slow-down in the liquid close to the glass transition temperature. Their concept is based on the assumption that temperature-dependent relaxation times in the dynamics of liquids are determined by the probabilities of cooperative rearrangements. To evaluate these transition probabilities, cooperatively rearranging regions are defined as subsystems which, upon a sufficient fluctuation in energy, can rearrange into another configuration independently of its environment. It turns out in their derivation of the average transition probability that the overwhelming majority of transitions are undergone by regions whose size differs negligibly from the smallest size that permits a transition at all. This is due to the fact that the transition of these smallest cooperative regions involve the smallest number of monomer units surmounting, essentially simultaneously, the individual activation barriers restricting their arrangement. This minimal size of cooperatively rearranging regions in turn is derived to be inversely proportional to the molar configurational entropy of the macroscopic sample. This results in the quantities describing relaxation, like the viscosity  $\eta$ , to depend on the system's configurational entropy  $S_c$ in the following way:

$$\eta(T) = A \cdot \exp \frac{B}{TS_c(T)}, \qquad (3.4)$$

where A is a constant. The parameter B is proportional to the energy barrier per molecular segment and the critical configurational entropy necessary for the cooperative region to move. It is therefore dependent on the type and strength of bonding in the system. The departure from Arrhenius behavior, however, comes from the temperature dependence of  $S_c$ .

A few years after Adam and Gibbs contributed the above ideas to the field, another approach to the topic of glass transition was brought forward in the work of Goldstein [72]: an *energy landscape* model. Independently from how much one estimates its potential to lead to quantitative statements about or the revealing of new insight into the physics of the glass formation in view of the large interest in the model's application in recent years [73, 74, 75, 68, 76, 77, 78, 79], the energy landscape concept is undoubtedly helplful in order to form a better understanding of the thermodynamics of undercooled liquids and glasses.

Goldstein's model is based on the idea that the limitation of configurational rearrangement is dominated by potential energy barriers and how they compare to thermal energies. Therefore he examined a potential energy hypersurface as a function of the 3N atomic coordinates in a 3N+1 dimensional space. The state of a system is represented by a point moving on the hypersurface with a 3N dimensional velocity whose average value is temperature dependent. The fact that glasses are solids implies that their atomic or molecular arrangement can be described by a point near the bottom of a local minimum in potential energy. Otherwise the system would continuously flow, which it does not at low enough temperatures. However, at elevated temperatures near the glass transition structural relaxation occurs implying the existence of more than one mechanically stable minimum. The observation that annealing proceeds more slowly the lower the applied temperature suggests that finding deeper minima becomes statistically more difficult as the temperature is decreased. This leads to a perception of a series of minima on a complex landscape where increasing depth coincides with a decreasing population of minima. [80]

The representation of such an energy landscape as given in Fig. 3.3 is of course a drastic oversimplification of a 3N dimensional hypersurface. Nevertheless, it seems legitimate to plot it in this way for the purpose of visualizing the concept. The individual minima on the potential energy hypersurface are the configurational microstates of the system. The configurational entropy is then related to the number of minima accessible at a given temperature, irrespective of whether the system can actually sample them all in given time. Thus a glass being confined to a single minimum still has

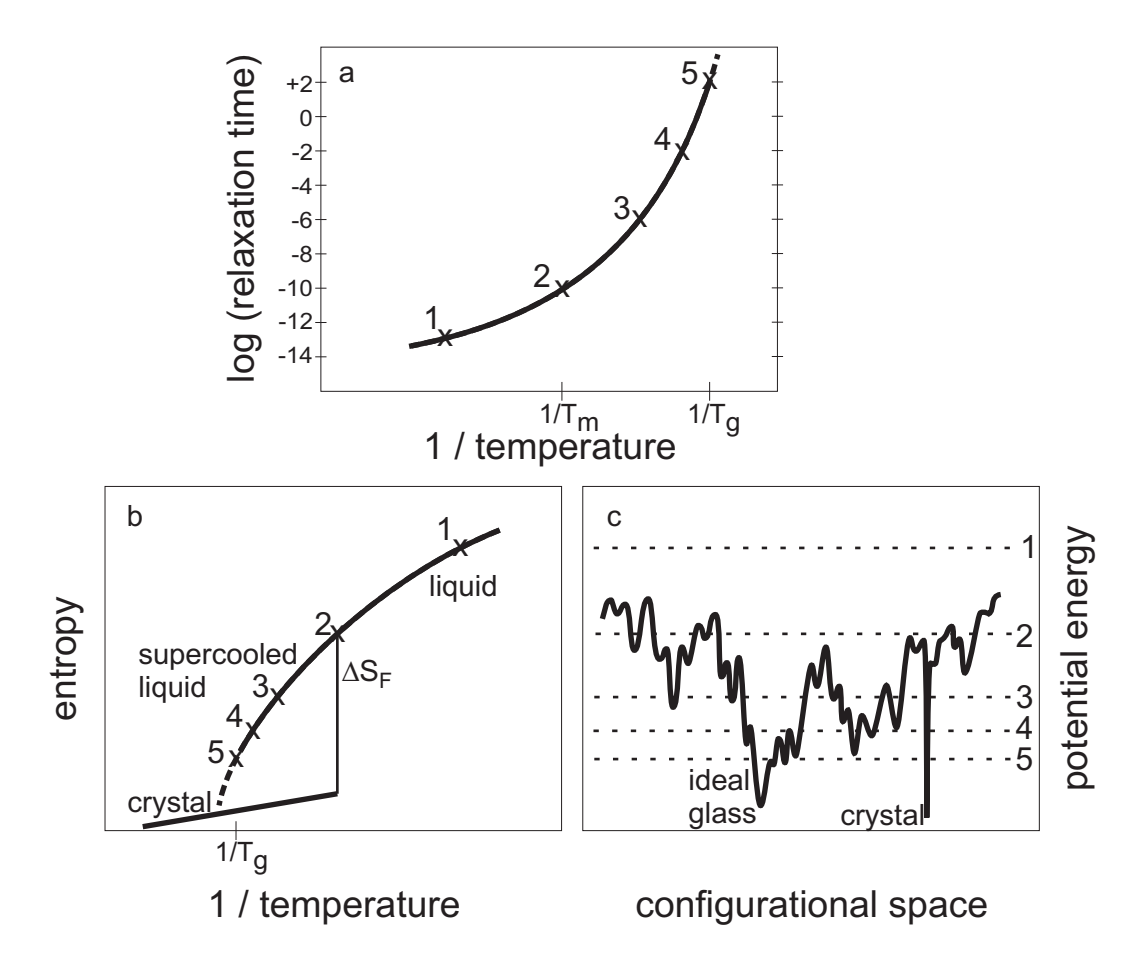


Figure 3.3: Illustration of the relation between relaxation time, entropy, and the potential energy hypersurface. At high temperatures, higher than the melting temperature, (1) structural dynamics of the liquid is unperturbed by any barriers to cross in order to establish new configurations. Around the melting temperature  $T_m$  (2) the energy landscape begins to influence the system. The liquid becomes increasingly rigid as the temperature T approaches the glass transition temperature  $T_g$ . With little excess entropy (much less than the entropy of fusion  $\Delta S_F$  at  $T_m$ ) remaining, the system falls out of equilibrium (5), becoming trapped in a single minimum. This transition into a glass state is accompanied by a rapid increase of the system's relaxation time beyond the experimental timescale. [80]

a residual entropy in excess of the perfect crystal. In equilibrium a system can visit a representative subset of the minima. [80]

In the framework of the energy landscape model the idea of Adam and Gibbs on the cooperative rearrangements can be rephrased as follows: There are two reasons for relaxations taking place more slowly at lower temperatures. Firstly, energy barriers have to be crossed in order to bring the system from one minimum to another. At lower available thermal energy it takes longer before some fluctuation of collective vibrations of the system is large enough to surmount the energy barrier. Secondly, entropic barriers have to be overcome: Lower energy minima are more distantly spaced. Thus the extent of collective rearrangements necessary to move from one low energy minimum to another increases.

While the connection between the mechanical and the thermodynamic properties of liquids and glasses has so far been built in a rather qualitative way, in the following this correlation will be manifested also more quantitatively: The Adam-Gibbs equation, Eq. (3.4), includes the configurational entropy  $S_c$  which itself is connected to the configurational heat capacity  $C_{p,conf}$  of the liquid by

$$C_{p,conf}(T) = T \left(\frac{\partial S_c(T)}{\partial T}\right)_p$$
 (3.5)

For a calculation of  $S_c$  in the liquid one could use the crystal as a reference point defined as a state with zero configurational entropy.

$$S_c(T) - S_c(T_K) \cong \int_{T_K}^{T} \frac{\Delta C_{p,lc}(T')}{T'} dT', \qquad (3.6)$$

wherein  $\Delta C_{p,lc}$  is the difference in specific heat between the liquid and the crystal.  $T_K$  is the Kauzmann temperature, defined as the temperature, where the entropy of the undercooled liquid equals the entropy of the crystalline phase [81].  $T_K$  has often been described as a lower boundary for the glass transition to take place, because otherwise the system would run into a violation of the third law of thermodynamics, stating that the entropy of a crystal vanishes at 0 K. It has also often been claimed that a liquid that is cooled infinitely slowly would have to turn into the *ideal glass* at the Kauzmann temperature, ideal for its configurational entropy being zero [82]. This view, however, neglects the fact that configurational entropy is not the only source of the total entropy of a system. There are also vibrational contributions to the entropy [66]. The latter are non-zero for all phases, even the crystalline ones, at non-zero temperatures. This is the reason why Stillinger et al. have been able to demonstrate in their work titled "The Kauzmann Paradox Revisited" [83] that a Kauzmann point can indeed occur without a third-law conflict arising, though not for all materials. The same

#### 3.3. THERMODYNAMICS

work also highlights the difference between the realization of a Kauzmann point and the ideal glass transition by clearly stating that no support was found for the latter effect. An undercooled liquid might have the same total entropy as the crystal phase at the same temperature without a vanishing configurational entropy. Nevertheless, this inaccurateness of Eq. (3.6) regarding the vibrational contributions to the entropy is frequently accepted setting  $S_c(T_K) = 0$  as a reasonable approximation:

$$S_c(T) \cong \int_{T_K}^T \frac{\Delta C_{p,lc}(T')}{T'} dT'.$$
(3.7)

While Adam and Gibbs themselves estimated  $\Delta C_{p,lc}$  to be constant in temperature, yielding a Vogel-Fulcher-Tammann equation only as an approximation valid near  $T_K$  [71], a more accurate assumption for the excess heat capacity might be [80]

$$\Delta C_{p,lc}(T) = \frac{K}{T}, \qquad (3.8)$$

with K being a constant. Substituting this into eq. 3.7 yields [84, 85]:

$$S_c(T) \cong K \int_{T_K}^{T} \frac{1}{(T')^2} dT'$$

$$= K \left(\frac{1}{T_K} - \frac{1}{T}\right). \tag{3.9}$$

The lower line of Eq. (3.9) into Eq. (3.4) leads to

$$\eta(T) = A \cdot \exp \frac{BT_K}{K(T - T_K)}, \qquad (3.10)$$

which coincides with the Vogel-Fulcher-Tammann equation, Eq. (3.3), if  $T_{FV} = T_K$ . Tanaka [85] compared values for  $T_{FV}$ , that have been determined by fitting experimental data for kinetic quantities, like relaxation times or viscosity, with values for  $T_K$  determined from thermodynamic experiments on a liquid's entropy. Surveying various materials he found a rather good agreement with  $T_{FV} = T_K$  for fragile glasses, while for strong glasses there were clear deviations from the equality.

The close relationship between kinetic quantities on the one hand and entropy on the other is also underlined by the comparison of the temperature dependence of these properties in the undercooled liquid phase: Martinez and Angell [66] compared the kinetic fragility, defined similar to Eq. (3.2), with a thermodynamic definition of fragility that is based on the temperature dependence of the liquid's excess of entropy over that of the crystal normalized to the excess entropy at the glass transition temperature. Although there were some exceptions, the correlation between kinetic and thermodynamic fragility became evident in this study for a wide variety of materials.

# Chapter 4

# Theory of Crystallization

Felix qui potuit rerum cognoscere causas.

Virgil

## 4.1 The driving force

In the preceding chapter the solidification of a liquid into a glass has been described. Although for a deeper understanding of the thermodynamics it seemed useful to refer to a crystalline phase at some points, e. g. to illuminate the Kauzmann paradox, in principle the dynamic processes in the liquid and glass phase can be and have been treated rather independently from the existence of crystalline phases. Since the solidification into a glass has been found to originate from a freezing of configurational dynamics, the models for the description of these processes focused on the probability of structural rearrangements. Therefore treating the case of a system arranging in crystalline order to be rather unlikely in view of the multitude of non-crystalline configurations appeared legitimate, especially as the resulting formulas agree nicely with experimental evidence for relaxation times or viscosity.

While a model explaining the hindrance of configurational rearrangement should be sufficient for the understanding of good glassformers, which are in some cases practically impossible to crystallize, the paradigm obviously has to be extended for liquids that show a strong tendency to crystallize. In these materials the configurational fluctuations are not small and rare enough to prevent the system from reaching at least locally crystalline phases. The latter is also often neglected in discussions of the energy landscape model: There is not only one deep absolute minimum of "the" crystalline phase. Instead clusters with crystalline order inside a surrounding liquid are forming pathways towards a completely crystalline phase<sup>1</sup>.

<sup>&</sup>lt;sup>1</sup>Even this term, "completely crystalline phase", could be slightly misleading. It does not take

#### 4.1. THE DRIVING FORCE

Once a large enough subset of particles is arranged in this state, it is unlikely that it will resolve again, as the necessary energetic fluctutations for leaving the according minimum in the energy landscape would be rather high. How much energy actually is needed for this depends on how energetically favourable the crystalline configuration of particles is compared to a more disordered assembly. The latter can be regarded as the "driving force" for crystallization.

A 'fundamentalist' might object that the one and only "driving force" of a system towards its equilibrium state is the maximization of the entropy. Why should a system ever turn irreversibly into a highly ordered crystal then? This argument overlooks, however, two important facts. The first is, that configurational disorder is not the only source of entropy. A system thus could add order of one apparent type, e.g. realize crystalline configuration, while compensating for this by increasing disorder of another type, e.g. vibrational entropy, and still fulfill the second law of thermodynamics [86]. The second important fact is, that in most experiments and especially applications we do not even nearly deal with isolated systems. Much more realistic is the assumption of a subsystem that can exchange heat and volume with its surrounding, which acts as a bath defining both temperature and pressure of the subsystem. The maximization of the entropy of the whole system is then fulfilled for the subsystem minimizing its Gibbs free energy G:

$$G = U + pV - TS = H - TS, (4.1)$$

with internal energy U, pressure p, volume V, temperature T, entropy S and enthalpy H. So the driving force towards crystallization must be described by the difference in Gibbs free energy of the liquid phase  $G_l$  and the crystalline one  $G_c$ :

$$\Delta G_{lc}(T) \equiv G_l - G_c = H_l - H_c - T(S_l - S_c) \equiv \Delta H_{lc}(T) - T\Delta S_{lc}(T). \tag{4.2}$$

As enthalpy H, entropy S and heat capacity at constant pressure  $C_p$  are related by

$$dH = C_p dT, (4.3)$$

$$dS = C_p \frac{dT}{T}. (4.4)$$

the difference in enthalpy  $\Delta H_{lc}$  and the difference in entropy  $\Delta S_{lc}$  between liquid and the crystal can be expressed by

$$\Delta H_{lc}(T) = H_l(T) - H_c(T) = \Delta H_f + \int_{T_m}^T \Delta C_{p,lc}(T') dT'$$
(4.5)

poly-crystallinity into account. The term "completely crystalline" should also be valid for these cases, but then a "completely crystalline" configuration is surely not unique, again implying the existence of many crystalline configurations on the energy landscape.

and

$$\Delta S_{lc}(T) = S_l(T) - S_c(T) = \Delta S_f + \int_{T_m}^{T} \frac{\Delta C_{p,lc}(T')}{T'} dT'.$$

$$(4.6)$$

using  $\Delta C_{p,lc} = C_{p,l} - C_{p,c}$  as the difference in heat capacity between liquid and crystal state.  $\Delta H_f = \Delta H_{lc}(T_m)$  is called heat of fusion and  $\Delta S_f = \Delta S_{lc}(T_m)$  entropy of fusion. At the melting temperature  $T_m$  the liquid and the crystal phase are in equilibrium, thus

$$\Delta G_{lc}(T_m) = 0. (4.7)$$

With Eq. (4.1) this leads to a relation between  $\Delta H_f$  and  $\Delta S_f$ :

$$T_m \Delta S_f = \Delta H_f \,. \tag{4.8}$$

Substituting Eq. (4.5), Eq. (4.6) and Eq. (4.8) into Eq. (4.2) yields

$$\Delta G_{lc}(T) = \Delta H_{lc}(T) - T\Delta S_{lc}(T)$$

$$= \Delta H_f + \int_{T_m}^T \Delta C_{p,lc}(T') dT' - T\Delta S_f - T \int_{T_m}^T \frac{\Delta C_{p,lc}(T')}{T'} dT'$$

$$= \Delta H_f \left(1 - \frac{T}{T_m}\right) + \int_{T_m}^T \Delta C_{p,lc}(T') dT' - T \int_{T_m}^T \frac{\Delta C_{p,lc}(T')}{T'} dT'$$

$$= \frac{\Delta H_f (T_m - T)}{T_m} + \int_{T_m}^T \Delta C_{p,lc}(T') dT' - T \int_{T_m}^T \frac{\Delta C_{p,lc}(T')}{T'} dT'. \quad (4.9)$$

Figure 4.1 plots qualitatively the Gibbs free energy G(T) for the various phases. Resulting from the above derivation, given the melting temperature  $T_m$  and the heat of fusion  $\Delta H_f$ , the exact temperature dependence of the change in Gibbs free energy upon crystallization  $\Delta G_{lc}(T)$  can be calculated using Eq. (4.9), if the heat capacities of the liquid and the crystal phase, and therewith  $\Delta C_{p,lc}(T)$ , are known as a function of temperature.

Heat capacities can in principle be determined experimentally by calorimetric measurements, like temperature modulated differential scanning calorimetry [87, 88, 89]. For materials with a strong tendency to crystallize, however, the undercooled liquid phase cannot be established for a period of time that would be long enough for a measurement of its heat capacity. To still calculate  $\Delta G_{lc}(T)$  despite the lack of direct experimental information about  $C_{p,l}(T)$ , one has to find reasonable estimations for the temperature dependence of  $\Delta G_{lc}(T)$  [90]. For cases in which incomplete or even no data are available for  $C_{p,l}(T)$ , different approximations for  $\Delta G_{lc}(T)$  have been proposed in the past.

#### 4.1. THE DRIVING FORCE

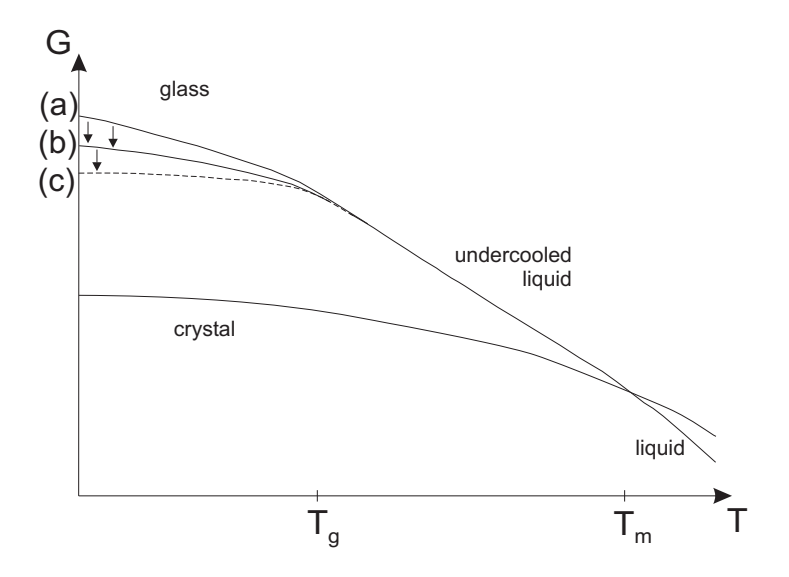


Figure 4.1: Gibbs free energy G as a function of temperature for the crystalline, liquid and amorphous phase: Above  $T_m$  the liquid is the most favourable phase, while below the crystal is energetically preferred. Cooling the liquid beyond  $T_g$  leads to the formation of a glass. For fast cooling (a) the glass transition takes place earlier, i. e. at higher temperatures, and results in a configuration that is energetically less favourable than glasses prepared by slower cooling rates (b). Curve (c) indicates the hypothetical glass prepared by infinitely slow cooling. Structural relaxation of the glasses (indicated by arrows) reduce their Gibbs free energy. The driving force for crystallization  $\Delta G_{lc}(T)$  rises with increased undercooling of the liquid.

The simplest assumption that can be made is  $\Delta C_{p,lc} = 0$  over the whole temperature range of the undercooled liquid. Application of this assumption to Eq. (4.9) leads to

$$\Delta G_{lc}(T) = \frac{\Delta H_f \left( T_m - T \right)}{T_m} \,, \tag{4.10}$$

the oldest linear approximation of  $\Delta G_{lc}(T)$ , used for example by Turnbull [91]. While  $\Delta C_{p,lc} = 0$  is a bad estimation for polymers, it is reasonable for metals, as  $\Delta C_{p,lc}/C_{p,c}$  is small [90].

With the goal to improve the above approximation Hoffman proposed another one [92], which assumes  $\Delta C_{p,lc}$  still to be constant as a function of temperature, though this time not zero, and  $\Delta H_{lc}$  to vanish at a temperature  $T_{\infty}$ , slightly below the glass transition temperature. For this case Eq. (4.5) yields

$$\Delta H_{lc}(T_{\infty}) = \Delta H_f + \int_{T_m}^{T_{\infty}} \Delta C_{p,lc}(T') dT'$$

$$0 = \Delta H_f + (T_{\infty} - T_m) \Delta C_{p,lc}$$
(4.11)

Substituting  $\Delta C_{p,lc}$  in Eq. (4.9) by  $\Delta H_f/(T_m - T_\infty)$  Hoffman argues that all terms in the formula for  $\Delta G_{lc}(T)$  can be neglected except for the following:

$$\Delta G_{lc}(T) = \frac{\Delta H_f (T_m - T)}{T_m} \left(\frac{T}{T_m}\right). \tag{4.12}$$

Thompson and Spaepen [90] have shown that Hoffman's approximation is not valid for a set of metals by calculating  $T_{\infty}$  from measured values of  $T_m$  and of  $\Delta C_{p,lc}$  at  $T_m$  using Eq. (4.11) and finding that the assumption  $T_{\infty} \cong T_g$  is clearly violated for these cases. For materials with a large  $\Delta C_{p,lc}(T_m)$  this contradiction does not occur and indeed for organic substances Hoffman's approximation seems adequate [90].

As a reaction to these limitations of Hoffman's approach, in the same work [90] Thompson and Spaepen proposed a new approximation for  $\Delta G_{lc}(T)$  themselves. They keep the idea of a constant  $\Delta C_{p,lc}$ . As a consequence of a small value for  $\Delta C_{p,lc}$  at  $T_m$ , as they found it to be the case for metals, they concluded that  $\Delta H_{lc}$  changes only slowly with temperature (see Eq. (4.5)) and can thus not become small compared to  $H_f$  around the glass transition temperature. So in contrast to Hoffman they do not assume  $\Delta H_{lc}$  but instead  $\Delta S_{lc}$  to vanish near  $T_g$ , or to be more precisely at the Kauzmann temperature  $T_K$ .

From Eq. (4.6) then follows

$$\Delta S_{lc}(T_K) = \Delta S_f + \int_{T_m}^{T_K} \frac{\Delta C_{p,lc}}{T'} dT'$$

$$0 = \frac{\Delta H_f}{T_m} + \Delta C_{p,lc} \ln \left(\frac{T_K}{T_m}\right). \tag{4.13}$$

Substituting

$$\Delta C_{p,lc} = \alpha \frac{\Delta H_f}{T_m} \tag{4.14}$$

with

$$\alpha = \frac{1}{\ln \frac{T_m}{T_K}} \tag{4.15}$$

into Eq. (4.9) yields

$$\Delta G_{lc}(T) = \frac{\Delta H_f \Delta T}{T_m} \cdot \left( \frac{(1-\alpha)T_m + (1+\alpha)T}{T_m + T} \right). \tag{4.16}$$

For a ratio of  $T_K/T_m$  near  $1/e \cong 0.37$  the parameter  $\alpha$  is approximately 1. In that case  $\Delta C_{p,lc} \cong \frac{\Delta H_f}{T_m}$  and Eq. (4.16) simplifies to

$$\Delta G_{lc}(T) = \frac{\Delta H_f \Delta T}{T_m} \cdot \left(\frac{2T}{T_m + T}\right). \tag{4.17}$$

From the observation of the ratio  $T_g/T_m \cong 1/2$  for typical metallic glass formers Thompson and Spaepen concluded that, if no other experimental evidence is available, Eq. (4.17) is a good approximation for metals.

Fig. 4.2 compares the temperature dependencies of  $\Delta G_{lc}$  resulting from the three approximations mentioned above, i. e. Eqs. (4.10), (4.12) and (4.17). The respective calculations are based on experimentally determined values for the heat of fusion  $\Delta H_f$  and the melting temperature  $T_m$  for  $\text{Ge}_2\text{Sb}_2\text{Te}_5$ , a typical phase change material. All three approximations reflect the continously increasing driving force for crystallization upon cooling. However, at temperatures around half of  $T_m$  the values for  $\Delta G_{lc}$  differ by a factor of two depending on the used model. This can be expected to make a significant difference for physical quantities that depend exponentially on  $\Delta G_{lc}$ .

Nevertheless, Eqs. (4.10), (4.12) and (4.17) are valuable tools for an extrapolation of the driving force of crystallization in cases like phase change materials, in which an experimental investigation of the undercooled liquid phase is largely prevented by the interference of crystallization. The required values for melting temperature and heat of fusion do not form a serious obstacle, as they are usually determined very easily by calorimetric measurements.

## 4.2 Crystal nucleation

In the preceding section 4.1 the Gibbs free energy has been identified to favour a crystalline structure against a disordered one at temperatures below the melting point. How this preference prevents the dissolution of afore stochastically generated local crystalline configurations and thus leads gradually towards permanent crystallinity of

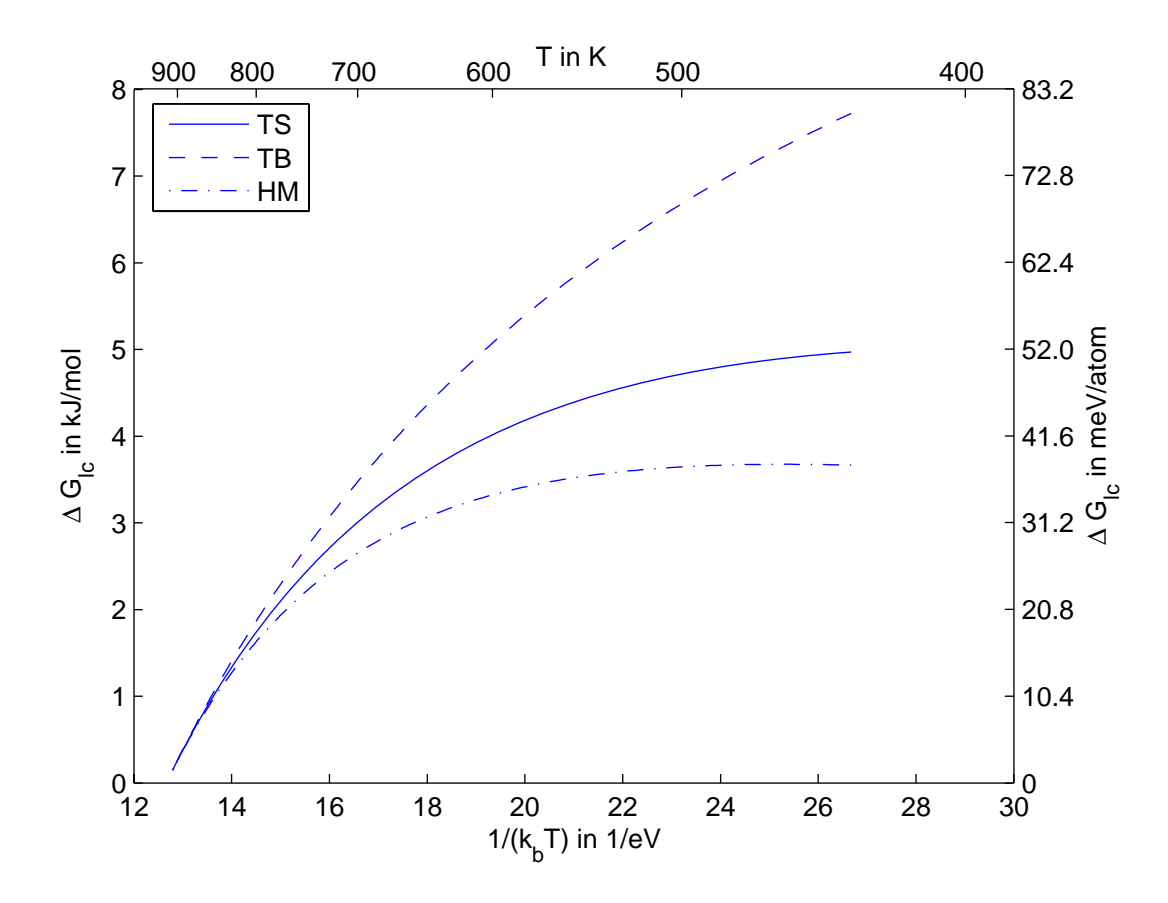


Figure 4.2: Approximations for the difference in Gibbs free energy between liquid and crystal: The curves are calculated using the approximation by Turnbull (Eq. (4.10), TB, dashed), by Hoffman (Eq. (4.12), HM, dot-dashed) and by Thompson and Spaepen (Eq. (4.17), TS, solid) respectively. The values used for the heat of fusion  $\Delta H_f = 14.7 \,\mathrm{kJ/mol}$  and the melting temperature  $T_m = 916.3 \,\mathrm{K}$  are experimentally determined values [69] for Ge<sub>2</sub>Sb<sub>2</sub>Te<sub>5</sub>, a typical phase change material.

#### 4.2. CRYSTAL NUCLEATION

a whole system has been elucidated only in a qualitative way at the beginning of this chapter (Ch. 4). A much more detailed and quantitative examination of the formation of stable crystalline clusters in a disordered surrounding, also referred to as *nucleation*, will follow now, leaving the treatment of the further progression of crystallization, the *growth* of stable crystalline regions, for the following section 4.3.

As it would certainly go far beyond the scope of this work to provide a review of all approaches to a physical description of nucleation that have been brought forward over the last century, a reasonable selection has become necessary. So the explanations in this text will largely concentrate on what is commonly called the *classical theory of nucleation* successively developed by Gibbs, Volmer, Weber, Becker, Döring, Turnbull and Fisher [93, 94, 95], not only because it proved to be capable of correctly describing various physical phenomena in the context of nucleation, but also since it has been and still is widely used for the interpretation of experimental data. This limitation to one approach shall in turn be legitimated both by highlighting and discussing the assumptions made in the framework of classical theory and by the amendment of a section (sec. 4.4) referring to alternative concepts for nucleation.

### 4.2.1 Basic classical nucleation theory

The essential driving force for crystallization is the difference in Gibbs free energy between the liquid and the crystalline phase  $\Delta G_{lc}$ , but the formation of small crystalline clusters implies an increase of free energy at first. This is due to the considerable fraction of atoms in these clusters being situated in transition regions between the two phases, where they have an environment neither characteristic of the crystalline nor the liquid in bulk. The frustration of these atoms is usually treated by the definition of an interface free energy ascribed to the interface region, while  $\Delta G_{lc}$  is assigned as a volume free energy. For sufficiently small clusters the surface term is dominant making them energetically less favourable than a homogeneously disordered phase.

A typical quantification of this paradigm expresses the Gibbs free energy difference due to the formation of a cluster containing n atoms  $\Delta G_{\text{cluster},n}$  as

$$\Delta G_{\text{cluster},n} = -n \cdot \Delta G_{lc,atom} + o \cdot n^{2/3} \cdot \sigma, \qquad (4.18)$$

wherein  $\Delta G_{lc,atom}$  is the Gibbs free energy difference between liquid and solid phase per atom,  $\sigma > 0$  is the interfacial energy per unit area and o is a shape factor making  $o \cdot n^{2/3}$  the surface area of a cluster. This formula already implies some extremely fundamental assumptions: It states that the cluster energy is the same for all clusters containing the same number of atoms. The shape factor o is only intended to take into account cluster shapes differing from one material to another, but not to vary for

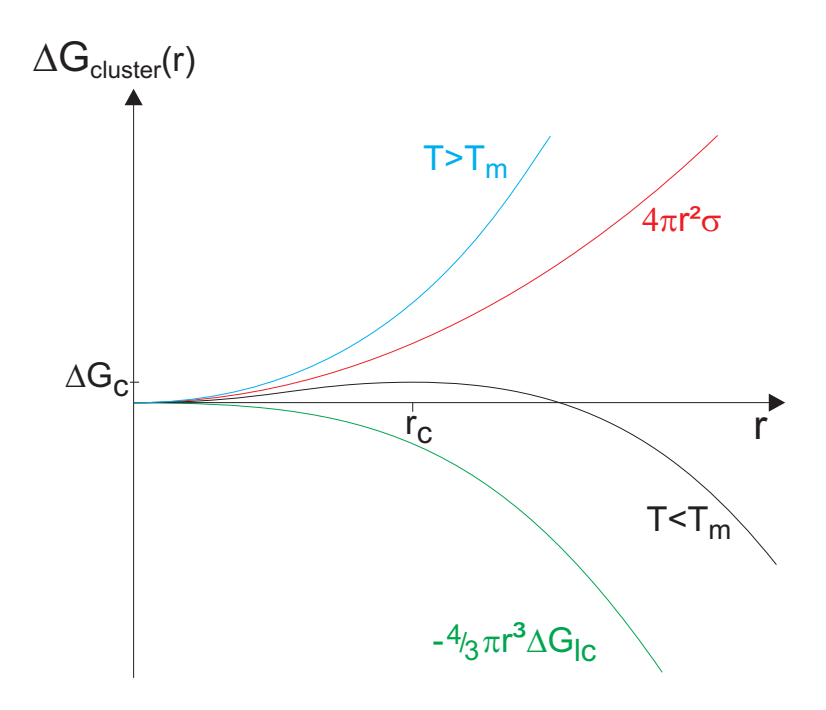


Figure 4.3: Gibbs free energy  $\Delta G_{cluster}(r)$  for the formation of a crystalline clusters of radius r in a liquid. Above the melting temperature the formation of a crystalline cluster of any size is energetically unfavourable. Moreover, the larger the cluster the more unfavourable is its formation. In contrast, below the melting temperature, i. e. in the undercooled liquid, on average clusters smaller than the critical size  $r_c$  decay, while those larger than  $r_c$  grow.

the clusters of one system. In addition, Eq. (4.18) assumes the interface between the cluster and the initial phase to be sharp. While both is surely not the case for very small clusters, made only of a couple of atoms, it can also be challenged how well this describes the reality for larger clusters. Further, a lack of isotropy of the interface free energy might lead to polyhedral nuclei, which would demand a term in the change of Gibbs free energy, Eq. (4.18), proportional to  $n^{1/3}$  representing an "edge free energy". Besides all that in solids elastic strain energy due to density changes upon the phase transition should have an influence on the driving force too. The latter effect, however, could be neglected for nucleation in a surrounding of rather low viscosity which can rapidly release the occurring stresses by flow.

If one is still willing to accept the approach in Eq. (4.18) and claim implicitly the interfacial energy's independency from the cluster size, then in principle this quantity could be determined from macroscopic measurements. Since such experiments are extremely difficult, in the application of the classical nucleation theory  $\sigma$  usually acts as a fitting parameter.

Under the additional approximation of the shape of the clusters being spherical the Gibbs free energy difference  $\Delta G_{\text{cluster}}$  can be expressed as a continuous function of the cluster radius r, which is otherwise equivalent to a discrete formulation using the

number of atoms n:

$$\Delta G_{\text{cluster}}(r) = -\frac{4}{3}\pi r^3 \cdot \Delta G_{lc} + 4\pi r^2 \cdot \sigma. \tag{4.19}$$

 $\Delta G_{lc}$  is the free energy difference between the liquid and the crystalline phase per volume. According to the discussion in the previous section it is negative above the melting temperature and positive below (Fig. 4.1 and 4.2). Together with the interfacial energy being always positive this leads to a size dependence of  $\Delta G_{cluster}$  as plotted qualitatively in Fig. 4.3.

Above the melting temperature,  $\Delta G_{\rm cluster}(r)$  is a monotonously increasing function, which is always positive. This indicates that in this temperature regime the formation of crystalline configurations is always energetically unfavourable and can thus only occur as temporal fluctuations of the equilibrium, but cannot persist. Below the melting temperature in contrast  $\Delta G_{\rm cluster}(r)$  shows a maximum as a consequence of the dominance of the interfacial energy for small clusters and the dominance of the contribution from the volume for large ones. From

$$\frac{\partial \Delta G_{\text{cluster}}(r)}{\partial r}\bigg|_{r_c} = 0 \tag{4.20}$$

the position of the maximum, the so-called *critical radius*  $r_c$ , can be derived:

$$r_c = \frac{2\sigma}{\Delta G_{lc}},\tag{4.21}$$

The corresponding critical Gibbs free energy equals

$$\Delta G_c := \Delta G_{\text{cluster}}(r_c) = \frac{16\pi}{3} \frac{\sigma^3}{(\Delta G_{lc})^2}.$$
 (4.22)

If such a cluster of critical size has formed, its decay is not the only possibility that is energetically favourable for the system, but a further growth of the cluster would also reduce the system's Gibbs free energy.

In classical nucleation theory it is assumed that a cluster evolves in a sequence of bimolecular reactions rather than by a sudden large fluctuation. Moreover, as reactions of a cluster  $C_n$  containing n atoms solely additions and subtractions of monomers  $C_1$  are allowed:

$$C_{n-1} + C_1 \stackrel{k_{n-1}^+}{\rightleftharpoons} C_n,$$

$$k_n^-$$

$$C_n + C_1 \stackrel{k_n^+}{\rightleftharpoons} C_{n+1}. \tag{4.23}$$

Here  $k_n^+$  is the rate of monomer addition to a cluster of size n,  $k_n^-$  the rate of the corresponding loss. Generally the corresponding time-dependent cluster density  $N_{n,t}$  is determined by solving a system of coupled differential equations:

$$\frac{\mathrm{d}N_{n,t}}{\mathrm{d}t} = N_{n-1,t}k_{n-1}^{+} - \left[N_{n,t}k_{n}^{-} + N_{n,t}k_{n}^{+}\right] + N_{n+1,t}k_{n+1}^{-}.$$
(4.24)

A nucleation rate  $I_{n,t}$  can then be defined as the time-dependent flux of clusters beyond a certain size n:

$$I_{n,t} = N_{n,t}k_n^+ + N_{n+1,t}k_{n+1}^-. (4.25)$$

In the paradigm of cluster growth by monomer addition the critical cluster size has to be realized on the path towards larger crystallites, so the Gibbs free energy  $\Delta G_c$  required for the formation of a critical cluster plays the role of an activation barrier against crystallization.

Volmer and Weber, who at that time worked on a problem related to the crystallization of under-cooled liquids, i. e. the condensation of supersaturated vapor, assumed that nuclei larger than the critical size  $n_c$  grow rapidly and so any back flux from such clusters to sub-critical clusters may be neglected. Accordingly they defined the nucleation rate as the rate of formation of post-critical clusters, i. e. clusters of size  $n > n_c$ :

$$I_{n_c,t} = k_{n_c}^+ \cdot N_{n_c} \,. \tag{4.26}$$

Further they assumed that the formation of sub-critical clusters can be viewed as regular configurational fluctuations of the liquid in equilibrium. The theory of thermodynamic fluctuations states that the probability to obtain a fluctation in equilibrium of the system is proportional to  $\exp(-\Delta G/k_BT)$ , wherein  $\Delta G$  is the change in Gibbs free energy according to the fluctuation. So in this equilibrium approximation Volmer and Weber arrived at the following equation for the nucleation rate:

$$I_{VW}^{equ} = k_{n_c}^+ \cdot N_{n_c}^{equ} = k_{n_c}^+ \cdot N_0 \cdot \exp\left(-\frac{\Delta G_c}{k_B T}\right),$$
 (4.27)

wherein  $N_0$  is the total number of atoms in the system. The two most apparent oversimplifications by Volmer and Weber, i. e. the assumption of equilibrium population of subcritical clusters and the denial of shrinking post-critical nuclei, have been replaced by Becker and Döring, who argued that a steady-state distribution of clusters  $N_n^{ss}$  was more realistic. So by allowing a back flux from post-critical nuclei the steady-state nucleation rate  $I^{ss}$  is derived from

$$I^{ss} = k_n^+ \cdot N_n^{ss} - k_{n+1}^- \cdot N_{n+1}^{ss}. \tag{4.28}$$

For ideal steady-state conditions the nucleation rate should be independent from the cluster size at which it is evaluated. As boundary conditions Becker and Döring assumed an equilibrium distribution for small cluster sizes and a vanishing number of

#### 4.2. CRYSTAL NUCLEATION

clusters for infinitely large clusters. Furthermore, they assumed that clusters near the critical size dominate the process of nucleation. Thus it is no surprise that their derivation of  $I^{ss}$  also resulted in an expression that includes the Gibbs free energy required for the formation of a critical cluster  $\Delta G_c$ :

$$I^{ss} = k_{n_c}^+ \cdot N_0 \cdot \underbrace{\frac{1}{n_c} \cdot \left(\frac{\Delta G_c}{3\pi k_B T}\right)^{\frac{1}{2}}}_{\Gamma_z} \cdot \exp\left(-\frac{\Delta G_c}{k_B T}\right) = \Gamma_z \cdot I^{equ}. \tag{4.29}$$

This steady state nucleation rate differs from the nucleation rate derived by Volmer and Weber (Eq. (4.27)) only by a factor  $\Gamma_z$ , called "Zeldovich factor". In most cases  $\Gamma_z$  is larger than 0.01, but smaller than 0.1.

In its early form the concept described above was developed for the description of the condensation of vapor. When turning towards the crystallization of a liquid or even a solid, the general form of the equation for the nucleation rate, i.e. the dependence on the driving force, was assumed to be the same. The rates of monomer addition and subtraction in contrast had to be reviewed. In the condensed phase such rates are expected to be determined essentially by an atomic jump frequency dependent on the product of an attempt frequency and a term containing an activation barrier that needs to be overcome. Turnbull and Fisher [95] worked out the preceding suggestions by Becker [96] assuming that in the process of addition or removal of a monomer to a cluster the system passes through an "activated complex", a configuration that has a higher energy then both the initial and the final state and by applying reaction rate theory to this problem. Later formulations of the classical nucleation theory [93] relate the molecular jump frequency  $\gamma$  to the jump frequency for bulk diffusion:

$$\gamma = \frac{6D}{\lambda^2} \,, \tag{4.30}$$

where D usually represents the diffusivity in the liquid, not in the crystal phase, and  $\lambda$  the atomic jump distance. Together with the number of sites at the surface of a critical cluster,  $O_c \propto (n^{2/3})$ , this gives the monomer addition rate:

$$k_{n_c}^+ = O_c \cdot \frac{6D}{\lambda^2} \,.$$
 (4.31)

The steady state nucleation rate for crystallization in a liquid can accordingly be expressed by:

$$I^{ss} = O_c \cdot \frac{6D(T)}{\lambda^2} \cdot N_0 \cdot \Gamma_z \cdot \exp\left(-\frac{\Delta G_c}{k_B T}\right). \tag{4.32}$$

Sometimes it is more practical to use the viscosity  $\eta$  instead of the diffusivity D as a measure for how easy an atomic configuration can rearrange at the interface of a cluster. The Stokes-Einstein equation provides a relation between both quantities:

$$D = \frac{k_B T}{6\pi \eta R} = \frac{k_B T}{3\pi \eta \lambda} \,. \tag{4.33}$$

Here the effective hydrodynamic radius R in the formula has been approximated by half of the atomic jump distance,  $\lambda/2$ , which should be roughly the atomic radius. In view of the fact that the Stokes-Einstein relation has been derived for diluted systems of spherical colloidal particles, it has been remarkably successful at correlating independently measured temperature dependencies of diffusivity and viscosity for many liquids [97, 98]. Substituting Eq. (4.33) into Eq. (4.32) yields

$$I^{ss} = O_c \cdot \frac{2k_B T}{\eta(T)\pi\lambda^3} \cdot N_0 \cdot \Gamma_z \cdot \exp\left(-\frac{\Delta G_c}{k_B T}\right). \tag{4.34}$$

Deviations from the Stokes-Einstein equation have been reported for undercooled liquids in a temperature regime below 1.2 times the glass transition temperature, where molecules translate faster than expected from the material's viscosity [99, 65, 100]. However, it is not clear if this implies Eq. (4.34) to be less valid than Eq. (4.32), since it is not obvious which is the better approximation for the rate of rearrangements at a cluster interface, viscosity or diffusivity. Regardless of which name one prefers to give to this term representing the rate of rearrangements during the formation of nuclei, in this text its temperature dependence is assumed to follow the Vogel-Fulcher-Tammann equation (Eq. (3.3)), which has been discussed in detail in the previous chapter.

The substitution of Eq. (4.22) for  $\Delta G_c$  displays the dependencies of the steady state nucleation rate even more clearly than Eq. (4.34) already does:

$$I^{ss} = O_c \cdot \frac{2k_B T}{\eta(T)\pi\lambda^3} \cdot N_0 \cdot \Gamma_z \cdot \exp\left(-\frac{16\pi}{3k_B T} \frac{\sigma^3}{(\Delta G_{lc,V})^2}\right). \tag{4.35}$$

The overall temperature dependence of the nucleation rate is dominated by two factors: on the one hand the driving force in form of the exponential term containing the Gibbs free energy difference between crystal and liquid  $\Delta G_{lc}$  counteracted by the interfacial energy  $\sigma$  between both phases and on the other hand the viscosity, also varying over several orders of magnitude in the undercooled liquid (Fig. 3.1).

The temperature dependence of the nucleation rate  $I^{ss}$  can be described qualitatively by discussing just the behaviour of these two components. Close to the melting point the crystal is energetically only slightly favourable against the undercooled liquid phase, and  $\Delta G_{lc}$  is very small (Fig. 4.1), so without a strong driving force the nucleation rate is negligible too. Near the glass transition temperature  $T_g$ , though the driving force is strong here, the nucleation rate vanishes, because the viscosity is high in this temperature regime (Fig. 3.1) hindering any structural rearrangement in the material.<sup>2</sup> Between these two limits, where the driving force is significant and the viscosity still rather low, the nucleation rate can rise over several orders of magnitude.

<sup>&</sup>lt;sup>2</sup>The idea of *collision-limited* crystallization shall only briefly be mentioned in this text as it is rather irrelevant to the topic of phase change materials. This becomes very apparent at this point

#### 4.2. CRYSTAL NUCLEATION

While this interplay of driving force and viscosity has been found to agree well with observations in experiments, the pre-exponential factors in Eq. (4.35) have been central to the controversy over the validity of the classical theory for describing nucleation in liquids and glasses. Experimental values for the product of all pre-exponential factors have been found to differ significantly from theoretical values, in some materials by as much as seven orders of magnitude [93].

In order to highlight the terms that incorporate the strength of the classical nucleation theory, the pre-exponential factors are merged into one factor, roughly estimated by  $O_c \sim 10$ ,  $T \sim 1000 \, \mathrm{K}$ ,  $\Gamma_z \sim 0.01$ ,  $\frac{1}{\lambda^3} \sim 10^{28} \frac{1}{\mathrm{m}^3}$  and  $N_0 \sim 10^{28} \frac{1}{\mathrm{m}^3}$ .

$$I^{ss} = \frac{10^{35}}{\eta(T)} \exp\left(-\frac{\Delta G_c}{k_B T}\right) \frac{\text{Pa s}}{\text{m}^3 s}.$$
 (4.36a)

Using Eq. (4.22), this can be rewritten as

$$I^{ss} = \frac{10^{35}}{\eta(T)} \exp\left(-\frac{16\pi}{3k_B T} \frac{\sigma^3}{(\Delta G_{lc}(T))^2}\right) \frac{\text{Pas}}{\text{m}^3 s}.$$
 (4.36b)

The uncertainty of the pre-exponential factor of  $10^{35}$  is typically about two to four orders of magnitude [69]. As mentioned above, the experience from the history of application of the classical nucleation theory does not permit a use of its formulas for the prediction of absolute numbers, but rather for a description of the change with temperature. The proportionality between  $\log(\eta I^{ss})$  and  $1/(T(\Delta G_{lc}(T))^2)$  has indeed been proven experimentally for a variety of materials [93]. In that sense it is legitimate to use Eq. (4.36) for a visualization of the dramatic temperature dependence of the nucleation rate in phase change materials applying it to the case of one of the most prominent representatives of this class of materials,  $Ge_2Sb_2Te_5$ .

Based on the temperature dependencies of viscosity  $\eta(T)$  (Fig. 3.2) and driving force  $\Delta G_{lc}(T)$  (Fig. 4.2) in Figure 4.4 the steady state nucleation rate is plotted as a function of temperature. One can see that the maximum value for the steady state nucleation rate is about ten orders of magnitude higher than the rate in the vicinity of the glass transition temperature. The graph also shows that a higher fragility leads to higher nucleation rates over the whole temperature range between melting and glass transition temperature, given that all other parameters remain the same.

of the discussion. The idea of collision-limited crystallization assumes the rate of monomer addition to a cluster  $k_{n_c}^+$  to be simply proportional to the velocity of sound in the material, characteristic for the vibrational motion of an atom, instead of being hindered by an activation barrier that has to be overcome to locally rearrange the structure. While this concept may have helped for the description of crystallization of elemental metals, it appears unreasonable for the description of phase change materials, which demand for a factor that strongly hinders crystallization at temperatures around the glass transition temperature.

<sup>&</sup>lt;sup>3</sup>In order to yield a nucleation rate per volume, it is necessary to enter an atomic density for  $N_0$ .

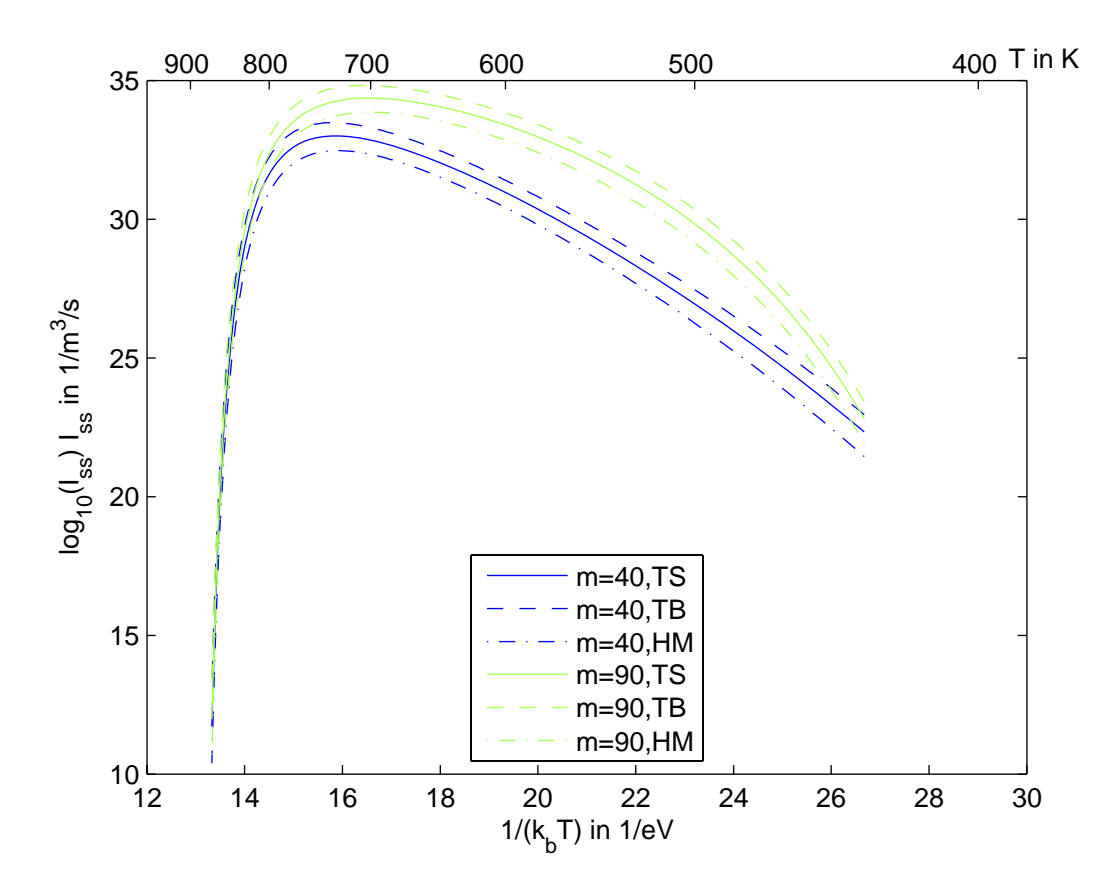


Figure 4.4: Steady state nucleation rate of as a function of temperature calculated from Eq. (4.36b) for two different temperature dependencies of the viscosity  $\eta(T)$ (Fig. 3.2), i.e. corresponding to a fragility of m=40 (blue curves) and m=90 (green curves), respectively. The difference in Gibbs free energy between the undercooled liquid and the crystal  $\Delta G_{lc}(T)$  has been approximated according to Fig. 4.2: approximation by Turnbull (Eq. (4.10), TB, dashed), by Hoffman (Eq. (4.12), HM, dot-dashed) and by Thompson and Spaepen (Eq. (4.17), TS, solid). The liquid-crystal interfacial energy  $\sigma$  is set to  $40 \,\mathrm{mJ/m^2}$ , the heat of fusion  $\Delta H_f$  to  $14.7 \,\mathrm{kJ/mol}$ , the melting temperature  $T_m$  to  $916.3 \,\mathrm{K}$  and the glass transition temperature  $T_g$  to  $428 \,\mathrm{K}$  as determined for  $\mathrm{Ge_2Sb_2Te_5}$  in [69].

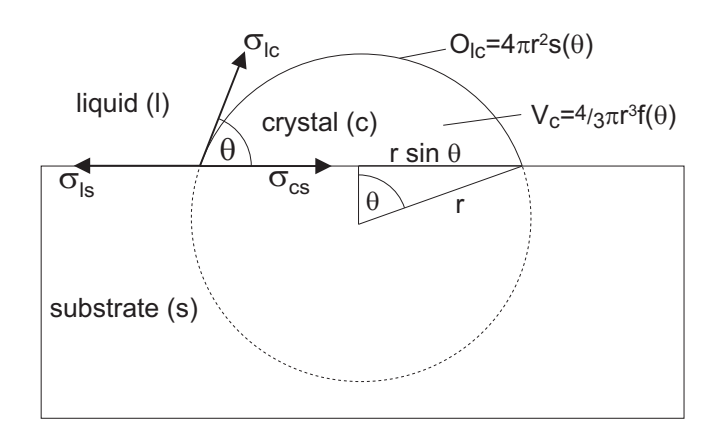


Figure 4.5: Heterogeneous cluster formation on a flat surface: The crystal cluster is assumed to have the form of a spherical cap. Its volume equals  $\frac{4}{3}\pi r^3 f(\theta)$ , with  $f(\theta) = \frac{(2+\cos\theta)(1-\cos\theta)^2}{4}$ , its interface with the liquid phase equals  $4\pi r^2 s(\theta)$ , with  $s(\theta) = \frac{1-\cos\theta}{2}$ , and the interface with the flat surface of the foreign particle or substrate equals  $\pi(r\sin\theta)^2$ . The wetting angle  $\theta$  is connected to the interfacial energies between the three phases by Young's equation:  $\sigma_{cs} - \sigma_{ls} = -\sigma_{lc}\cos\theta$ .

## 4.2.2 Heterogeneous nucleation

The classical theory of nucleation described so far is inherently based on the intrinsic properties of the crystallizing material, like the interfacial energy  $\sigma$  between crystalline and liquid phase and the difference in Gibbs free energy  $\Delta G_{lc}$ . The crystallizing volume is treated to be homogeneous, without any foreign particles or other heterogenities included. Also any effects of the boundaries of the volume are neglected. As a consequence nucleation is expected to occur with equal probability in all parts of the volume. In reality, however, the occurrence of heterogenities is very difficult to avoid. Naturally present in practically all applications they can catalyze nucleation by reducing the interfacial energy of crystalline clusters.

A popular approach to extend the existing theory to include heterogeneous nucleation is the introduction of another parameter, the wetting angle  $\theta$  [94]. The latter is meant to represent the conditions of a cluster attached to a flat side of a particle or substrate with respect to the different interfacial energies between the three phases, crystal, liquid and foreign substance. Assuming isotropy of all phases the crystalline cluster should then grow like a spherical cap on the flat substrate (Fig. 4.5).

Analogous to the homogeneous case, Eq. (4.19), the Gibbs free energy required for the formation of a heterogeneous cluster  $\Delta G_{\text{cluster}}^{\text{het}}(r)$  can then be obtained by

$$\Delta G_{\text{cluster}}^{\text{het}}(r) = \Delta G_{lc} \cdot f(\theta) \cdot \frac{4}{3} \pi r^3 + \sigma_{lc} \cdot s(\theta) \cdot 4\pi r^2 + \pi (r \sin \theta)^2 (\sigma_{cs} - \sigma_{ls}), \quad (4.37)$$

the indices c, l, and s referring to crystal, liquid, and substrate, respectively. The dependencies on  $\theta$  are illustrated in Fig. 4.5.

Young's equation on the relation between wetting angle and the three interfacial energies (see also Fig. 4.5),

$$\sigma_{cs} - \sigma_{ls} = -\sigma_{lc}\cos\theta\,, (4.38)$$

simplifies Eq. (4.37) into

$$\Delta G_{\text{cluster}}^{\text{het}}(r) = \left(\Delta G_{lc} \cdot \frac{4}{3}\pi r^3 + \sigma_{lc} \cdot 4\pi r^2\right) f(\theta) = \Delta G_{\text{cluster}}^{\text{hom}}(r) \cdot f(\theta). \tag{4.39}$$

So the Gibbs free energy for a heterogeneous cluster  $\Delta G_{\text{cluster}}^{\text{het}}(r)$  differs from  $\Delta G_{\text{cluster}}^{\text{hom}}(r)$ , the Gibbs free energy for homogeneous cluster formation given by Eq. (4.19), only by a factor  $f(\theta)$ , with  $0 \leq f(\theta) \leq 1$ , that takes account of the interplay of the interfacial energies between the three phases.

As a consequence, the critical radius for heterogeneous nucleation, defined by

$$\frac{\partial \Delta G_{\text{cluster}}^{\text{het}}(r)}{\partial r}\bigg|_{r} = 0, \qquad (4.40)$$

equals the critical radius for homogeneous nucleation. The corresponding number of atoms  $n_c$  forming such a critical heterogeneous cluster, however, is by factor  $f(\theta)$  smaller than a critical homogeneous cluster:

$$n_c^{\text{het}} = n_c^{\text{hom}} \cdot f(\theta) \,. \tag{4.41}$$

Therefore, also the Gibbs free energy to form a critical cluster is reduced by the factor  $f(\theta)$  for heterogeneous nucleation:

$$\Delta G_c^{\text{het}} := \Delta G_{\text{cluster}}^{\text{het}}(r_c) = \Delta G_c^{\text{hom}} \cdot f(\theta). \tag{4.42}$$

Only if there is no wetting ( $\theta = 180^{\circ}$ , f = 1) due to an energetically very unfavourable interface between the crystal and the foreign substance, the heterogeneities do not catalyze the nucleation process. There the above equations for the heterogeneous case reduce to the ones describing homogeneous nucleation. A formula for the steady state heterogeneous nucleation rate similar to Eq. (4.36) can be derived in the framework of the classical theory simply by adapting the energy barrier  $\Delta G_c$  and reducing the total number of atoms relevant to the process by a factor  $\epsilon$ , as not all  $N_0$  atoms, but only the fraction in contact with a cluster next to a heterogeneous nucleation:

$$I^{ss,\text{het}} = \epsilon \cdot \frac{10^{35}}{\eta(T)} \exp\left(-\frac{\Delta G_c}{k_B T} \cdot f(\theta)\right) \frac{\text{Pa s}}{\text{m}^3 s}. \tag{4.43a}$$

Using Eq. (4.22), this can be rewritten as

$$I^{ss,\text{het}} = \epsilon \cdot \frac{10^{35}}{\eta(T)} \exp\left(-\frac{16\pi}{3k_B T} \frac{\sigma^3}{(\Delta G_{lc}(T))^2} \cdot f(\theta)\right) \frac{\text{Pas}}{\text{m}^3 s}.$$
 (4.43b)

## 4.2. CRYSTAL NUCLEATION

The smaller the volume of the crystallizing material, the higher is the relative fraction of atoms in contact with the surrounding. So especially in the miniaturized cells of phase change material used in memory devices, the probability for heterogeneous nucleation can be expected to be much higher than for homogeneous nucleation.<sup>4</sup>

The derivation described here for the case of a flat side of a particle as heterogenity is meant as an example for a whole set of similar derivations [94] that describe nucleation at heterogenities with other geometries, like edges or corners. The formulas of course turn out to be different in detail, while the main trend remains the same: Heterogenities catalyze nucleation by reducing the number of required atoms and thus the Gibbs free energy needed for the formation of a critical cluster.

Although these derivations of a heterogeneous nucleation rate might look sensible, their result should be used with great caution for several reasons: A uniform flat heterogenity is not a good approximation for the real world. Statistical surface roughening will always be present to an appreciable extent, at least on an atomic length scale effectively varying the geometry for clusters of the size of tens or hundreds of atoms. So the assumption of only one type of heterogenity present in the system must be regarded as very unrealistic. Additionally this roughness of interfaces on the molecular level is in conflict with the assumption of homogenity of physical properties, which macroscopic concepts, like the definition of a wetting angle, are based on. This violation makes macroscopic concepts inapplicable to processes on the molecular level.

Finally, it is problematic, that for most materials there are no values for the macroscopic wetting angle measured in separate experiments. In those cases the application of Eq. (4.43) for an explanation of experimentally observed nucleation rates may be considered to simply give another *free* parameter to fit the data. One should thus be very careful to interpret the ability to fit some data as evidence for the correctness of the model. Any parameter that cannot be cross-checked by different experiments makes it more difficult to gather enough experimental evidence to prove or disprove a model. It is certainly appropriate to have this general truth in mind dealing with the topic of crystal nucleation in liquids.

## 4.2.3 Transient nucleation

The above derivation of nucleation rates was carried out assuming steady state cluster distributions. This condition is not necessarily fulfilled in practice. Especially when the temperature of a liquid is changed very rapidly, the cluster distribution may not

<sup>&</sup>lt;sup>4</sup>However, in the presence of a crystalline phase next to the switchable volume both homogeneous and heterogeneous nucleation will loose importance. The further the spatial dimensions of a structure are scaled down, the more dominant is crystal growth from the existing crystal front.

reach the steady state in the relevant time-window. In condensed phases the activation barrier for rearrangements at the boundary of a cluster slows down the approach of the cluster distribution towards the steady state. Thus it is necessary to investigate the *transient* nucleation rate. For that purpose the coupled differential equations, Eq. (4.24),

$$\frac{\mathrm{d}N_{n,t}}{\mathrm{d}t} = N_{n-1,t}k_{n-1}^{+} - \left[N_{n,t}k_{n}^{-} + N_{n,t}k_{n}^{+}\right] + N_{n+1,t}k_{n+1}^{-},\tag{4.44}$$

need to be solved more generally allowing for the time-dependence of the cluster distribution  $N_{n,t}$ . There are two conceptually different mathematical approaches to this problem. The first is to solve the coupled differential equations analytically.

Zeldovich was the first, who showed that the master equation, Eq. (4.44), describing a discrete process of adding and loosing single monomers to a cluster can be approximated by a continuous equation, the so-called Zeldovich-Frenkel equation:

$$\frac{\partial N_{n,t}}{\partial t} = \frac{\partial}{\partial n} \left\{ k_n^+ N_n^{equ} \frac{\partial}{\partial n} \left( \frac{N_{n,t}}{N_n^{equ}} \right) \right\}. \tag{4.45}$$

Substituting the equilibrium distribution by  $N_n^{equ} = N_0 \cdot \exp(-\Delta G_n/k_B T)$  yields [101]

$$\frac{\partial N_{n,t}}{\partial t} = \frac{\partial}{\partial n} \left\{ k_n^+ \frac{\partial N_{n,t}}{\partial n} \right\} + \frac{1}{k_B T} \frac{\partial}{\partial n} \left\{ k_n^+ N_{n,t} \frac{\partial \Delta G_n}{\partial n} \right\} , \qquad (4.46)$$

which is formally equivalent to the diffusion equation for a set of particles distributed along an axis n and moving under the influence of a force field specified by a potential  $\Delta G_n$ , often referred to as Fokker-Planck equation, which is known from the description of Brownian motion [94].

Most treatments of transient nucleation in the framework of classical theory have solved the Zeldovich-Frenkel equation by approximating the rate constants and the Gibbs free energy of cluster formation [93, 102]. The possibly most thorough analytical treatment due to Kashchiev, for example, approximates the Gibbs free energy of cluster formation  $\Delta G_n$  by the first two nonzero terms of a Taylor expansion around the critical cluster size  $n_c$  and sets the rates  $k_n^+$  equal to  $k_{n_c}^+$  for all cluster sizes n, which results in a time-dependent nucleation rate at the critical size [103, 93]

$$I_{n_c,t} = I^{ss} \left[ 1 + 2 \sum_{m=1}^{\infty} (-1)^m \exp\left(-\frac{m^2 t}{\tau_K}\right) \right],$$
 (4.47)

with the transient time  $\tau_K$ 

$$\tau_K = \frac{4}{\pi^3 k_n^+ \, \Gamma_z^2} \,, \tag{4.48}$$

wherein  $\Gamma_z$  is the Zeldovich factor, known from Eq. (4.29). Much more recently Reguera et al. [102] presented a very general discussion of the Fokker-Planck equation in the context of nucleation processes.

## 4.3. CRYSTAL GROWTH

Alternatively to such analytical approaches the master equation (4.44) can also be solved numerically. This has the advantage that numerical calculations simulate directly the discrete steps of cluster evolution, which are central to the classical theory. The continuum approximation itself and the many other approximations neccessary in the course of the analytical solutions can be omitted. Another advantage is the rather simple implementation of arbitrary initial cluster distributions [101] and of non-isothermal annealing [104] into the finite difference calculation, which divides the time into a large number of small intervals  $\delta t$  and calculates the cluster distribution after the time interval by

$$N_{n,t+\delta t} = N_{n,t} + \delta t \frac{\mathrm{d}N_{n,t}}{\mathrm{d}t}, \qquad (4.49)$$

where  $dN_{n,t}/dt$  is given by Eq. (4.44).

A comparison of the results from numerical calculations with analytical solutions showed best agreement for the predictions from the expressions by Kashchiev [105].

Pre-existing clusters have a great influence on the transient nucleation rate. The assumption of the absence of clusters larger than a few atoms is, although often used, rarely realistic. Instead, the consideration of the exact thermal history of a sample is appropriate.

## 4.3 Crystal growth

The preceding section described the formation of crystalline entities from the liquid as a process of overcoming a critical cluster size. Once formed the growth of the entity, i. e. addition of another monomer, is energetically more favourable and thus more likely than shrinking, i. e. subtraction of a monomer from the cluster. A mathematical formulation of the subsequent growth of a cluster can be obtained according to the ansatz of Turnbull and Fisher [95] for nucleation assuming the system has to pass through an "activated complex" on its way from a cluster of size n to a cluster with one monomer more or less, respectively (see Fig. 4.6).<sup>5</sup>

In the framework of reaction rate theory the jump frequency  $\gamma$  of a monomer accross the liquid-crystal interface at the boundary of a cluster is exponentially dependent on the energy step according to the activated complex  $\Delta G^*$ :

$$\gamma = \nu \cdot \exp\left(-\frac{\Delta G^*}{k_B T}\right), \tag{4.50}$$

<sup>&</sup>lt;sup>5</sup>This approach would be not valid for collision limited growth, which, however, can be excluded from being a good model for crystal growth in phase change materials, as has already been mentioned before.

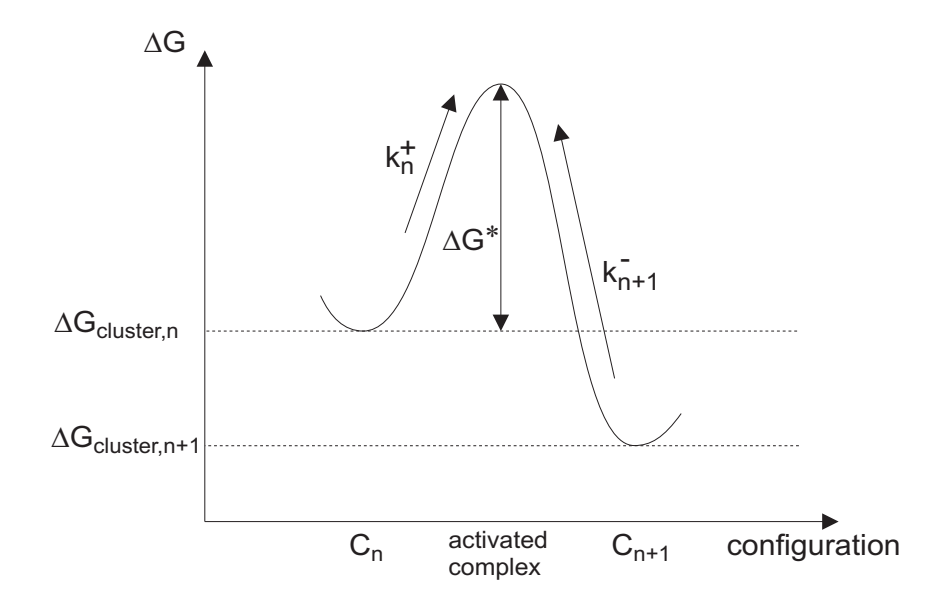


Figure 4.6: Gibbs free energy difference for interface-controlled crystal growth: The growth rate of a cluster is given by the difference between the rate of monomer addition  $k_n^+$  to a cluster of size n and the rate of monomer subtraction  $k_{n+1}^-$  from a cluster of size n+1. During the process of monomer addition and subtraction the system's configuration is assumed to go through an activated complex, activated by an additional Gibbs free energy of  $\Delta G^*$ . The depicted case, where the energy  $\Delta G_{cluster,n}$  for the formation of a cluster of size n is larger than the energy  $\Delta G_{cluster,n+1}$  for the formation of a cluster of size n+1, is valid for clusters larger than the critical size  $n_c$  (see Fig. 4.3), which is the relevant range of cluster sizes for crystal growth.

wherein  $\nu$  is the attempt frequency. This jump frequency  $\gamma$  is assumed to correlate with the bulk diffusivity D in the liquid phase, a measure for how easy a configuration can be changed.  $\Delta G^*$  can generally be temperature dependent, which corresponds to the diffusivity behaving not necessarily Arrhenius-like. As already stated in Eq. (4.30) in the context of nucleation

$$\gamma = \frac{6D}{\lambda^2} \,, \tag{4.51}$$

with  $\lambda$  representing the molecular jump distance.

The rate of monomer addition to a cluster containing n atoms is then analogous to Eq. (4.31):

$$k_n^+ = 4n^{2/3} \cdot \nu \cdot \exp\left(-\frac{\Delta G^*}{k_B T}\right)$$

$$= 4n^{2/3} \cdot \gamma$$

$$= 4n^{2/3} \cdot \frac{6D}{\lambda^2}, \qquad (4.52)$$

with the number of available attachment sites on the surface of a cluster assumed to equal  $4n^{2/3}$  [93]. The rate of the reverse process, the subtraction of a monomer from a

cluster of size n+1, is then given as

$$k_{n+1}^{-} = 4n^{2/3} \cdot \nu \cdot \exp\left(-\frac{\Delta G^* + (\Delta G_{cluster,n} - \Delta G_{cluster,n+1})}{k_B T}\right)$$

$$= 4n^{2/3} \cdot \gamma \cdot \exp\left(-\frac{\Delta G_{cluster,n} - \Delta G_{cluster,n+1}}{k_B T}\right)$$

$$= 4n^{2/3} \cdot \frac{6D}{\lambda^2} \cdot \exp\left(-\frac{\Delta G_{cluster,n} - \Delta G_{cluster,n+1}}{k_B T}\right), \tag{4.53}$$

where  $\Delta G_{cluster,n}$  and  $\Delta G_{cluster,n+1}$  are the Gibbs free energies of clusters of size n and n+1 respectively, less the free energy of the completely liquid state (see Eqs. (4.18) and (4.19) and Fig. 4.3).

The growth rate  $\partial n/\partial t$  of a cluster of size n can be defined as

$$\frac{\partial n}{\partial t} = k_n^+ - k_{n+1}^- \tag{4.54}$$

$$= 4n^{2/3} \cdot \frac{6D}{\lambda^2} - 4n^{2/3} \cdot \frac{6D}{\lambda^2} \cdot \exp\left(-\frac{\Delta G_{cluster,n} - \Delta G_{cluster,n+1}}{k_B T}\right)$$
(4.55)

$$= 4n^{2/3} \cdot \frac{6D}{\lambda^2} \cdot \left[ 1 - \exp\left(-\frac{\Delta G_{cluster,n} - \Delta G_{cluster,n+1}}{k_B T}\right) \right] . \tag{4.56}$$

It makes sense to define the crystal growth velocity u as the velocity of the crystal front, i. e. the time derivative of a cluster's radius r:

$$u = \frac{\partial r}{\partial t} = \frac{\partial n}{\partial t} \cdot \frac{\partial r}{\partial n} \ . \tag{4.57}$$

The term  $\partial r/\partial n$  can be derived from the increase of the volume of a cluster  $\Delta V$  upon the addition of  $\Delta n$  atoms, each of which filling the volume  $V_{atom}$ :

$$\Delta V = V_{atom} \cdot \Delta n = 4\pi r^2 \Delta r \,, \tag{4.58}$$

resulting in

$$\frac{\Delta r}{\Delta n} = \frac{V_{atom}}{4\pi r^2} = \frac{\partial r}{\partial n} \,. \tag{4.59}$$

Substituting Eqs. (4.59) and (4.54) into Eq. (4.57) yields

$$u = \frac{\partial r}{\partial t} = 4n^{2/3} \cdot \frac{6D}{\lambda^2} \cdot \left[ 1 - \exp\left(-\frac{\Delta G_{cluster,n} - \Delta G_{cluster,n+1}}{k_B T}\right) \right] \cdot \frac{V_{atom}}{4\pi r^2} \ . \tag{4.60}$$

The correlation between n and r via the volume V of a cluster of radius r containing n atoms

$$V = \frac{4}{3}\pi r^3 = n \cdot V_{atom} \tag{4.61}$$

allows the replacement of  $n^{2/3} = n/n^{1/3}$  in Eq. (4.60):

$$\frac{\partial r}{\partial t} = 4 \frac{\frac{4}{3}\pi r^3}{V_{atom}} \cdot \left(\frac{V_{atom}}{\frac{4}{3}\pi r^3}\right)^{1/3} \cdot \frac{6D}{\lambda^2} \cdot \left[1 - \exp\left(-\frac{\Delta G_{cluster,n} - \Delta G_{cluster,n+1}}{k_B T}\right)\right] \cdot \frac{V_{atom}}{4\pi r^2}$$

$$= \frac{4}{3} \cdot \left(\frac{3V_{atom}}{4\pi}\right)^{1/3} \cdot \frac{6D}{\lambda^2} \cdot \left[1 - \exp\left(-\frac{\Delta G_{cluster,n} - \Delta G_{cluster,n+1}}{k_B T}\right)\right]$$

$$= \left(\frac{3V_{atom}}{4\pi}\right)^{1/3} \cdot \frac{8D}{\lambda^2} \cdot \left[1 - \exp\left(-\frac{\Delta G_{cluster,n} - \Delta G_{cluster,n+1}}{k_B T}\right)\right]. \tag{4.62}$$

Finally using Eq. (4.19)

$$\Delta G_{\text{cluster}}(r) = -\frac{4}{3}\pi r^3 \cdot \Delta G_{lc} + 4\pi r^2 \cdot \sigma \tag{4.63}$$

the exponent in Eq. (4.62) can be replaced by a continuous representation using the radius r

$$\Delta G_{cluster,n+1} - \Delta G_{cluster,n} = \frac{\partial \Delta G_{cluster,n}}{\partial n} 
= \frac{\partial \Delta G_{cluster}(r)}{\partial r} \cdot \frac{\partial r}{\partial n} 
= \left[ -4\pi r^2 \Delta G_{lc} + 4\pi r^2 \sigma \right] \cdot \frac{\partial r}{\partial n} 
= -4\pi r^2 \cdot \Delta G_{lc} \left[ 1 - \frac{r_c}{r} \right] \cdot \frac{\partial r}{\partial n} 
= -V_{atom} \cdot \Delta G_{lc} \left[ 1 - \frac{r_c}{r} \right] .$$
(4.64)

wherein  $r_c$  is the critical radius defined in Eq. (4.21). The product of the volume per atom  $V_{atom}$  and the difference in Gibbs free energy between liquid and crystal  $\Delta G_{lc}$  in Joule per volume can also be expressed as  $\Delta G_{lc,atom}$ , the Gibbs free energy difference per atom. The growth velocity of a cluster of radius r can then be written as [106, 104]

$$u = \frac{\partial r}{\partial t} = \left(\frac{3V_{atom}}{4\pi}\right)^{1/3} \cdot \frac{8D(T)}{\lambda^2} \cdot \left[1 - \exp\left(-\frac{\Delta G_{lc,atom}(T)}{k_B T} \left[1 - \frac{r_c}{r}\right]\right)\right] . \tag{4.65}$$

Using the Stokes-Einstein relation  $D = (k_B T)/(3\pi \eta \lambda)$  from Eq. (4.33), the diffusivity can be replaced by the viscosity:

$$u = \frac{\partial r}{\partial t} = \frac{4k_B T}{3\pi\eta(T)\lambda^2} \cdot \left[1 - \exp\left(-\frac{\Delta G_{lc,atom}(T)}{k_B T} \left[1 - \frac{r_c}{r}\right]\right)\right] . \tag{4.66}$$

The last step also included the approximation for the atomic radius  $[(3V_{atom})/(4\pi)]^{1/3} \cong \lambda/2$ , where  $\lambda$  is the interatomic distance (see comment on Eq. (4.33)).

It shall be emphasized that the formula for the crystal growth velocity is based on the very same assumptions that are used for the derivation of the nucleation rates. At this point it becomes apparent that there is no fundamental distinction in classical crystallization theory between the variations in cluster size around the critical value resulting in nucleation on the one hand and the growth of crystal fronts, the surfaces of larger clusters, on the other hand.

Equation (4.66) clearly includes a hindering contribution from the interfacial energy between the crystalline and the liquid phase for finite cluster sizes represented by the critical radius  $r_c$ . Only for clusters much larger than the critical cluster  $(r >> r_c)$  the interface remains practically constant upon crystal growth and thus in this limit the growth velocity u becomes constant in time too:

$$u = \frac{4k_B T}{3\pi\eta(T)\lambda^2} \cdot \left[1 - \exp\left(-\frac{\Delta G_{lc,atom}(T)}{k_B T}\right)\right] (r >> r_c) . \tag{4.67}$$

#### 4.3. CRYSTAL GROWTH

This limitation of the validity of the upper formula (4.67) is often neglected and accordingly the growth velocity being constant in time is claimed to be a general fact for interface-controlled growth.

It should be mentioned that in the derivation of the formula for crystal growth, it was implicitly assumed, that the atoms necessary for the correct continuation of the crystalline configuration at the cluster's surface are available in the direct proximity of the respective position. If, however, the stoichiometry of the crystalline phase differs from the composition of the liquid, the zone next to the cluster will be depleted by at least one type of atom, which then has to diffuse to the liquid-crystal interface from more distant parts of the liquid before it can be attached to the cluster. In those cases the long-range diffusion process effectively limits the crystal growth, if the interface mobility is reasonably high. Here the growth velocity decreases with time, u typically being proportional to  $(D/t)^{1/2}$ , with diffusivity D and time t. [94]

Back to the simpler case of transformation of a liquid into a crystalline phase with the same stoichiometry and thus to interface-controlled growth: the overall temperature dependence in the limit of large clusters can be most easily seen, when all parameters that are not varying with temperature are merged into one constant.

$$u(T) = u_0 \cdot \frac{T}{\eta(T)} \cdot \left[ 1 - \exp\left(-\frac{\Delta G_{lc,atom}(T)}{k_B T}\right) \right] (r >> r_c) . \tag{4.68}$$

For illustration of this temperature behaviour the function  $u(T)/u_0$  is plotted logarithmically in Fig. 4.7. At the melting temperature  $\Delta G_{lc}$  vanishes and hence the whole right hand term in Eq. (4.68) and the whole growth velocity equals zero. This is trivial as without a driving force, no transformation should occur. For slight undercoolings of the liquid the growth velocity exhibits a sharp increase resulting in a maximum value not far below the melting temperature. Below this point the increasing viscosity, which hinders any reconfiguration, leads to the growth velocity to decrease for lower temperatures despite a steady increase of the driving force. The graph in Fig. 4.7 shows that for phase change materials the classical crystallization theory predicts the growth velocity near the glass transition temperature to be several orders of magnitude lower than at its maximum.

In comparison with the nucleation rate (Fig. 4.4) one can observe that in the framework of classical theory the crystal growth velocity is expected to depend much more on the temperature dependence of the viscosity than on the temperature dependence of the driving force. The fragility has a much larger impact on u than the choice of the model for the temperature dependence of  $\Delta G_{lc}$  does. Furthermore, the temperature of maximum growth velocity is predicted to be higher than the temperature of maximum nucleation rate. Finally, similar to nucleation also crystal growth velocities turn out

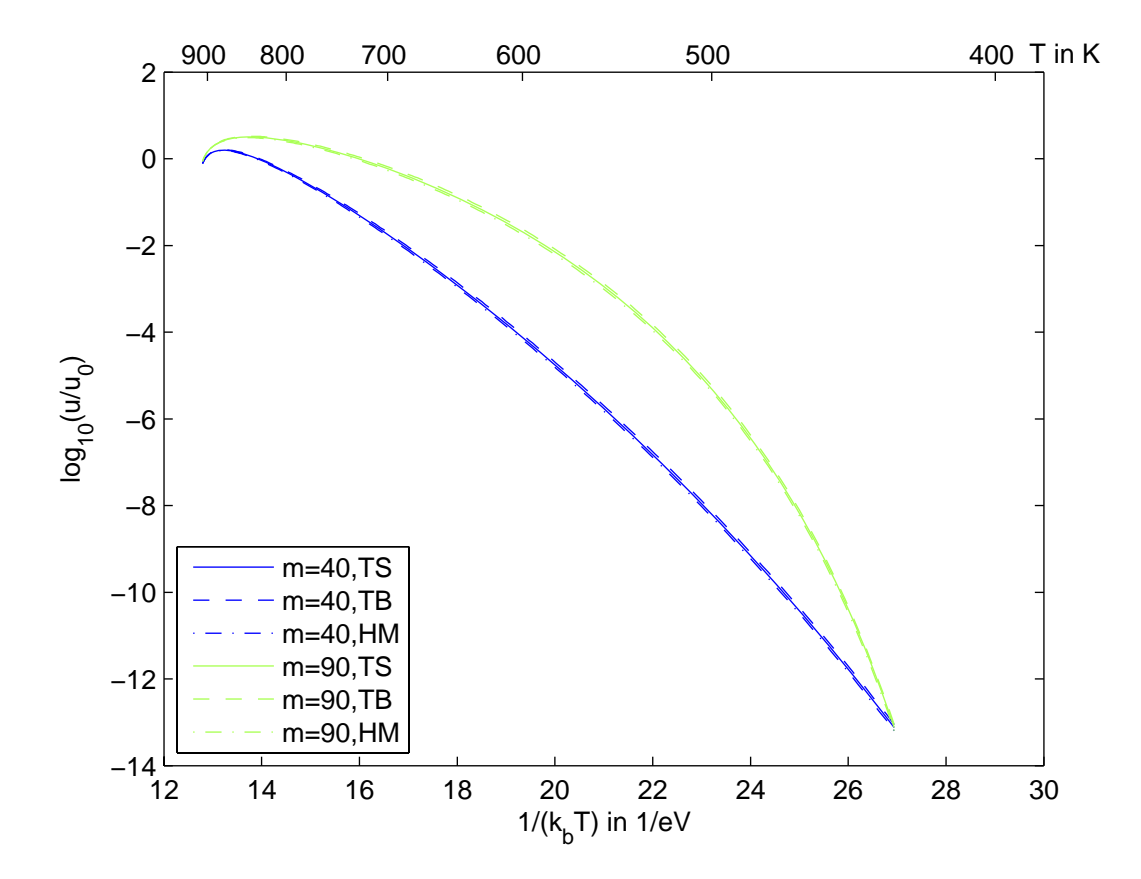


Figure 4.7: Relative temperature dependence of crystal growth velocity calculated from Eq. (4.68) for two different temperature dependencies of the viscosity  $\eta(T)$  (Fig. 3.2), i. e. corresponding to a fragility of m=40 (blue curves) and m=90 (green curves), respectively. The difference in Gibbs free energy between the undercooled liquid and the crystal  $\Delta G_{lc}(T)$  has been approximated according to Fig. 4.2: approximation by Turnbull (Eq. (4.10), TB, dashed), by Hoffman (Eq. (4.12), HM, dot-dashed) and by Thompson and Spaepen (Eq. (4.17), TS, solid). The liquid-crystal interfacial energy  $\sigma$  is set to 40 mJ/m<sup>2</sup>, the heat of fusion to 14.7 kJ/mol, the melting temperature to 916.3 K and the glass transition temperature to 428 K as determined for Ge<sub>2</sub>Sb<sub>2</sub>Te<sub>5</sub> in [69].

higher over the complete range of the undercooled liquid for larger fragilities.

## 4.4 Beyond classical theory

Classical nucleation theory has been used many times to describe experimental data of crystal nucleation. Still caution is advised, as there is a chronic lack of data of the temperature dependence of the driving force  $\Delta G_{lc}(T)$  and the viscosity  $\eta(T)$  leaving the formula for nucleation rate with two practically free parameters. This is even more true for the interfacial energy  $\sigma$ . It is often known only from fitting nucleation data, which show the inability to cross check their values with independent experiments. In view of these uncertainties about the physical quantities incorporated in the equations for the nucleation rate it is not surprising, that the concept of the classical theory itself has rarely been challenged by experimental evidence. Crucial assumptions of the model, like clusters having bulk properties inside of a sharp surface, which in turn is described by the interfacial energy of a flat plane <sup>6</sup>, or the atomic rearrangements at the crystal-liquid interface being controlled by the bulk mobility in the liquid, are still not checked rigorously and their validity is therefore unclear. Especially for small clusters these assumptions seem bold.

For this reason it would be disingenuous to conceal the existence of alternative approaches to the phenomenon of nucleation. Since the 1950s, when Cahn and Hilliard [107, 108] published their pioneering work, a field-theoretic approach to nucleation has been constantly advanced over the years. While Cahn and Hilliard concentrated on the correct form of the free energy for critical cluster formation with diffuse interfaces, Langer and co-workers [109, 110, 111, 112] extended the existing analysis by taking properly account for the fundamental fluctuations leading to nucleation and considering fluctuations in cluster size and shape. Density functional theory, molecular dynamics and Monte Carlo simulations have also been applied to the problem of nucleation. In this text it shall be sufficient to just mention these activities beyond classical nucleation theory and refer to the literature for a more in depth study of these topics. A good overview of the different approaches is given by Kelton [93] and more recently by Gunton [113].

The different theoretical models of nucleation do not only explain the underlying fundamental processes in alternative ways, but also lead to differing values for the nucleation rates. This should be kept in mind, when applying any of the theories to crystallization of a specific material. Because crystallization in phase change materials takes place on extremely short time scales, the measurement of their crystallization

<sup>&</sup>lt;sup>6</sup>This is often referred to as "the capillarity approximation".

kinetics is experimentally not trivial. The temptation is great to measure crystallization only where it is slow and extrapolate the characteristics in the framework of a theory to temperatures, where the phase transition is much faster. It might well be the case, but is far from certain, that classical theory is capable of giving a closed description of the crystallization kinetics in phase change materials over the whole temperature range between melting and glass transition temperature. So estimations based on the equations resulting from classical theory should be carefully checked by experiments in all temperature regimes. Part III will describe an experimental setup that offers the capability to investigate crystallization kinetics especially where it is fast.

## 4.5 General models on transformation

In the past numerous experiments have been developed that are capable of measuring the crystalline fraction of a sample  $\chi$ . In isothermal and also in non-isothermal experiments this degree of crystallization is measured as a function of time  $\chi(t)$ . Data from these experiments are often analyzed applying the so-called *Kissinger analysis*[114]. Despite its rigorous application in literature, the validity of Kissinger's method and its results must be strongly doubted for all cases where his starting assumption about the Arrhenius-like temperature dependence of the reaction rate  $\partial \chi/\partial t$  (see Eq. (4.69) below) or any of the approximations in the course of his subsequent derivation is unrealistic. In view of the formulas for nucleation rate and growth velocity, even without involving transient effects, the Kissinger ansatz

$$\frac{\mathrm{d}\chi}{\mathrm{d}t} = A \cdot (1 - \chi)^n \cdot \exp\left(\frac{E_{kiss}}{k_B T}\right), \tag{4.69}$$

wherein A,  $E_{kiss}$  and 0 < n < 1 are constant for a specific material, can at least not generally be expected to be correct for crystallization in phase change materials. A more detailed discussion of the limited validity of the Kissinger analysis is given in [115] and references within.

Another method for the analysis of  $\chi(t)$  traces back to Johnson, Mehl, Avrami and Kolmogorov [116, 117, 118]. The accordingly called JMAK-model starts with three crucial assumptions in order to statistically compute the effect of impingement of growing crystal clusters on the crystallization kinetics [115]: First, the sample size is much greater than any individual transformed region. Second, the growth proceeds homogeneously throughout the sample. And third, the nucleation is spatially random. If these requirements are fulfilled, the fraction of transformed material  $\chi$  can, for the

## 4.5. GENERAL MODELS ON TRANSFORMATION

three dimensional case, be expressed as

$$\chi(t) = 1 - \exp\left(-\frac{4\pi}{3V_0} \int_0^t I(T, t') \left(\int_{t'}^t g(T, t'') dt''\right)^3 dt'\right), \tag{4.70}$$

where  $V_0$  is the sample volume. However, to really take advantage of the JMAK-model further simplifications are necessary. A core assumption is the time-independence of the crystal growth velocity g(T,t). The aim to match this requirement as well as possible is the reason why in almost all cases the JMAK-model is used together with isothermal experiments. As we learned in the above section on crystal growth, though, classical theory predicts a time dependent growth velocity not only for diffusion-controlled growth but also for interface-controlled growth of small clusters.

Nevertheless, if, for example, additionally to constant growth a constant nucleation rate I is assumed, Eq. (4.70) simplifies to

$$\chi(t) = 1 - \exp\left(-\frac{4\pi}{3V_0}Ig^3t^4\right). \tag{4.71}$$

In other cases often a general form of the JMAK expression is claimed to describe isothermal phase transformations:

$$\chi(t) = 1 - \exp(-(kt)^n) . (4.72)$$

The effective kinetic parameter k and the so-called Avrami exponent n include information about both the dimensionality of the problem and the crystallization kinetics, e.g. the time dependence of nucleation. While it seems appropriate to fit a typically S-shaped experimental curve for  $\chi(t)$  with no more than two free parameters, it is in turn obvious that a disentanglement of non-trivial time dependencies of nucleation and growth can hardly be derived from only two parameters without making bold assumptions.

So a critical review of the JMAK analysis, as found in [115], leads to the understanding that for a legitimate use of this analysis it is required to ensure that reality is consistent with the original assumptions and those necessary for the interpretation of the fitting parameters. In other words, the JMAK model may become useful to check, if existing functions for the crystallization kinetics can correctly describe an experiment measuring  $\chi$ , or even to determine kinetic parameters, after the general functional dependence on temperature and time has been proven in a different, more direct way. An unambiguous identification of the crystallization mechanism by JMAK-analysis of  $\chi(t)$  measurements alone is impossible. [119, 120]

Experimental challenges with respect to the achievement of isothermal conditions in very fast annealings, when approaching higher temperatures and faster crystallization,

## CHAPTER 4. THEORY OF CRYSTALLIZATION

are, although severe, deliberately left out in this consideration in order to stress that major shortcommings in the applicability of the JMAK analysis to reality are *intrinsic* to the concept and not due to experimental difficulties.

4.5. GENERAL MODELS ON TRANSFORMATION

# Part II Prediction of Glass Transition

Temperatures

## Motivation

We haven't got the money, so we've got to think!

ERNEST RUTHERFORD

Before anyone could possibly be willing to read about the topic of the second part of this thesis, the prediction of glass transition temperatures, an important question has to be answered first: Why should anyone be interested in the glass transition at all?

Various requirements a phase change material has to fulfill to be useful for data storage originate from the specific application it should serve, while they are irrelevant for other applications. A high reflectivity contrast between the amorphous and the crystalline state, for example, is crucial for the application in rewritable optical discs in order to have a sufficient signal-to-noise ratio during the read out process, while this attribute is completely irrelevant inside an electronic memory device. It can be even detrimental there, because optical contrast is often related to a large change in mass density which can lead to void formation upon repeated cycling. On the other hand any material property associated with the electrical properties of a phase change material, discussed in some detail in section 2.2.3 on the topic of PCRAM, will certainly be of no interest when aiming for optical storage media. Unlike those, however, there are some material parameters that are equally crucial for all kinds of applications of phase change materials in the field of data storage. Two major ones surely are switching speeds and thermal stability against data loss. The latter is probably even more important for solid state memory devices than for optical discs, as the operation temperature can be significantly higher in PCRAM. For embedded storage applications, e.g. on the mainboard of a computer, the memory has to withstand 350 K and for some potential applications in the automobile industry even 420 K without loosing the stored information. Removable storage media for the consumer market typically have to guarantee retention times of 10 years at up to 320 K. Thus tailoring the stability zone of a phase change material's amorphous state spanning sufficiently beyond these temperatures is essential for achieving optimum performance of a solid state device.

Apparently both aspects, switching speeds and thermal stability, are ultimately de-

termined by the crystallization kinetics of a phase change material. The switching speed mainly depends on the maximum in the temperature dependence of crystal nucleation rate (Fig. 4.4) and growth velocity (Fig. 4.7), respectively. The challenges of investigating these extremely fast processes at high temperatures are presented in part III. The long-term thermal stability of the amorphous phase against crystallization, in contrast, is linked to the low temperature tail of the nucleation and growth rates. As derived in chapter 4 both quantities depend on the viscosity, which is changing dramatically as a function of temperature (see Fig. 3.2). The configurational freezing of the undercooled liquid at the glass transition serves as a critical point, below which any structural rearrangement is largely frustrated. An increase of the glass transition temperature thus can be expected to enlarge the stability zone of the amorphous phase shifting the temperature region of fast crystallization kinetics towards higher temperatures.

Changing the composition of known phase change materials that already fulfill most other criteria for a successful application by alloying them with new elements has been shown to be capable of achieving this stability increase of the amorphous phase. Several examples of experimental studies of the change of crystallization behavior upon doping Sb<sub>70</sub>Te<sub>30</sub> with Ag [121, 122], In [121], Cu [122], Ge [123] or Si [124], doping prominent stoichiometries of GeSbTe with Cu [125], Sn [126], Si [127], B [128], F [129], O [130, 131, 129], N [131, 26, 129] or a combination of N and O [131] and very recently doping of Sb<sub>80</sub>Te<sub>20</sub> with W [132] can be found in the literature. In many cases this doping led to a higher stability of the amorphous phase at elevated temperatures<sup>7</sup>. However, the efficiency in producing this change in crystallization kinetics varies a lot and in some cases, e. g. doping GeSbTe with F [129], doping even reduced the extent of the regime of stability. The multitude of possible dopants, in principle almost all elements in the periodic table, combined with the ever limited time and resources for experiments based solely on trial and error calls for a method to predict how a change in composition influences the structural stability of a glass before starting experiments.

For this purpose an algorithm has been programmed in the scope of this work predicting the glass transition temperature for a given stoichiometry. Before the physical basis for this calculation and the program itself will be described in chapter 6, chapter 5 gives an overview of other existing models on the compositional dependence of the glass transition. Afterwards, in chapter 7, the calculated glass transition temperatures for some phase change materials are compared with measured values for this quantity. Closing this second part of this thesis in chapter 8 the potential of the algorithm to indicate the change in thermal stability of a glass against crystallization is evaluated.

<sup>&</sup>lt;sup>7</sup>Often also an increased resistivity in the crystalline phase is observed implying the advantageous reduction of the reset current in electronic memories.

Therefor its predictions for the effect of different dopants on this stability is compared with the respective experimental results for different parent phase change alloys.

# Chapter 5

# Models of Glass Transition in Literature

If I have seen further it is by standing on the shoulders of giants.

ISAAC NEWTON

## 5.1 Constraint theory

In chapter 3 the temperature dependencies of the kinetic and thermodynamic properties of a material's undercooled liquid phase have been discussed introducing amongst others the concept of fragility. In the present chapter the focus is shifted towards models that describe the dependence of the glass transition temperature on the stoichiometry of the respective material.

As a first of these models the pioneering work of Phillips and Thorpe [133, 134] developing the so-called constraint theory shall be mentioned. This atomic model for predominantly covalently bonded materials is based on the comparison of the number of topological degrees of freedom with the number of interatomic force field constraints. The latter are differentiated into two body central forces associated with bond stretching and three body non-central forces associated with bond bending. As a simplification of the problem it is assumed that all bond bending forces are equally strong and topologically equally significant, i. e. independent of the coordination number of an atom. The total number of constraints per atom  $N_{cons}$  is then calculated as a function of an atom's coordination number r:

$$N_{cons} = r/2 + r(r-1)/2 = r^2/2,$$
 (5.1)

the first term of Eq. (5.1) representing bond stretching, the second one bond bending constraints. For the constraint theory as well as for all other models on glass transition

in predominantly covalently bonded materials mentioned below, the coordination number of an element from group N is assumed to be equal to 8-N. So a group IVB element, like Ge, is expected to have four nearest neighbors, while a chalcogen supposedly has only two nearest neighbors. The latter is the reason for a cluster of chalcogen atoms often being referred to as chains (see for example the discussion of the Gibbs-DiMarzio equation in this chapter).

Thus the number of constraints for an  $As_xSe_{1-x}$  alloy is calculated following Eq. (5.1) as

$$N_{cons}(x) = x \cdot 3^2 / 2 + (1 - x) \cdot 2^2 / 2.$$
 (5.2)

In Phillips' constraint theory the glass forming condition is fulfilled when the number of constraints equals the number of degrees of freedom  $N_D$ .

$$N_{cons}(x_c) = N_D. (5.3)$$

In the case of a three-dimensional solid ( $N_D = 3$ ) of, for example,  $As_xSe_{1-x}$  this condition is met at a critical concentration  $x_c = 0.40$ , corresponding to an average coordination number per atom  $\bar{r}$  of 2.4. This critical value is also called the rigidity percolation threshold. Below this threshold a glass is underconstrained or floppy while structures with  $\bar{r}$  larger than 2.4 are overconstrained or rigid. More recently simulations of random bond models [135] theoretically and temperature modulated differential scanning calorimetry [136] experimentally revealed that in some covalently bonded alloys like  $Si_xSe_{1-x}$  there is not only one rigidity transition but there are two. The Intermediate region between these two transitions, being rigid but not stressed, separates the floppy glasses ( $\bar{r}$  below 2.4) from the stressed rigid compositions ( $\bar{r}$  above 2.67). The origin of the physical anomalies near  $\bar{r}$ =2.67 is still controversial. While Tanaka [137] associated this critical coordination number in As- and Ge-chalcogenide glasses with a dimensionality change from two-dimensional structures to three-dimensional networks, Boolchand et al. [138] propose nanoscale phase separation as the molecular origin of the second threshold.

## 5.2 Segmental motions

Although these models can predict stoichiometric thresholds for the elastic or structural properties of glasses such as the molar volume or the glass forming tendency for a quantitative description of the dependence of a material's glass transition temperature on its composition other approaches are necessary. A rather basic one by Tanaka [139]

starts from an Arrhenius equation for the viscosity of a liquid

$$\eta = \eta_0 \cdot \exp\left(\frac{E}{k_B T}\right) \,. \tag{5.4}$$

Assuming that the fluidity of liquids is due to segmental motions of polymer or chalcogen chains or slipping movements of distorted layers, he identifies the glass transition temperature with the event of van der Waals bonds freezing in. He therefore relates the activation energy E of Eq. (5.4) with such cooperative rearrangements in the expression

$$E \cong E_0 \cdot n^{\bar{r}-1} \,, \tag{5.5}$$

 $E_0$  describing the strength of the van der Vaals bonding per atom and  $n^{\bar{r}-1}$  the number of binding atoms belonging to an atomic unit. At the glass transition temperature  $T_g$  with viscosity  $\eta_g$ , equations (5.4) and (5.5) lead to

$$\ln\left[\frac{k_B T_g}{E_0} \cdot \ln\left(\frac{\eta_g}{\eta_0}\right)\right] \cong (\overline{r} - 1) \cdot \ln(n) , \qquad (5.6)$$

a proportionality between  $\ln(T_g)$  and the average coordination number  $\bar{r}$ . In his work Tanaka fits this linearity to experimentally determined glass transition temperatures of a set of chalcogenides and organic compounds resulting in the equation

$$ln(T_g) \cong 1.6 \cdot \overline{r} + 2.3.$$
(5.7)

## 5.3 Gibbs DiMarzio equation

A much more successful formula for the description of the compositional dependence of the glass transition temperature was found by Gibbs and DiMarzio [82, 140]. Their theory was based on statistical mechanics, i. e. equilibrium principles instead of a kinetic approach. They described the glass transition of polymers by the crosslinking of long chains of a certain length and stiffness. The mechanism for stress relaxation was identified by the shifting of one chain over another. For this to take place another configuration needs to be accessible, meaning there has to be both enough thermal energy for the bonds rotating on the chain and sufficient free volume providing free sites for the atoms of the chain to move to. The model results in the following formula for the glass transition temperature  $T_g$  of the crosslinked glass

$$T_g = \frac{T_0}{1 - \kappa X},\tag{5.8}$$

where  $T_0$  is the glass transition temperature of the non-crosslinked parent chain,  $\kappa$  is a constant and X is the density of crosslinking chain units relative to the total number of

units. This model proved to work well for long chains. For glasses with a high degree of crosslinking, however, the assumed mechanisms of stress relaxation might not be applicable.

## 5.4 Modified Gibbs DiMarzio equation

Much later Varshneya et al. [141] modified the Gibbs-DiMarzio equation, Eq. (5.8), to include the crosslinking in terms of the average coordination number  $\bar{r}$  for chalcogenide glasses. For this the crosslink density X is redefined to be equal to the average coordination number of the composition less the coordination number of the parent chalcogenide chain, i. e. 2:

$$T_g = \frac{T_0}{1 - \beta(\overline{r} - 2)}. ag{5.9}$$

In contrast to the old definition the new one handles a fourfold coordinated atom, like Ge, to be twice as effective in crosslinking as a threefold coordinated atom, like Sb. Moreover, the replacement of the old constant  $\kappa$  by a new one,  $\beta$ , is more than just a nominal one, but shall also represent a change of view: while Gibbs and DiMarzio stated  $\kappa$  as a universal constant, Varshneya et al. consider  $\beta$  to be only a system constant. For several chalcogen-rich alloys, like GeSbSe and GeSbSeAsTe, it has been possible to fit the increase of the glass transition temperature with increasing average coordination number well with Eq. (5.9).

## 5.5 Stochastic agglomeration theory

After the Gibbs-DiMarzio equation had been adapted to covalently bonded glasses at first in a quite empirical way, some years later Kerner and Micoulaut gave a theoretical foundation for this formula, Eq. (5.9), by developing the stochastic agglomeration theory (SAT) [142, 143].

In this theory the time dependence of the fluctuations of the local configuration is evaluated based on the probabilities for the formation of the possible covalent bonds. These probabilities are assumed to be proportional to the relative concentrations of the atoms involved, their valencies and a Boltzmann factor involving the respective bond energies. The minimization of the configurational fluctuations yields a metastable configuration. The presence of a stable (attractive) solution of this minimization problem is interpreted as the manifestation of the tendency of the system to become structurally arrested or trapped in an amorphous state.

For a binary chalcogenide  $A_{1-x}C_x$  in the limit of high chalcogen concentrations ( $x \cong 1$ ) the following parameter-free equation is predicted by the stochastic agglomeration

## 5.5. STOCHASTIC AGGLOMERATION THEORY

theory to describe the change of the glass transition temperature  $T_g$  with varying average coordination number  $\bar{r}$  of the alloy.

$$\frac{dT_g}{d\overline{r}}\Big|_{\overline{r}=r_C} = \frac{T_0}{(r_A - r_C) \cdot \ln(\frac{W_{AC}}{2 \cdot W_{CC}})}.$$
(5.10)

The variation of the glass transition temperature with respect to the glass transition temperature of the pure chalcogen glass  $T_0$  is entirely controlled by connectivity, i. e. the coordination number of the chalcogen atoms and the modifier atoms,  $r_C$  and  $r_A$ , respectively. Neither kinetic nor thermal contributions arise. Also the bond energies do not appear in the equation, although they are used in its derivation. Instead the entropy of the network  $\Delta S_{AC}$ , which is based on  $W_{AC}$  and  $W_{CC}$ , the number of equivalent ways A and C atoms can join each other to built A-C and C-C bonds, is part of the denominator of Eq. (5.10):

$$\Delta S_{AC} = \ln(\frac{W_{AC}}{2W_{CC}}) = \ln(\frac{2r_A r_C}{2r_C^2}) = \ln(\frac{r_A}{r_C}). \tag{5.11}$$

Substitution into Eq. (5.10) yields

$$\frac{dT_g}{d\bar{r}}\Big|_{\bar{r}=r_C} = \frac{T_0}{(r_A - r_C) \cdot \ln(\frac{r_A}{r_C})}.$$
(5.12)

The first order Taylor expansion of the modified Gibbs-DiMarzio equation, Eq. (5.9), in the vicinity of the pure chalcogen region, i. e. near  $\bar{r} = r_C$ , gives a linear dependence on the average coordination number  $\bar{r}$ :

$$T_q \cong T_0 \left[ 1 + \beta(\overline{r} - 2) \right] . \tag{5.13}$$

The comparison of the slope of this line with Eq. (5.12) allows the identification of the constant  $\beta$  as

$$\beta \cong \frac{1}{(r_A - r_C) \cdot \ln(\frac{r_A}{r_C})}.$$
 (5.14)

A comparison of the slope calculated in the framework of the stochastic agglomeration theory with the experimentally observed one has shown excellent agreement for  $Si_xTe_{1-x}$ ,  $Ge_xTe_{1-x}$ ,  $Ga_xTe_{1-x}$ ,  $As_xS_{1-x}$ ,  $Ge_xSe_{1-x}$ ,  $Si_xSe_{1-x}$ ,  $As_xSe_{1-x}$  and  $P_xSe_{1-x}$  for x near zero. [143]. However, the relative maximum in glass transition temperature at lower chalcogen contents, as it occurs for many covalent glasses, cannot be predicted by such a random covalent network approach. The position of such a maximum rather implies a chemically ordered covalent network (COCN) [144]. The latter model is based on the assumption of a glass being composed of cross-linked stable chemical compounds surrounded by excess elements dispersed among these units. Lucovsky et al. [145] applied this idea to the structural interpretation of infrared and Raman spectra in  $Ge_{1-x}S_x$  (with  $0.90 \ge x > 0.67$ ) postulating each Ge atom being bonded to four

S atoms and the resulting GeS<sub>4</sub> tetrahedra being interconnected by chains of S atoms. Within the COCN model the relative maximum in the glass transition temperature's dependence on an alloy's stoichiometry is identified as a chemical threshold. It corresponds to compositions that can be formed solely with heteronuclear bonds. Tichy and Ticha clearly demonstrated the validity of this correlation for the GeSbSe, GeGaSe and GeInSe systems [146].

## 5.6 Glass transition and bond energy

All preceding models do not distinguish elements of the same group, e.g. Te from Se, in their predictions of the glass transition temperature, with the exception that the Gibbs-DiMarzio equation, valid only for chalcogen-rich alloys, relates  $T_g$  to different  $T_0$  according to the parent chalcogens. It was again Tichy and Ticha [147] who overcame this limitation. They started from the concept that coming from low temperatures to reach the glass transition an energy barrier has to be overcome which represents two steps of softening: the first being the creation of mobile entities by breaking the network apart, the second being the reorientation of the entities to move. Supposing that the first contribution is dominant, the activation barrier is further assumed to be proportional to the overall mean bond energy  $\overline{E}_{bond}$ , which is a function of the average coordination number, the type of bonds, the degree of cross-linking and the bond energies.

Regarding coordination numbers for elements from group IVB, VB and VIB the 8-N rule is applied as it is described above in the context of Phillips' constraint theory (Sec. 5.1) leading to four-, three- and twofold coordination, respectively. In chalcogenides containing elements from group IIIB, i. e. Ga and In, however, these elements are assumed to be fourfold coordinated due to the formation of dative bonds, i.e. using two electrons of a chalcogen atom, that are not taking part in its "normal" two bonds. The coordination number of those chalcogen atoms donating two electrons to an additional bond with a group IIIB element is increased accordingly. The justification for those dative bonds is given by Liu and Taylor, who stated such a formal charge transfer in their work on a general structural model for semiconductor glasses [148]. Based on Extended X-ray Absorption Fine Structure (EXAFS) measurements they found threeand four-fold coordination of Se atoms in CuAsSe and CuAsS glasses to be determined by the copper concentration, while a fourfold coordination of Cu atoms has been confirmed for Cu concentrations up to 25 atomic percent. In case of an exhaustion of chalcogen atoms Liu and Taylor claim As atoms to provide the electrons for dative bonds with group IB, IIB or IIIB elements increasing the coordination number of As from three to four.

For the counting of the type of bonds and the calculation of the degree of crosslinking Tichy and Ticha state the alloys' preference for heteronuclear chalcogen bonds. Only atoms that cannot find a partner for such a covalent bond are allowed to bond to each other.

Finally a specific energy is linked to each bond.<sup>1</sup> Thus there is a clear distinction between different elements from the same group. The overall mean bond energy is calculated as the weighted average of the energies of the various bonds formed in the glass, weighted according to the number of realizations of the respective bond. The comparison of the glass transition temperature  $T_g$  with this overall mean bond energy  $\overline{E}_{bond}$  for 186 binary and ternary chalcogenide glasses produced empirical evidence for a linear relationship between both values:

$$T_g \cong 311 \,\mathrm{K/eV} \cdot \left(\overline{E}_{bond} - 0.9 \,\mathrm{eV}\right) \,. \tag{5.15}$$

From this Tichy and Ticha concluded that the overall compositional trend in the glass transition temperature is influenced mainly by the chemical bond arrangement. The latter probably is also the main reason, why the correlations Lasocka [149] found for some chalcogen glasses could not succeed in predicting the occurrence of features at the chemical threshold. He compared  $T_g$  of an alloy with the atomization enthalpy  $\overline{H}_{at}$ , that he calculated based on its composition. However, his calculation oversimplifies the situation in an alloy by approximating the atomization enthalpy of a composition by the weighted average of the atomization enthalpies  $H_{at,i}$  of its components i

$$\overline{H}_{at} = \sum_{i} x_i H_{at,i} \,. \tag{5.16}$$

The weighting is done according to the atomic fractions  $x_i$  of the components.

Nevertheless, an approach [150] via a composition's enthalpy of atomization, indeed calculated in a more bond oriented and thus more sophisticated way compared to what Lasocka did, renders the prediction of  $T_g$  possible. This will be shown in the next chapter.

<sup>&</sup>lt;sup>1</sup>Unfortunately publication [147] only states the values used for the bond energies, but does not mention the source.

## Chapter 6

## The Model Used

Hypothesen sind Netze; nur der wird fangen, der auswirft.

Novalis

Each of the concepts on glass transition described in chapter 5 is able to explain some characteristic features in the dependence of a material's glass transition temperature on its composition. The most promising approach for a prediction of this temperature, especially with respect to the applicability to a wide range of materials, seems to be its correlation with the enthalpy of atomization [150] representing the cohesive energies that stabilize an amorphous structure [151].

In order to calculate the enthalpy of atomization for a given composition it is assumed that in a covalent material virtually this whole enthalpy can be represented by the sum of the enthalpies of all covalent bonds formed in the system, as suggested by Bicerano and Ovshinsky [151]. This obviously neglects the contribution of electron correlations, apart from the formation of covalent bonds, that also stabilize the system. While this assumption of course breaks down for molecular solids, like pure sulfur, where it is sufficient to break the weak Van der Waals interactions between the basic molecules to melt the solid, it has been demonstrated to be a reasonable approximation for glasses that are dominantly covalently bonded [151].

For the summation of the bond enthalpies two sets of data are necessary: On the one hand the number of bonds of each type  $n_{AB}$  has to be counted, the index referring to a bond between element A and B. On the other hand a specific bond enthalpy  $H_{AB}$  has to be identified with each bond type. Then the total bond enthalpy  $H_{tot}$  for a given composition is determined by:

$$H_{tot} = \sum_{A,B} n_{AB} H_{AB} . \tag{6.1}$$

The counting of bonds is based on a preferred coordination number  $r_A$  for each element A, which is determined by the number of its valence electrons N. For elements

from group IVB, VB and VIB the 8-N rule is applied, yielding a coordination number of 4, 3 and 2, respectively. For elements from group IB, IIB and IIIB, however, a formal charge transfer of otherwise non-bonding valence electrons from group VIB or, if not available, from group VB atoms is applied [148], so that elements from group IB, IIB and IIIB always end up to be fourfold coordinated. Each of such bonds based on transfer charges of course acts as an additional bond of the electron donating atom, too. Thus group VB and VIB atoms can participate in one or two charge transfers, respectively, before reaching the maximum covalent coordination of four themselves. Due to the assumption of this mechanism the whole model is inapplicable for compositions with an average number of valence electrons of  $\overline{N} < 4$ , because there would be not enough group VB or VIB atoms available to transfer charges to group IB, IIB or IIIB atoms. Fortunately good phase change materials, which are under consideration for being doped with further elements, usually contain high amounts of group VIB or VB elements (see section 2.1.2) and therefore are well above this critical number of four valence electrons.

Based on this predefinition of the total number of available bonding partners the formation of bonds, i. e. the connection of two "loose ends" for each bond, is assumed to follow two rules [150, 151]:

- 1. The priority of hetero-nuclear over homo-nuclear bonds.
- 2. The preference of stronger bonds, meaning bonds of higher enthalpy, over weaker bonds.

The first rule has been assumed to be valid already when Zachariasen proposed his covalently bonded continuous random network model [152]. It is equivalent to expecting chemical ordering to be predominant. The first rule also excludes the possibility of phase separation or even the formation of a molecular solid, like solid sulfur composed out of  $S_8$  units, but claims instead a homogeneous mixture of the elements.

Due to the second rule already in the formation of bonds a data basis of bond enthalpies becomes important. The homo-nuclear bond enthalpies of group IVB, VB and VIB elements are calculated from literature values for the enthalpy of atomization by dividing the latter by half of the coordination number, again following the 8 - N rule [150]. The factor one half accounts for the fact that two atoms participate in each covalent bond. Table 6.1 shows the enthalpy of atomization<sup>1</sup>, the coordination number

<sup>&</sup>lt;sup>1</sup>Values are taken from http://www.webelements.com. Therein referred to both A.M. James and M.P. Lord in Macmillan's Chemical and Physical Data, Macmillan, London, UK, 1992 and H. Ellis (Ed.) in Nuffield Advanced Science Book of Data, Longman, London, UK, 1972.

**Table 6.1:** Enthalpy of atomization  $H_{atom}$ , coordination number n, homo-nuclear bond enthalpy  $H_{bond}$  and electronegativity EN for group IVB, VB and VIB elements.

Element	Si	Ge	As	Sb	Se	Те
$H_{atom}$ (kJ/mol)	456	377	302	262	227	197
n	4	4	3	3	2	2
$H_{bond}$ (eV/bond)	2.36	1.95	1.81	2.09	2.35	2.04
EN	1.9	2.01	2.18	2.05	2.55	2.1

**Table 6.2:** Homo-nuclear bond enthalpy  $H_{bond}$  and electronegativity EN for group IB, IIB and IIIB elements. The value for the bond enthalpy of Cu equals the mean of the two values provided in [150].

Element	Al	Ga	In	Cu
$\overline{H_{bond} \text{ (eV/bond)}}$	1.10	0.93	0.52	-0.25
EN	2.18	1.61	1.78	1.9

and the homo-nuclear bond enthalpy calculated from the first two numbers for several elements from the periodic table.

Pauling's equation [153] is used to relate the enthalpy of a hetero-nuclear bond  $H_{AB}$  to the homo-nuclear bond enthalpies  $H_{AA}$  and  $H_{BB}$  and the electronegativities  $EN_A$  and  $EN_B$  of the bonding partners:

$$H_{AB} = (H_{AA} + H_{BB})^2 + 96.14 \frac{\text{kJ}}{\text{mol}} \cdot (EN_A - EN_B)^2.$$
 (6.2)

The homo-nuclear bond enthalpy for group IB, IIB and IIIB elements used in this work have been derived by Lankhorst [150] from the enthalpies of atomisation of *compounds* of the respective element with elements, of which the homo-nuclear bond enthalpy is known (Table 6.1), using Pauling's equation, Eq. (6.2). For a selection of four elements the resulting bond enthalpies are given in Table 6.2.

The set of bond enthalpies derived in this way differs from the source the calculations of both the overall mean bond energy by Tichy and Ticha [147] and the cohesive energy by Bicerano and Ovshinsky [151] are based on. They used energy values for single bonds derived from the dissociation of *molecules* [153], which might be not the best choice for dealing with covalent bonds in *solids*.

After the sum of all bond enthalpies in a material of arbitrary composition is determined following the hierarchy of bonds mentioned above, it needs to be related quantitatively to the glass transition temperature of that material. In order to establish such a connection, experimentally determined glass transition temperatures of many chalcogenide glasses have been compared with the enthalpy of atomization calculated as described in this chapter. This comparison revealed a linear relation between both quantities, which could be fitted by the following equation:

$$T_{g} = 3.44 \frac{K}{\frac{kJ}{mol}} \cdot H_{tot} - 480 K$$

$$= 332 \frac{K}{\frac{eV}{atom}} \cdot H_{tot} - 480 K$$

$$= 332 \frac{K}{\frac{eV}{atom}} \cdot (H_{tot} - 1.45 \frac{eV}{atom}).$$
(6.3)

This empirical relationship is used to predict the glass transition temperature of a material based on its total bond enthalpy, which in turn is calculated from its composition.

The summation of the enthalpy of all individual bonds in a covalent solid accounts for the increase of the glass transition temperature not only with a higher number of bonds but also with increased bond strengths. Thus the enthalpy of atomization should even be able to indicate the features of the glass transition temperature at the chemical threshold, where the stronger hetero-nuclear bonds are predominant compared to the weaker homo-nuclear ones. The biggest advantage of the algorithm presented in this chapter over the stochastic agglomeration theory is the larger versatility in contrast to SAT's limitation to chalcogen-rich alloys.

# Chapter 7

# Comparison with Glass Transition Temperatures

The great tragedy of science - the slaying of a beautiful hypothesis by an ugly fact.

T. H. Huxley

Lankhorst was the first who applied the empirically observed correlation between the atomization enthalpy and the glass transition temperature, Eq. (6.3), to make quantitative predictions for the shift of the regime of stability against crystallization upon changes in stoichiometry [150]. He argued that because at "normal" heating rates amorphous materials would "generally" crystallize "just above" the glass transition temperature this temperature could be seen as a lower limit for the crystallization temperature<sup>1</sup>. Furthermore, he recognized that crystallization below the glass transition temperature is much slower than for higher temperatures because of the high activation energy for atomic rearrangements. From that fact he concluded that the glass transition temperature was a good parameter for a "first-order estimation of the archival life stability" of data storage media using phase change materials.

For checking the performance of such predictions Lankhorst first compared experimentally determined glass transition temperatures with the according calculated values for some materials. After coming to a satisfying result there, he predicted glass transition temperatures for phase change materials and compared them with crystallization temperatures of sputter deposited thin films of the respective compositions measured at a heating rate of 20 K/min. Here he found that for all these materials the experimentally determined crystallization temperature is, with only one exception, "typically" 50 to 100 K higher than the calculated glass transition temperature. Remarkably this was

 $<sup>^{1}</sup>$  The crystallization temperature in this context is understood to be the one observed for heating rates comparable to those used for measurements of the glass transition temperature.

not interpreted as a contradiction against the earlier statement of amorphous materials "generally" crystallizing "just above" the glass transition temperature. Instead, the difference of the two temperatures was regarded as supporting the statement that the glass transition temperature can be seen as a lower limit for the crystallization temperature at "normal" heating rates.

At first glance one might think, that the combination of the two above statements simply defines the understanding of "just above" to be "50 to 100 K". The impression is left that the model actually predicts the glass transition temperature rather well also for phase change materials, one just has to add the "typical" temperature difference between crystallization and glass transition in order to yield the crystallization temperature at "normal" heating rates. The arguments put forward in this chapter, however, will not only show that this interpretation is not correct, but shall lead to a deeper understanding of the uniqueness of the properties of phase change materials.

It is important to see that Lankhorst did not distinguish between chalcogenide glasses in general and phase change materials in particular. The crucial step in his argumentation is the assumption of the *same* connection between crystallization and glass transition for both groups of materials.

The data basis for the empirical linear relation between a material's glass transition temperature and the calculated atomization enthalpy naturally consisted of alloys that have been experimentally accessible and therefore can be produced rather easily as a glass. The typical way of preparing glasses is melt-quenching of a bulk sample, weighing at least around one milligram, in order to provide a good signal-to-noise ratio when its glass transition is calorimetrically investigated. The fact that materials can be prepared via the common way of melt-quenching means that these materials can be categorized as rather good glass formers. In other words, the temperature range between melting temperature and glass transition temperature is crossed without crystallization despite an only moderately shortened time the material is in that region. This implies that these materials' tendency to crystallize can be ranked as relatively low compared to phase change materials. The latter are actually useful for data storage applications especially due to their fast crystallization speeds.

In contrast, in order to amorphize a phase change material cooling rates are required that are several orders of magnitude higher than those realized inside of bulk samples during common melt-quenching. It requires a very small volume of phase change materials from which the heat can be drained fast enough to reach these cooling rates. Laser amorphization of few square micrometer large areas of some tens of nanometer thin films is accomplished only with substrates with high thermal conductivity which act as an effective heat sink. The only alternative for preparing a macroscopic vol-

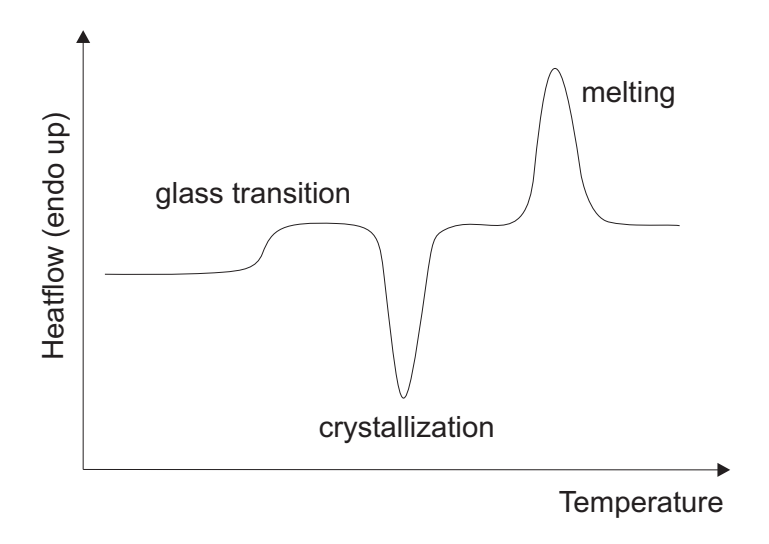


Figure 7.1: Schematic of the heat flow into an initially amorphous sample while heating with a constant rate, a measurement often performed with a Differential Scanning Calorimeter (DSC). The glass transition is measured as an endothermic step, since the heat capacity of the liquid phase is higher due to the addition of mainly configurational entropy compared to the glass (see Fig. 3.3). For good glass formers the glass transition takes place significantly before the crystallization. In this case the decrease of the network's rigidity after the glass transition evolves too slowly for an immediate crystallization bringing the material into its energetically more favourable state. In contrast to crystallization, glass transition and melting are both endothermic processes. In reality heat flow signals from crystallization and melting are usually much stronger than that from the glass transition.

ume of phase change material in its amorphous state is continuous cooling during the deposition of the material from the plasma or the gas phase.

This difference between good glass formers and phase change materials in their tendency to crystallize becomes obvious considering the pronounced difference in calorimetric measurements. Good glass formers show a clear separation of the glass transition from crystallization when heated at rates typical for annealing macroscopic samples inside of a furnace, i. e. less than 500 K/min [154, 155, 156]. This behaviour is visualized in the schematic of a characteristic heat flow signal during an annealing with constant heating rate in Fig. 7.1. An according experiment could for example be performed with a differential scanning calorimeter. So having an interval of 50 to 100 K between glass transition and crystallization is not uncommon in good glass formers such as various sulfides and selenides. For some good glass formers it is even necessary to strongly reduce the cooling rate in order to realize crystallization when cooling down from the liquid phase.

Phase change materials however behave very different. Very recently Kalb [157] investigated the heat flow signal for a small selection of phase change materials focusing

on the temperature range just below the crystallization temperature. Fig. 7.2 (left) shows exemplarily the results for  $Ge_2Sb_2Te_5$ . The amorphous as-deposited samples of  $Ge_1Sb_2Te_4$ ,  $Ge_2Sb_2Te_5$  and  $Ge_4Sb_1Te_5$  did not show any endothermic step before crystallization, which would otherwise indicate a glass transition. From this experimental evidence the existence of a glass transition must be excluded for these materials, at least in a temperature range more than 20 K below the crystallization temperature <sup>2</sup>. Instead, already up to 90 K below the crystallization peak structural relaxation in the amorphous phase was observed as an exothermic shoulder in the heat flow signal.

However, in the same work other samples of these compositions were pre-annealed at elevated temperatures for almost two days in order to let the amorphous phase structurally relax as far as possible, yet without crystallizing them. In the subsequent temperature scans (Fig. 7.2, right) the exothermic shoulder of structural relaxation had disappeared in the heat flow signal. Additionally, the onset of an endothermic step emerged around 30 K below a crystallization peak, which itself had shifted around 10 K towards higher temperatures compared to the crystallization of the not pre-annealed samples. The endothermic step indicating the glass transition was not completed before the strong exothermic signal from crystallization emerged.

How these results can be interpreted is probably best explained with the help of a graph that shows how the structural rigidity evolves depending on the different thermal treatments of the samples, because it is this physical property that both hinders crystallization and undergoes a change by glass transition and also by relaxation. Figure 7.3 is such a graph plotting the viscosity versus the reciprocal temperature. It shows, that the onset of the glass transition is not revealed for the pre-annealed sample simply because the crystallization peak in the heat flow signal is shifted towards higher temperatures, but because the glass transition temperature itself has dropped significantly, i.e. by more than 10 K, upon the structural relaxation during pre-annealing. The conclusion of Kalb that in phase change materials, at least in those he investigated,  $T_q$  is within 10 K of the crystallization temperature upon continuous heating at 40 K/min is not the whole truth. There is actually no indication for a glass transition taking place before crystallization in the as-deposited amorphous samples. Thus for these samples it cannot be differentiated between a crystallization coinciding with glass transition on the one hand and the respective phase change materials crystallizing even before the onset of a glass transition on the other.

However, Kalb's experiments do not only remind of the fact that the glass transi-

<sup>&</sup>lt;sup>2</sup>The strong crystallization peak could hide the rather weak signal from a glass transition in its direct proximity. However, around 20 K below its center the signal from the crystallization peak is too small to be able to disguise the glass transition.

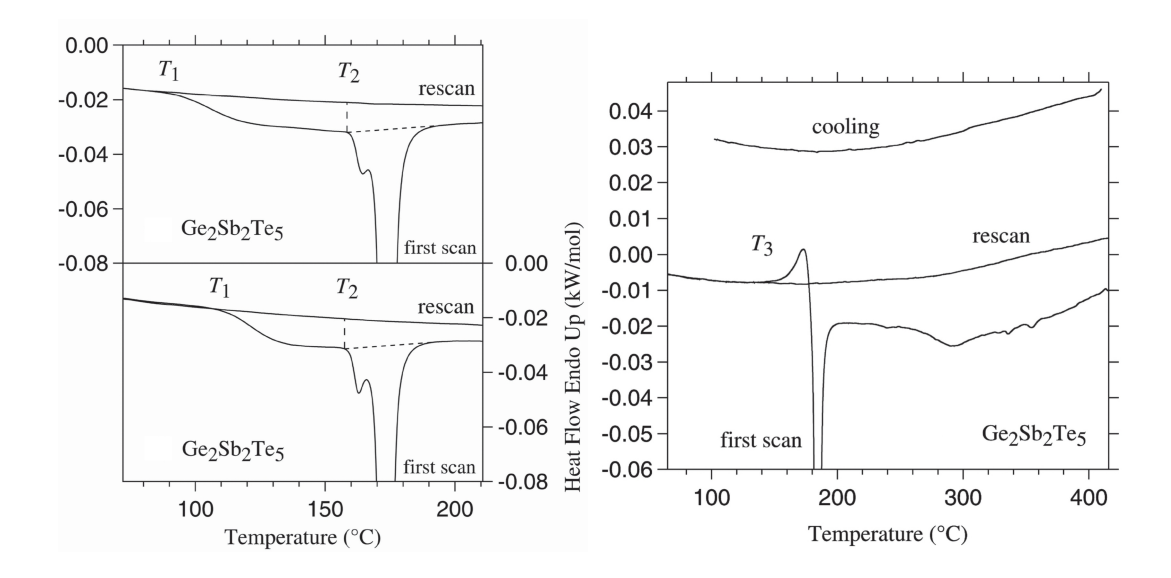


Figure 7.2: Heat flow results of  $Ge_2Sb_2Te_5$  from Kalb [157]. Heat flow as a function of temperature (left:) for a three days old (top) and a 39 days old (bottom) as-deposited amorphous sample and (right:) for a sample that had been pre-annealed for 37 hours at 387 K before the heat flow experiment. The heating rate was 40 K/min for all experiments. The rescan serves as a baseline for the first scan, revealing the onset of structural relaxation at  $T_1$ , of surface crystallization at  $T_2$  and of the glass transition temperature at  $T_3$ .

tion temperature varies for glasses that differ solely in their degree of relaxation. They also reveal that for phase change materials glass transition and crystallization are at least in direct proximity, likely even coinciding with each other. Lankhorst's assumption of phase change materials generally showing glass transition 50 to 100 K below crystallization is clearly wrong. Based on this insight it is advisable to review the correlation of the predictions of the glass transition temperature with experimental values of this quantity for phase change materials. For a lack of alternatives the compositions from the experimental work discussed above [157] are chosen for a comparison with the calculations based on the enthalpy of atomization.

Figure 7.4 shows a ternary diagram of the glass transition temperature for the Ge-Sb-Te system calculated in the way described in chapter 6. Such diagrams can be automatically generated for an arbitrary set of elements by a code that has been programmed by the author of this thesis using Matlab, a numerical computing environment. A general increase of the glass transition temperature for a higher atomic percentage of Ge in the alloy is striking. Red marks in Fig. 7.4 indicate where the three different stoichiometries of GeSbTe investigated in [157] are located. From their positions one can already qualitatively state an increase of the glass transition temperature in the sequence Ge<sub>1</sub>Sb<sub>2</sub>Te<sub>4</sub>, Ge<sub>2</sub>Sb<sub>2</sub>Te<sub>5</sub> and Ge<sub>4</sub>Sb<sub>1</sub>Te<sub>5</sub>.

To calculate the glass transition temperature an accurate book-keeping is required

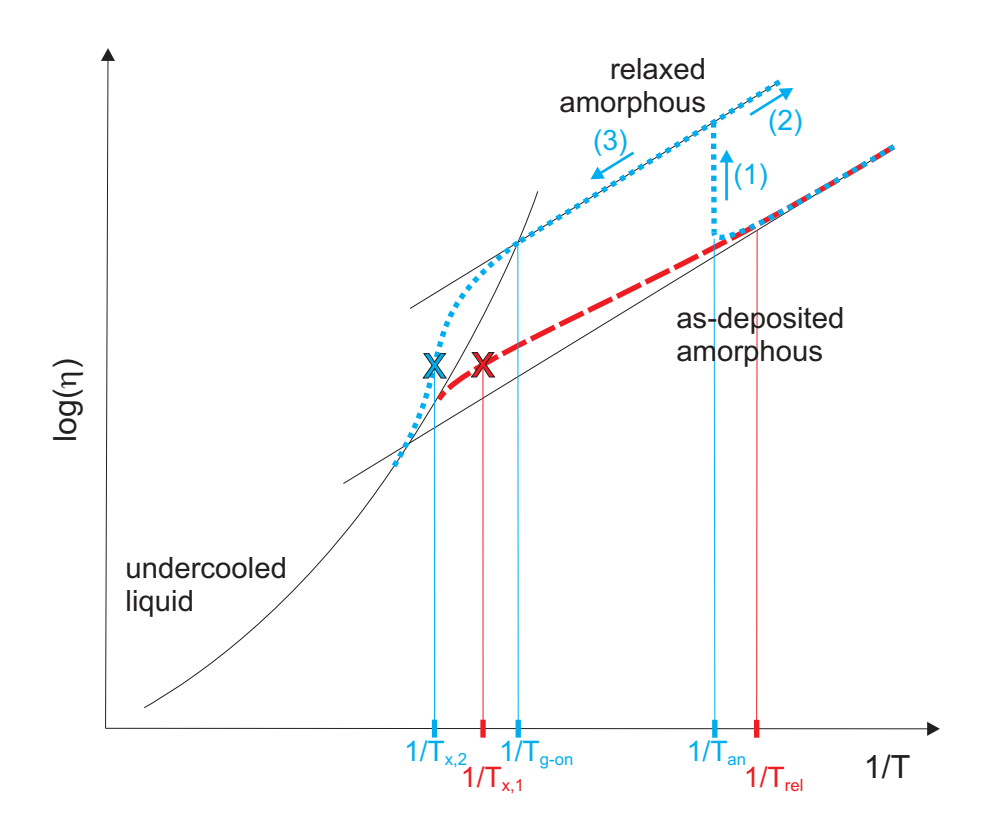
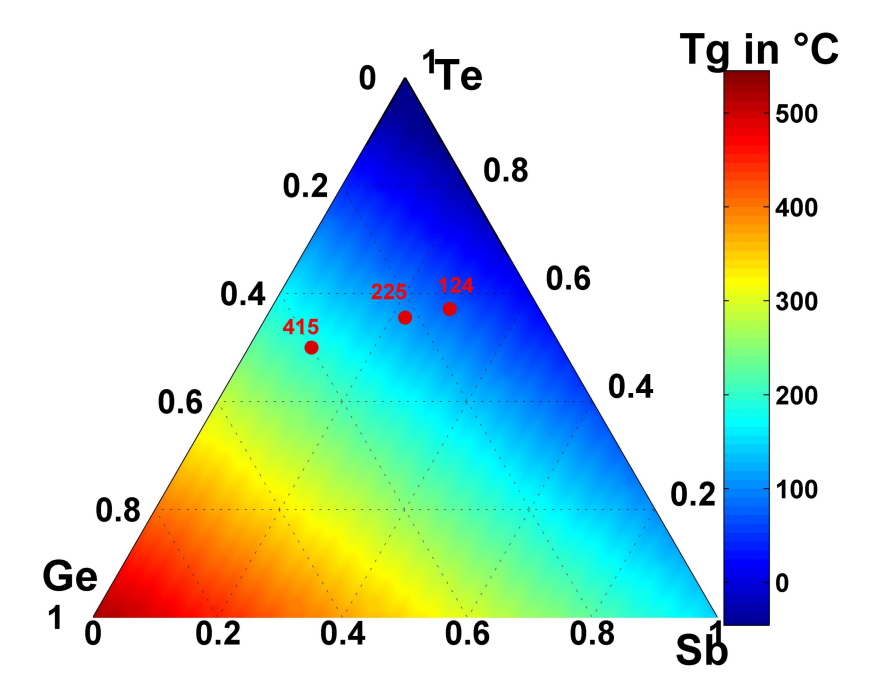


Figure 7.3: Viscosity plot explaining relaxation, glass transition and crystallization measurements in Fig. 7.2. The red, dashed line represents the heating experiment of an as-deposited sample, where only structural relaxation can be observed starting at temperature  $T_{rel}$  (equal to  $T_1$  in Fig. 7.2) and ending with crystallization at  $T_{x,1}$ . The blue, dotted curve describes what happens to the pre-annealed sample. It is kept at the annealing temperature  $T_{an}$  for a long time (1) and cooled down (2) before it is heated up again beyond its crystallization temperature  $T_{x,2}$ . The structural relaxation during the pre-annealing increases the viscosity of the glass. As a consequence the viscosity curve of the undercooled liquid phase is met at a lower temperature than it would have been the case for the first sample, if crystallization had not interfered before. Actually, the onset of the glass transition in the structurally relaxed sample takes place even at a lower temperature  $T_{g-on}$  than the crystallization temperature in the as-deposited sample. The completion of the glass transition is intercepted by the crystallization of the sample at  $T_{x,2}$ .



**Figure 7.4:** Ternary diagram of calculated glass transition temperatures for the GeSbTe system. The stoichiometries of Ge<sub>1</sub>Sb<sub>2</sub>Te<sub>4</sub>, Ge<sub>2</sub>Sb<sub>2</sub>Te<sub>5</sub> and Ge<sub>4</sub>Sb<sub>1</sub>Te<sub>5</sub> are marked by red dots.

for the type of bonds that are realized, their number and their enthalpies. This information is saved in a log file together with the according arguments that lead to the decision to form a distinct number of bonds of a certain type, e.g. its comparably large strengths or the depletion of one of the bonding partners. Table 7.1 is an excerpt of the log files for the three compositions mentioned above.

Because Ge-Te is the strongest hetero-nuclear bond, it is formed as long as both Ge and Te atoms are available. In the case of Ge<sub>1</sub>Sb<sub>2</sub>Te<sub>4</sub> and Ge<sub>2</sub>Sb<sub>2</sub>Te<sub>5</sub> all Ge atoms are completely surrounded by Te atoms. This means that the chemical ordering results in Ge only occurring inside of GeTe<sub>4</sub> tetrahedrons. The remaining open bond arms of Te atoms then form bonds to Sb atoms. The Sb atoms that so far did not find a bonding partner form homo-nuclear bonds. So in the framework of the model used the higher glass transition temperature of Ge<sub>2</sub>Sb<sub>2</sub>Te<sub>5</sub> compared to that of Ge<sub>1</sub>Sb<sub>2</sub>Te<sub>4</sub> has its origin in the larger number of strong Ge-Te bonds, which in turn are possible due to the higher portion of Ge atoms in the alloy. This can even compensate the partial substitution of Sb-Te bonds by energetically less favourable Sb-Sb bonds.

Although the reason for  $Ge_4Sb_1Te_5$  having the highest glass transition temperature of all three compositions can essentially be attributed again to the even higher amount of Ge-Te bonds, its bond arrangement deserves an additional remark. Unlike in  $Ge_1Sb_2Te_4$  and  $Ge_2Sb_2Te_5$  the Ge content in  $Ge_4Sb_1Te_5$  is so high that Te is depleted

Table 7.1: Calculated glass transition temperature  $T_g$  and total bond enthalpy  $H_{tot}$  for three GeSbTe alloys. The number of bonds of each type  $n_{AB}$  and the enthalpy contributed from each bond type to the total bond enthalpy  $n_{AB}H_{AB}$  is given. The sequence in which the bonds are listed from top to bottom accounts for their preference of formation in the model used.

Composition	$T_g$	$H_{tot}$	bonding	$n_{AB}$	$n_{AB}H_{AB}$
	K	$\mathrm{kJ/mol}$	elements		$\mathrm{kJ/mol}$
$Ge_1Sb_2Te_4$	350	241	GeTe	0.57	110
			SbTe	0.57	106
			$\operatorname{GeSb}$	-	-
			TeTe	-	-
			GeGe	-	-
			SbSb	0.14	25
$Ge_2Sb_2Te_5$	384	251	GeTe	0.89	171
			SbTe	0.22	41
			$\operatorname{GeSb}$	-	-
			TeTe	-	-
			GeGe	-	-
			SbSb	0.22	39
$Ge_4Sb_1Te_5$	464	274	GeTe	1.00	192
			SbTe	-	-
			$\operatorname{GeSb}$	0.3	54
			TeTe	-	-
			GeGe	0.15	28
			SbSb	-	-

first, even though the atomic fraction of Te in the alloy is higher than the Ge fraction. The fourfold coordination of group IVB elements leads to the fact that unbonded Ge atoms remain when all twofold coordinated Te atoms are already saturated. These Ge atoms are then free to bond to Sb. In the case of  $Ge_4Sb_1Te_5$  the 10% Sb are even to few to serve as hetero-nuclear bonding partners for all open Ge valences, resulting in an additional small number of homo-nuclear Ge bonds.

For a comparison Fig. 7.5 plots the glass transition temperatures resulting from the calculations (Table 7.1) against the temperatures, where the onset of a glass transition was detected experimentally (Fig. 7.3). The calculated glass transition temperature can be assessed to be in good agreement with the experiment for Ge<sub>4</sub>Sb<sub>1</sub>Te<sub>5</sub>, not only

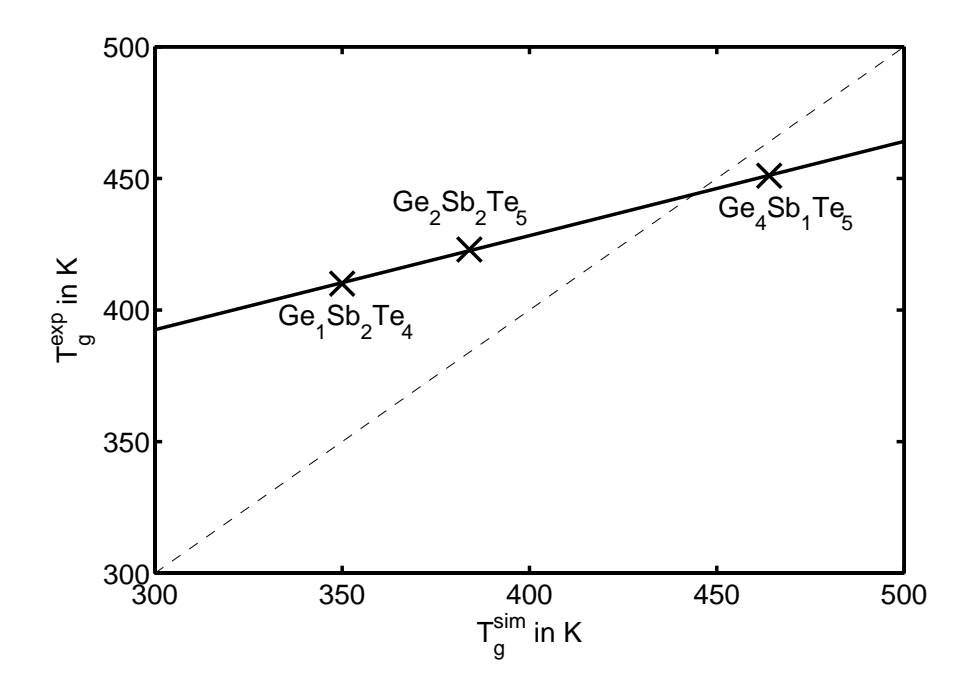


Figure 7.5: Comparison of the predicted glass transition temperatures  $T_g^{sim}$  for  $Ge_1Sb_2Te_4$ ,  $Ge_2Sb_2Te_5$  and  $Ge_4Sb_1Te_5$  with the respective experimental data  $T_g^{exp}$  from [157, 69]. The dashed line indicates perfect matching between simulation and experiment. A linear fit (solid line) resulted in the following relation:  $T_g^{exp} = 0.36T_g^{sim} + 285 \,\mathrm{K}$ .

because the experimental value represents the *onset* of the transition, but also since the not pre-annealed glass must have its glass transition at higher temperatures. In contrast, for Ge<sub>1</sub>Sb<sub>2</sub>Te<sub>4</sub> and Ge<sub>2</sub>Sb<sub>2</sub>Te<sub>5</sub> the prediction clearly underestimates the real value of the glass transition temperature.

It seems difficult to point at a single reason for this discrepancy. There are at least four different possible sources for errors in the calculation. The first is the data basis for the homo-nuclear bond enthalpies of the elements. In their derivation from experimental values of the enthalpy of atomization it is assumed that the all cohesive forces can be localized in the covalent bonds. The neglect of other contributions to the enthalpy of atomization, e. g. those from non-covalent electron correlations, is likely not equally large for all components. Especially for pure Te the conceptional limitation on two covalent bonds seems disputable [158]. While the role of the interactions between the chains of twofold coordinated atoms in elemental Te might be not negligible, the approximation of four covalent bonds per atom representing most of the cohesive enthalpy in solid Ge can be assessed to be much better. Thus, in the data basis for the model used to predict the glass transition temperature the bond enthalpy for Te bonds is likely overestimated compared to the one for Ge bonds.

A second source of error in the model could be an in fact limited validity of Pauling's

equation, Eq. (6.2), for covalent bonds in solids. The equation was established on the basis of data for the heat of formation of molecules [153]. Similar to the first argument, the presence of neighboring atoms might influence the strength of a bond between two atoms in a way, that is not taken into account by Pauling's equation.

Thirdly, the rules for the determination of the hierarchy of the possible bonds, i.e. the sequence of formation, in an alloy might be more strict than nature itself. The influence of chemical ordering, which is undoubtedly important, apparent in the occurrence of chemical thresholds (see chapter 5), might be exaggerated against the power of thermal activation and entropy. A concept that also takes into account the latter aspects without sacrificing its validity over a wide range of compositions, unlike the stochastic agglomeration theory, is truly desirable.

The fourth source of error is the linear fit to the empirical relation between the glass transition temperature and the calculated enthalpy of atomization. It is based on a limited set of data, which in individual cases already showed a significant deviation from the fit. Moreover, the underlying data for this fit did not contain any phase change material, which differ from other covalent glasses at least in the accessibility of an amorphous state from the melt as discussed above. It is conceivable that the cause for this difference could also result in a somewhat different correlation between glass transition temperature and enthalpy of atomization.

Whatever the reason is for the disagreement between the absolute values of predicted and measured glass transition temperatures, it is remarkable how well the trend in the experimental data is reproduced by the model. The data of the first comparison between calculated and experimental glass transition temperature for phase change materials (plotted in Fig. 7.5) follow suprisingly well a linear behaviour.

In view of this evaluation of the described model, the potential of this algorithm to predict glass transition temperatures for phase change materials can be estimated to be good for comparitive statements. However, the number of phase change materials for which an experimental glass transition temperature is available is very small. Therefore, an empirical adaption of the model to improve the absolute matching with experiments by changing parameters would be quite easy, but for the same reason rather senseless too. Thus the unmodified algorithm is used, when compositional trends of the stability against crystallization are investigated in the next chapter.

## Chapter 8

# Comparison with Crystallization Temperatures

After an overview has been given on various existing models dealing with the dependence of a material's glass transition temperature on its composition, one model has been explained in detail and its potential in the field of phase change materials has been evaluated. In this chapter finally the application, mentioned in the motivation at the very beginning of this second part of this thesis, can be addressed. The task is to improve known phase change materials regarding their thermal stability against crystallization by purposeful adding of further elements to the composition.

The model has been applied to many material systems by the author of this thesis in the course of his research at the IBM Almaden Research Center in San Jose, California, for identifying promising dopants and minimizing the number of uneffective experiments. Though, at this point only a set of four examples will be presented: Aland Cu-doping of both SbTe and GeSb. It will become evident in the course of this chapter, however, that these few examples alone demonstrate several different effects that occur in the context of doping of phase change materials.

For an overview of the compositional dependence of the calculated glass transition temperatures in a ternary alloy, the diagrams of the type of Fig. 7.4 are quite useful. Thus such figures are also created for the systems Al-Ge-Sb (Fig. 8.1), Cu-Ge-Sb (Fig. 8.2), Al-Sb-Te (Fig. 8.3) and Cu-Sb-Te (Fig. 8.4). They are based on the bond enthalpies listed in Tables 6.1 and 6.2. The color scales are optimized to show as many details as possible in each graph at the cost of direct comparability from one diagram to another.

As both Al and Cu are elements with less valence electrons than group IVB elements, in the framework of the model used they require transfer electrons via dative bonds from group VB or VIB elements in order to achieve a fourfold coordination. The

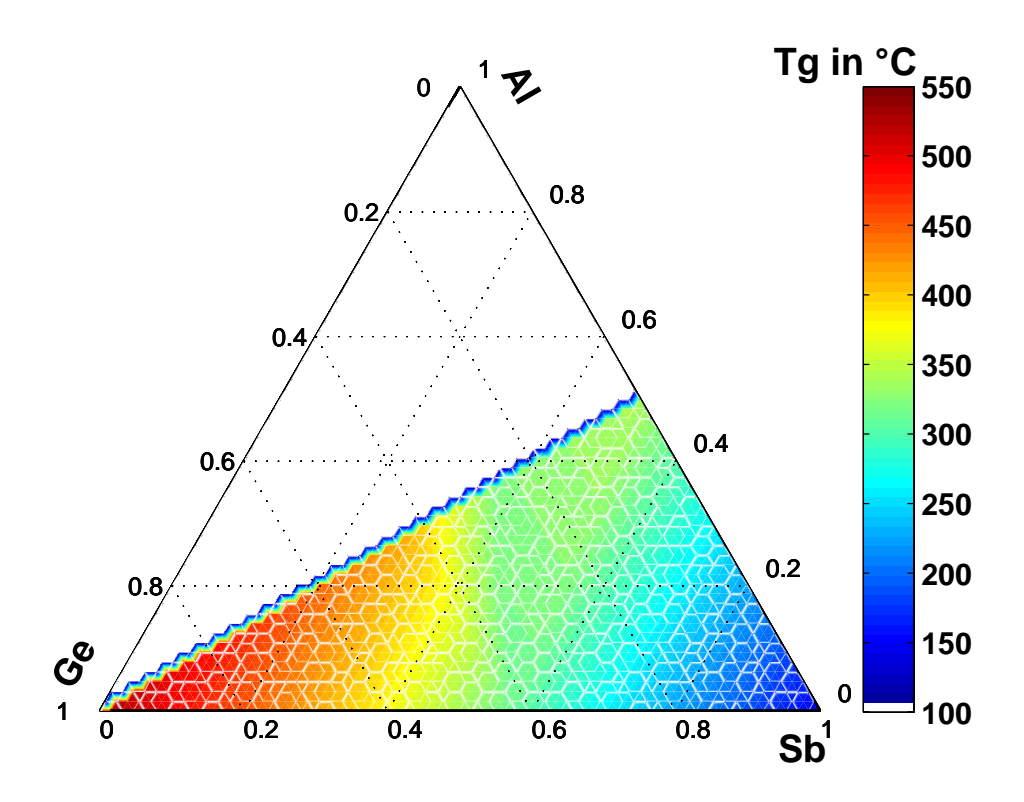


Figure 8.1: Calculated glass transition temperatures for AlGeSb

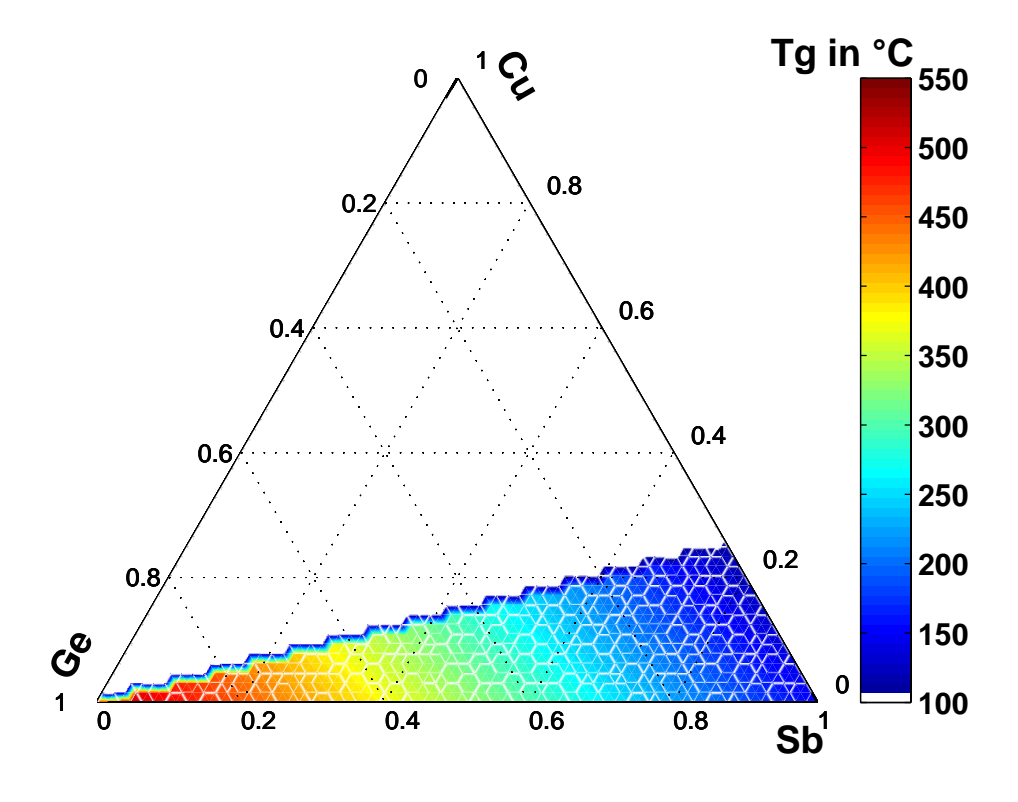


Figure 8.2: Calculated glass transition temperatures for CuGeSb

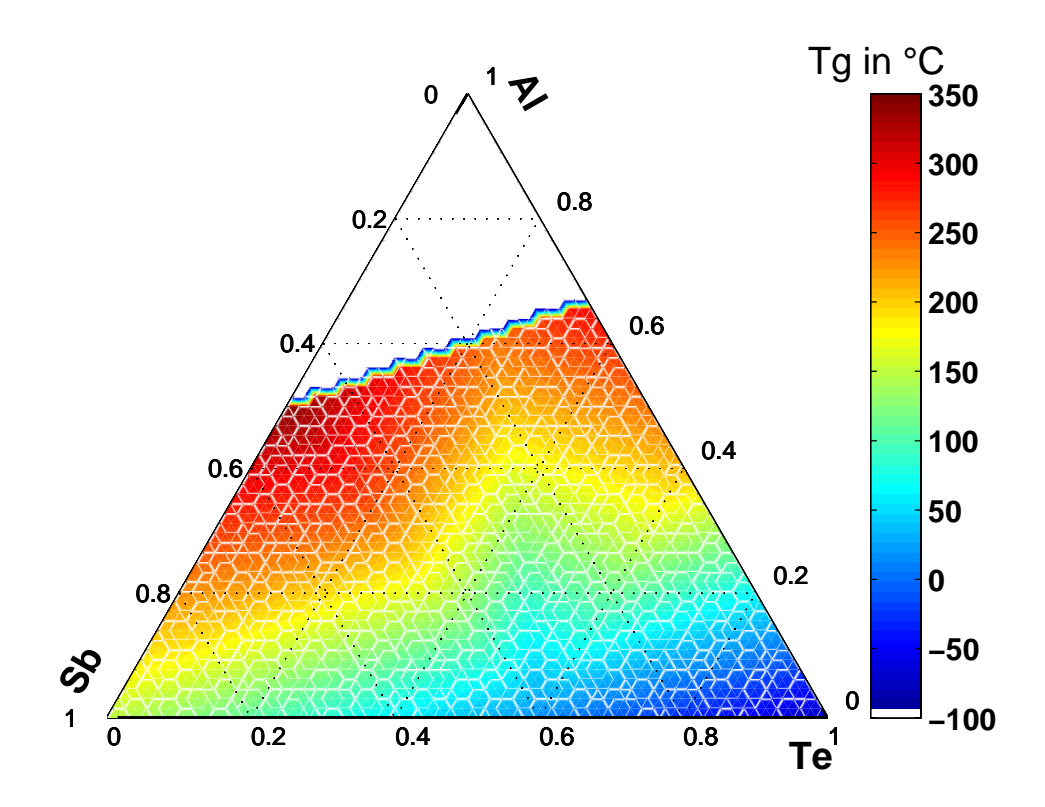


Figure 8.3: Calculated glass transition temperatures for AlSbTe

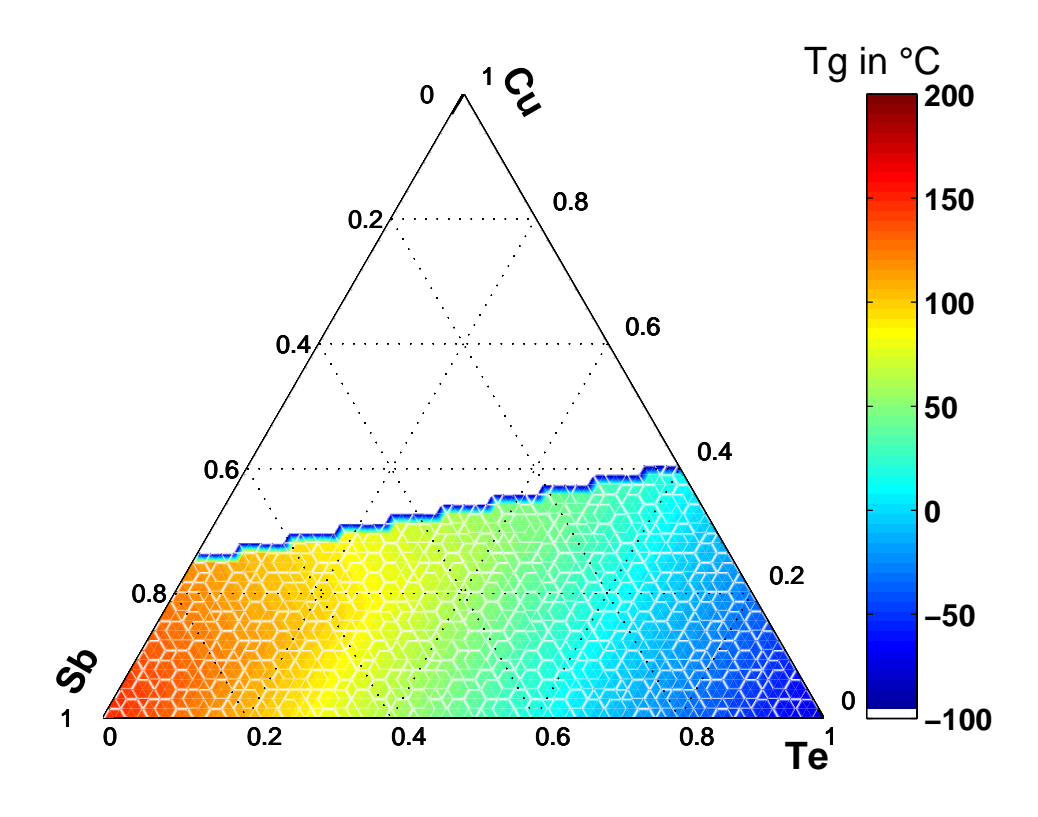


Figure 8.4: Calculated glass transition temperatures for CuSbTe

model does not make any predictions for the bond coordination and the atomization enthalpy for cases where the demand for transfer electrons by group IB to IIIB elements is higher than what group VB and VIB elements can supply. The areas with too high amounts of Cu or Al remain white in the ternary diagrams in Fig. 8.1 to 8.4.

In the case of doping GeSb with Al (Fig. 8.1) it is the contribution of such dative bonds, here between Al and Sb, that can together with regular Al-Sb or Al-Ge bonds compensate for the reduction of the number of Ge-Sb bonds, which are the strongest bonds in Al-Ge-Sb alloys. Thus the main trend in Al-Ge-Sb is an increase in the total bonding enthalpy and thus an increase in  $T_q$  for a larger amount of Al.

In contrast in Cu doped GeSb (Fig. 8.2) the enthalpy of Cu bonds is too low for such a compensation. In this case the decrease of strong bonds leads to a reduction in total bond enthalpy and thus to a lower calculated glass transition temperature.

Besides the general trend of increasing glass transition temperature with higher Al doping, the diagram for Al-Ge-Sb reveals another effect. It shows an area of relatively low values for  $T_g$  around compositions with a Ge:Sb ratio of 3:4. This reflects a lack of hetero-nuclear bonding partners for the Al atoms where Ge and Sb atoms match perfectly to form solely Ge-Sb bonds, which are preferred due to their higher enthalpy. In such compositions most Al atoms can only form homo-nuclear bonds, with the exception of dative bonds to Sb atoms. According to Pauling's equation, Eq. (6.2), the homo-nuclear Al bonds have a significantly lower enthalpy than Al-Sb or Al-Ge bonds. The latter can only be formed at compositions further away from the Ge:Sb ratio of 3:4, where the mismatch between Ge and Sb atoms provides a sufficient number of free Ge or Sb valences.

The calculations for Al-Sb-Te (Fig. 8.3) lead to a very similar diagram as for Al-Ge-Sb. The general trend is an increase of the glass transition temperature with a higher amount of Al. This is because the loss of strong Sb-Te bonds, strong compared to Al-Sb or Al-Te bonds, is overcompensated by dative Al-Te or Al-Sb bonds, respectively. And again compositions with a specific ratio of Sb:Te, in this case 2:3, show a relatively low glass transition temperature compared to compositions with the same amount of Al, but higher or lower ratios of Sb:Te. Analogous to Al-Ge-Sb for this ratio the establishment of stronger Sb-Te bonds leaves the Sb and Te atoms without any free valences for the formation of regular Al-Sb or Al-Te bonds besides the dative bonds.

Finally the ternary diagram for the Cu-Sb-Te system (Fig. 8.4) shows an increase of the glass transition temperature with higher Cu doping until the ratio of Cu:Te reaches the value 2:3. Up to this point Cu atoms can establish all their dative bonds with Te atoms. Beyond the Cu:Te ratio of 2:3 additional Cu atoms can only build dative bonds with Sb atoms, which are weaker than Cu-Te bonds. Similar to the Cu-Ge-Sb system

these dative Cu-Sb bonds are then too weak to compensate for the loss of stronger bonds with increasing amount of Cu in the material.

For a comparison between these results from calculations and the corresponding effect of doping on the stability against crystallization in reality, thin films of doped phase change materials were prepared for annealing experiments [159]. All films were 50 nm thick deposited by co-sputtering from elemental targets. The Ge:Sb and Sb:Te ratio was fixed close to the eutectic  $Ge_{15}$ :Sb<sub>85</sub> and close to Sb<sub>2</sub>Te, respectively, while the Al and Cu concentrations were varied by tuning the power at the according sputter guns. The depositions were done at room temperature in an Ar atmosphere with a pressure of 0.27 Pa. The obtained stoichiometries were determined by Rutherford Backscattering Spectrometry. The results of these measurements are listed in the first column of Table 8.1. For each composition the table also contains the detailed output of the  $T_g$  simulating algorithm including the calculated glass transition temperature and the atomization enthalpy besides the number of all formed bonds and their contribution to the total bond enthalpy.

Resistivity is commonly chosen as a highly sensitive indicator for the crystallization upon heating of phase change materials because of the strong contrast of this quantity between the amorphous and the crystalline state. For this purpose two 100 nm thick Al pads were deposited on each thin film sample and contacted electrically in a two-point-probe setup. In order to prevent a current to flow in parallel to the phase change film from one electrode to the other and thus to corrupt the measurement the Si substrates used were coated with  $SiO_2$  before deposition of phase change material. The resistivity was measured while heating the sample with a constant rate of  $1 \, \text{K/s}$  in a nitrogen atmosphere to minimize oxidation of the phase change material especially at elevated temperatures, where reactivity is increased.

The resulting resistivity data are plotted against temperature in Figures 8.5 to 8.8. For all samples a rather sharp drop in resistivity can be observed indicating crystallization. To illustrate how the predictions for the trends of the glass transition temperature  $T_g$  relate to the experimentally determined crystallization temperature  $T_x$ , the relative change of the glass transition temperature upon doping  $T_{g,doped}^{cal}/T_{g,undoped}^{cal}$  was projected to a prediction for the crystallization temperature  $T_{x,doped}$  of the doped material via the measured crystallization temperature of the undoped one  $T_{x,undoped}^{measured}$ .

$$T_{x,doped} = \frac{T_{g,doped}^{cal}}{T_{g,undoped}^{cal}} \cdot T_{x,undoped}^{measured},$$
(8.1)

where all temperatures are in K. Such an adjustment to a reference point is the natural consequence of the finding in chapter 7, that in phase change materials the calculated glass transition temperature does not match the actual glass transition temperature

given. The sequence in which the bonds are listed (from left to right) accords to their preference of formation in the used model. Al, respectively. The number of bonds of each type  $n_{AB}$  and the enthalpy contributed from each bond type to the total bond enthalpy  $n_{AB}H_{AB}$  is Table 8.1: Calculated glass transition temperature  $T_g$  and total bond enthalpy  $H_{tot}$  for several degrees of alloying Sb<sub>2</sub>Te and Ge<sub>12</sub>Sb<sub>88</sub> with Cu or

Composition	$T_g$	$H_{tot}$	$n_{SbTe}$	$n_{SbTe}H_{SbTe}$	$n_{AlTe}^a$	$n_{AlTe}H^a_{AlTe}$	$n_{AlSb}$	$n_{SbTe}H_{SbTe}$	$n_{SbSb}$	$n_{SbSb}$ $n_{SbSb}H_{SbSb}$
	°°	${\rm kJ/mol}$		${ m kJ/mol}$		$\mathrm{kJ/mol}$		${ m kJ/mol}$		${ m kJ/mol}$
${ m Sb}_{66.7}{ m Te}_{33.3}$	75	241	0.670	124	0.670	117				
${ m Al}_{2.1}{ m Sb}_{65.3}{ m Te}_{32.6}$	86	244	0.653	122	0.021	4	0.063	10	0.621	109
${ m Al}_{3.5}{ m Sb}_{64.3}{ m Te}_{32.2}$	93	246	0.643	120	0.035	6	0.105	17	0.591	103
${ m Al}_{8.5}{ m Sb}_{61.0}{ m Te}_{30.5}$	119	253	0.610	114	0.085	15	0.255	41	0.483	84
	$T_g$	$H_{tot}$	$n_{GeSb}$	$n_{GeSb}H_{GeSb}$	$n_{AlSb}^a$	$n_{AlSb}H^a_{AlSb}$	$n_{AlSb}$	$n_{AlSb}H_{AlSb}$	$n_{SbSb}$	$n_{SbSb}H_{SbSb}$
$\rm Ge_{18.0}Sb_{82.0}$	218	282	0.720	130	0.870	152				
$Al_{6.1}Ge_{12.4}Sb_{80.6}$	221	283	0.501	90	0.062	10	0.185	29	0.877	154
$Al_{10.7}Ge_{11.5}Sb_{76.7}$	235	287	0.465	84	0.108	17	0.325	52	0.768	134
$\rm Al_{19.2}Ge_{10.9}Sb_{68.8}$	266	296	0.441	79	0.194	31	0.582	93	0.532	93
	$T_g$	$H_{tot}$	$n_{SbTe}$	$n_{SbTe}H_{SbTe}$	$n^a_{CuTe}$	$n_{CuTe}H^a_{CuTe}$	$n_{CuSb}$	$n_{CuSb}H^b_{CuSb}$	$n_{SbSb}$	$n_{SbSb}H_{SbSb}$
${ m Sb}_{66.7}{ m Te}_{33.3}$	75	241	0.670	124	0.670	117				
$\mathrm{Cu_{9.3}Sb_{65.3}Te_{25.4}}$	92.6	245.8	0.508	94.6	0.279	25.2	0.093	7.2	0.679	118.8
$\mathrm{Cu}_{20.1}\mathrm{Sb}_{58.3}\mathrm{Te}_{21.6}$	93.2	246.0	0.432	80.5	0.432	39.0	0.372	28.9	0.558	97.6
	$T_g$	$H_{tot}$	$n_{GeSb}$	$n_{GeSb}H_{GeSb}$	$n^a_{CuSb}$	$n_{CuSb}H^a_{CuSb}$	$n_{CuSb}$	$n_{CuSb}H_{CuSb}$	$n_{SbSb}$	$n_{SbSb}$ $n_{SbSb}H_{SbSb}$
${ m Ge_{18.0}Sb_{82.0}}$	218	282	0.720	130	0.870	1 52				
$\mathrm{Cu_{13}Ge_{15.7}Sb_{71.3}}$	192	275	0.626	113	0.390	30	0.130	10	0.692	121
$Cu_{21}Ge_{14.2}Sb_{64.8}$	175	270	0.569	103	0.630	49	0.210	16	0.582	102

well in an absolute sense, while it reproduces *relative* compositional trends quite satisfactorily. These projected values for the cystallization temperature are marked in Figures 8.5 to 8.8 by vertical lines.

Fig. 8.5 documents a steady rise of the crystallization temperature of Sb<sub>2</sub>Te upon increased Al doping up to a fraction of 9.5 at.% of Al. The agreement between the experimental data and the calculations is remarkably good. The prediction of a shift of the stability regime of the amorphous phase towards higher temperatures for Cu doping of Sb<sub>2</sub>Te is also confirmed, as can be seen in Fig. 8.6. For the alloy with the highest amount of Cu realized in this measurement series, i. e. 38.8 at.% of Cu, no comparison with the calculations is possible, because the model is not applicable to such high concentrations of Cu, as there is a lack of group VB and VIB atoms that could supply Cu atoms with dative bonds. The very low resistivity in the as-deposited state also hints towards a severe change in the electronic configuration of this composition, justifying the limitation of the model to smaller degrees of doping. The deviation between prediction and experiment for the composition with 20.1 at.% of Cu is likely to be at least partially also due to its close proximity to the validity border of the model.

One can conclude already at this point, that the experimentally verified increase of the crystallization temperature of Sb<sub>2</sub>Te by Al- and Cu-doping could only be predicted correctly, because the formation of dative bonds between group VB and VIB elements on the one hand and group IIIB and IB elements on the other have been assumed in the calculations.

The same effect can be observed in Fig. 8.7 plotting the resistivity versus temperature curves for Al-doped Ge<sub>18</sub>Sb<sub>82</sub>. The increase of the crystallization temperature with higher degree of doping is significant, though less pronounced than in the case of Al-Sb<sub>2</sub>Te. The comparatively lower effectiveness of Al doping in Ge<sub>18</sub>Sb<sub>82</sub> becomes even more apparent, when the maximum dopant concentrations are considered: addition of 8.5 at.% of Al lets the crystallization temperature of Sb<sub>2</sub>Te increase more than adding 19.2 at.% of Al does in Ge<sub>18</sub>Sb<sub>82</sub>. Besides, the influence of such a high Al content is overestimated by the model, while for dopant concentrations of up to 10 at.% there is still a good agreement with the experimental data.

While Cu doping increases the glass transition temperature of  $\mathrm{Sb_2Te}$ , the calculations predict a decrease of the stability of the amorphous network when doping  $\mathrm{Ge_{18}Sb_{82}}$  with the same element. And indeed, Fig. 8.8 shows a shift of the crystallization towards lower temperatures in good agreement with the projected behaviour.

To cross-check if the drop in resistivity correctly indicates the crystallization of the sample, the same thin films of doped  $Ge_{18}Sb_{82}$  and  $Sb_2Te$  were deposited also on

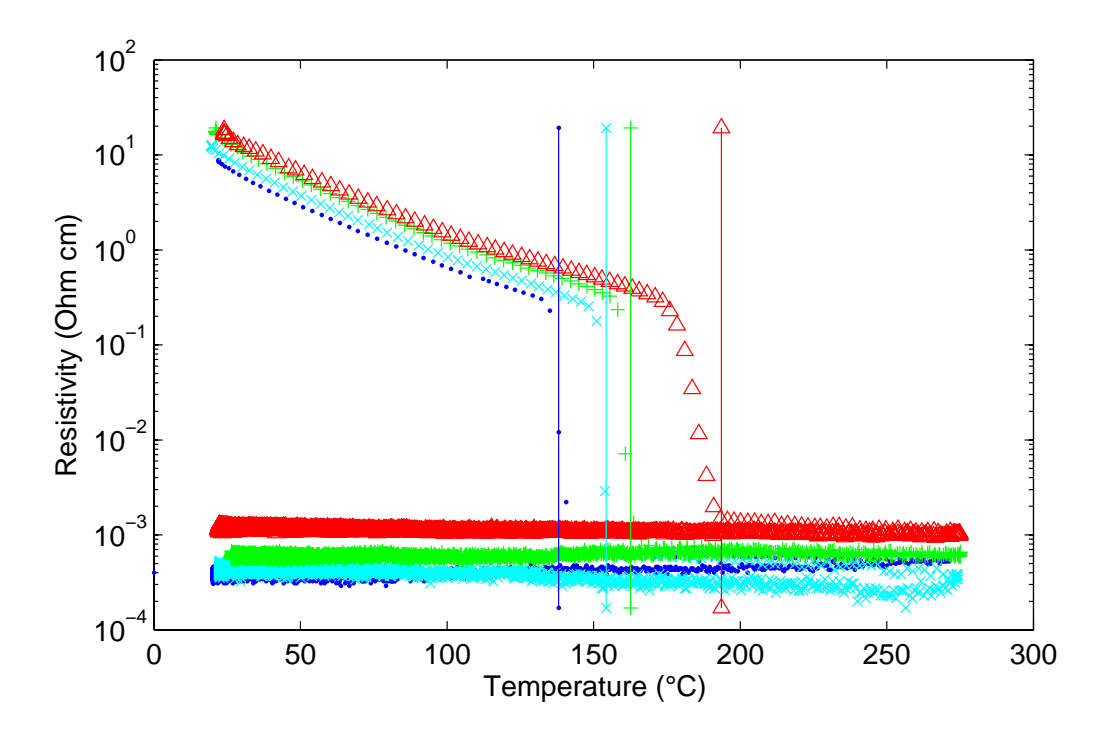


Figure 8.5: Resistivity versus temperature measured during heating with a constant rate of  $1 \,\mathrm{K/s}$  and subsequent cooling [159]. The degree of Al doping varied as follows: Sb<sub>2</sub>Te without any Al (blue dots), 2.1 at.% Al (cyan crosses), 3.5 at.% Al (green plusses) and 8.5 at.% Al (red triangles). The vertical lines indicate the results of the calculation of the glass transition temperature projected to the crystallization temperature according to eq. 8.1.

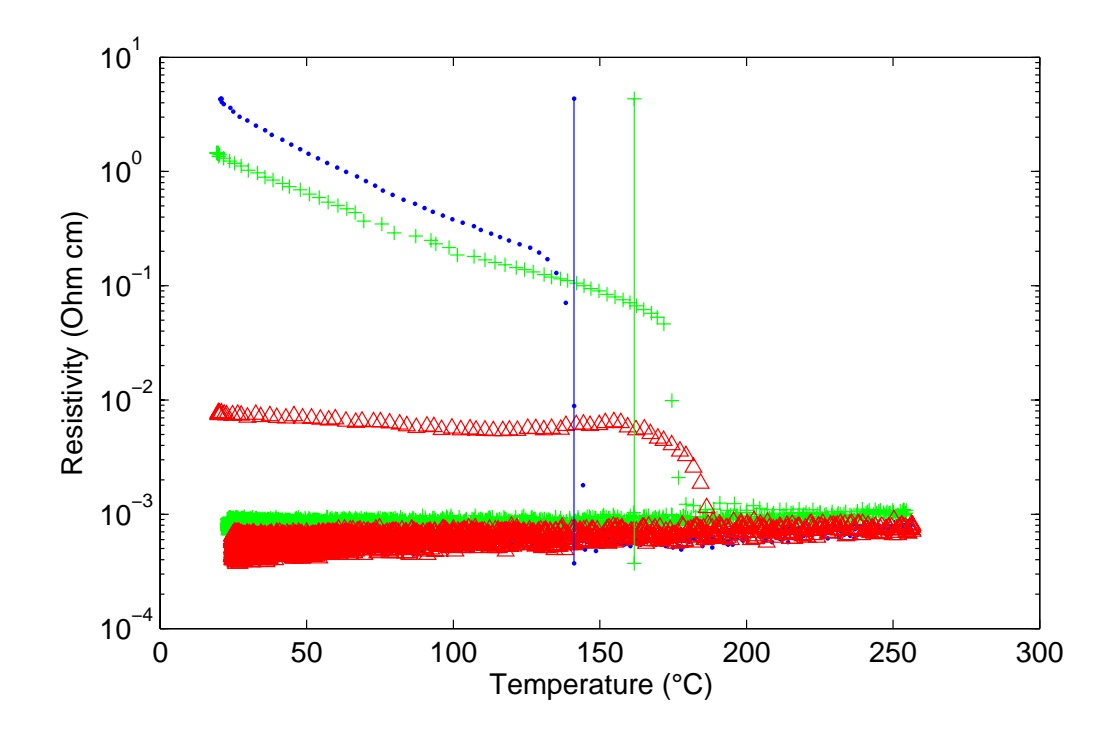


Figure 8.6: Resistivity versus temperature measured during heating with a constant rate of 1 K/s and subsequent cooling [159]. The degree of Cu doping varied as follows: Sb<sub>2</sub>Te without any Cu (blue dots), 20.1 at.% Cu (green plusses), 38.8 at.% Cu (red triangles). The vertical lines indicate the results of the calculation of the glass transition temperature projected to the crystallization temperature according to eq. 8.1.

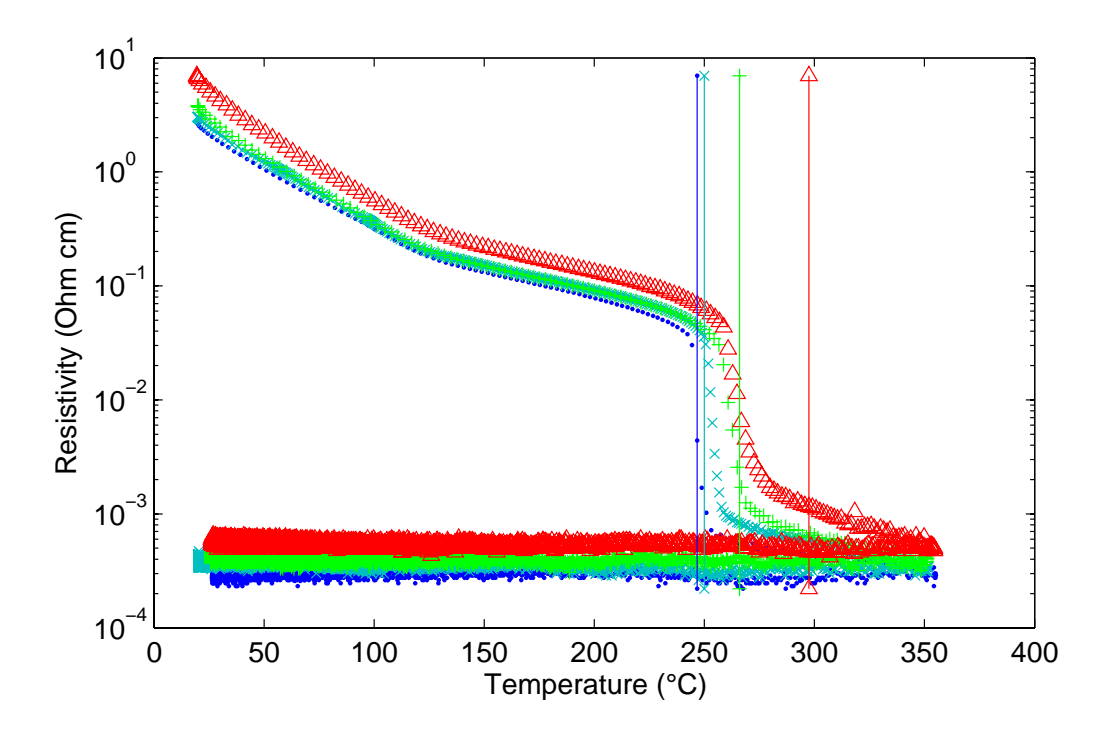
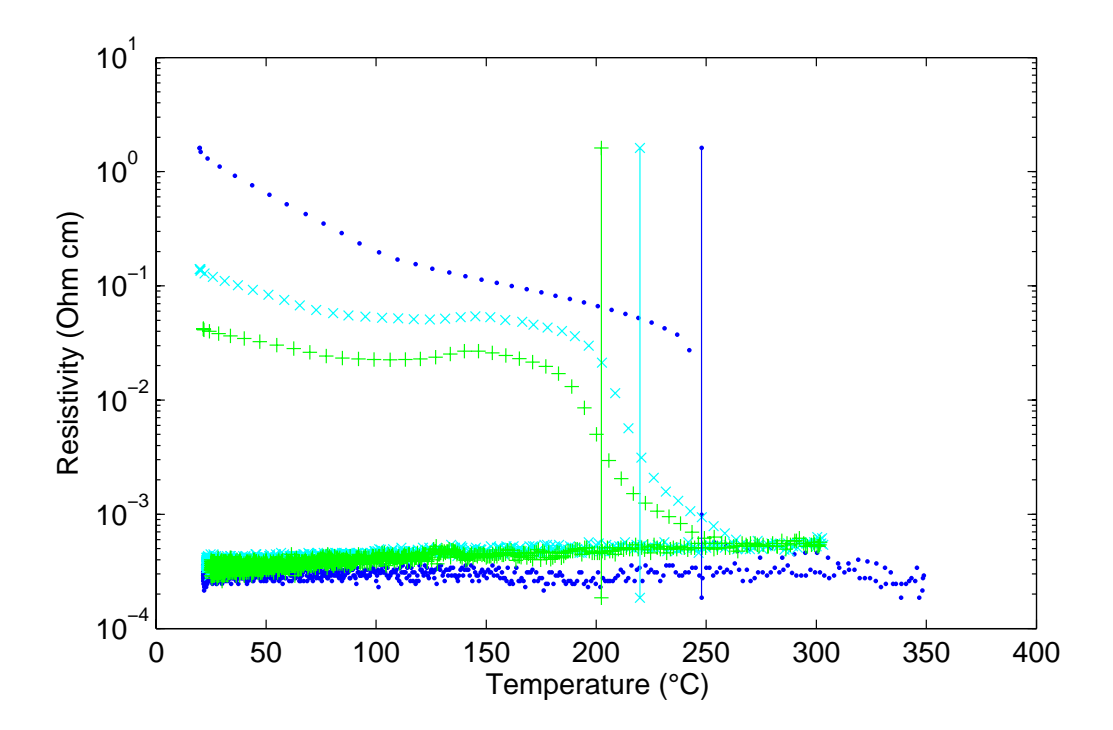


Figure 8.7: Resistivity versus temperature measured during heating with a constant rate of 1 K/s and subsequent cooling [159]. The degree of Al doping varied as follows:  $Ge_{18}Sb_{82}$  without any Al (blue dots), 6.1 at.% Al (cyan crosses), 10.7 at.% Al (green plusses) and 19.2 at.% Al (red triangles). The vertical lines indicate the results of the calculation of the glass transition temperature projected to the crystallization temperature according to eq. 8.1.



**Figure 8.8:** Resistivity versus temperature measured during heating with a constant rate of 1 K/s and subsequent cooling [159]. The degree of Cu doping varied as follows: Ge<sub>18</sub>Sb<sub>82</sub> without any Cu (blue dots), 13 at.% Cu (cyan crosses), 21 at.% Cu (green plusses). The vertical lines indicate the results of the calculation of the glass transition temperature projected to the crystallization temperature according to eq. 8.1.

uncoated Si substrates for x-ray diffraction experiments. These samples were heated at a rate of 1 K/s in a He atmosphere while their structural condition was monitored by time resolved x-ray diffraction. These measurements confirmed the results of the resistivity versus temperature measurements presented in Figures 8.5 to 8.8 [159].

The examples given show convincingly that a material's stability against crystallization can be lowered or increased by doping depending on the chosen dopant. They also revealed that the same dopant can increase the crystallization temperature for one material and decrease it for another. All compositional trends were predicted correctly by the calculations of the glass transition temperatures in the framework of the model described before. For that reason this method can be regarded as a good guide to tailor phase change materials for technological applications where an increased stability against crystallization is desirable [159].

# Part III

# Measurements of Crystallization Kinetics

#### Motivation

It is much easier to make measurements than to know exactly what you are measuring.

J. W. N. SULLIVAN

The unusual crystallization kinetics of phase change materials has been referred to repeatedly in the course of this thesis, so the attentive reader of the first two parts will regard the *experimental* treatment of crystallization kinetics as a natural imperative arising from what has been presented so far. Nevertheless, a brief motivation accumulating the various incitements for the engagement in this direction seems reasonable at this point.

Phase change materials can remain in their amorphous state at room and slightly elevated temperature for years while they can crystallize in few nanoseconds when brought to higher temperatures. This tremendous change of structural stability with varying temperature is core to these materials' application in data storage. The exact temperature dependence of crystallization kinetics determines the performance of data storage media incorporating phase change materials. Not only ultimate switching speed and retention times, but also thermal cross-erasing or multi-level storage can only be addressed properly when the temperature dependence of crystallization kinetics is known for the used material.

Even for the investigation of the most peculiar *electrical* property of phase change materials, the so-called threshold-switching, one is in need of a precise knowledge of crystallization kinetics. Threshold-switching means the transition from a highly resistive amorphous ground state to a much more conductive, though still amorphous, excited state upon the application of a critical electric field. In order to draw a conclusion about the critical electric field, it is necessary to know the extension of the amorphous volume the measured critical voltage drops across *at the moment of switching*. Crystallization kinetics is not only decisive in the *preparation* of a well-defined volume of melt-quenched amorphous<sup>1</sup> phase change material as initial state of a threshold-

<sup>&</sup>lt;sup>1</sup>This is at least the technologically relevant state. It may differ in its structural and thus also electrical properties from the as-deposited amorphous state. The reader is referred to the topic of structural relaxation in glasses, e.g. in Chapters 3 and 7. However, this does not mean that any

switching experiment. The same is true also for the heat generation by electrical current passing the distinct resistivities or amorphous and crystalline volumina in the device. The latter effects the temperature distribution and therewith again the degree of crystallinity of the device during an electrical experiment. Only if the extent of the amorphous volume in the testing structure is known at every point in time, it can be taken into account for the determination of a material specific threshold field. The latter is not only the property that is needed when predicting the performance of devices differing from the testing structures in size or shape. It is also the quantity that is actually interesting from a basic research point of view aiming for a fundamental correlation between composition and properties of materials.

Having therewith crossed the gap between applied and basic research, which is admittedly often rather small in the field of phase change materials, a second view from this side on crystallization kinetics itself might be worthwhile. Chapter 4 should have made apparent that, besides the technological relevance of crystallization kinetics of phase change materials, its basic mechanism and how it can be incorporated into a theoretical description of crystallization is still unclear when it comes to experimental evidence. And even if the basic theories are correct, what are the right values for the multitude of parameters going into the formalism? What fragility of the undercooled liquid, for example, matches the temperature dependence of crystal growth velocity best?

The major reason for the lack of data, despite the great demand for it, is the extremely high crystal nucleation rate and growth velocity at high temperatures making experiments challenging. To cover at least most of the temperature dependence of crystallization kinetics in the range between melting point and glass transition, the experimental time resolution should be by far faster than in the classic experiments performed on a seconds to days timescale. Laser annealing experiments seem to be the natural solution to cope with this task and have thus been used to investigate crystallization behaviour of phase change materials.

Those tools, commonly used in the field of phase change materials today, are described and their capabilities regarding the goals defined above are assessed in chapter 9. In view of the shortcomings of those methods the concept of a new experimental setup overcoming those limitations is displayed in chapter 10, before chapter 11 gives a detailed description of this setup, named  $POET^2$ , as it has been realized by the author of this thesis. Finally, chapter 12 illuminates a wide spectrum of different experiments

experiments on the as-deposited amorphous phase were irrelevant. They are perfectly legitimate as long as their results are not blindly generalized, but discussed with respect to the consequences of the named distinction.

<sup>&</sup>lt;sup>2</sup>acronym for Phase change Optical Electrical Tester

that have been performed using the described setup ending in a proposal of a selection of even further new experiments POET enables.

# Chapter 9

# **Existing Techniques**

Es ist nicht das Ziel der Wissenschaft, der unendlichen Weisheit eine Tür zu öffnen, sondern eine Grenze zu setzen dem unendlichen Irrtum.

Bertolt Brecht: Leben des Galilei

Over the years various approaches have been taken to experimentally determine the crystallization kinetics of phase change materials. Most of them focus on the low temperature branch of crystallization kinetics (see Sec. 9.1). Those temperatures are high enough for crystal nucleation and growth to take place on a laboratory time scale, but low enough for high viscosities to keep both processes quite slow, meaning experiments to happen on a tenth of seconds to days time scale.

A different type of rather slow experiments aims for the high temperature end of crystallization, i. e. slightly below the melting temperature (Sec. 9.2). Here the driving force of crystallization is still comparably small resulting in rather long periods of time for the formation of post-critical nuclei.

In the intermediate temperature regime crystallization happens much faster than near the melting point or at low temperatures, because the driving force is large while viscosity is still low. The only way this regime was investigated is by using laser pulses for annealing. A brief overview of different approaches in that direction is given in Section 9.3.

#### 9.1 Slow crystallization at low temperatures

The traditional way of investigating crystallization is calorimetry. It utilizes the fact that crystallization being an exothermic process is accompanied by a usually quite strong heat release. A macroscopic mass of a material, which may such as powder consist of small particles is heated up at a constant temperature increase while monitoring the heat that needs to be supplied to maintain the temperature ramp. The latter is

commonly achieved with high accuracy by simultaneously heating a second container, constructed in the same way as the one holding the sample, as reference.

Experimental heat flow curves taken during such annealings have been discussed in some detail already in Part II and can be seen in Fig. 7.2. While information about the thermodynamics is found in the *amount* of heat released during crystallization, the kinetics of crystallization can be revealed with calorimetry by varying the constant speed of heating and measuring the corresponding *changes of the peak* in the heat flow signal.

For an analysis of the predominant shifting of the crystallization peak towards higher temperatures for higher heating rates Kissinger [114] developed a method in 1957 which is still widely used. However, as has been already discussed in Section 4.5, the basic assumptions as well as some simplifications might not be applicable to a lot of experiments, which regardless of this fact have been analyzed using Kissinger's method. In these cases the resulting "activation energies" do therefore not have any direct physical meaning.

The heat release upon crystallization is a very general physical effect accompanying this phase transition in practically all materials. The same is true for the formation of long range order, which is actually by definition the key difference between the crystalline and amorphous state. So also the time dependent x-ray diffraction (XRD) pattern taken during annealing should reflect the crystallinity of a sample. To yield a sufficient time resolution such experiments are carried out at a synchrotron [159]. While the diffraction pattern has the advantage of unequivocally proving crystallinity, it is difficult to quantify the degree of how "strong" the diffraction signal is, not to mention any conclusions about the degree of crystallization in the sample.

These two effects, heat release and long range order, are generally applicable to the distinction between crystalline and amorphous. In addition, phase change materials offer further physical properties that can be used to monitor the degree of crystallization. The strong contrast in resistivity between the amorphous and the crystalline state, often a factor of several orders of magnitude, is one of them. So this quantity is assumed to indicate the progress of the phase transition during the annealing of an electrically contacted sample. This is generally legitimate to do, for example to compare the influence of changes in the sample, as has been described in Chapter 8. However, such experiments have also been used to study the crystallization kinetics [160]. Therefore sets of annealing experiments are performed with varying heating rates and are often analyzed using Kissinger's method. Again, the significance of the resulting "activation energies" is doubtful, if reality does not match Kissinger's assumptions. Besides, another important limitation of electrical experiments with the goal of the determina-

#### 9.1. SLOW CRYSTALLIZATION AT LOW TEMPERATURES

tion of crystallization kinetics should be borne in mind: electrical conduction through a partially crystallized sample generally has to be treated as a percolation problem. This means, amongst others, that the correlation between the resistivity and the degree of crystallization is strongly non-linear. The formation of the first few crystalline and thus highly conductive paths between the two electrodes inside of a largely amorphous sample lets the resistivity of the whole sample drop much more than what the crystallization of the rest of the volume causes.

This problem of percolation is addressed in a work [161] that compares the reduction in resistivity of a thin film of phase change material upon annealing with the simultaneous increase in reflectivity. Similar to the contrast in resistivity most phase change materials also exhibit a significant difference in their optical properties becoming manifest in the dielectric function. Otherwise they would have never been used in optical discs. Accordingly, the reflectivity of a flat sample has been found to be a conveniently measurable indicator for its degree of crystallization.

Although reflectivity does not show an as strong non-linearity in the correlation with the crystallized fraction as resistivity does, it would be dangerous to assume that there would be generally a one-to-one connection. Depending on the geometry of the experiment it needs to be considered that the reflectivity depends more strongly on the conditions at the surface of a sample than on what is underneath. If the degree of crystallization near the surface of a bulk sample is different than in the interior, e.g. due to heterogeneous nucleation, than reflectivity is not indicating the fraction of crystallized volume correctly.

Both the percolation problem in electrical measurements as well as the optical measurement of a bulk sample just mentioned highlight that the dimensionality of the used probe (electrical=1D, optical=2D, calorimetric=3D) should always match the dimensionality of the crystallization problem in the used sample. This is the reason why reflectivity measurements are particularly suited for thin films where inhomogenities vertical to the surface can be neglected.

However, this use of the term dimensionality shall not be confused with the fact that all these experiments, regardless of measuring resistivity, reflectivity or heat flow of a sample during annealing, generate only a zero-dimensional information, i. e. a single number, for any given point in time. This is why without any additional information about the particular crystallization process it is not possible to discriminate between the time and temperature dependence of nucleation on the one hand and of crystal growth on the other. This is true both for annealings with constant heating rates as well as for isothermal annealings (see Section 4.5).

This limitation of the experiments mentioned so far is overcome in another class of

experiments, which produce a two-dimensional set of data for each step of crystallization of a practically two-dimensional sample. A first kind of such experiments [162] uses atomic force microscopy (AFM) to scan the surface of a thin film of phase change material. The resulting topography of the film contains information about crystallization due to the density contrast between the amorphous and crystalline state, which leads to a lowered surface of the film wherever it is crystalline. The AFM images are taken ex-situ after each step of a sequence of isothermal annealings in the furnace of a differential scanning calorimeter (DSC). The occurrence of new crystallites and their subsequent growth is captured in a rather direct way, making a precise determination of nucleation rate and growth velocity possible. The price for this experimental disentanglement of the crystallization kinetics is the loss of in-situ capability. As a consequence these experiments are limited to temperatures with rather slow crystallization that can be efficiently interrupted on the time scale necessary for cooling the sample down at the end of an annealing step.

A second sort of experiments delivering two-dimensional information about the crystallization in a two-dimensional sample is based on transmission electron microscopy (TEM) [163, 164, 165]. This technique brings with it a whole package of advantages over AFM with respect to the described purpose. The spatial resolution is much better, the sensitivity to the films' unavoidable surface roughness is much lower and the border of neighboring crystallites is detectable. Also *in-situ* observation during annealing is possible. And information can be obtained about crystal orientations, which can reveal anisotropies in the growth mechanism.

Nevertheless, the time resolution of this type of experiment, although repeatedly applied to the crystallization kinetics of phase change materials, has so far not gone much below the range of seconds. There are efforts to built TEMs with extremely high time resolution (even faster than nanoseconds) not giving up on the field of view. But even the protagonists of those activities described in a recent article [166] that there are still enabling technologies that require further development before such an instrument could be realized in practice. In their opinion the most crucial ones are high beam quality short-pulse electron guns and powerful magnetic lens systems capable of operating in the several MeV range.

One should also keep in mind that high temporal and high spatial resolution does not come for free. Already in their early studies using today's tools [167, 168], Kooi and coworkers observed crystallization of phase change films to be sensitive to irradiation by the electron beam of the TEM. It concerned them enough to not only have a closer look at this effect [169], but also to depart from their original strategy of continuous image acquisition in order to avoid such an influence of the probe as much as possible. Thus

in their more recent works [164] they performed *ex-situ* experiments, interrupting the isothermal annealings by cooling down the sample to nearly room temperature before each TEM measurement. In this way the sample was at least not exposed to the electron beam at elevated temperatures.

#### 9.2 Slow crystallization at high temperatures

While all techniques mentioned above work on the low temperature end of the crystallization kinetics, it is also possible to investigate crystallization at the high temperature end, i. e. just below the liquidus temperature, without requiring very high temporal resolution. For that purpose droplets of molten alloys are undercooled. The calorimetric signal of the crystallization event is interpreted as the point in time when the probability of nucleation during cooling from the liquidus temperature is unity.

Kalb et al. [170] applied this kind of experiments to typical phase change materials, reaching undercoolings of 40 to 80 K below the liquidus temperature in a differential thermal analyzer. In their conclusion they claim to have determined an upper limit for the homogeneous steady-state nucleation rate this way, since heterogeneous nucleation could not be excluded.

The analysis of such an experiment is based on a lot of assumptions and allows therefore only rather indirect conclusions about the crystallization kinetics. If for example the experimental results are discussed in the framework of classical nucleation theory and if all other parameters, such as the temperature dependence of the driving force for crystallization, are either determined by independent experiments or approximated by models, respectively, the formula for steady-state nucleation Eq. (4.36b) is used to fit the data for undercooling typically by adapting the interfacial energy as a "free" parameter.

# 9.3 Fast crystallization at intermediate temperatures

If one wishes to investigate extremely fast crystallization in phase change materials, one needs to accomplish at least one of two experimental tasks: a fast detection system monitoring the degree of crystallization and a method of extremely fast heating and especially cooling of the material. The latter can compensate for a lack of the first ensuring the feasibility of ex-situ experiments by bringing the material rapidly from a temperature regime of neglectable crystallization speeds into the annealing condition and back again. Both tasks can be coped with by employing laser irradiation.

Since commercially available optical storage media, also those containing phase change materials, work with laser light, it is not surprising that methods utilizing laser light have been applied to the topic of crystallization kinetics by various research groups over the last two decades.

On the one hand there are dynamic testers [171] working very similar to the principle of optical storage. A pulsed laser irradiates a film of phase change material locally on a  $spinning\ disc$ , and the state of the material is determined by detection of the reflected light. Such setups are mostly employed in materials research closely related to the storage application. This does not contradict the fact that by the additional use of ex-situ tools, like for example TEM, many insights into the material dependence of the crystallization behaviour have been found.

However, for basic research on crystallization kinetics *static* testers are preferred, since they concentrate on a fixed volume of phase change material over a complete experiment [172, 173, 174, 175]. The most ordinary experiment in a static tester measures how the change of a film's reflectivity *after* a laser pulse, compared to the reflectivity *before*, depends on the power and on the duration of the pulse. The results of these *ex-situ* measurements are commonly visualized in a pseudocolor plots, often referred to as power-time-effect (PTE) diagrams [173, 175]. Despite the conceptual simplicity of these experiments some serious mistakes can easily be made in both conducting them and interpreting their results. A more detailed discussion about such mistakes is given in Section 12.1.

Although such ex-situ laser experiments can already give some insight into the crystallization behaviour of a material and be useful, for example, to compare the maximum crystallization speeds for alloys of varying stoichiometry, e.g. in [176, 161, 177, the full potential of a static tester can only be exploited, if it is equipped with a detection system that allows in-situ reflectivity measurements during the annealing with the laser pulse [38]. Mansuripur and coworkers proposed a scheme employing two laser beams [178] amongst others for the investigation of the crystallization kinetics in phase change materials [179, 180]. The resulting reflectivity data can be compared to numerical simulations of the crystallization process [179]. However, it is important to obtain confidence in the parameters that are adapted to fit the simulations to the experimental data. The number of parameters included in any simulation of a process as complex as crystallization is large. Therefore it is necessary to cross-check the results by additional evidence from complementary ex-situ measurements, using e.g. AFM or TEM [172, 174], on the same locations on the sample the in-situ reflectivity data have been taken. Without this or any other cross-check, numerical simulations are not very convincing. Accordingly, the promise of *in-situ* reflectivity measurements leading to a

#### 9.3. FAST CRYSTALLIZATION AT INTERMEDIATE TEMPERATURES

quantitative determination of fast crystallization kinetics waits to be kept.

## Chapter 10

# Concept for a New Experimental Setup: *POET*

It may be so, there is no arguing against facts and experiments.

ISAAC NEWTON

Confronted with the task of characterizing phase change materials for the use in electronic memory, there are two main problems that need to be addressed. The temperature dependence of crystallization kinetics and the in general non-linear electronic response to an applied voltage. In a PCRAM cell both effects are strongly interweaved. How exactly they influence each other depends strongly on the shape and size of the cell. To yield a material specific description of crystallization kinetics and electronic properties, which is independent of the geometry of the sample it has been determined with, the two effects need to be decoupled. Otherwise a prediction of the performance not only of the switching in a new cell, but also of the experimentally inaccessible long-term behaviour of known cells cannot be successful.

This disentangling of both effects is identified as the paramount goal of the study of phase change materials aiming at electronic memory applications. Hence, within the scope of his work the author of this thesis designed and built a new experimental setup, which enables its user to achieve this goal.

The concept of the setup is essentially the combination of optical and electrical both probing and annealing facilities which is expanded by purely thermal annealing capabilities. A sample in the phase change optical electrical tester (*POET*), as it is depicted in Fig. 10.1, can be heated with a pulsed laser to be crystallized or melt-quenched, respectively, while its reflectivity is monitored *in-situ* with a temporal resolution of a few nanoseconds. This optical branch of the setup alone forms a state-of-the-art static tester for the investigation of fast crystallization kinetics outperforming most of the existing tools discussed in Chapter 9, for example laser setups that measure the

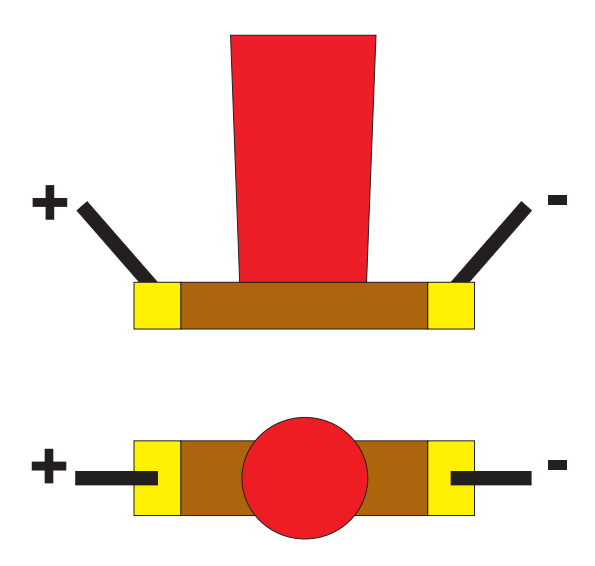


Figure 10.1: Concept of *POET*: A lateral sample of phase change material (brown) can be annealed optically by a pulsed laser (red), or electrically by a voltage applied via two electrodes (yellow). Concentrically with the pulsed laser another laser with a different wavelength operated in continuous wave mode is used to monitor the reflectivity of the sample during a pulse experiment. Also electrically the sample's transient response to a voltage pulse is monitored *in-situ*. For precise measurement of the resistance of the sample a periodic signal is used together with a lock-in amplifier before and after pulse experiments. Additionally the sample holder can be heated above 600 K enabling measurements of dependencies on the ambient temperature. The different components of the system can be combined in a modular way allowing for a wide variety of new experiments.

reflectivity only ex-situ. Accordingly in Chapter 12 several experiments are presented, which used POET purely for studies on the crystallization kinetics.

The second branch is a complete electrical tester that can apply voltage pulses to a sample, which can be several volts high and as short as 10 ns. It records the according current passing through the device *in-situ* with a temporal resolution in the nanosecond range. While this measurement of the transient resistance is optimized for high temporal resolution, a more precise measurement of the device resistance is achieved by using a periodic low voltage signal and a lock-in amplifier before and after pulse-experiments.

The optical and the electrical system can be used modularly opening the gates to a wide range of new experiments. New questions, such as how laser irradiation influences threshold switching or generally conduction in phase change materials, can be addressed. However, as explained in the motivation at the beginning of Part III, the determination of the threshold field under "normal" conditions is already challenging. For the correct interpretation of a current versus voltage characteristic recorded during the application of a voltage pulse it is important to know which parts of the phase

change material inside the tested sample are crystalline and which parts are amorphous at the point in time when the break-down of the resistivity occurs.

This is difficult to determine, if a sample is set into its highly resistive state by a strong electrical current. The resistance of a sample alone can only hint to the size of the amorphous volume provided its shape. For a complete description it is not sufficient.

Often numerical simulations are then applied to the problem. This is in principle not a bad thing to do, unless the extensive cross-checking of the correctness of the simulation, making allowance for the implicit assumptions and especially the multitude of parameters it is based on, is skipped. The immense calculating power of today's computers surely is a mixed blessing with respect to numerical simulations. Easy to use software provides solutions to complex problems in beautiful graphs, which obviously make many people forget that the results might actually be wrong.

A healthy suspicion about numerical simulations ultimately yields a strategy of separating the different effects contributing to a complex problem experimentally and adapting the respective parameters in the simulation to this more direct evidence. In the case of electrical switching of phase change materials this means that crystallization kinetics should first be investigated in experiments that do not involve any heating by electrical currents. Also it seems advisable to initialize a sample for a threshold switching experiment via laser induced melt-quenching. This way the starting conditions of the electrical experiments should be defined much better and be more reproducible than in case of an initialization with a current pulse, where more unknown effects play a role. The result of thermal initialization via laser heating also promises to be less dependent on a sample's previous degree of crystallinity than in case of an electrical initialization.

# Chapter 11

#### Realization of *POET*

Poets in our civilization, as it exists at present, must be difficult.

T. S. Eliot

#### 11.1 Overview

Before each part of *POET* will be explained more detailed, it seems sensible to give an overview of the whole system first. Fig. 11.1 shows a schematic that divides the setup into substructures. The descriptions in the course of this chapter will largely follow these logic units.

In order to use laser light to both heat a localized volume of a sample and to monitor the reflectivity at the same location, it is necessary to first generate the required laser beams, to combine them, so they propagate in the same way, and to shape them so that a controlled intensity profile is guaranteed at the sample (see Sec 11.2).

Longterm fluctuations of laser power are coped with by permanently sampling the incoming light (see Sec. 11.3).

A video microscope unit allows to visually monitor, where the laser beams hit the sample (Sec. 11.4). The latter can be positioned by an electronically controlled three axis stage system (Sec. 11.5) that carries a heated sample holder (Sec. 11.6). Alternatively the laser beams can be moved relative to the sample, keeping the position of the stages fixed (Sec. 11.7).

The reflected light is coupled out of the optical path of the incoming beams by a Faraday isolator (Sec. 11.8). One part of this light is detected and its intensity is recorded for the determination of the sample's reflectivity (Sec. 11.9). The rest is used as input signal for an autofocus control (Sec. 11.10).

The long working distance of the microscope objectives used allow the contacting of the sample via pneumatically launching electrical probes. These connect the sample

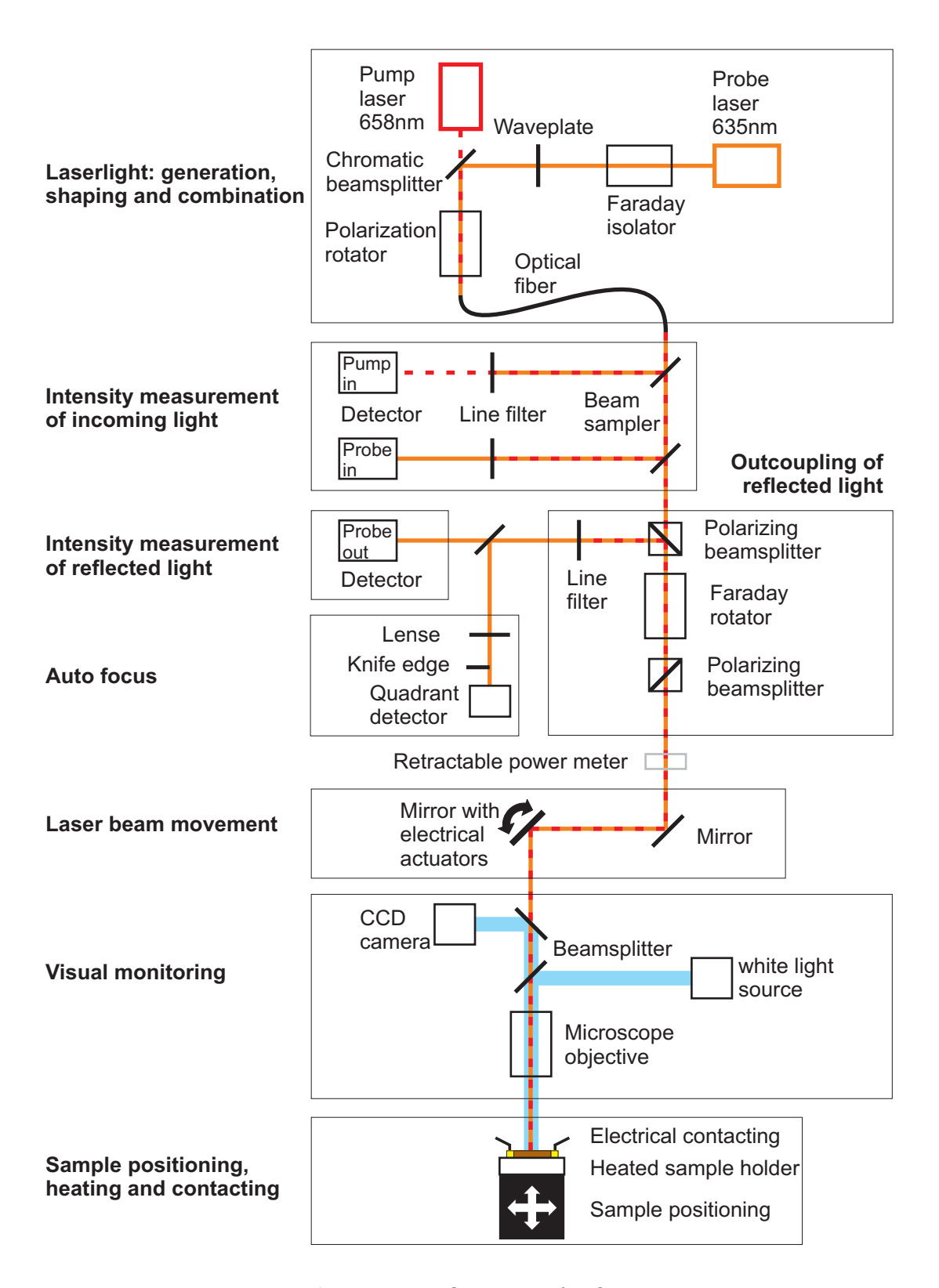


Figure 11.1: Overview of *POET* 

to electrical circuits measuring the electrical properties of the sample (Sec. 11.11).

Not depicted in Fig. 11.1 for clarity are peripheral devices, which are nevertheless important for the functioning of the setup. Therefore they are mentioned where appropriate in the context of this chapter.

Last, but certainly not least, the control software on the personal computer the experiments are operated from is explained (Sec. 11.12).

# 11.2 Laserlight: generation, shaping and combination

POET employs two lasers with different wavelengths. For heating, a diode laser with 658 nm wavelength is used to output intensities of more than 200 mW in pulses, that can be as short as few nanoseconds and as long as tens of microseconds. The laser diode, a Mitsubishi ML240G21, is driven by a National Semiconductor LMH6525 four-channel laser diode driver. The diode is soldered on a custom-made printed circuit board together with the necessary electronic components. The driver circuit itself receives its pulse signals from a Hewlett and Packard 8131A 500 MHz pulse generator. This defines the length of the laser pulse, while its intensity is controlled by a DC voltage.

The pulse laser and all other optical components described in this section are shown in a commented photograph in Fig. 11.2, as they were assembled by the author of this thesis in the scope of his work.

In order to gather information about the progress of crystallization during the heating pulse, a second, low-power laser, a ChromaLase 635 from BlueSkyResearch, with a wavelength of 635 nm is used in continuous wave mode. The wavelength of this probe laser differing from the one of the pulsed laser enables to filter out the contribution to the reflected light that originates from the high intensity heating laser. This way small changes of the reflectivity can be detected by the probe laser. The wavelengths were selected to be similar to reduce effects of chromatic aberration in those optical components that are passed by both laser beams.

Pump and probe laser are combined with a chromatic beamsplitter, which transmits most of the incident light at  $658 \,\mathrm{nm}$  while reflecting a good portion of the light at  $635 \,\mathrm{nm}$ . Two main objectives are set regarding the combined laser beams. The first is the shape of the beam. The intensity profile of the contributions of both wavelengths should reproduce a  $\mathrm{TEM}_{00}$  mode, i.e. the light intensity hitting the sample should radially decline like a gaussian distribution. The second is to have the best possible overlap of the  $\mathrm{TEM}_{00}$  modes for the two wavelengths, i.e. optimum alignment of the

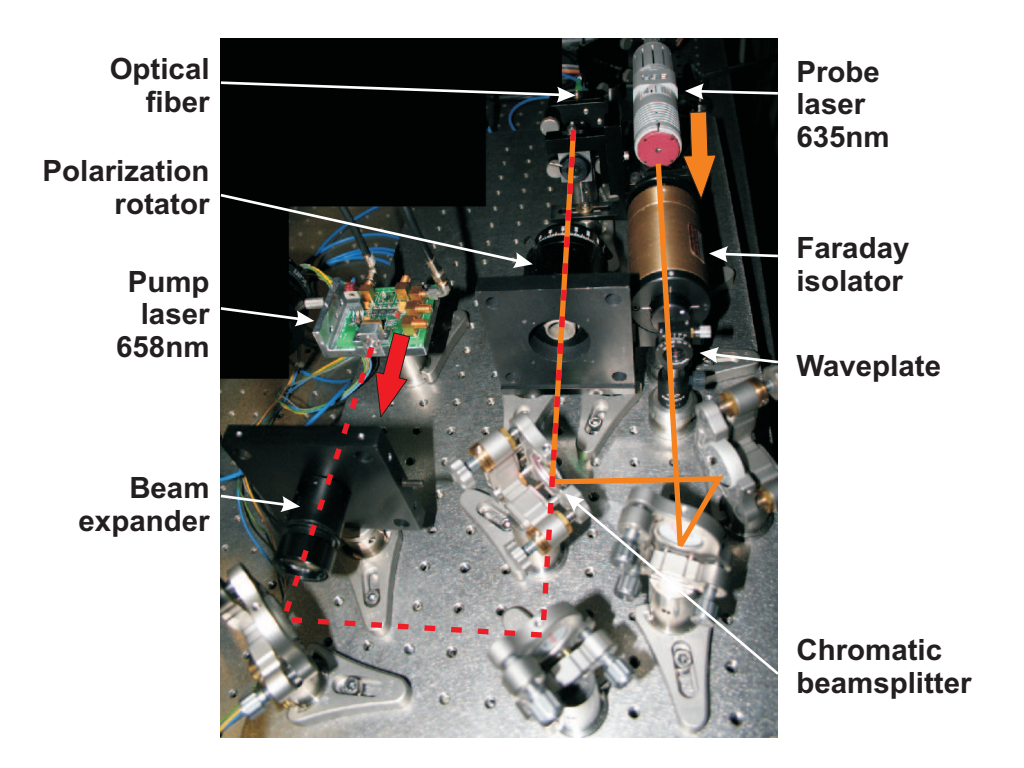


**Figure 11.2:** Laserlight creation and combination in reality: The mirrors, although not marked, are important for a successful combination of the two laser beams, because they provide the experimenter with enough degrees of freedom not only to hit the end of the optical fiber but also to align the lasers' direction of propagation at that point in space.

centers of highest intensity on the sample.

Both objectives are achieved in POET quite well by coupling the combined beams into an optical monomode fiber that allows propagation only for a single mode, the  $TEM_{00}$ . So even if the laser sources do not provide a perfect monomode and the chromatic beamsplitter does not allow for a perfect alignment of propagation direction for both wavelengths, the light that passes the optical fiber should fulfill the mentioned requirements satisfactorily.

The implementation of a monomode fiber into the system does not only bring these undisputed advantages, it also emphasizes the importance of temporal stability of the laser sources with respect to intensity, but even to propagation direction and laser modes. The latter two would obviously also change the net intensity leaving the fiber towards the sample. Therefore the ChromaLase 635 has been used as probe laser source due to its good power and pointing stability and its low optical noise. Accordingly, it is connected to an ILX Lightwave LDX-3620 ultra low noise current source.

As will be discussed in more detail in Sec. 11.8, the mechanism for separating the light reflected by the sample from the incoming beam is based on polarization. As a consequence, both parts of the laser beam, the probe and the pulse laser, need to be linearly polarized in the same direction. The light each of the two laser sources provides

is already reasonably well polarized. Thus only a half-wave plate is necessary to rotate the polarization direction of the probe laser to match the one of the pulse laser. After the beams are combined, an achromatic polarization rotator adjusts the polarization direction to what is needed by the outcoupling mechanism mentioned above. The optical fiber must therefore be polarization maintaining.

An additional feature of the optical fiber is that its ends are polished at an angle for low back reflection. This is desirable because minimum light should be reflected back into the laser cavity. Such reflection can seriously disturb the electro-magnetic fields forming the mode inside the cavity, which determines the mode of the light that is sent out. Especially at the front end of a fiber it is not possible to just tilt the optics slightly in order to let the light reflect out of the optical path, since the coupling efficiency into the fiber would be severely reduced at the same time.

The Faraday isolator directly in front of the probe laser serves the same purpose. It allows the linearly polarized light emitted from the laser diode to transmit to a large extent, while most of the light that passes the isolator and is reflected at some later point is not transmitted through the isolator back towards the laser cavity. The working principle of a Faraday isolator is described in more detail in Sec. 11.8.

How well all the provisions described in the present section have been able to achieve a controlled laser profile on the sample can be seen in Fig. 11.3. There the results of a measurement of the beam profile at the sample position are plotted. Those measurements have been accomplished with a scanning knife-edge beam profiler positioned in the focal plane of the microscope objective, where otherwise the sample is hit by the laser beams.

# 11.3 Intensity measurement of incoming light

After the combined beams of pump and probe laser have been aligned and shaped by the monomode optical fiber, a beam sampler reflects a small portion of the light, i. e. few percents of the power, of both beams out of the optical path.

The fact that the beam sampler is several millimeters thick allows the separated use of both reflected beams, i. e. the one reflected at the front surface of the beam splitter and the one reflected at its back surface. It has the advantage that the addition of another beam sampler for the outcoupling of a second beam can be avoided. This is part of the general strategy of putting as few optical components as possible into the path of the pulsed laser in order to maximize the available heating power on the sample.

One of the two beam samples passes a spectral band filter that only allows the light

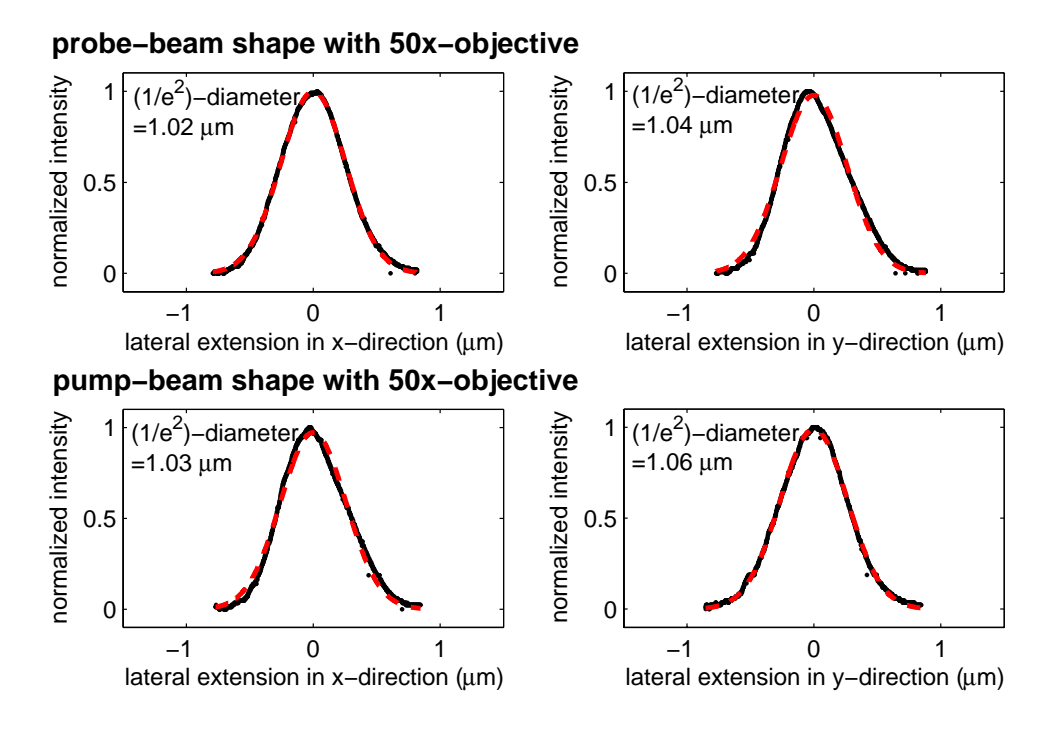


Figure 11.3: Laser beam profile on sample: Result from measurements with a scanning knife-edge beam profiler (black dots). The profiler has been positioned in the focal plane of the microscope objective, which otherwise focuses the beams on the sample. The intensity profile has been detected for the 50x objective, which has been used for laser annealings. Microscope objectives with lower magnification are only used for monitoring the sample position between laser annealing experiments. At low magnification the spot size is too large and the corresponding intensity is too low for heating the phase change sample above the melting temperature in order to achieve amorphization. Both the probe (top) and the pump beam (bottom) have been scanned along orthogonal axes inside the focal plane. Fits of a Gaussian distribution (red dashed lines) yield very good agreement with the experimental beam profiles. The intensity distribution of both lasers can therefore be considered to be in TEM<sub>00</sub> mode. Moreover, the beam diameter, defined as the diameter, where the intensity drops to  $1/e^2 \cong 13.5\%$  of the maximum intensity, is around  $1 \mu m$  for both the pump and the probe beam.

of the pump laser to transmit but not the light of the probe laser. In contrast, from the second beam sample the 658 nm wavelength components of the pump beam are filtered out by a line filter, letting only the light from the 635 nm probe laser transmit. This way the detection of the power of the filtered beams represents the separate measurement of the power of the incoming probe and the incoming pulse laser light.

For the pump laser detection a Hamamatsu S5973 silicon PIN photodiode is used for its high speed response (cut-off frequency of 1.5 GHz). Like all detectors in *POET* it is mounted on a custom-made printed circuit board. The electronic circuits, especially regarding the implementation of suited operational amplifiers, are designed to match the speed and power requirements of the respective laser light to be detected. In the case of the incoming pump laser the comparably large intensity does practically not act as a limitation, so the detector and the attached electronic circuit is optimized mainly for high temporal resolution.

For the incoming probe laser light the situation is reversed. It is measured to take care of long-term drifts of the power of the probe laser. Thus a high time resolution is not important and can therefore be traded for higher sensitivity in the design of the detector. Accordingly a Hamamatsu S1223 silicon PIN photodiode with 20MHz cut-off frequency is implemented into an adapted circuitry providing a good signal even for low laser powers. The low powers are unavoidable, since the probe laser light hitting the sample needs to be minimized in order to guarantee that heating by the probe laser can be neglected in the experiments.

The amplified signal from the slow detector measuring the power of the incoming probe laser can be read out by a simple analog input of a computer interface. The fast signal from the pump laser detector, in contrast, is fed into a fast oscilloscope, here a Tektronix TDS7404 Digital Phosphor Oscilloscope with 4 GHz bandwidth and maximum sampling rate of 20 Gigasamples per second.

A calibration of the height of the output signals from the two detectors can be carried out by the system automatically before each series of experiments, provided the user wants it to do so. For this calibration a Newport 818-SL detectorhead, which is connected to a 2832-C Newport dual channel power meter, is pneumatically moved into the beam path almost directly before it enters the video microscope unit. The power loss from this point to where the beam hits the sample has been determined before and is assumed to stay constant in time. The latter has been confirmed repeatedly by sporadic power measurements directly at the sample's position.

It is advisable to position the power meter as late as possible in the optical path in order to be sure of the mentioned constancy in power loss on the lasers way to the sample. In constrast, the powerloss of the light passing e.g. polarization discriminating optical components, like the Faraday isolator described in Sec. 11.8, can vary if the polarization of the entering laser light should change unintentionally. Thus the power meter should definitely be positioned behind those components.

This way the power of the beam measured before entering the microscope unit can be extrapolated to the power at the sample, which is then used as reference for the heights of the output signals of the photo detectors.

The calibration procedure copes with a possible non-linearity of the detectors by recording a whole calibration curve, meaning the power at the sample extrapolated from the values measured with the power meter as a function of the signal height of the detector. Only the interpolation between two data pairs of the calibration curve is linear.

### 11.4 Visual monitoring

The beam sampler couples out only a small representative portion of the photons for the determination of the power of the incoming light. The main part of the laser light passes. Also the polarizing beamsplitters around the Faraday rotator are oriented in a way so that the transmission of the incoming beam is maximized.

In order to heat the sample to high temperatures, higher than the melting temperature of phase change materials, the pulsed laser beam needs to be focussed significantly. This is achieved with a 50x microscope objective. The Mitutoyo M Plan Apo 50x has been used for its combination of a quite long working distance, important for electrical contacting of the sample, at a still rather large numerical aperture of 0.55. As already shown in Fig. 11.3 the resulting beam diameter in the focal plane is around  $1 \mu m$  small.

To monitor where exactly the laser hits the sample, the microscope objective is attached to a video microscope unit (also by Mitutoyo). It essentially illuminates the sample through the microscope objective with white light and projects an image of the sample out of the laser beam path onto a CCD camera, a Pulnix TM-1400CL. Both is done with beamsplitters that are largely transparent in the red, i.e. for both laser wavelengths. This maximizes the pulse laser power on the sample and lets most of the reflected probe signal leave the video microscope unit 'upstream' in the path of the beam. Moreover, the CCD chip is protected from destruction by high power laser pulses. However, since the beamsplitter's reflectivity in the red spectral range is not zero and because the laser light is much more intense than the white light, the reflection of the laser spot is also visible on the image taken by the CCD camera.

To allow the user to navigate the laser on the sample with a convenient field of view, a revolver for four microscope objectives is equipped with less magnifying objectives besides the 50x one. In the course of setting up the optics, care is taken for the higher magnification objectives to zoom roughly into the center of the field of view of the lower magnification objectives. Also the laser is aligned so that it hits almost the same spot on the sample irrespective of the used microscope objective.

### 11.5 Sample positioning

To bring a sample into the focal plane of the laser beams, which at the same time produces a sharp image of the sample at the CCD camera, a Newport VP-5ZA precision vertical linear stage is used. It provides a travel range of 4.8 mm with a resolution of  $0.2 \,\mu\text{m}$ . This resolution is sufficient for a good control over the focusing on the sample, which will be discussed in more detail in the section on the autofocus (Sec. 11.10).

Its comparably high load capacity of 50 N for normal centered load allows to stack further stages on top of the vertical stage and still have good margin to design a heated sample holder (see Sec. 11.6) without too tight restrictions with respect to its weight.

Two Newport VP-25XA precision linear stages mounted orthogonal to each other move the sample within the focal plane to steer a chosen location on the sample into the focal point of the laser beams. These stages have a 25 mm travel and  $0.2 \,\mu\text{m}$  resolution. This resolution of the horizontal stages turns out to be sufficient for most experiments. However, for a certain type of experiment, where the control over the position of the laser on the sample needs to be better than 100 nm (see Sec. 12.3), alternative ways to shift the laser across the sample's surface had to be considered. One solution of this problem improving the precision of such shifts has finally been implemented into POET. It is described in Sec. 11.7.

All stages are motorized and electronically controlled via a Newport XPS Motion Controller, which itself communicates with the control software (Sec. 11.12) for the whole setup which is run on a personal computer.

## 11.6 Sample heating

The most primitive version of a sample holder one could think of will at least keep the sample fixed with respect to the stages it is mounted on. In *POET*, however, the sample holder is much more sophisticated than that.

In order to minimize stress inside the sample, which could easily be introduced when clamping the sample, in *POET* the sample is sucked down by low pressure in a cavity inside the holder right underneath the sample.

This has the further advantage of high reproducibility in establishing a perpendicular incidence of the laser beams onto the sample surface. The latter is necessary to reflect the probe laser light exactly in opposite direction to the incoming beams. This is crucial for the detection system (Sec. 11.9) and the autofocus (Sec. 11.10) to work properly.

To accomplish this the only additional requirements are to have a sufficiently flat surface of the sample holder and reasonably plane-parallel surfaces of the samples. The latter is given, when using silicon wafers as substrates. The one-time leveling of the sample holder is done by checking how the sample leaves the focal plane of the microscope objective, when it is nominally moved in one of the two horizontal directions. The alignment works like in a standard kinematic mirror mount with three actuators. Three screws with fine pitch threads press the sample holder away from its base plate, against the force of two pull-springs. The base plate is attached to the stack of stages.

In POET the sample holder does not only help positioning the sample, but it can also heat it. A three dimensional drawing of the heater is given in Fig. 11.4(a). A gold-plated copper block acts as heat bath for the sample. It is heated by two cartridge heaters fit into the block. A thermocouple measures the temperature inside the copper block closely below the sample. The temperature signal is fed into a Watlow controller that drives the cartridge heaters. The temperature controller itself communicates with POET's main control software.

At its bottom the copper block has fins, between which compressed air can be blown out of the sample holder to cool it down more rapidly after an annealing experiment at high temperatures. To achieve a high air flux there are openings in the shielding. The shielding prevents the enclosed copper block from loosing too much heat to its surrounding by radiation and convection. To minimize heat loss by conduction the copper block stands on stainless steel tubes. The latter act not only as mechanical posts but also as feed pipes for the low pressure that sucks the sample down to the holder, and for the compressed air that cools the fins.

Another very useful detail about the sample holder is the set of three pins at the top of the copper block. They are used to lock the usually roughly rectangular substrates in place. As long as the user keeps track of the general orientation of a sample, i. e. where its front side is, *POET* can return to a previously investigated part of the sample, the position of which has been saved automatically. This is extremely useful especially when exchanging samples frequently.

A photograph of the realization of such a heated sample holder implemented into POET is given in Fig. 11.4(b). With this holder temperatures higher than 600 K were

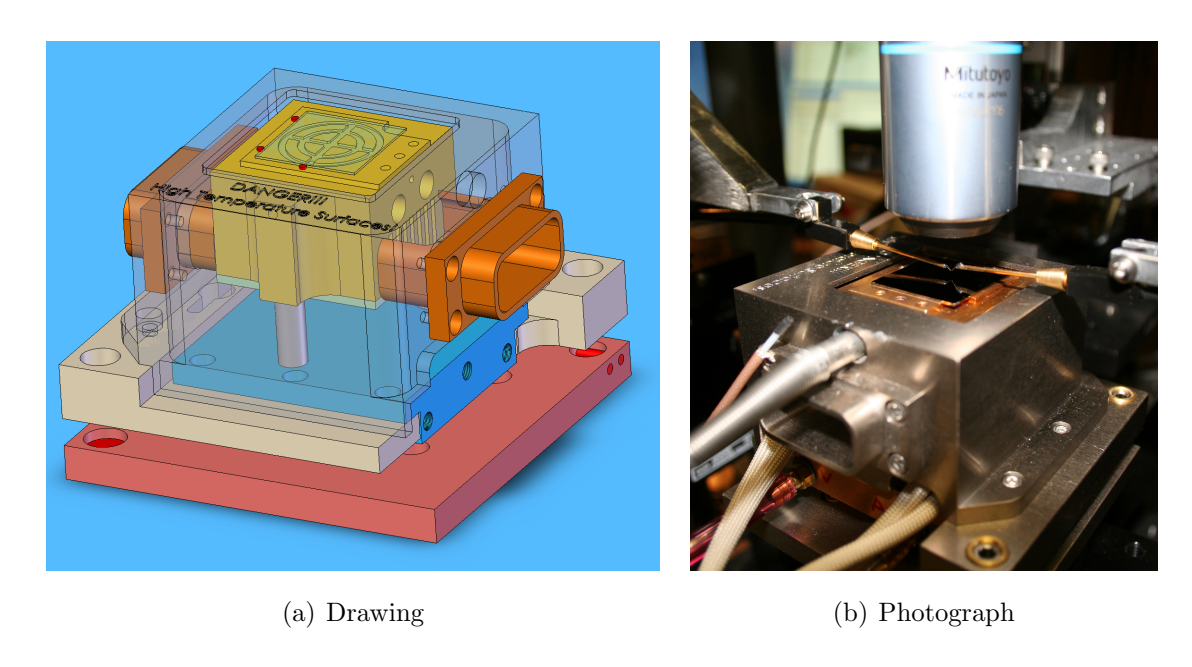


Figure 11.4: Heated sample holder: The three-dimensional drawing (left) shows a quadratic sample (semi-transparent) on top of the copper block (yellow) that is locked in place by three pins (red). The small blind hole and the two large ones at the right hand side of the copper block are drilled for a thermocouple and two cartridge heaters, respectively. The fins at the bottom of the copper block are oriented so that the flux of cooling air can leave the heat shielding (semi-transparent) through its openings (orange). The stainless steel tubes (grey) serve the copper block as mechanical posts and as feed lines for both low pressure and compressed air, respectively. The sample surface is aligned perpendicular to the laser beam in a way similar to a kinetic mirror mount: Three fine thread screws push the sample holder against the base plate (pink), which is connected to the stages. The photograph of the implemented heated sample holder (right) also shows a sample on a silicon substrate, electrical probes approaching the device from the sides and a microscope objective introducing the laser from the top.

obtained.

The reason why this heated sample holder is described so extensively is not the obvious high level of sophistication of its design, but its novelty inside a system like *POET* and the great potential for a whole new field of experiments it adds to the setup. While one specific type of experiments on the determination of crystal growth velocities over several orders of magnitude will be explained in detail in Sec. 12.6.1, here only a few examples shall highlight this potential.

The importance of numerical simulations in the calculation of the performance of phase change devices has already been discussed in Chapter 10. A universally valid need in this context is the locking down of simulation parameters by experimental evidence. The heated sample holder provides an experimentally controlled and tunable physical parameter: the offset temperature of the sample's substrate. A series of experiments varying this quantity can be used to double-check the validity of simulations, e.g. of crystallization kinetics in thin films. The reason is that the varied quantity directly influences the results of a simulation without introducing a new unknown parameter. The functional dependence of the outcome of an experiment on that quantity can thus be used to determine simulation parameters that are not directly accessible by fitting them to the experimental evidence.

Another interesting field of experiments is the temperature dependent electrical testing. On the one hand such experiments are necessary for a fundamental understanding of the peculiar electrical properties of phase change materials' amorphous phase, culminating in the effect of threshold-switching. On the other hand they have a very practical relevance in the context of an application of those materials in electronic memories. The high density of frequently switching cells inevitably leads to an increased working temperature of a PCRAM cell. How an increased base temperature degrades a cell's performance until it ultimately prevents it entirely from switching will obviously have implications for the design of a PCRAM memory.

#### 11.7 Laser beam movement

As mentioned briefly in the section on sample positioning (Sec. 11.5) the resolution of the stages carrying the sample is not always sufficient. For experiments that require a high precision in horizontal motion of the sample relative to the laser beams, e.g. like those described in Sec. 12.3, a higher resolution is necessary.

A replacement of the stages by more precise ones would not only have been very expensive, but more precise stages are also often layed out for less load. The latter would have implied further major changes in the setup, especially regarding the heated

sample holder.

A much more cost-effective improvement of the situation has been achieved by reversing the solution for the problem of relative motion of sample and laser beam. The sample position is kept fixed and the laser beam is actually scanned across it. Therefore, the micrometers in the mount of a mirror that deflects the laser beam briefly before it enters the video microscope unit are replaced by Newport NSA12 actuators. This way the tilt of the mirror and therewith the shift of the laser spot on the sample can be set electronically from POET's control software.

The geometry of the optical path, especially the distance from the actuated mirror to the video microscope unit and the refraction power of the optical components, foremost the microscope objective, let the resolution of the actuator motion result in a control of the laser beam position on the sample that clearly exceeds the resolution of the stages. The AFM images resulting from the demanding experiments in Sec. 12.3 will give an impression of what has been achieved.

### 11.8 Outcoupling of reflected light

As already mentioned in Sec. 11.6 the sample surface is positioned perpendicular to the incident laser beam. Thus the reflected beam will exactly follow the path of the incoming one, just in opposite direction. In order to detect the reflected laser light it is therefore necessary to separate it from the incoming laser beam. In *POET* a Faraday isolator serves this purpose. It consists of three optical components: an entrance polarizing beam splitter cube, a Faraday rotator and an exit polarizer.

Fig. 11.5 illustrates the working principle of this assembly. The incoming light is linearly polarized in the direction that allows maximum transmission through the entrance polarizing beam splitter cube. This is achieved by an achromatic polarization rotator before the laser beams are coupled into the optical fiber (see Fig. 11.1). Imperfections in the polarization of the incoming light are cleaned up by the entrance beam splitter cube the better the higher its extinction ratio is.

The Faraday rotator following next in the beam path utilizes a magneto-optical phenomenon, the so-called Faraday effect, to rotate the plane of polarization by 45°. Inside the Faraday rotator a permanent magnetic field is applied to a dielectric material parallel to the light's direction of propagation through this dielectric. The angle of rotation of the plane of polarization  $\beta$  is proportional to the magnetic field B, the length d of the path, where the light and the magnetic field interact, and the so-called Verdet constant of the used material  $\nu$ :

$$\beta = \nu Bd \quad . \tag{11.1}$$

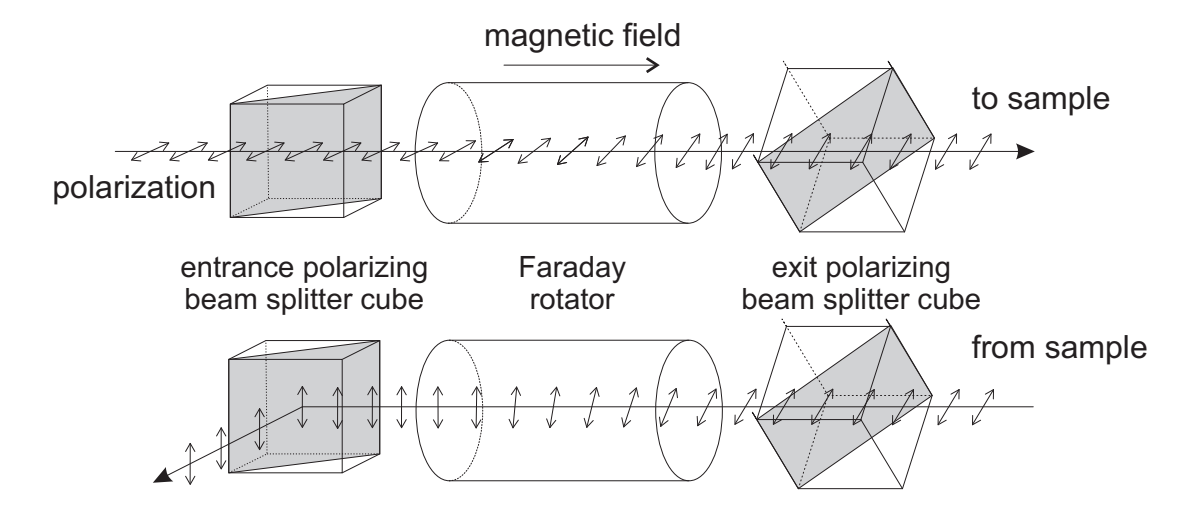


Figure 11.5: Faraday isolator: Linearly polarized light is transmitted through the entrance polarizer. The strong magnetic field in the Faraday rotator causes the light's plane of polarization to rotate by 45°. The exit polarizer, tilted by the same 45° relative to the entrance polarizer, allows the resulting light to transmit with maximum intensity. Since the reflection at the sample preserves the plane of polarization, the exit polarizer transmits also the largest portion of the reflected light. The Faraday effect lets the plane of polarization rotate into the same direction as before. The resulting total tilt of 90° compared to the polarization of the original laser beam causes the entrance polarizing beam splitter cube to deflect most of the light from the sample to the side.

The material specific  $\nu$  is an empirical proportionality constant that is in general dependent on wavelength and temperature.

The exit polarizer, often also a polarizing beam splitter cube, is tilted by 45° relative to the entrance polarizer so that the light coming from the Faraday rotator transmits with minimal loss. At this point again imperfections in the linear polarization of the laser light propagating towards the sample are cleaned up.

The sample reflects the incident laser light preserving the plane of polarization. Thus the reflected beam experiences maximum transmission through the exit polarizer.

The Faraday rotator turns the plane of polarization again by 45° into the same direction as before. This results in a total rotation of 90° compared to the original laser beam entering the entrance polarizer at first. With this polarization the reflected light from the sample is almost completely deflected by the entrance polarizing beam splitter cube.

On the one hand this makes most of the reflected light available for detection (Sec. 11.9) and autofocussing, respectively (Sec. 11.10). On the other hand the reflected light, especially that from the high power pulsed laser, is prevented from propagating all the way back into the laser cavities, where it could harm the laser diodes or at least disturb their performance.

#### 11.9 Intensity measurement of reflected light

After the reflected light from the sample is deflected by the Faraday isolator, one fraction of the intensity of the continuous wave probe laser light is used to determine the reflectivity of the sample. The light with 658 nm wavelength from the pump laser is filtered out by a chromatic line filter that is transparent only around the probe laser's 635 nm.

The detector for the intensity measurement of the reflected probe beam is the one with the most demanding requirements in the whole setup. It needs to be as fast as the detector sampling the incoming pump beam, because a high temporal resolution of a sample's reflectivity during its annealing is desired. At the same time the detector needs to be extremely sensitive, similar to the detector sampling the incoming probe beam, because the power of the probe laser needs to be as low as possible to minimize unintentional heating of the sample. A custom-made printed circuit board driving a Hamamatsu S5973 silicon PIN photodiode has been optimized regarding the combination of these challenging demands.

The amplified signal from the detector is recorded by the fast oscilloscope mentioned above. In order to draw a conclusion about the absolute reflectivity of the sample it is necessary to calibrate the voltage scale of the detector output. Therefore a reference with known reflectivity is placed, where otherwise the samples are positioned. Only the probe laser irradiates the sample. Given a calibration of the detector sampling the incoming probe beam, as described in Sec. 11.3, the absolute power of the incident probe beam on the sample can be derived from this detector's signal. Multiplying this value with the absolute reflectivity of the reference sample gives the absolute probe beam power that is reflected by the sample. The latter is then linked to the measured height of the output signal of the detector for the reflected light.

Like in the case of the detectors sampling the incoming beams, here also no linearity needs to be preassumed in the relation between laser power and detector output signal. Instead a whole series of calibration points for varying laser power can be taken automatically by *POET*. Again like for the other detectors, the calibration is interpolated linearly, which is legitimate for a reasonably dense set of calibration points.

The traces in Fig. 12.4 give an impression on how typical signals from the reflectivity detection in *POET* look like.

### 11.10 Autofocus

Besides the time-resolved determination of the absolute reflectivity of a sample, the reflected light is also used as the input signal of a regulation that automatically focuses the sample. A beamsplitter deflects a part of the reflected laser beam centric onto a quadrant detector resulting in an equal irradiation of the different quadrants. Before it reaches the detector, however, the beam is focussed by a lens. Further, one focal length behind the lens a knife-edge is positioned so that the light can merely pass on its way to the quadrant detector, given the sample is in focus. If the sample leaves the focal plane of the microscope objective, the reflected beam hitting the lens will diverge more or less causing the focal point behind the lens to shift relative to the knife-edge. The latter will consequently cut off certain parts of the light that would have otherwise irradiated distinct quadrants of the detector. The resulting change in the signals from the detector indicates in which direction and how much the vertical stage has to move to steer the sample back into focus.

A more detailed explanation of which change of the sample position has what effect on the detector signals is given in the caption to Fig. 11.6, where the parts of the beam path relevant for the autofocus are depicted.

The autofocus facility enables *POET* to automatically perform large sequences of optical annealing experiments. Not only could the sample position drift over longer periods of time. Also, during experiments, wherein each annealing pulse needs to be applied to a virgin area of the sample (see Sec. 12.1), the horizontal stages have to travel long distances, whereupon the sample could easily run out of focus. To guarantee a reproducible spotsize and therewith a controlled intensity of the laser pulses, it is indispensable to have the sample in the focal plane of the microscope objective during each pulse. For thousands of laser pulses it would be not only very unpractical, but also much less reproducible to have the user refocus the sample manually. The control software of *POET* utilizing the autofocus is the only sensible solution for this task.

The same implementation is also very useful, when thermal expansion of the sample holder due to heating lifts the sample with respect to the microscope objective. A regulation of the vertical stage based on the autofocus signals can compensate for this unintended fluctuations in the height of the sample holder. A fixed position of the sample's surface is also desirable in purely electrical experiments, because the electrical contact to the electrodes of a cell is sensitive to the force, with which the electrical probes are pressed on the contact pads. The latter would change upon expansion of the heater during a temperature variation in the course of an electrical experiment. So in this case the regulation of the sample height via the autofocus is beneficial to the stability of the electrical contacting.

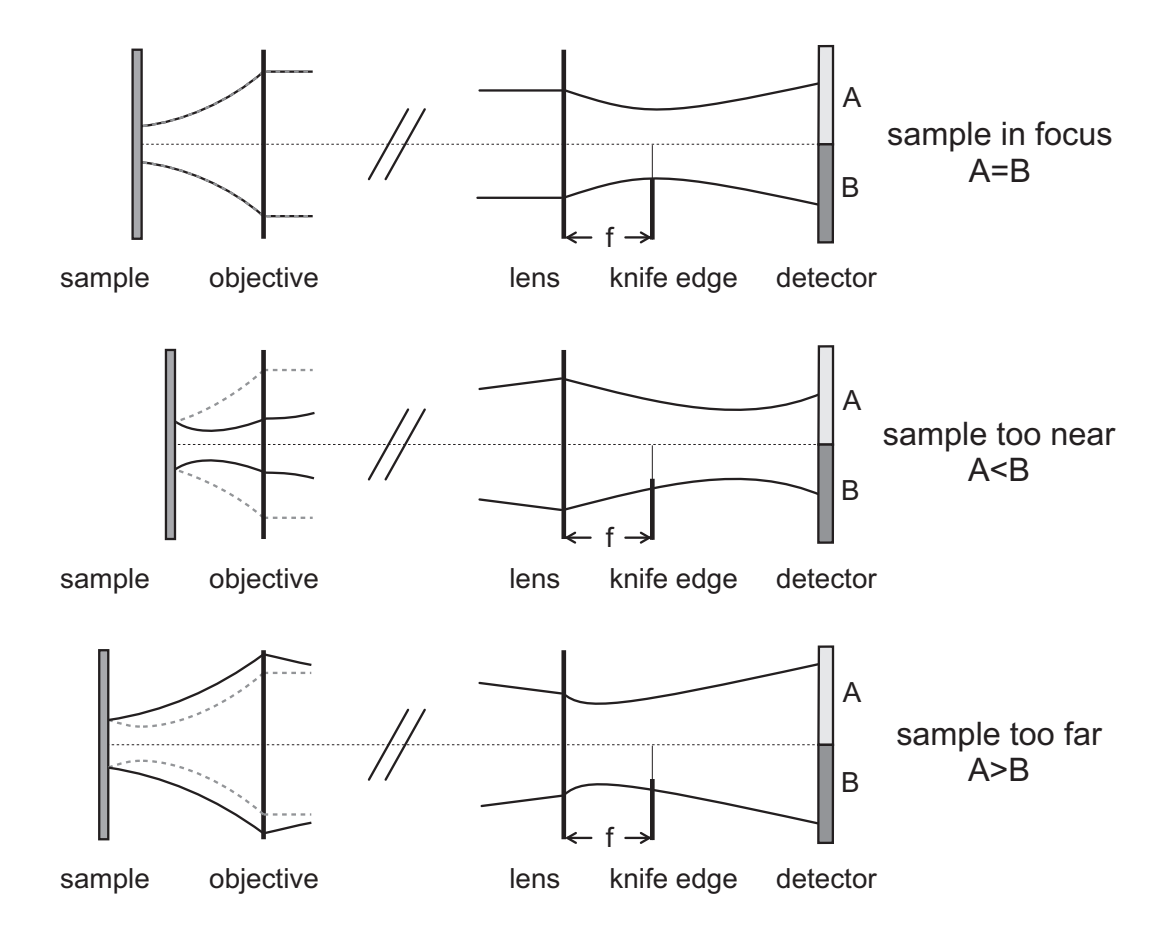


Figure 11.6: Illustration of the working principle of *POET*'s autofocus: The incoming laser beam (dashed grey) is focussed by the microscope objective. After hitting the sample the reflected light (solid black) is collected by the objective again. If the sample is positioned in the focal plane (top), the microscope objective will produce a collimated laser beam from the reflected light. This beam is ultimately refracted by the lens of the autofocus optics to form a waist just one focal length away from the lense. There the knife-edge is positioned in such a way, that it does not block any light resulting in a balanced irradiation of the quadrant detector. If the sample is positioned too close to the microscope objective (middle), the latter cannot totally collimate the reflected light. The diverging beam causes the focal point behind the lens to shift towards the detector. Consequently the knife-edge blocks light, that would have otherways hit the upper part (A) of the detector. In case the sample is too far away from the microscope objective (bottom), the reflected light is refracted into a converging beam. This results in a shift of the waist of the beam closer to the lens. Accordingly, the knife-edge partially screens the bottom part (B) of the quadrant detector. All effects are exaggerated for clarity.

#### 11.11 Electrical testing

For electrical testing of phase change cells a transmission line scheme has been chosen to be implemented into *POET*. As illustrated in Fig. 11.7 in this method two coaxial probes (by Picoprobe) are used to contact the two electrodes of a cell with their signal lines while handing over their shield potential via a separate, continuous contact pad located next to the device under test.

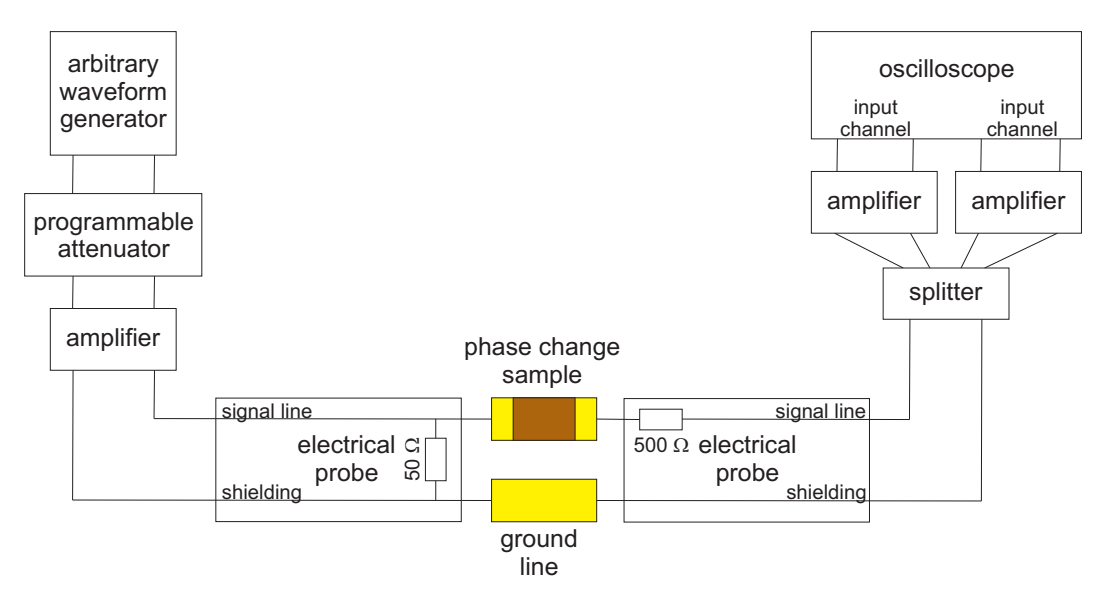
Due to the high resistance of typical phase change cells, especially in the amorphous state, fast AC voltage signals would face strong reflection at the device under test. In order to cancel out such reflections a  $50\,\Omega$  resistor connects signal and ground line next to the tips at the end of the coaxial probe, that applies the voltage to the device. The spatial proximity of less than 5 mm between that resistor and the device under test is sufficient to let incoming voltage signals effectively "see" a  $50\,\Omega$  termination on a nanoseconds time scale zeroing any reflection. The AC signal leaving the cell at the opposite electrode is picked up by the second probe, which incorporates a  $500\,\Omega$  resistor in the signal line just behind its tips.

The applied voltage signal is created by a Tektronix AWG520 1 GHz arbitrary waveform generator. It gives the user valuable freedom to choose any pulse shape that seems useful for the investigation of the electrical properties of phase change materials. At the same time the waveform generator's maximum output voltage into  $50\,\Omega$  is just 1 V. To have higher voltages available for testing an amplifier has been inserted, unfortunately at the price of reduced temporal resolution.

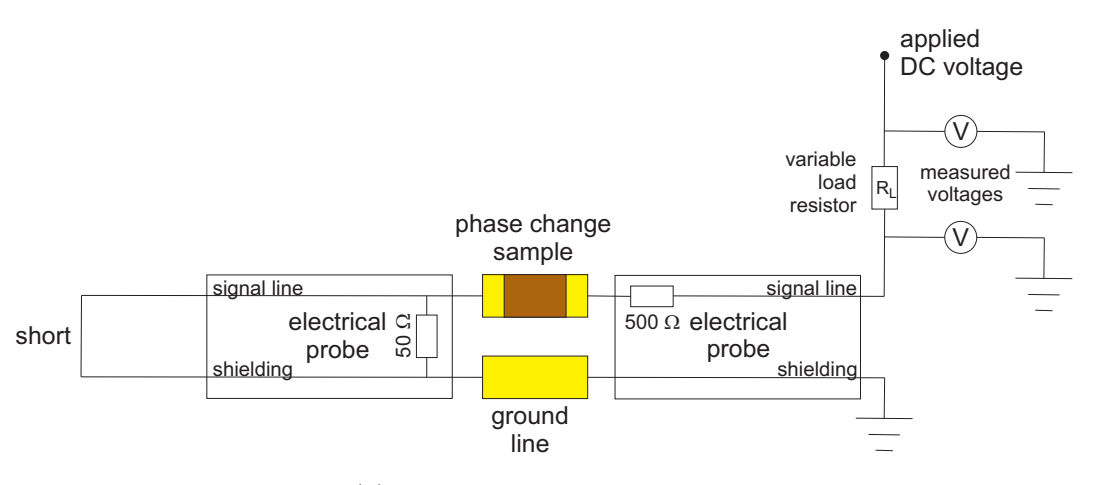
In order to modify the voltage pulse one should not simply vary the height of the waveform generator's output signal. The signal shape would loose resolution in voltage that way. Instead in *POET* programmable attenuators reduce the height of the 1 V signal coming from the waveform generator, before it is then amplified by a constant factor and finally applied to the device under test. This combination of arbitrary waveform generator, programmable attenuators and amplifier increases the maximum voltage applicable to the sample to around 6 V.

Not only the signal that is applied to the device under test, but also the outgoing signal is amplified before it is read out by the digital oscilloscope. In order to have a wider range of sensitivity the signal is split in two with a  $50\,\Omega$  impedance signal devider and then amplified with different factors. This strategy is chosen, because amorphous phase change cells change their resistance rapidly by several orders of magnitude during threshold switching. One fixed amplification could not cope with the corresponding wide range of currents through the device.

While this scheme provides the opportunity to apply *fast* pulses and to monitor the time evolution of the resulting current, it is not suitable for a *precise* determination



(a) Application of fast voltage signals



(b) Slow resistance measurement

Figure 11.7: Electrical testing: In the chosen transmission line concept the signal lines of two coaxial probes are attached to the electrodes of a phase change cell. For the application of fast voltage pulses to the cell (top) a  $50\Omega$  termination at the probe that introduces the signal to the device is needed in order to avoid signal reflections. The same  $50\Omega$  resistor would hinder a precise measurement of the cell resistance (bottom) applying DC voltages via a load resistor. Therefore the back ends of the electrical probes are switched between the two according electrical circuits with computer controlled relays.

of the resistance of a sample. For the latter a slow *ex-situ* measurement is performed before and after each pulse and whenever the user wishes to have an additional measurement.

Two options have been implemented into the setup for this measurement. The first is the application of low DC voltage of around 200mV via a load resistor of known resistance in series with the device under test. The voltage drop across this load resistor is measured. Together with the known resistance, both the current through and the voltage across the sample can be calculated from that.

While the  $50\,\Omega$  termination resistor inside the electrical probe is crucial for avoiding reflections in fast AC measurements, it produces a total resistance of around  $50\,\Omega$  in DC. Even large changes of the always comparably high cell resistance let the total resistance deviate only slightly from  $50\,\Omega$  and are therefore difficult to measure.

To solve this problem, for the DC measurement the roles of the two electrical probes are switched compared to the situation in the fast measurement described above. Now the voltage is applied to the sample via the probe with the  $500\,\Omega$  series resistor. This way there is no small resistor in parallel to the device under test. Actually, the  $50\,\Omega$  termination in the second probe is even bypassed by shorting its signal and shield line.

This reconfiguration of the electrical circuitry is of course not performed manually, but is realized using a relay to switch the electrical connections at the back ends of both probes.

To cover a wide range of possible cell resistances the load resistor can be exchanged, again via computer controlled relays. In POET the load resistors span four orders of magnitude. This way neither the voltage drop across the load resistor nor the voltage applied to the device under test disappears in the noise of the electronics.

Tests of this DC resistance measurement with reference resistors between  $100\,\Omega$  and  $10\,\mathrm{M}\Omega$  showed less than one percent deviation from values determined with a Fluke Ohmmeter.

An alternative way for a precise but slow measurement of the sample resistance that has also been implemented into *POET* is the employment of an EG&G Princeton Applied Research 5210 Lock-in Amplifier together with a rather slowly (less than 100 kHz) oscillating excitation signal. To achieve the same precision the maximum applied voltage could be reduced compared to the DC method mentioned first.

#### 11.12 Control software

In the course of this chapter it has been explicitly pointed out several times that certain tasks are not carried out manually by the user, but automatically by the control software of *POET*. Moreover, the present section will show that the code written in National Instruments Labview is both "backbone" and "brain" of the setup. The autofocus and the automatic calibrations of the detectors mentioned above are only "the tip of the iceberg".

First and most obviously the control software establishes communication channels to all devices that collect any kind of data, foremost to the oscilloscope recording the outcome of the fast experiments. These data together with all available information about the conditions, under which the respective experiments have been carried out, need to be saved completely and unambiguously.

It has been a very conscious decision to not let the control software fully analyze the experiments and store only final results. A later, likely deeper understanding of the physical processes involved in the switching of phase change samples might necessitate a different mathematical treatment of the raw data. This way an old analysis and its results might become obsolete, but experimental facts will not. Therefore POET's control software stores the data in a rather raw, only slightly pre-processed condition.

However, this implies at the same time that the extent of data, which are produced by large numbers of experiments with high temporal resolution in several observed quantities, is huge. In few months a single user could create several Gigabyte of raw data this way.

Consequently a well thought-out strategy of data management is necessary. There are two main columns the data management of *POET* is based on. The first is to save the raw data of each experimental event, mostly the application of an optical or an electrical pulse, in a separate file. One important purpose of this rather fine structuring of data is to limit the size of the files that need to be opened during data analysis. The raw data file is accompanied by another file that contains all available information about the conditions the experimental event has been recorded in, such as the position on the sample, i. e. the coordinates of the stages, the calibration curves for the detectors that have been used to preprocess the raw signals, or the version of control software and electronic components that are implemented into *POET*, when the measurement was carried out. Finally, as a help for fast browsing through the results, additionally screen shots of the preprocessed oscilloscope traces are stored as small image files (in png format). All files are named unambigously with the number of the according event the respective sample has experienced.

To maintain an overview of the vast number of files, produced for a variety of different samples, a rigorous hierarchy is established for sorting the experiments. Whenever a user lets *POET* bring the sample holder into exchange position, he is asked which material he is going to investigate and which sample he just placed. He may pick the

name of an existing sample he has already used earlier or enter a new material and sample name. In the case of phase change cells for electrical testing, next the device that is actually contacted needs to be specified similarly. In case of thin film samples for purely optical experiments the latter level of the hierarchy is used to group events of one measurement series (e. g. power-time-effect measurements in Sec. 12.1) instead. POET's control software creates a folder structure according to this hierarchy, which the files for all events are sorted into.

Whenever a new material, sample, device or measurement series is established, the user may input a more detailed description. Also it is always possible to enter a comment, which is saved as an event in the flow of experiments. Therewith *POET*'s control software provides the user with a digital lab book along the way of performing the experiments. This lab book not only has the advantage of reminding the user to take notes at crucial moments during the experiments. Also later searching for a specific experiment is much easier. More detailed information is always just a few mouseclicks away from the general hierarchy. Browsing through experiments is not limited to a chronological order. For further assistance in this regard *POET*'s software additionally keeps book of the experiments within html files. Therefore browsing through experiments can actually be done with a (web) browser, like Firefox.

Besides this sophisticated data handling, *POET*'s control software indeed *controls* all electronically accessible parts of the setup. On one side of the wide spectrum of devices there are the more complicated instruments, like the oscilloscope, the pulse generator or the arbitrary waveform generator. They need to be prepared for each pulse experiment, e. g. with respect to their resolution, their range or to the triggering. The electrically opening and closing of valves to pneumatically move retractable parts, like the powermeter head or the electrical probes, might mark the other end of the spectrum.

Somewhere in between there is the communication with the linear stages carrying the sample. One of the indispensable features of *POET*'s control software is the very intuitive graphical user interface for sample navigation. Providing a permanently refreshed CCD image of the sample on the monitor, the software assists the user in bringing the sample into the right position by either continuous or stepwise movement at adjustable speed or step size, respectively. In a long series of measurements the sample positioning is of course totally automated.

Besides the critical components of POET's control software, without which the setup would not be usable at all or only in an extremely laborious way, it includes numerous very handy details.

One example is the marking of that area of a thin film sample, where a series of laser

#### 11.12. CONTROL SOFTWARE

annealings has been performed on. Near to the laser marks of the actual experiments, but still in sufficient distance to not corrupt those marks, a frame is written into the film with the heating laser continuously pulsing at high powers. Additionally the consecutive numbering of the experimental series is written next to the top left corner of this frame.

An experiment marked this way can easily be identified under an optical microscope. This is extremely useful for the *ex-situ* investigation of laser experiments via atomic force microscopy, which locates crystalline regions due to their higher density and therefore lower film thickness. The marking of performed experiments also helps identifying virgin areas of the phase change film for new experiments even on heavily tested samples. This would otherwise become very difficult, where extended regions had been annealed with low power laser pulses resulting in an indiscernable change in reflectivity of the material.

A second example for a quite handy, since time-saving, feature of the control software is its ability to find back the location of any old experiment. After placing a previously tested sample onto the holder the user just picks the number of the measurement series of interest and the stages will move the sample to the recorded position. The user is assisted in the necessarily reproducible placement of the sample on the holder by the design and construction of the latter (see Sec. 11.6).

The selection of features of *POET*'s control software presented in the present section let the experienced reader sense both the capabilities and the complexity of the code. And although the implementation of electronically addressable components and the according programming demanded significant time and effort from the author of this thesis, a more thorough discussion of all facets of the program would go far beyond the scope of this text.

# Chapter 12

# Experiments Using *POET*

Es gibt kein größeres Hindernis des Fortgangs in den Wissenschaften als das Verlangen, den Erfolg davon zu früh verspüren zu wollen.

GEORG CHRISTOPH LICHTENBERG

Despite the level of sophistication in all its details, both in hardware and software, the most outstanding characteristic of POET is its versatility. To justify this appreciation to the reader, in this chapter experimental results are given rather to exemplify the variety of the different methods than to give a concluding discussion about their interpretation. Nevertheless, after having read this thesis to this point, one does not need to be an expert in this field to recognize the scientific and technological value of these results, too.

#### 12.1 Power-time-effect measurements

Likely the most basic measurement one can perform on phase change materials with a static laser tester is the determination of the change of reflectivity of a thin film sample upon annealing with a single laser pulse. The dependence of this change on power and duration of the laser pulse is usually looked at in a two-dimensional pseudocolor plot. It is not surprising that also POET is capable of producing this kind of data. Fig. 12.1 shows a power-time-effect diagram for a thin film sample of  $Ge_2Sb_2Te_5$ .

Although it sounds rather straight forward, there are some easy mistakes one could make, and people in the past actually did. Instead of extensively displaying those, the following paragraphs will concentrate on the provisions the author made for the experiments with *POET* being meaningful.

The reflectivity trace *POET* records during and therefore also *directly* before and after each laser pulse gives good confidence in the determination of the reflectivity change *right at the location*, where the pulsed laser heated the sample. Limited drift

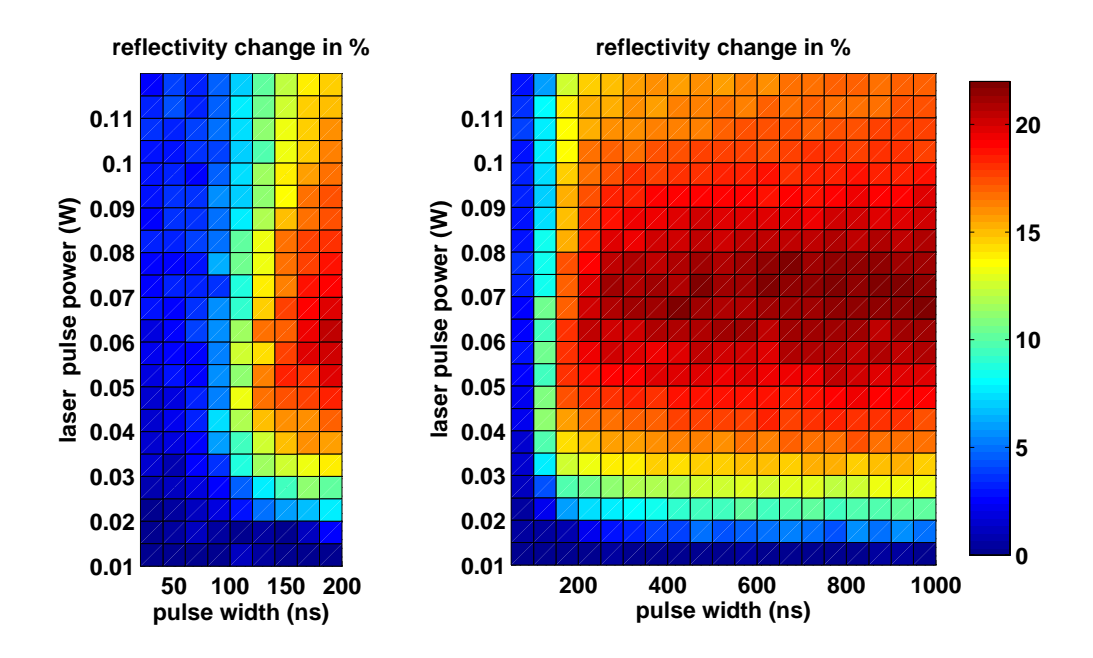


Figure 12.1: Power-time-effect diagrams for as-deposited Ge<sub>2</sub>Sb<sub>2</sub>Te<sub>5</sub>: The sample is a 30 nm thin film of Ge<sub>2</sub>Sb<sub>2</sub>Te<sub>5</sub> deposited on top of a silicon wafer, which has previously been covered with 20 nm of Al<sub>2</sub>O<sub>3</sub>. It is amorphous as-deposited. The power is the output power of the pulsed laser, the time the duration of a pulse. The colors indicate the relative change in reflectivity of the sample due to laser annealing. The left diagram is taken for better resolution at the short times edge of the crystallization region.

stability of real stages makes this detection scheme an advantage against setups, where the ex-situ reflectivity measurements before and after a pulse are more distant in time and thus possibly also in space. A laser annealing experiment typically takes place on a micrometer length scale on the sample. Small spatial deviations of the sample or the optics can therefore make a significant difference in reflectivity.

An indicator for good reproducibility is a setup's ability to produce quite homogeneous power-time-effect measurements, i. e. measurements without large fluctuations in the reflectivity change, when pulse parameters are varied only marginally. However, such a judgement of the quality of the measurement is not possible, if the data points are interpolated in the plot. Therefore a discrete representation of the results has been chosen by the author knowing that smoother plots might be subconsciously more appealing to the readers eye. That way Fig. 12.1 can serve as a prove for good reproducibility of the laser experiments in *POET* alongside.

A second important detail of the author's laser experiments, which might be less obvious than the first, is the choice of substrates for the thin film samples. All samples for optical testing are sputter deposited on a silicon wafer that is covered only with a thin heat barrier, either out of sputter-deposited Al<sub>2</sub>O<sub>3</sub> or SiO<sub>2</sub>. At the very beginning

of this thesis Fig. 1.1 illustrates the switching principle of phase change materials. The time for which a material experiences a temperature in the regime of fast crystallization decides on whether a volume crystallizes or not. A long thermal time constant of a sample can significantly change those time spans both in crystallization pulses and in attempts to amorphize. It is thus not surprising that materials, that can crystallize very rapidly, are impossible to melt-quench, if a glass (SiO<sub>2</sub>) substrate showing low thermal conductivity is used. The other extreme is a substrate that carries away the heat from the phase change layer so efficiently, that the maximum available laser power could not melt the phase change material. Any melt-quenching would of course be prevented in this case too. For that reason in the samples, the author prepared for his studies, a heat barrier, few tens of nanometers thin, is placed between the phase change material and the silicon substrate.

The choice of the substrate is so important already for the interpretation of a simple power-time-effect diagram, because the time axis could be misleading especially for short pulses. The duration of a laser pulse can be much shorter than the overall time the phase change material sojourns in the temperature regime of fast crystallization (see again Fig. 1.1). Therefore a crystallized mark on a phase change film as a result of a laser pulse of a certain duration is no evidence for the crystallization process being completed in the same duration.

Good indicators for a check of the thermal time constant of an experiment are iso-effect lines, though, not those of crystallization, but the ones of amorphization or ablation. The temperature evolution is more strictly connected to the latter effects than to crystallization, which can be linked to temperature only via rather complicated kinetics (Chapter 3). To give an example, the case of amorphization shall be discussed briefly. After the thermal steady state is reached, a molten volume of distinct size is established and maintained. The effects of two laser pulse experiments with identical power but different pulse durations will be the same, as long as both pulse durations are longer then the time needed to establish the steady state. For pulses of such duration iso-effect lines should therefore be horizontal in power-time-effect diagrams, and the starting point of such a line hints to the thermal time constant of the sample. Fig. 12.15 showing a typical amorphization experiment performed with *POET* gives evidence for a thermal time constant of the respective sample to be shorter than 30 ns.<sup>1</sup> Fig. 12.15 in particular and amorphization experiments in general are discussed in more detail later (in Sec. 12.4).

<sup>&</sup>lt;sup>1</sup>For completion the reader's attention is drawn to the fact, that the constant duration of the finite slopes of the laser pulses also has an influence on the starting point of an horizontal iso-effect line. However, a detailed discussion of this topic seems inappropriate at this point.

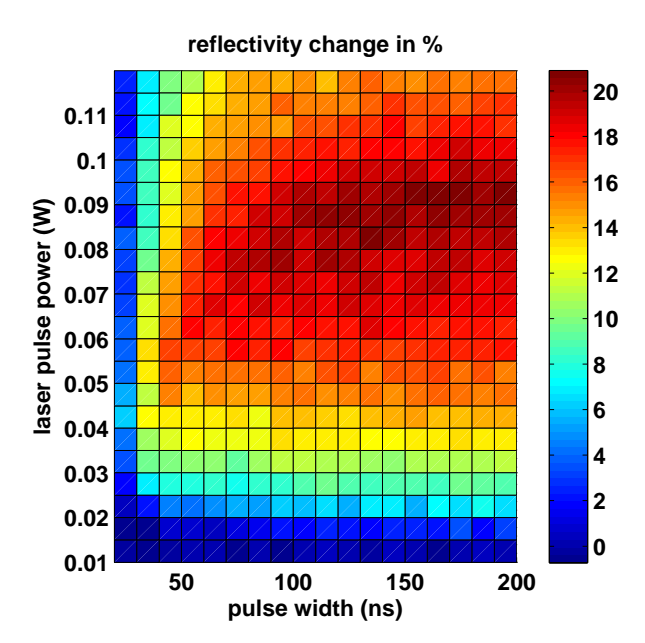


Figure 12.2: Power-time-effect diagram for as-deposited  $Sb_2Te$ : The sample is a 30 nm thin film of  $Sb_2Te$  deposited on top of a silicon wafer, which has previously been covered with 20 nm of  $Al_2O_3$ . It is amorphous as-deposited. The power is the output power of the pulsed laser, the time the duration of a pulse. It has been increased from 20 ns to 200 ns in increments of 20 ns. The colors indicate the relative change in reflectivity of the sample due to laser annealing.

Besides these more technical, but therefore not less important discussions, the power-time-effect diagrams in Fig. 12.1 allow also an interpretation with respect to the physics of crystallization of the investigated material.

First of all one can state that Ge<sub>2</sub>Sb<sub>2</sub>Te<sub>5</sub>, like Sb<sub>2</sub>Te (Fig. 12.2) and Ge<sub>15</sub>Sb<sub>85</sub> (Fig. 12.3), shows a very strong contrast in reflectivity between its amorphous and its crystalline state, which is nothing new, since these materials are known to be good phase change materials.

The lower reflectivity at the highest powers, lower compared to the reflectivity caused by laser pulses with intermediate power, can be explained by melt-quenching of the material in the center of the laser beam, where the temperature is the highest.

In contrast to the optical properties, the crystallization kinetics of  $Ge_2Sb_2Te_5$  and  $Sb_2Te$  on the one hand and  $Ge_{15}Sb_{85}$  on the other differ strongly.  $Ge_2Sb_2Te_5$  crystallizes from the as-deposited amorphous state after around 130ns. In  $Sb_2Te$  crystallization is even faster. For both materials the incubation times change only slightly over a rather large range of laser powers. In  $Ge_{15}Sb_{85}$ , however, crystallization does not only take much longer than in  $Ge_2Sb_2Te_5$  and  $Sb_2Te$ . It is even difficult to identify an incubation time at all.

While in Ge<sub>2</sub>Sb<sub>2</sub>Te<sub>5</sub> (Fig. 12.1) and Sb<sub>2</sub>Te (Fig. 12.2)the crystallization depends

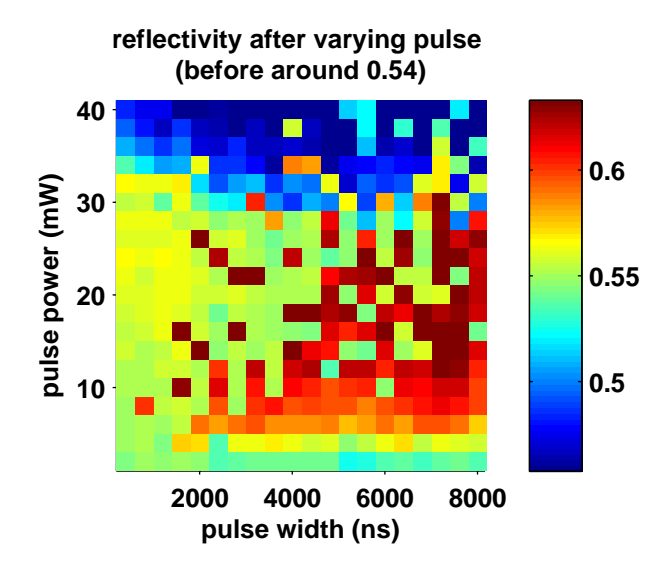


Figure 12.3: Power-time-effect diagram for as-deposited  $Ge_{15}Sb_{85}$ : The sample is a 30 nm thin film of  $Ge_{15}Sb_{85}$  deposited on top of a silicon wafer, which has previously been covered with 20 nm of  $Al_2O_3$ . It is amorphous as-deposited. The pulse power is the power of the incident pulsed laser at the sample, the time is the duration of a pulse. It has been increased from 400 ns to  $8 \mu s$  in increments of 400 ns. The colors indicate the absolute reflectivity of the sample after laser annealing. Before the absolute reflectivity was around 0.54.

very continuously on the parameters of the laser pulses, in  $Ge_{15}Sb_{85}$  (Fig. 12.3) there are many pulses, that do not lead to crystallization, although shorter pulses of the same power do. Crystallization looks much more stochastic in the latter case.

This observation can be explained by a strong difference in nucleation rates between  $Ge_2Sb_2Te_5$  and  $Sb_2Te$  on the one hand and  $Ge_{15}Sb_{85}$  on the other. In the case of the first two materials many nuclei are formed inside the irradiated volume, so the statistical fluctuations in the time of formation of a nucleus are smoothed out by the large number of nuclei that are formed simultaneously. In  $Ge_{15}Sb_{85}$ , in contrast, the probability of forming even a single post-critical nucleus inside the whole irradiated volume is far lower than unity for annealing times below 1  $\mu$ s and even longer for certain laser powers.

For a deeper understanding and a more quantitative analysis of nucleation in materials like  $Ge_{15}Sb_{85}$  it is obviously necessary to perform many more experiments than the few hundred pulses a typical power-time-effect diagram is based on. The next section will show that the fact that POET detects the reflectivity of the sample during the annealing becomes very useful for this task.

#### 12.2 Incubation time experiments

At the end of the preceding section an interpretation was given for the rather stochastic occurence of crystallization in  $Ge_{15}Sb_{85}$ : A comparably low probability of nucleation. And indeed this hypothesis has been confirmed by the study of the *in-situ* reflectivity data for the crystallization experiments. A typical reflectivity trace of a successful crystallization is shown in Fig. 12.4. Besides the increase of reflectivity due to the irradiation and heating of the sample by the pump laser, one can clearly identify a point in time, when the reflectivity sharply rises to a higher level. This observation supports strongly the hypothesis of identifying the occurence or absence of a crystallized mark at the end of a laser pulse experiment with the event of a *single* nucleation. Furthermore, the reflectivity traces are evidence of a fast crystal growth velocity in  $Ge_{15}Sb_{85}$  in spite of the slow formation of nuclei.

To quantify the probability of crystallization for the annealing with a certain laser power, a large number of experiments is necessary to cope with the stochastic nature of nucleation. But instead of varying the pulse parameters like in a power-time-effect measurement, now only the laser power is changed. The pulse length is fixed at a very long time, in case of  $Ge_{15}Sb_{85}$  some tens of microseconds, for which nucleation and therefore also full crystallization is likely to take place during the pulse. The time necessary to form the first nucleus is then determined from the reflectivity trace for each pulse. This way practically every laser pulse yields a value for the incubation time. In contrast, a strategy of pulse length variation would produce a vast amount of experiments without crystallization lacking any precise information about how long nucleation would have taken. Thus the chosen strategy allows to significantly reduce the number of experiments and therewith the overall time necessary for the study of the probability of crystallization.

Since the manual analysis of hundreds of reflectivity traces would be totally unfeasible, the author programmed an algorithm in Matlab for this purpose. This code determines both the different levels of reflectivity and the times of transitions between these levels. Besides the reflectivity trace itself, Fig. 12.4 shows also, what results the algorithm produced for this set of data. A person, who tried to automate an analysis of similar data, will understand that it can be challenging to teach a code to do what seems to be so easy for human eyes and brains. However, to not tire out the majority of the readers of this thesis, the details about how the algorithm copes with a sometimes rather low signal to noise ratio will not be discussed.

The reliability of the program's analysis has been approved by visually checking the correctness of the results, which are for that purpose plotted by default like in Fig. 12.4 during the analysis. This procedure utilizes the human abilities for fast final inspection

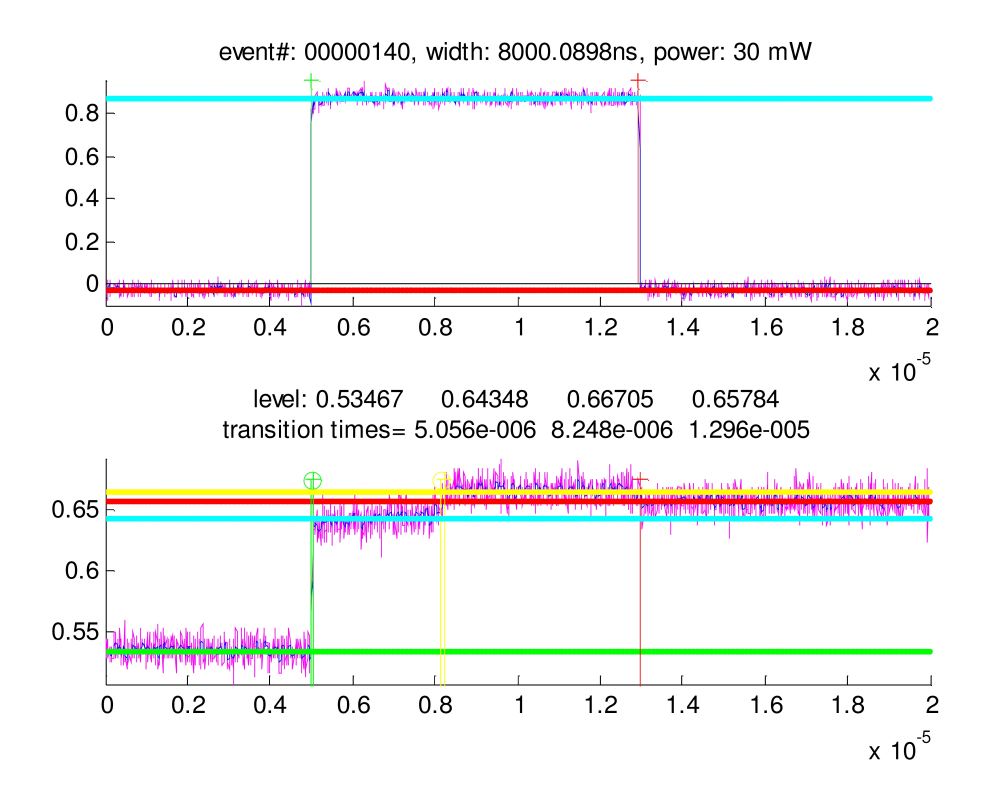


Figure 12.4: Analysis of reflectivity traces: The irradiation from the applied laser pulse (top) causes the absolute reflectivity (bottom) to increase immediately. An additional sharp rise in reflectivity indicates crystallization, or more precisely formation of a crystal nucleus and subsequent fast growth. A Matlab code, programmed for the automatic analysis of such traces, finds all levels of reflectivity (horizontal lines), i.e. the level of the initial (green), the excited (cyan) and the final state (red) and, if occurring, the level of the excited and transformed state (yellow). The algorithm additionally determines the according times of transition between these states (vertical lines). The incubation time is identified with the time span between the phase transformation (yellow) and the start of the irradiation (green).

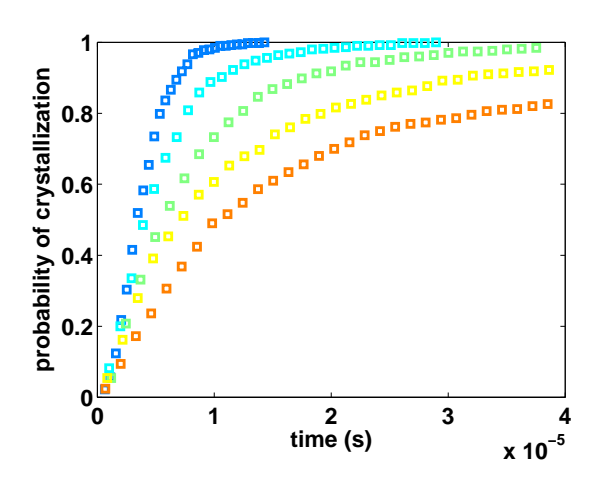


Figure 12.5: Incubation time for varying laser power: The probability of crystallization of a Ge<sub>15</sub>Sb<sub>85</sub> sample is plotted versus the duration of laser irradiation. The sample is a 30 nm thin film of Ge<sub>15</sub>Sb<sub>85</sub> sputter deposited on top of a silicon wafer, which has previously been covered with 20 nm of sputtered Al<sub>2</sub>O<sub>3</sub>. The phase change material is amorphous as-deposited before the application of a laser pulse. The laser power at the sample is varied from 10 mW (blue) over 15 mW (cyan), 20 mW (green) and 25 mW (yellow) upto 30 mW (orange). Each of these sets of measurements consists of more than 500 pulse experiments. A clear and very continuous trend is apparent: The higher the laser power the longer the time necessary for nucleation.

while keeping the tedious numerical analysis off the user's hands and mind.

The values for reflectivity levels and transition times are stored together with the pulse parameters of the respective experiment, wich are also cross-checked by the same code analyzing the trace of the pulse power. The combined results of a large measurement series repeating long pulses for hundreds of times at a fixed power form the data basis for further analysis.

To get a grip on incubation times, the time between the beginning of the heating pulse and the discrete step in reflectivity indicating crystallization is sorted into the bins of a histogram. The integration of the filling of all bins below a certain time equals the probability of crystallization up to that time. Figs. 12.5, 12.6 and 12.7 show plots of the probability of crystallization determined that way.

The used strategy has a further advantage over the variation of pulse length and checking the final reflectivity to determine success or failure in crystallization: The phase of cooling down, after the laser is shut off, is systematically excluded from the experiment. Any uncertainties about this process have thus no influence on the results for the incubation time.

The influence of the pulse power on the probability of crystallization in  $Ge_{15}Sb_{85}$  is visualized in Fig. 12.5. What could be recognized only qualitatively in a power-

time-effect diagram (Fig. 12.3) is now quantified by the new kind of experiments: The higher the laser power the slower is the formation of a nucleus. It is obviously not allowed to extrapolate this trend towards powers lower than the range of measurements. Somewhere near a laser power of 10 mW one may expect a maximum probability of nucleation.

Quantitative results like the ones plotted in Fig. 12.5 are ideal to study the theory of nucleation. In order to draw any further conclusions about the crystallization kinetics in a material, the temperature distribution needs to be taken into account. Numerical simulations are a valuable tool for this task. However, to arrive at a point, where parameters of the kinetics of the phase change material are the only remaining fit parameters, it is important to fix the other, rather free parameters by matching the results of controlled variations of experimental conditions.

For that purpose a variety of thin film samples was prepared, which all contain the same materials, i. e. Ge<sub>15</sub>Sb<sub>85</sub> as phase change material and Al<sub>2</sub>O<sub>3</sub> as a heat barrier on the silicon substrate, but differ in thickness of the layers. The latter critically determines the temperature distribution during a laser pulse experiment. How the thickness of the heat barrier and that of the layer of phase change material influence the process of crystallization during laser annealing is shown in Figs. 12.6 and 12.7, respectively.

Besides the delay of crystallization with increasing laser power, there are two further trends that can be clearly recognized: First, the thicker the heat barrier the longer is the time necessary for nucleation. A likely interpretation is the following. For identical applied laser powers a thinner heat barrier causes an overall reduction of temperature. This argument is in line with the decrease of laser power in the first series of experiments, also causing a lower temperature and faster nucleation.

Second, the thicker the layer of phase change material the shorter is the time necessary for nucleation. This correlation can either have its origin again in a change of the temperature distribution in the layer stack due to a modified contribution from the phase change material's own thermal conductivity. Another explanation for the higher probability of nucleation could be that a larger volume of heated phase change material offers more potential nucleation sites. The truth is likely to be a mixture of both. In order to undoubtedly separate the contributions from these effects, it is necessary to gain confidence in simulations of the sample's thermal behaviour during laser annealing.

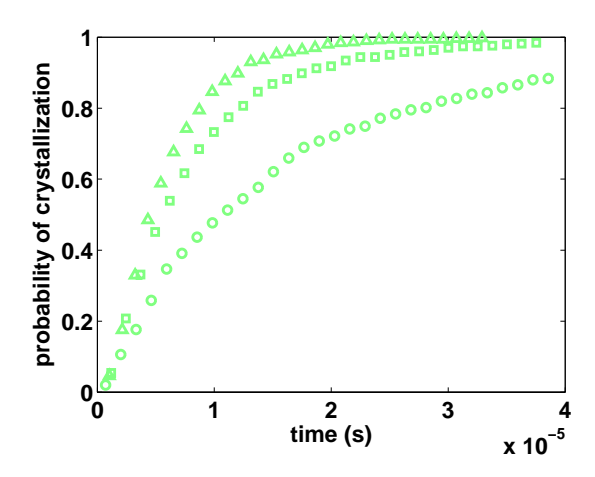


Figure 12.6: Incubation time for varying heat barrier thickness: The probability of crystallization of Ge<sub>15</sub>Sb<sub>85</sub> samples is plotted versus the duration of laser irradiation. The samples consist of a 30 nm thin film of Ge<sub>15</sub>Sb<sub>85</sub> sputter deposited on top of a silicon wafer, which has previously been covered with a sputtered layer of Al<sub>2</sub>O<sub>3</sub>. The thickness of the heat barrier is varied between 10 nm (triangles), 20 nm (squares) and 40 nm (circles). The phase change material is amorphous as-deposited before the application of a laser pulse. The laser pulse power at the sample is kept constant at 20 mW. Each of these sets of measurements consists of more than 500 pulse experiments. A clear trend is apparent: The thicker the heat barrier the longer the time necessary for nucleation.

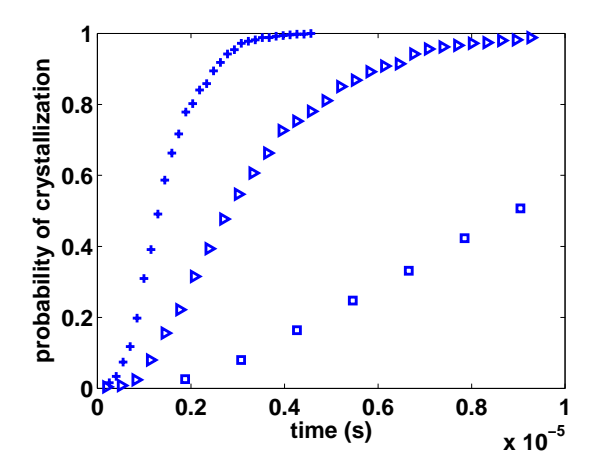


Figure 12.7: Incubation time for varying phase change layer thickness: The probability of crystallization of Ge<sub>15</sub>Sb<sub>85</sub> samples is plotted versus the duration of laser irradiation. The samples consist of a thin film of Ge<sub>15</sub>Sb<sub>85</sub> sputter deposited on top of a silicon wafer, which has previously been covered with 20 nm of sputtered Al<sub>2</sub>O<sub>3</sub>. The thickness of the layer of phase change material is varied between 60 nm (plusses), 30 nm (triangles) and 15 nm (squares). The phase change material is amorphous as-deposited before the application of a laser pulse. The laser pulse power at the sample is kept constant at 10 mW. Each of these sets of measurements consists of more than 500 pulse experiments. A clear trend is apparent: The thicker the layer of phase change material the shorter the time necessary for nucleation.

#### 12.3 Dual-spot experiments

The sharp transition steps in the reflectivity traces taken for incubation time experiments on  $Ge_{15}Sb_{85}$  indicate that as soon as the first crystal nucleus is formed, crystallization of the whole heated volume of the film proceeds very fast (Sec. 12.2). This stongly suggests that the crystal growth velocity is so high that pure growth can crystallize a more than  $1 \mu m^2$  large area of a thin film in much shorter time than it needs to form the first nucleus in the according volume. This turns out to make a study of crystal growth in materials with crystallization kinetics similar to that of  $Ge_{15}Sb_{85}$  challenging, as will be explained in the coming paragraphs.

In order to investigate how crystallization actually proceeds in space, it is necessary to look at the annealed spot on the sample with high resolution microscopy. Atomic force microscopy (AFM) is chosen for this task, because it is capable of non-destructively measuring the thin film samples described above. For transmission electron microscopy (TEM), the silicon wafer substrate, which is crucial to ensure the right thermal conditions in laser annealing experiments (see Sec. 12.1), would need to be removed, at least locally. Returning to laser testing with a sample that has already been prepared for TEM would thus be impractical. AFM, however, has the disadvantage that it can only indicate that an area of a film is crystalline or amorphous. Thus a completely crystallized annealing spot will look the same irrespective of how it crystallized.

For a spatial information about the progress of crystallization it is therefore necessary to interrupt it by shutting down the heating laser before complete crystallization is reached. Since a signal feedback from the reflectivity to the laser source would be much too slow, the decision about when the laser should be switched off needs to be made before the experiment. Because in Ge<sub>15</sub>Sb<sub>85</sub> the fluctuations of the incubation times are much larger than the duration of crystal growth, the result of any laser pulse will most probably be either a completely crystalline mark or a totally non-crystalline area.

To overcome this problem a new type of laser annealing experiments has been established in the course of this study: the dual-spot experiment. Its fundamental idea is to separate nucleation and growth by the consecutive application of two laser pulses. The first provides an amorphous-to-crystalline interface at the rim of the amorphous volume heated by the second pulse, where then pure crystal growth can be observed.

More specifically, a spot on a phase change film is irradiated for a sufficiently long time to surely crystallize it, i. e. longer than the time of practically 100 % probability of crystallization, which has been determined via incubation time experiments (Sec. 12.2). A second, much shorter laser pulse is then applied to the sample with slight lateral offset

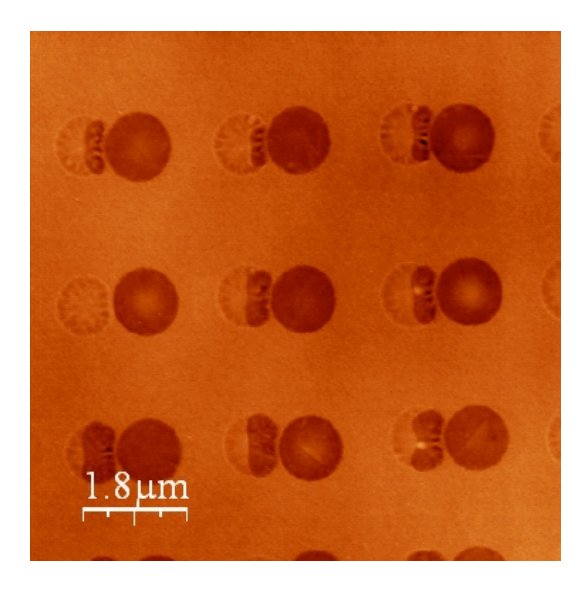


Figure 12.8: AFM image of dual-spot laser experiments: In each of the nine dual-spot experiments, at first, a long laser pulse was applied to guarantee complete crystallization of the irradiated area (right mark). Thus the area under the second, shifted laser spot (left mark) can crystallize by pure growth from the existing crystalline-to-amorphous interface, as long as the elevated temperature induced by the second laser pulse reaches this interface. The second pulses are short enough to interrupt the crystal growth process before its completion.

compared to the first one. This way the material under the second laser spot does not need to "wait" for nucleation in order to crystallize, but can crystallize by pure growth starting at the border of the already crystallized area of the first spot. Fig. 12.8 shows an AFM image of typical results of dual-spot experiments on Ge<sub>15</sub>Sb<sub>85</sub>. The duration of the second pulses, less than 100 ns, is far too short to let Ge<sub>15</sub>Sb<sub>85</sub> crystallize relying on a nucleation event. Fig. 12.8, however, shows clearly partial crystallization in several cases, always beginning at the interface of the existing crystallite of the first spot.

Additionally, in Fig. 12.9 images of dual-spot experiments are shown that were taken with a secondary electron microscope (SEM). SEM has not been mentioned in the above discussion about the right tool for investigating the spatial extension of crystalline and amorphous regions. Actually, to the best of the author's knowledge a visualization of the difference between crystalline and amorphous phase change material with such a contrast in an SEM has never been published before. For the purpose of determining the size of crystalline areas, however, SEM, unlike TEM, does not bring any advantage over AFM. Instead, it has been difficult to reliably produce this contrast in SEM. Therefore AFM has been used as standard procedure to gain spatial information about crystallinity of a laser annealed sample.

Because of the rather sharp temperature profile created by the focussed laser beam in lateral dimension the outcome of a dual-spot experiment is very sensitive to the

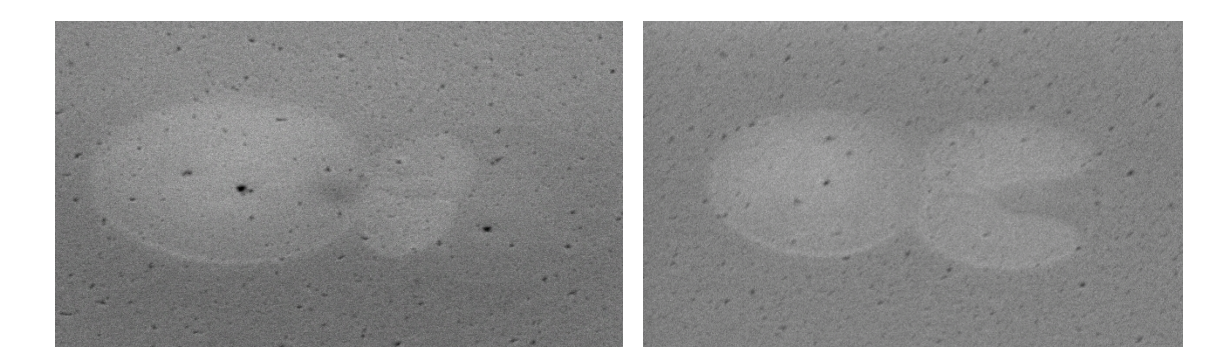


Figure 12.9: SEM images of dual-spot laser experiments: The images were taken with a non-zero angle to the surface normal. The crystalline area is much brighter than the remaining amorphous film. One could even guess to see the whole rim of the second laser spot similarly to what is detected with AFM (Fig. 12.8).

distance between the positions of the two laser spots on the sample. Since the control of the stages position in *POET* is limited, one cannot rely on the nominal value for the lateral shift. Therefore the distance between the two laser spots needs to be determined in an alternative way. The circular rim that a laser pulse produces on the surface of a phase change film even without crystallizing it (see Fig. 12.8) can be used to measure the spots' distance in the AFM images, which are taken anyway to see the degree of crystallization.

In order to make this determination time effective and, much more importantly, reproducible an image processing code has been programmed in Matlab for that purpose. It identifies the crystalline regions and also the distance between the centers of the two laser spots based on AFM images.

First the code just searches for dual-spot experiments in the image. Fig. 12.10 visualizes this procedure. Based on an image exported from WSxM, a program allowing standard analysis of AFM data, a greyscale image is created. On the latter a so-called edge-filter is applied. This filter essentially searches for extremal values of the brightness gradient of an image. In the next step those edges are dilated joining all edges of a single spot. This way edges originating from a locally higher surface roughness or from particles on top of the film can be identified and neglected from here on. Finally the procedure makes sure that two spots, which do not touch but are in near proximity to each other, are recognized as parts of a single dual-spot experiment.

Secondly the code separately analyses each dual-spot experiment. Therefor again an edge-filter is applied to the sector of the AFM image showing a certain dual-spot experiment. This time it is a filter working with two threshold values, though. This turned out to be most successful in finding both the borders between crystalline and amorphous regions and at the same time the rim of the second laser spot, which has

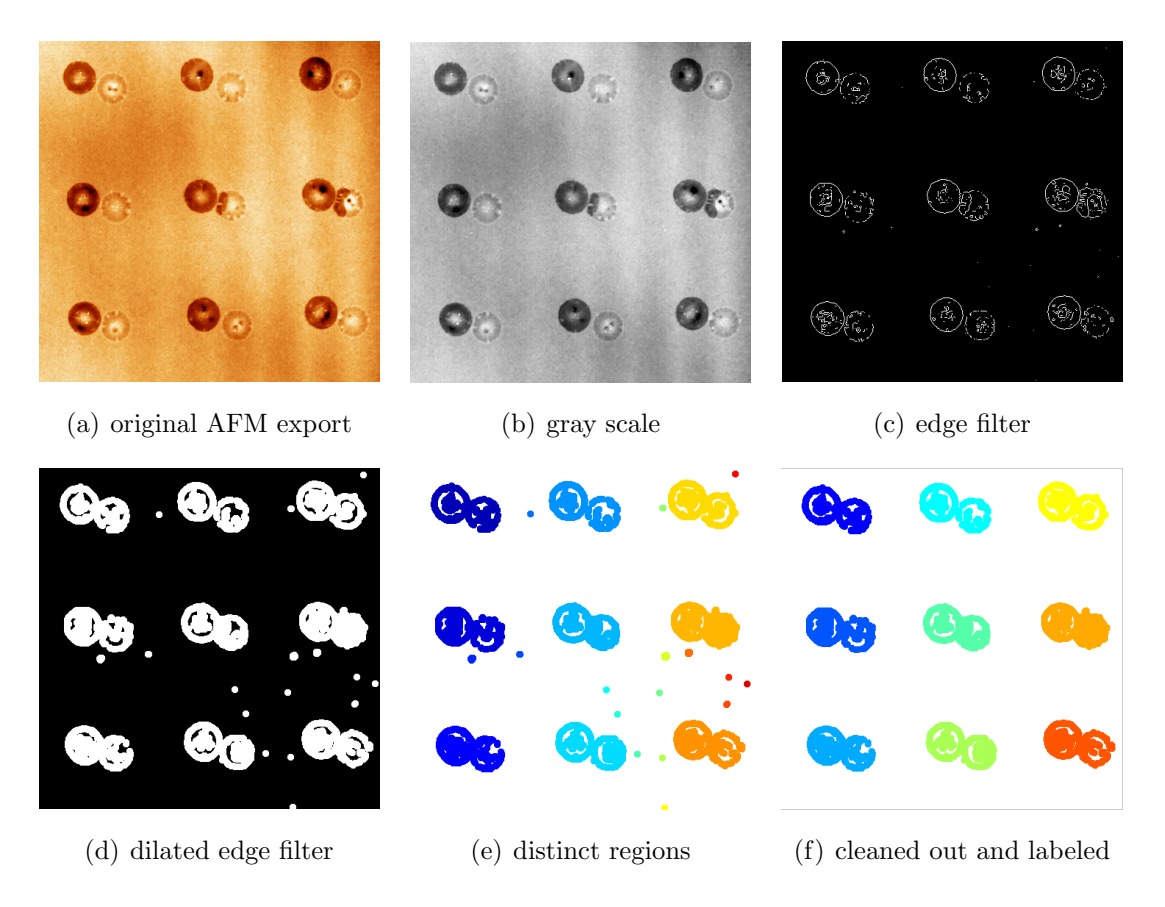


**Figure 12.10:** Image processing of dual-spot experiments I - searching for spots in AFM image: A standard AFM image (a) is converted into greyscale image (b). An edge-filter is applied to the grey-scale image. The resulting edges (c) are dilated (d). Edges that are not part of the distinct regions according to laser spots (e) are sorted out. Finally spots are grouped in pairs, i. e. dual-spot experiments (f).

much lower contrast. In the next step these detected edges are correlated with a circle of variable radius. Such correlation images are shown in the first two rows of Fig. 12.11. The correlation image with the sharpest and most pronounced maximum is regarded as best fitting the edges of a spot. The positions of the maxima of the two best correlation images represent the centers of the two laser spots. Comparison between the identified circles and the edge-filter image the correlation analysis has been applied to shows a very good agreement (exemplarily also in Fig. 12.11).

After having localized the two marks, next the crystalline area inside the second mark is searched for. For that purpose discretized areas of the surface, i.e. the pixels of the image, are sorted into the bins of a histogram according to their height, i.e. brightness of the pixels. This is done separately for the pixels inside of the circular mark of the first and the second laser pulse. Based on this distribution of the brightness of pixels inside the fully crystallized first spot a brightness level is determined that distinguishes crystalline from amorphous regions inside the second mark. Finally the code identifies the rim and the area of the largest continuous crystalline region inside the second laser mark. The histograms of a set of nine dual-spot experiments are plotted in Fig. 12.12.

How well the results from the Matlab code agree with the original AFM images is illustrated exemplarily for the same nine dual-spot experiments in Fig. 12.13. This set of experiments serves also as an example for the typical fluctuation of the shift between the two laser spots that occurs, when the linear stages carrying the sample are used for the respective movement. Apparently, dual-spot experiments are not well controlled in this mode of operation. Although the described Matlab code still enables the analysis of these experiments, it is inefficient to perform a large number of experiments that finally do not provide useful data. Especially AFM measurements consume much time, when the scanned dual-spots frequently turn out to be so far apart that there is no crystallization at all in the second spot.

Therefore an alternative way of moving the position of the laser spot on the sample has been developed. As described in Sec. 11.7, the implementation of electronically controlled actuators replacing the micrometers of a mirror mount allows the movement of the laser beam. This method provides much better control over the movement of the laser spot relative to the sample, because the stages are resting.

This is demonstrated by the series of dual-spot experiments depicted in Fig. 12.14. The increase of both power and duration of the second pulse continuously changes the outcome of an experiment. Especially for the shortest pulse durations the sequences of AFM images for fixed pulse power almost look like snapshots of a single continuing experiment. This is in strong contrast to the dual-spot experiments achieved by moving

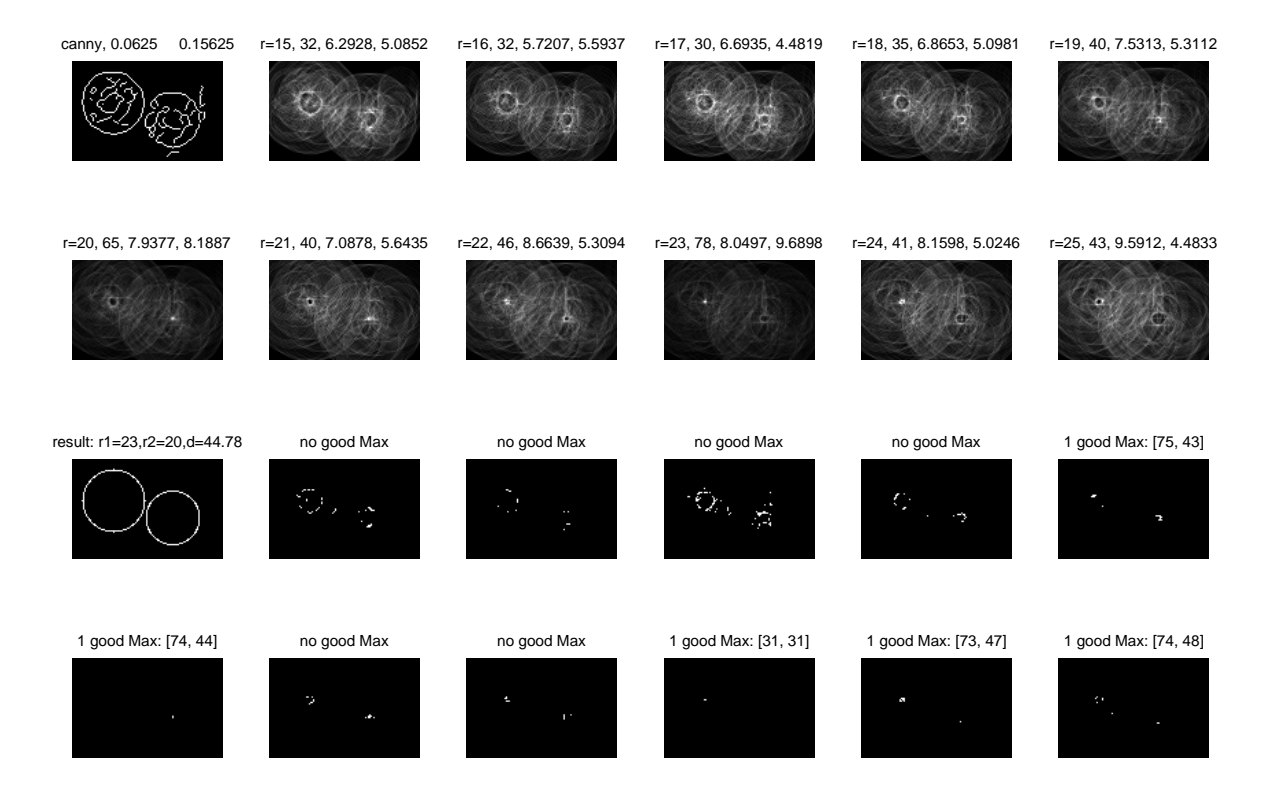


Figure 12.11: Image processing of dual-spot experiments II - circle correlation analysis: The result of the application of an edge-filter with two thresholds on a dual-spot experiment (top left image, title states filter type and threshold values) is correlated with a circle of variable radius r (here: 15 pixel  $\leq r \leq 25$  pixel). The resulting correlation images are shown in the top two rows. The title refers to the used radius r, the global maximum of the correlation, the average and the ratio of maximum and average. The latter are taken as indicators for the evaluation of the goodness of a correlation. The results of these evaluations are given in the titles of the images showing the local maxima of each correlation (bottom two rows). Each of the latter images corresponds to the correlation plotted exactly to rows above. If a correlation has a good maximum, additionally its position is given in the title. The positions of the maxima of the two best fitting correlations represent the centers of the two laser spots. The resulting circles are plotted two rows below the analyzed edge-filter result (i. e. first column, third row). The radii of the two identified circles r1 and r2 are given in the title of this image together with the distance d between their centers.

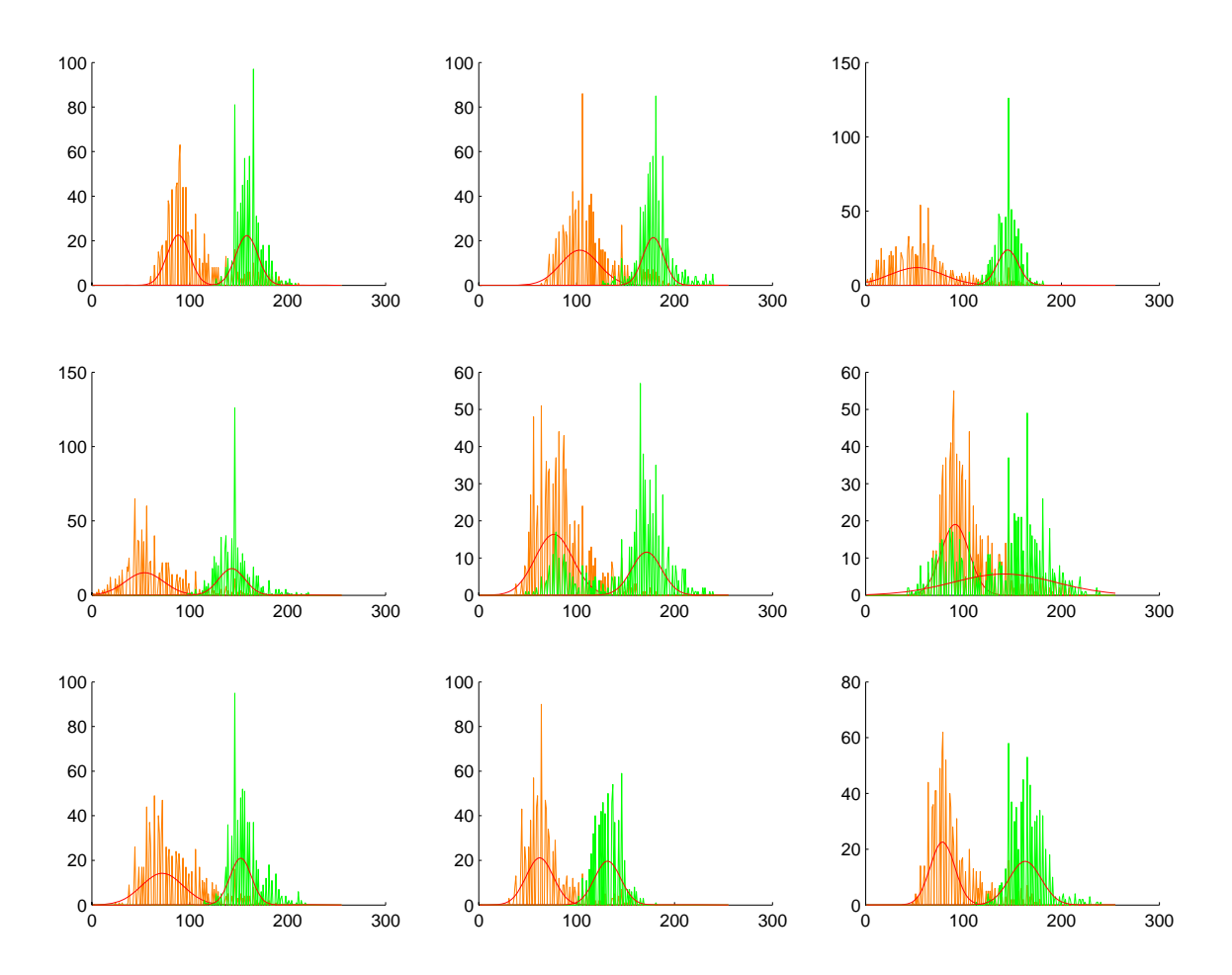


Figure 12.12: Image processing of dual-spot experiments III - histograms of surface height: Histograms of a set of nine dual-spot experiments. The pixels of the AFM image are sorted into the bins of a histogram according to their brightness indicating the height of the sample's surface. This is done separately for the pixels inside of the circular marks of the first (orange) and the second laser pulse (green). The red curves represent fits of a Gaussian distribution to the pixels of each spot. The distribution of the brightness of pixels inside the fully crystallized first spot define a brightness regime that corresponds to crystallinity for this sector of an AFM image. The pixels inside the second spot showing a brightness in this regime are therefore identified as indicating crystallinity of the film.

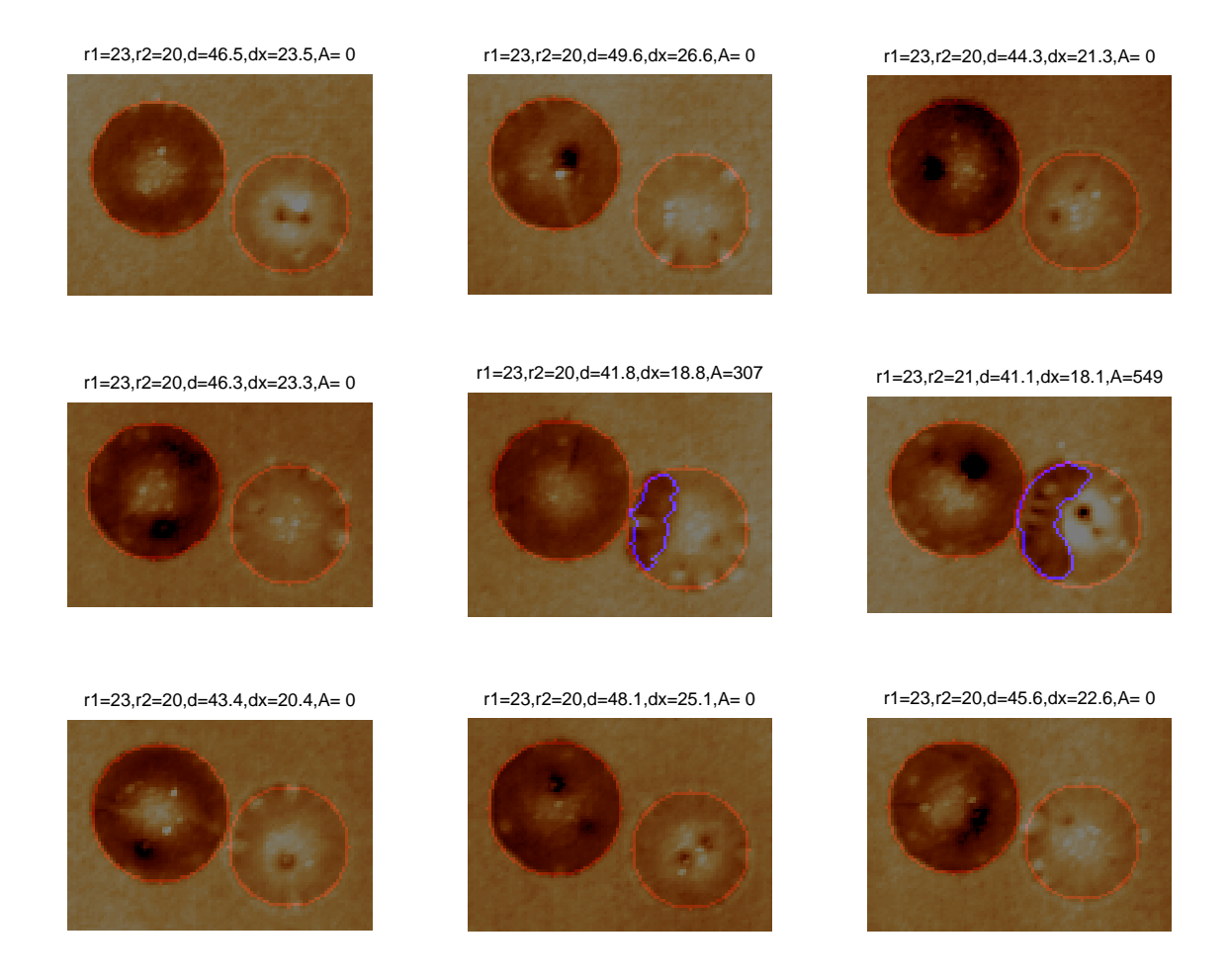


Figure 12.13: Image processing of dual-spot experiments IV - results: The rims of the laser spots (orange) and of the crystalline area inside the second spot (purple) as identified by the Matlab image processing code are plotted on top of the respective cutouts of the original AFM image. The examples are the same nine dual-spot experiments the histograms in Fig. 12.12 correspond to. Above each picture the code puts out some characteristic numbers it determined: the radius of the first r1 and the second laser mark r2, the distance d between their centers, the distance dx between the center of the second mark and the crystalline interface given by the first mark, the area A of the crystalline region inside the second mark. The unit of all numbers is a pixel.

the stages. The variations in the outcome of the experiments in Fig. 12.13 are solely due to fluctuations in shift distance. Both power and duration of the second pulse have been kept constant, as well as the nominal shift between the two laser spots. Obviously, in that case one is comparably far away from *seeing* trends in crystallization behaviour due to varying laser power and pulse duration.

The newly incorporated experimental possibilities for shifts of the laser spot are very promising to produce high quality data that can be used to fit the parameters of crystal growth in numerical simulations. While this can be expected to lead to unprecedented quantitative results on crystal growth for high temperatures, the image in Fig. 12.14 itself allows already to draw some direct qualitative conclusions. The crystallization of an around  $1\,\mu\mathrm{m}^2$  large area of amorphous as-deposited  $\mathrm{Ge_{15}Sb_{85}}$  is completed in less than 80 ns by crystal growth only. Further the "half moon like" shape of the crystalline regions evidences, that laser pulses of 24 mW and higher increase the temperature in the phase change material around the center of the beam beyond the regime of fastest crystal growth velocities.

### 12.4 Amorphization and recrystallization

Incubation time experiments, as they are described in Sec. 12.2, are only possible, if the amorphous volume under investigation is not in contact with crystalline material. The crystal growth from the existing interface would interfere with the nucleation of new crystallites in the annealed volume preventing a separate measurement of nucleation. The higher the crystal growth velocity (and it is very high especially for phase change materials that are relevant for application) the less is the process of crystallization determined by nucleation and the lower is the chance to characterize nucleation with such an experiment. Exactly this phenomenon has been utilized when studying the crystal growth velocity via dual-spot experiments (Sec. 12.3).

The entanglement of crystal nucleation and growth is the reason why incubation time experiments usually start from the as-deposited amorphous state. Here no pre-existing crystallites disturb the measurement of incubation times. For application, however, both in optical and electrical storage, it is important to know how crystallization of a melt-quenched amorphous volume takes place in a crystalline environment. A melt-quenched amorphous state can in general differ in its physical properties from an as-deposited amorphous state.

Therefore, melt-quenched amorphous marks were created by high power laser pulses in completely crystalline thin film samples. The samples were identical to the ones used for the optical experiments described above, except for having additionally been

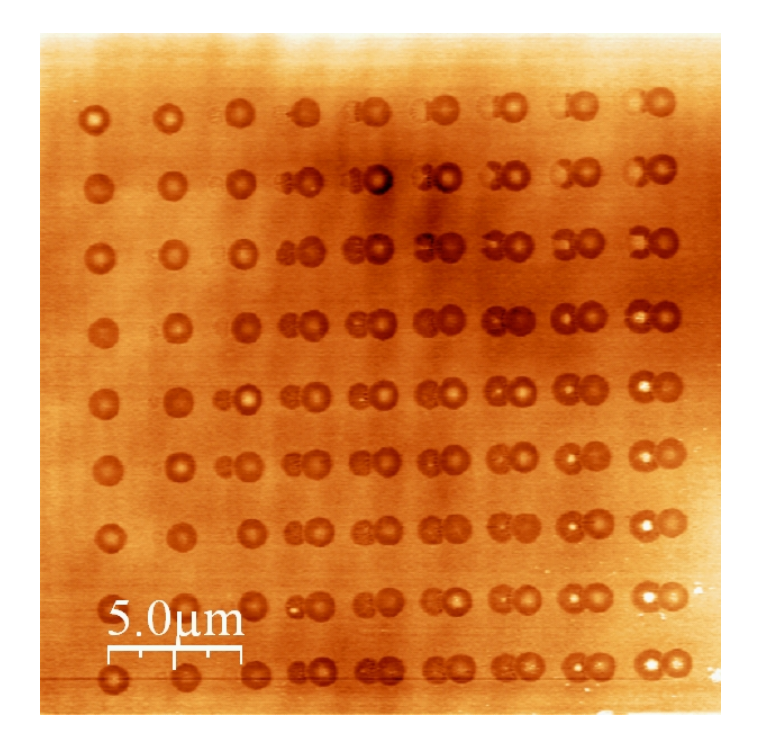


Figure 12.14: AFM image of dual-spot experiments with improved shift precision: Both the pulse parameters of the first laser pulse (right mark) and the shift between first and second spot are kept constant throughout the series of experiments. The power of the second laser pulse rises from 4 mW (in the left column) to 36 mW (in the right column) in increments of 4 mW. Its duration increases from 20 ns (in the top row) in increments of 20 ns up to 180 ns (in the bottom row). The increase of both power and duration of the second pulse continuously changes the outcome of the experiment. The experiments in a given column almost look like snapshots of a single continuing annealing experiment. That there is still a remaining fluctuation of the relative position of the two laser spots can be seen in the third column. In two of those experiments the existing crystalline boundary from the first laser pulse was just a little closer to the center of the second spot than for the other experiments in that column. This implied the temperature at the crystalline boundary to be just high enough to grow with a significant velocity in these two cases, while in the other cases the temperature at the pre-existing crystalline interface was too low for an observable growth. Both the pronounced temperature profile in the sample and the strong temperature dependence of crystal growth velocity at moderate temperatures are responsible for the outcome of the experiment to be that sensitive to the relative position of the two spots.

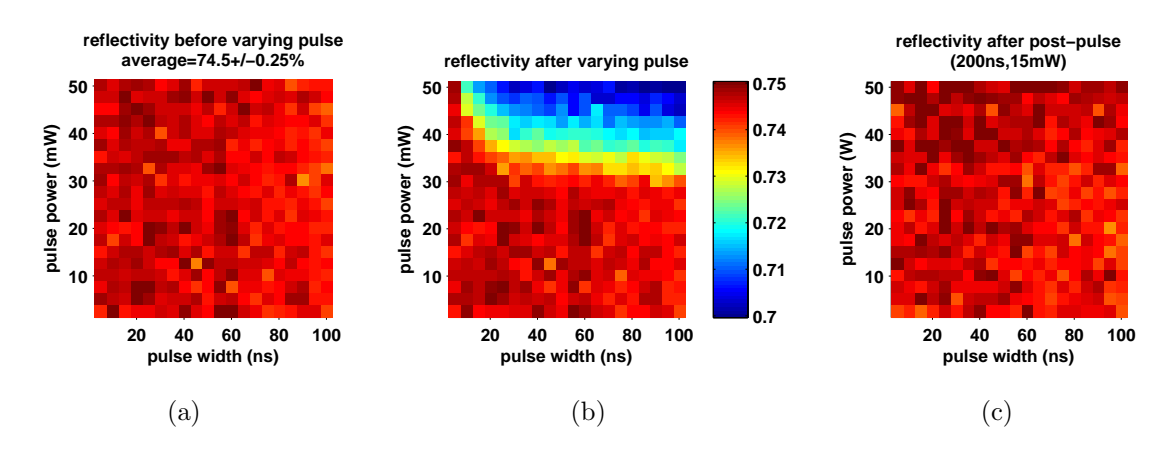


Figure 12.15: Reflectivity change upon amorphization: The absolute reflectivity of a thin film sample consisting of  $30 \,\mathrm{nm}$  of  $\mathrm{Ge_{15}Sb_{85}}$  on  $20 \,\mathrm{nm}$  of  $\mathrm{Al_2O_3}$  on silicon is plotted in pseudocolors. Initially (a) the sample is completely crystalline, since it was annealed for  $5 \,\mathrm{min}$  at  $583 \,\mathrm{K}$ . After the application of a laser pulse of varying power and duration (b) the reflectivity is unchanged for low powers, but significantly reduced by high power pulses. Irrespective of the parameters used for this attempt to amorphize the sample, the same location is irradiated by a second  $15 \,\mathrm{mW}$  pulse for  $200 \,\mathrm{ns}$ . The resulting reflectivity (c) agrees well with the original values indicating good reversibility of the amorphization.

annealed for five minutes at 583 K in Helium atmosphere. In this way the phase change material was completely crystallized.

The plots in Fig. 12.15 show that the reduction in reflectivity due to amorphization by high power laser pulses is totally reversible, at least in the range of laser parameters applied there, i.e. up to 50 mW for maximum 100 ns. Reversibility is an important provision for using a certain pair of pulse power and duration values to prepare a melt-quenched mark for further experiments.

Based on the measurements depicted in Fig. 12.15, a 70 ns long laser pulse of 45 mW power was chosen to reliably prepare an amorphous mark of fixed size in the otherwise crystalline phase change film. Fig. 12.16 shows how a second pulse following this amorphization pulse changes the reflectivity of the sample again. Apparently it takes only few nanoseconds to crystallize the amorphous region. A 20 ns long pulse can fully recrystallize the sample, at least in the ideal power range. This experiment proves, that a material, e. g. Ge<sub>15</sub>Sb<sub>85</sub>, that shows extremely slow nucleation and therewith crystallization from its as-deposited amorphous state, can crystallize a melt-quenched mark in crystalline environment much faster. And since the latter is the case in applications, Ge<sub>15</sub>Sb<sub>85</sub> or similar alloys should also be considered as potential materials for data storage, at least from a crystallization kinetics point of view.

To obtain a deeper insight into the crystallization kinetics or at least to gain a better view on what happened during a laser annealing experiment, it is always advis-

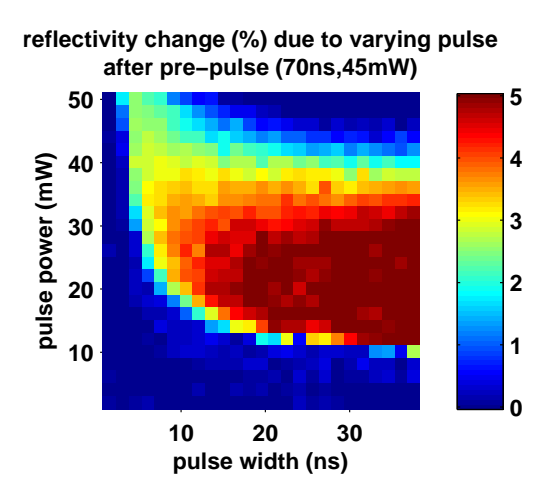


Figure 12.16: Reflectivity change upon recrystallization: The relative change in reflectivity of a thin film sample upon irradiation with a laser pulse of variable power and duration is plotted in pseudocolors. The sample consists of 30 nm of Ge<sub>15</sub>Sb<sub>85</sub> on 20 nm of Al<sub>2</sub>O<sub>3</sub> on silicon. It has been crystallized by a 5 min annealing at 583 K. A 70 ns long 45 mW pulse amorphized the sample, before the second variable laser annealing is applied to the same location of the sample. A 20 ns laser pulse is long enough to fully recrystallize the melt-quenched amorphous volume in a crystalline environment.

able to investigate the respective location of the sample ex-situ with a high resolution microscope. For phase change materials with a significant density contrast between crystalline and amorphous phase atomic force microscopy (AFM) can detect local differences in the thickness of a thin film sample indicating the existence of crystalline and amorphous regions. Fig. 12.17 shows AFM images of laser amorphization and recrystallization experiments in  $Ge_{15}Sb_{85}$ . The respective laser experiments are equivalent to those depicted in Fig. 12.15(b) and 12.16. Just the variation of laser parameters is coarser so a single AFM image can contain a wider range of experiments. The image of the amorphization experiments, Fig. 12.17(a), attests that increasing power leads to larger melt-quenched areas. It also demonstrates that an extension of the pulse length beyond 20 ns has practically no influence on the outcome of the experiment. As discussed in Sec. 12.1 this is evidence for the sample reaching thermally steady state after that period of time.

The AFM image on the recrystallization experiments, Fig. 12.17(b), shows that the amorphization due to a pulse of 45 mW and 70 ns is completely reversible not only with respect to the reflectivity, but also regarding the topography, which indicates the spatial extension of an amorphous region. Any kind of destruction such as ablation of the film can be excluded based on this evidence. Again in total agreement with the reflectivity measurement in Fig. 12.16 the AFM image indicates that for powers between 15 and 30 mW full recrystallization takes place in less than 20 ns.

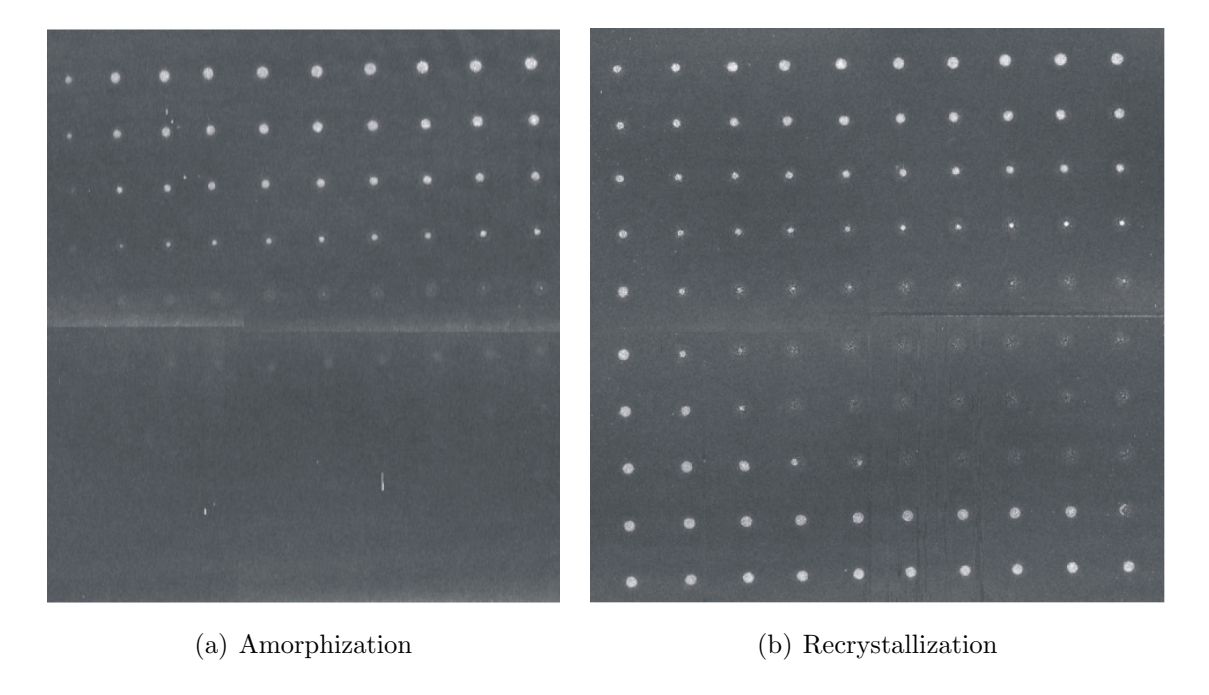


Figure 12.17: AFM image of amorphization and recrystallization marks created by laser pulses with variable power and duration. The brighter the image the higher is the surface. The extension of the scanned areas are around  $30\,\mu\mathrm{m}$  (in vertical direction of the images). The sample consists of  $30\,\mathrm{nm}$  of  $\mathrm{Ge_{15}Sb_{85}}$  on  $20\,\mathrm{nm}$  of  $\mathrm{Al_2O_3}$  on RF-cleaned silicon. It has been crystallized by a 5 min annealing at  $583\,\mathrm{K}$ . Laser pulses of experiments in the same column have identical pulse lengths, while those in the same row have the same power. The laser power is  $50\,\mathrm{mW}$  for the top row experiments, decrementing by  $5\,\mathrm{mW}$  to the next lower row. The laser pulses attempting amorphization (a) range in duration from 10 to 100 ns (from left to right) with increments of  $10\,\mathrm{ns}$ . Only for powers above  $35\,\mathrm{mW}$  melt-quenched amorphous marks are obtained. For recrystallization experiments (b) a  $70\,\mathrm{ns}$  long  $45\,\mathrm{mW}$  pulse amorphized the sample, before the second, variable laser pulse is applied to the same location of the sample. Pulse duration ranges here from  $4\,\mathrm{ns}$  (left column) incrementing by  $4\,\mathrm{ns}$  upto  $40\,\mathrm{ns}$  (right column).

Especially the marks that are partially recrystallized due to shorter pulses offer a great opportunity for a determination of the crystal growth velocity by matching simulations to the experimental results. This approach is novel to the field of phase change materials. Preliminary results from numerical analysis of the experimental evidence presented in this section have been presented very recently at the 2008 Spring Meeting of the Materials Research Society [181].

### 12.5 Optically assisted electrical measurements

In the preceding sections of this chapter several methods were presented, that are capable of quantitatively characterizing fast crystallization kinetics in phase change materials. This is surely scientifically relevant by itself.

However, as has been motivated at the beginning of the third part of this thesis, a good knowledge about crystallization kinetics is also essential to really understand the electrical switching in phase change devices. Without the ability to distinct between electrical field induced effects and purely thermally driven crystallization there is no chance to unambiguously identify the physical mechanisms controlling this switching.

An in-depth investigation of a material's crystallization kinetics based on the kind of experiments presented above is already much more than what is most often done before experimenting with electrically switching of phase change devices. Thus one could think that, since independent experimental evidence on crystallization kinetics is provided to numerical simulations, the obligation to scientific accurateness is fulfilled and one could therefore start with the typical electrical switching experiments. With the results from the optical experiments the simulations of electrical switching would be already much better validated than any other, the author is aware of.

Nevertheless, an intermediate step was taken instead on the way from purely optical to purely electrical testing: the initial state for electrical threshold switching experiments was prepared by laser induced melt-quenching. This has the advantage, that much more is known about how laser pulses anneal a sample than about how current pulses do. The latter is actually part of the investigation. It does not seem wise to conduct an experiment, in which its results are needed to know about its conditions.

In order to perform both optical and electrical experiments on the same samples, they need to be designed accordingly. For that reason in the course of this study line devices have been used, like the one depicted in Fig. 12.18.

The samples are structured by electron beam lithography and lift-off of a photoresist. Phase change material and alumina are deposited by sputtering. RF-cleaning before each sputter deposition has been a standard step in order to provide uncon-

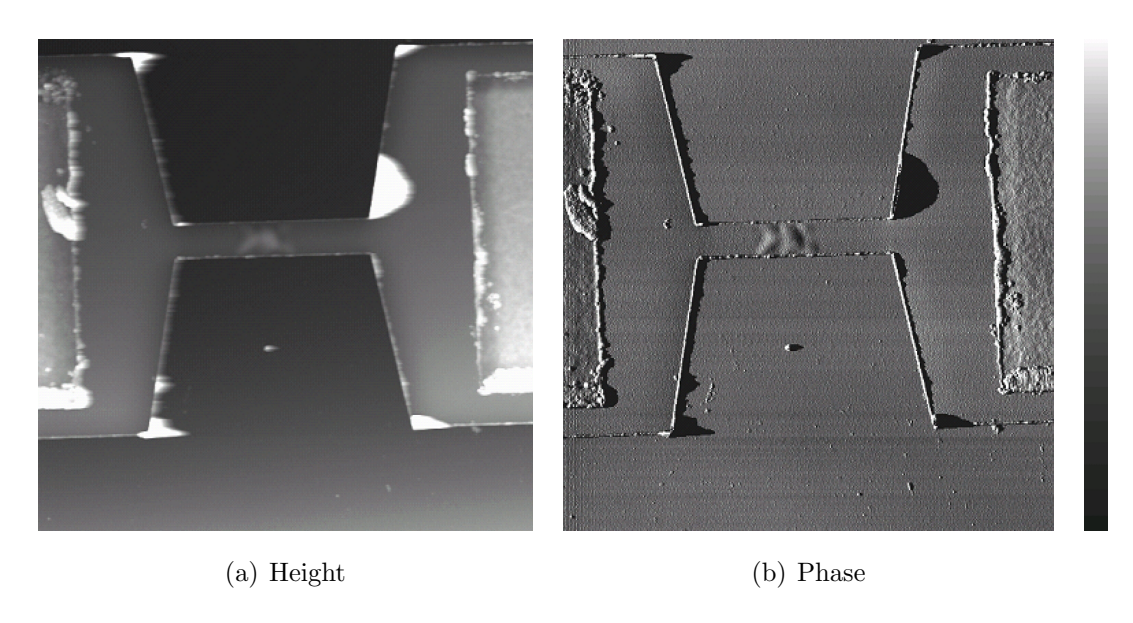


Figure 12.18: AFM image of electrical line cell: A  $3 \mu m$  long, 600 nm wide and 30 nm high line of  $Ge_{15}Sb_{85}$  bridges two larger  $Ge_{15}Sb_{85}$  areas of the same thickness. The latter are deposited on top of platinum electrodes (partially visible as rectangles at both sides of the image), which serve as contact pads for POET's electrical probes. Phase change material and Pt electrodes are electrically isolated from the RF-cleaned silicon substrate by a continuous layer of 30 nm  $Al_2O_3$ . A 10 nm thick  $Al_2O_3$  capping layer is deposited on top of the device. The wrinkled area in the center indicates where intensive laser annealing melt-quenched the phase change material. The field of view of the AFM scan is  $8 \mu m$ . The gray scale on the right applies to both the height image (a) and the phase image (b) ranging from 0 nm to 100 nm and from  $0^{\circ}$  to  $20^{\circ}$ , respectively.

taminated interfaces, especially between the phase change material and the platinum contact but also between the phase-change material and the heat barrier.

A line length of  $3 \mu m$  is enough to make sure that the laser spot does not hit the line at its ends, where the situation is geometrically and therewith thermally less simple than in the middle. In the preceding optical experiments,  $30 \, \text{nm}$  of  $\text{Al}_2\text{O}_3$  underneath the  $\text{Ge}_{15}\text{Sb}_{85}$  layer proved to act as a suitable heat barrier allowing melt-quenching via pulsed laser irradiation.

A 10 nm Al<sub>2</sub>O<sub>3</sub> capping layer prevents oxidation, which would otherwise be enhanced at high temperatures during switching experiments. As the AFM image in Fig. 12.18 reveals, the heavily tested line structure is bulging where it has been repeatedly melt-quenched by laser annealing. Interestingly, this change in the device's topography turned out to have a surprisingly small influence on the electrical resistance of the cell. Nevertheless, it can only improve the reproducibility of experiments on the switching kinetics, if this structural integrity of the line is preserved. Increasing the thickness of the capping layer would seem to be the natural solution. The capping layer thickness in the devices shown in Fig. 12.18 is limited by the lift-off process. Herein the phase change material is removed together with the capping layer on top of it everywhere except where the device remains. With a thicker capping layer this lithographic step would be in danger of producing a device with unsharp edges, which definitely needs to be avoided. Later adding of another capping layer is an alternative option to solve the problem, though, it might lead to a reduction of contrast between the phase change line and its surrounding in *POET*'s CCD camera image. The latter is used to steer the laser's focal point onto the center of the line structure. A third solution for preventing the device from bulging could be the exchange of alumina by a material with different thermo-mechanical properties.

Before describing the switching experiments themselves, a brief discussion of one more detail of the device geometry might be appropriate: the platinum contact pads. From an electrical point of view the contact pads cannot be too small, since all additional capacitance near the device under test brings about the danger of unintentional discharging through the device. The faster the applied voltage pulses, especially the steeper the leading and trailing edges, the more undesirable capacitances next to the device become. Consequently in the design of the used samples the contact pads have been reduces to be just large enough to enable a reproducible contacting with POET's electrical probes.

Common setups for resistance versus temperature measurements, in contrast, are rarely equipped with an optical microscope and micrometer stages for contacting a sample. The measurement of the temperature dependence of a device's resistance, however, is highly desirable. As an example the technologically highly relevant comparison of the crystallization temperature of melt-quenched and of as-deposited amorphous phase change material is discussed in the next section (12.6.2). This incompatibility of common heating setups with fast electronic devices is another argument making clear, that the implementation of a heated sample holder into *POET* does not only serve the user's convenience and efficiency by relieving him of alternating between different setups, but it does enable experiments that would not be possible otherwise.

The resistivity of line devices, like the ones described above, was repeatedly switched by the irradiation with laser pulses. As-deposited amorphous structures were completely crystallized by scanning a continuously pulsing laser spot across. Samples that were crystallized in a furnace were locally amorphized by melt-quenching and recrystallized with laser pulses in the middle of the line, also switching the resistance of the device. The latter type of laser annealings, with pulse parameters typically around 40 ns and 30 mW, were used to prepare the line structures for electrical testing. Therein a voltage pulse was applied to the device, while the induced current was measured (see 12.5 for details).

Fig. 12.19 shows a typical result of such an experiment in form of a current versus voltage curve. Starting in a highly resistive state a sudden breakdown of the device resistance is observed, when the applied voltage exceeds the so-called threshold voltage. The increased current heats the device significantly. If the current is held up long enough, the amorphous regions have sufficient time to recrystallize. Only then, i. e. in the case of structural transition, the resistance remains permanently low after the electrical pulse is over.

Often the low resistance after electrical pulses, even after long ones, is slightly higher than the value for a completely crystalline, furnace annealed device. This indicates that the electrical current might not be able to heat the *whole* amorphous volume up to a temperature regime of fast crystallization. The likely interpretation is the formation of a crystalline channel through residues of the amorphous volume. The presence of these residues can only marginally increase the total resistance of the device.

Also, it was always possible to bring the device back to a resistance equal to the resistance of the completely crystallized state, i. e. 450 to  $550\Omega$ , by irradiating it with a longer laser pulse of medium intensity, i. e. around 200 ns and  $10 \,\mathrm{mW}$ , respectively. This fact does not only support the above interpretation of incomplete crystallization due to electrical switching. It also underlines the appropriateness of preparing the initial state of a threshold switching experiment using laser irradiation instead of risking a history effect building up due to amorphous residues.

With shorter voltage pulses it was also possible to only temporarily excite the

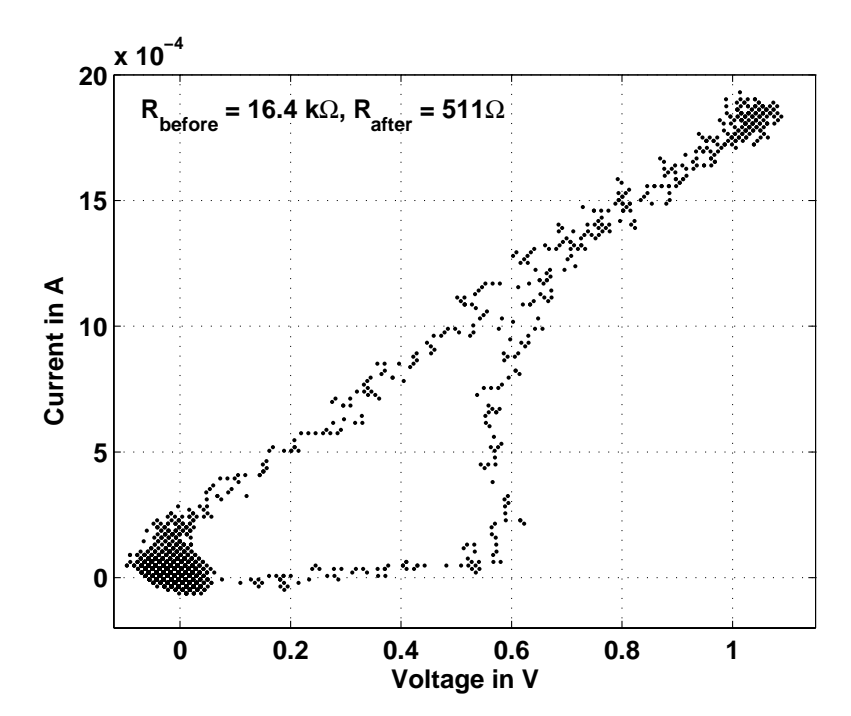


Figure 12.19: Threshold switching in a  $Ge_{15}Sb_{85}$  line cell: Current versus voltage characteristic of a line cell like the one described in Fig. 12.18. The current is induced by a voltage pulse of around 50 ns length, including leading and trailing edge each around 20 ns long. The pulse height is around 1.1 V driving at maximum a current of around 1.9 mA through the cell. The device resistance was determined before and after the application of the pulse. The pulse reduced the device resistance from initially 16.4 kΩ permanently to a value of 511 Ω. The initial state of the device was prepared by a laser pulse locally melt-quenching the phase change material in the middle of the line.

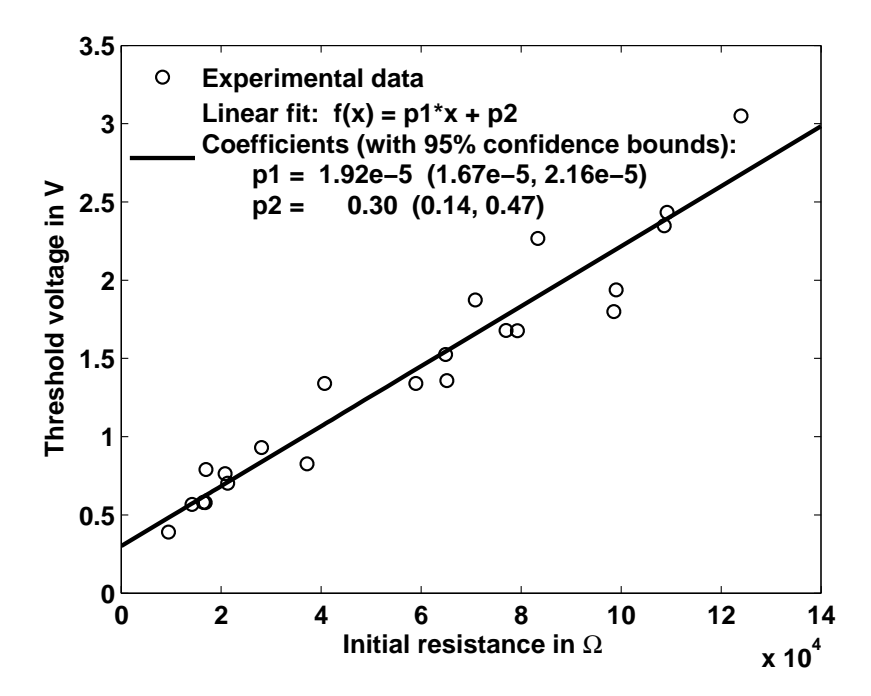


Figure 12.20: Threshold voltage dependence on initial resistance for Ge<sub>15</sub>Sb<sub>85</sub> line cells: Experimental values for threshold voltages and initial resistances are taken from pulse experiments like the one described in Fig. 12.19. The linear dependence agrees with the interpretation of the initial resistance representing the spatial extension of the melt-quenched amorphous volume that blocks the line.

amorphous material into a state of high conductivity. For a determination of the threshold voltage it is irrelevant what happens to the devices after the breakdown of resistance, so experiments of both kinds could be analyzed for studying the threshold voltage.

In Fig. 12.20 a collection of threshold voltages determined with the described line structure is plotted versus the resistance, measured before the application of the voltage pulse. The different initial resistances result from varying conditions for laser induced amorphization causing melt-quenched volumes of varying size.

It is obvious that the spatial extension of an amorphous volume in the direction of the applied voltage influences the strength of the electric field inside this volume. For sufficiently well-natured shapes of the amorphous volume the electrical field should be approximately inversely proportional to the volume's length.

In the scope of this study there was a lack of measurement capabilities for a direct determination of the extension of the amorphous material. Hence, the resistance before applying the pulses has been taken as the closest representation of that extension that is available. As such it is used in Fig. 12.20 to plot the threshold voltage against in order to see a material or at least device specific property.

The linear increase of the threshold voltage with rising initial resistance agrees with the given interpretation. The higher the resistance, the longer is the amorphous volume, the larger needs the applied voltage to be in order to produce a material specific critical electrical field inside of the amorphous volume.

Although the scattering of the data points prevents an unambiguous statement, the trend of the treshold voltages seems to point at a non-zero value for infinitesimal initial resistances. It is comforting, though, that the group at NXP, Netherlands, observed a similar offset for another phase change material, i. e. doped Sb<sub>2</sub>Te [182]. The source of this effect, may it be specific to the phase change material, caused by the electrical contacts or something completely different, should be the aim of further investigations.

## 12.6 Proposal of new experiments

Besides the types of experiments described above, some of which have never been published or even proposed before, POET is capable of many more with only small adaptations of the setup or even without any modification. Only a few ideas for new experiments shall be examplarily proposed in this section to illustrate the potential and versatility of the new setup.

# 12.6.1 Fast and isothermal measurement of crystal growth velocity

It has been mentioned at several occasions in the course of this thesis, that the temperature dependence of the crystal growth velocity in phase change materials is a highly desirable function, not only for science, but also for application. Such measurements have been realized with AFM or TEM at rather low temperatures, where crystal growth velocities are slower than  $10^{-6}$  m/s. [162, 163, 164, 165]

To perform faster experiments at higher temperatures laser annealing is used for the fast heating and cooling rates it provides. The major disadvantage of this method is the wide distribution of temperatures in a single experiment making it strongly nonisothermal both in time and in space. A quantitative determination of crystallization kinetics is therefore only possible via fitting of numerical simulations to the experimental results.

As a solution to this problem the following isothermal experiment is proposed. *POET*'s heated sample holder keeps the base temperature of the experiment at a constant elevated temperature. A completely crystalline phase change thin film is locally melted by a strong but short laser pulse. The reflectivity is measured at this

location during and especially directly after the application of this laser pulse.

As evidenced by the laser experiments described in the previous chapter, the thermal time constant of the typical thin film samples suggests the period of time, the melt needs to cool down to the base temperature, to be in the range of tens of nanoseconds. So at latest after one microsecond one could assume the sample to be isothermally at the base temperature. Any change in reflectivity can then be ascribed to crystallization at the location of the laser spot.

It is not unlikely that, at least for some materials, crystallization happens purely by growth from the crystalline border. This is indicated by the optical experiments on Ge<sub>15</sub>Sb<sub>85</sub> described in this work. In this case the diameter of the amorphous mark could be calculated directly from the value of the reflectivity. The propagation of the crystalline rim in time gives a value for the growth velocity at the base temperature. This way a much more direct evidence is given for the temperature dependence of crystal growth velocity than fitting of numerical simulations could provide.

One can expect to measure in sufficiently isothermal conditions on timescales as short as one microsecond and as long as tens of seconds. This conservative estimation gives this method already a range of seven orders of magnitude. Based on the size of amorphized marks realized with *POET* it seems reasonable to assume the disc of the not yet crystallized phase change material to have a radius of 300 nm after it cooled down to the base temperature. Together with the value of one microsecond for the shortest time measurement this yields an equivalent value of 0.3 m/s for the maximum detectable crystal growth velocity. This is several orders of magnitude higher than what common isothermal measurements achieve.

Due to their limitation until now it has always been necessary to assume a shape for the temperature dependence of crystal growth velocity in order to extrapolate the experimental data. In contrast, with the results from the proposed experiment it should be possible to measure a good part of it. For some phase change materials almost the full range of growth velocities should be accessible. With this experimental evidence one could really check, wether the theory describes the reality of phase change materials correctly.

An investigation of different alloys should reveal systematic trends in the crystal growth velocity, which one could correlate to fundamental material parameters.

# 12.6.2 Resistance versus temperature measurements for the melt-quenched amorphous state

The determination of the temperature dependence of the crystal growth velocity (12.6.1) is surely aiming for a very fundamental characterization and, in a second step, understanding of phase change materials. Compared to this the next experiment is much closer to the application in electronic memories.

It has been pointed out several times in this thesis, that the melt-quenched amorphous state is more relevant for any phase change based data storage application than the as-deposited amorphous state. The laser experiments on Ge<sub>15</sub>Sb<sub>85</sub> presented in this work have shown, that recrystallization of a melt-quenched amorphous mark is much faster than crystallization in the as-deposited state.

Therefore the common resistivity measurements during temperature ramps indicating crystallization by a drop in resistivity performed on as deposited amorphous films are less meaningful, if one wants to estimate the stability of amorphized phase change material in a PCRAM cell. Besides the actual structural state of the material, also the size and the shape of the amorphous volume inside a cell will influence how the resistivity changes upon heating.

POET can measure the resistivity versus temperature for electrical cells that have been melt-quenched either electrically or optically. The way of preparation will have an influence on size and shape of the amorphous volume. Preliminary results of the author have shown that in  $Ge_{15}Sb_{85}$  the thermal stability against crystallization is much lower for the melt-quenched amorphous state than for the as-deposited case.

### 12.6.3 Influence of capping layers

Recent studies have demonstrated that the crystal nucleation and growth is affected by the presence of a capping layer [164]. Again most studies have focussed on measurements at low temperatures where nucleation and growth proceed on a time scale of seconds. In any storage application, however, the desired processes will take place on a time scale several orders of magnitude shorter than that. *POET* is predestined for an extension of these investigations.

The bulging of the line cells upon laser annealing (Fig. 12.18) showed that there are also mechanical effects causing deformations of the sample structure. Similar behaviour has been observed by the author in laser experiments on SiO<sub>2</sub> and Al<sub>2</sub>O<sub>3</sub> capped phase change thin films. These mechanical effects are not only of obvious practical relevance for application. It is also not yet studied thoroughly how stress and strain of the capping interact for example with a changing viscosity of the phase change material.

### 12.6.4 Electronic properties of phase change materials

The combination of both optical and electrical measurement and excitation in *POET* also enables the user to study the electronic properties of phase change materials beyond the standard experiments. For example the time dependent current through a phase change sample could be measured while an intensity modulated laser optically excites charge carriers in the material. Or the arrival of charge carriers at the electrodes of a biased phase change sample could be detected as a function of time after a short laser pulse created charge carriers at a singular point in time. With these kinds of experiments, especially when performed at variable temperatures the user may be able to learn more about carrier lifetime, trapping, mobility and other related *electronic* effects in phase change materials.

### 12.7 Conclusion

The novel experimental setup POET, as it has been realized in the scope of the author's work, proved to be capable of performing new types of experiments. Further innovative experiments that can be performed with the setup are proposed. By this pioneering work future users of a POET are enabled to win unprecedented quantitative insight into crystallization kinetics, even on very short time scales, and, in a second step, also into the electrical behaviour of phase change materials. This insight can be expected to lead to a much deeper understanding of the fundamental physics of these materials, which is crucial for a further progress in phase change technology.

### 12.7. CONCLUSION

# Acknowledgements

Die beste Bildung findet ein gescheiter Mensch auf Reisen.

JOHANN WOLFGANG VON GOETHE

Many persons have supported me during my work on this thesis in various ways. It is my pleasure to use this opportunity to thank them for it.

At first, I thank my thesis advisor, Matthias Wuttig, for letting me work on such an interesting and challenging topic. Moreover, it was my privilege to have close insights into his style of working and thinking during the months, in which we were office- and housemates in California.

I am especially grateful for having had the chance of working abroad during the first twenty months of my doctoral research. The stay at the IBM Almaden Research Center in San Jose, California, had a huge impact on my life. It let me mature both as a physicist and as a person. Therefore, I am grateful to many of my colleagues at IBM.

I thank Simone Raoux for providing me with the raw data of her resistivity measurements I used for the comparisons in part II. I am grateful for her hospitality, for introducing me to the variety of different tools in the Almaden lab, for her encouragement to participate in the Stanford-Berkeley summerschool, for sending me to the Brookhaven National Lab and for being a great example for how well one can organize one's work. I appreciated her driving me in my research efforts without limiting my freedom to follow up on my own ideas while at the same time supplying me with books and tickets for the symphony. Finally, I thank her for following up the progress of my thesis even after I left California, not least for correcting my phrasing and punctuation in this text.

I am indepted to Bob Shelby for his help with the setting up of *POET*, especially for teaching me how to work with optics in the lab, but also for the many instructive and enjoyable discussions about all kinds of physics he knows so much about.

To Mike Jefferson I am grateful for his manifold help on the setting up of *POET*, foremost the design and construction of the sample heater and all custom-made electronics. Furthermore, I thank him for allowing me to use his lab space for this project

and even letting me take apart some of his beloved old setups for parts for *POET*. Even if some colleagues might not believe me, I am truly grateful for his sometimes endless "philosophy lessons" I had to listen to. Mike's permanent stimulations to think outside of the box repeatedly ignited my own thinking not only about his pieces of wisdom, but about my environment and life as a whole.

I thank Geoff Burr for the html programming for *POET*, for his numerical simulations on my experiments and for many fruitful discussions about the physics of phase change materials. I am especially grateful for his advice even after my departure from California.

I thank Charlie Rettner for his help with the fabrication of the phase change line devices for electrical testing. Without his skills in lithography these samples could not have been realized. I also appreciate his interest in my laser experiments taking the SEM images on dual-spot samples. Not least, I am grateful for our not work-related activities. Foremost, I thank Charlie, Don, Bruce and of course Bob, who introduced me, for admitting me to their lunch time cycling group. To me it was much more than just a valuable balance to long working days in the lab.

I thank Mark Jurich for his assistance with sputter depositions, but especially for his readiness to help with all kinds of problems knowing all "secret doors", hidden places and resources in the Almaden lab.

I thank Yi-Chou Chen for a very pleasant working atmosphere despite the somewhat difficult legal boundary conditions we faced.

Manny Hernandez helped with the fabrication of the custom-made electronics for *POET*. The people in the workshop of the IBM Almaden Research Center manufactured many mechanical parts for *POET*. For this work essential to my thesis I am very grateful.

Jane Frommer allowed me to use the AFMs in her lab. I appreciated especially the experimenting with nanotube tips off the beaten track of standard AFM. Kerem Ünal I am grateful to for our joined activities on conducting AFM on phase change materials. I thank Andy Kellock for letting me use his furnace for sample annealing and for the determination of phase change films with RBS.

Gary McClelland allowed me to work with him on the electrical testing of phase change samples in his lab. For this experience I am very grateful.

I thank Bülent Kurdi for his support of my plan to build *POET* and for the naming of the experiment. Besides that, he gave me an example for how a good management of a group of researchers can look like.

I am very grateful to Liz Fedde for her helpfulness with respect to a lot of organizational questions I had in Almaden. The same is true for Josefine Elbert at the RWTH Aachen. It helped a lot to always find her willing to listen to my problems.

I thank Christian Salinga, Günther Kluck-Ehlen and Ralf Detemple for their help with financial and administrative issues during the last three years, especially regarding my stay in California.

Both Johannes Kalb and Ursula Nellen made the digital documents of their own theses available to me, which I appreciate. Gunnar Bruns was a valuable help in solving problems with Latex.

I thank all members of the I. Physikalisches Institut IA at the RWTH Aachen for the kind reception back in Aachen.

During the last year and especially in the weeks of writing this thesis I have been glad to experience encouragement by old and new friends in Aachen.

Finally, I want to thank my family, especially my parents, Lothar and Christel Salinga, for their unreserved support during the past three years of my life and beyond.

In a moment like this when thinking about how few one would have achieved without the help of others, the own limitation becomes apparent. Not taking the helpfulness of all those people for granted I shall not forget the one who blessed me with this environment, the one who is my greatest help himself.

Soli deo gloria

# **Bibliography**

- [1] M. Wuttig and N. Yamada. Phase-change materials for rewriteable data storage. Nature Materials, 6(11):824–832, November 2007.
- [2] H. J. Borg, M. van Schijndel, J. C. N. Rijpers, M. H. R. Lankhorst, G. F. Zhou, M. J. Dekker, I. P. D. Ubbens, and M. Kuijper. Phase-change media for high-numerical-aperture and blue-wavelength recording. *Japanese Journal Of Applied Physics Part 1-Regular Papers Short Notes & Review Papers*, 40(3B):1592–1597, March 2001.
- [3] S. R. Ovshinsky. Reversible Electrical Switching Phenomena In Disordered Structures. *Physical Review Letters*, 21(20):1450–&, 1968.
- [4] J. Feinleib, J. Deneufville, S. C. Moss, and S. R. Ovshinsky. Rapid Reversible Light-Induced Crystallization Of Amorphous Semiconductors. *Applied Physics Letters*, 18(6):254–&, 1971.
- [5] S. R. Ovshinsky and H. Fritzsche. Amorphous Semiconductors For Switching, Memory, And Imaging Applications. *Ieee Transactions On Electron Devices*, ED20(2):91–105, 1973.
- [6] D. Adler, H. K. Henisch, and N. Mott. Mechanism Of Threshold Switching In Amorphous Alloys. *Reviews Of Modern Physics*, 50(2):209–220, 1978.
- [7] D. Adler, M. S. Shur, M. Silver, and S. R. Ovshinsky. Threshold Switching In Chalcogenide-Glass Thin-Films. *Journal Of Applied Physics*, 51(6):3289–3309, 1980.
- [8] D. Adler, M. S. Shur, M. Silver, and S. R. Ovshinsky. Threshold Switching In Chalcogenide-Glass Thin-Films - Reply. *Journal Of Applied Physics*, 56(2):579– 580, 1984.
- [9] K. Homma, H. K. Henisch, and S. R. Ovshinsky. New Experiments On Threshold Switching In Chalcogenide And Non-Chalcogenide Alloys. *Journal Of Non-Crystalline Solids*, 35-6(JAN-):1105-1110, 1980.

- [10] W. D. Buckley and S. H. Holmberg. Electrical Characteristics And Threshold Switching In Amorphous-Semiconductors. Solid-State Electronics, 18(2):127–&, 1975.
- [11] A. J. Hughes, P. A. Holland, and A. H. Lettington. Control Of Holding Currents In Amorphous Threshold Switches. *Journal Of Non-Crystalline Solids*, 17(1):89–99, 1975.
- [12] M. Kastner. Bonding Bands, Lone-Pair Bands, And Impurity States In Chalcogenide Semiconductors. *Physical Review Letters*, 28(6):355–&, 1972.
- [13] M. Kastner, D. Adler, and H. Fritzsche. Valence-Alternation Model For Localized Gap States In Lone-Pair Semiconductors. *Physical Review Letters*, 37(22):1504– 1507, 1976.
- [14] M. Kastner and H. Fritzsche. Defect Chemistry Of Lone-Pair Semiconductors. Philosophical Magazine B-Physics Of Condensed Matter Statistical Mechanics Electronic Optical And Magnetic Properties, 37(2):199–215, 1978.
- [15] N. F. Mott. Conduction In Non-Crystalline Systems .11. On-State Of Threshold Switch. *Philosophical Magazine*, 32(1):159–171, 1975.
- [16] K. E. Petersen and D. Adler. On State Of Amorphous Threshold Switches. Journal Of Applied Physics, 47(1):256–263, 1976.
- [17] K. E. Petersen and D. Adler. Electronic Nature Of Amorphous Threshold Switching. *Applied Physics Letters*, 27(11):625–627, 1975.
- [18] D. K. Reinhard, F. O. Arntz, and D. Adler. Field-Dependent Conductivity Of Chalcogenide Glasses. Applied Physics Letters, 23(9):521–523, 1973.
- [19] H. K. Rockstad and M. P. Shaw. Electrical Stability Of Bulk S-Shaped Negative Differential Conductivity Media. *Ieee Transactions On Electron Devices*, ED20(6):593–595, 1973.
- [20] M. P. Shaw, S. H. Holmberg, and S. A. Kostylev. Reversible Switching In Thin Amorphous Chalcogenide Films - Electronic Effects. *Physical Review Letters*, 31(8):542–545, 1973.
- [21] M. Chen, K. A. Rubin, and R. W. Barton. Compound Materials For Reversible, Phase-Change Optical-Data Storage. Applied Physics Letters, 49(9):502–504, September 1986.

- [22] E. Ohno, N. Yamada, T. Kurumizawa, K. Kimura, and M. Takao. TeGeSnAu Alloys For Phase-Change Type Optical Disk Memories. Japanese Journal Of Applied Physics Part 1-Regular Papers Short Notes & Review Papers, 28(7):1235–1240, July 1989.
- [23] N. Yamada, E. Ohno, N. Akahira, K. Nishiuchi, K. Nagata, and M. Takao. High-Speed Overwritable Phase-Change Optical Disk Material. *Japanese Journal Of Applied Physics Part 1-Regular Papers Short Notes & Review Papers*, 26:61–66, 1987.
- [24] N. Yamada, E. Ohno, K. Nishiuchi, N. Akahira, and M. Takao. Rapid-Phase Transitions Of Gete-Sb2 Te3 Pseudobinary Amorphous Thin-Films For An Optical Disk Memory. *Journal Of Applied Physics*, 69(5):2849–2856, March 1991.
- [25] R. Kojima, S. Okabayashi, T. Kashihara, K. Horai, T. Matsunaga, E. Ohno, N. Yamada, and T. Ohta. Nitrogen doping effect on phase change optical disks. Japanese Journal Of Applied Physics Part 1-Regular Papers Short Notes & Review Papers, 37(4B):2098–2103, April 1998.
- [26] H. Seo, T. H. Jeong, J. W. Park, C. Yeon, S. J. Kim, and S. Y. Kim. Investigation of crystallization behavior of sputter-deposited nitrogen-doped amorphous Ge2Sb2Te5 thin films. Japanese Journal Of Applied Physics Part 1-Regular Papers Short Notes & Review Papers, 39(2B):745-751, February 2000.
- [27] A. Ebina, M. Hirasaka, and K. Nakatani. Oxygen doping effect on Ge-Sb-Te phase change optical disks. *Journal Of Vacuum Science & Technology A-Vacuum Surfaces And Films*, 17(6):3463–3466, November 1999.
- [28] R. Kojima and N. Yamada. Acceleration of crystallization speed by Sn addition to Ge-Sb-Te phase-change recording material. *Japanese Journal Of Applied Physics Part 1-Regular Papers Short Notes & Review Papers*, 40(10):5930–5937, October 2001.
- [29] C. M. Lee, T. S. Chin, and E. Y. Huang. Optical properties and structure of tellurium-germanium-bismuth-antimony compounds with fast phase-change capability. *Journal Of Applied Physics*, 89(6):3290–3294, March 2001.
- [30] T. Nakai, T. Tsukamoto, S. Ashida, K. Yusu, N. Yoshida, K. Umezawa, N. Ohmachi, N. Morishita, N. Nakamura, and K. Ichihara. Dual-layer rewritable phase-change recording media for HD DVD system. *Japanese Journal Of Applied Physics Part 1-Regular Papers Short Notes & Review Papers*, 43(7B):4987–4991, July 2004.

- [31] N. Ohmachi, N. Morishita, K. Yusu, N. Nakamura, T. Nakai, and S. Ashida. High-speed recording media for HD DVD rewritable system. *Japanese Journal Of Applied Physics Part 1-Regular Papers Brief Communications & Review Papers*, 45(2B):1210–1212, February 2006.
- [32] K. Hirota and G. Ohbayashi. PdGeSbTe alloy for phase change optical recording. Japanese Journal Of Applied Physics Part 1-Regular Papers Short Notes & Review Papers, 37(4A):1847–1851, April 1998.
- [33] H. Iwasaki, Y. Ide, M. Harigaya, Y. Kageyama, and I. Fujimura. Completely Erasable Phase-Change Optical Disk. *Japanese Journal Of Applied Physics Part* 1-Regular Papers Short Notes & Review Papers, 31(2B):461–465, February 1992.
- [34] T. Kato, H. Hirata, T. Komaki, H. Inoue, H. Shingai, N. Hayashida, and H. Utsunomiya. The phase change optical disc with the data recording rate of 140 Mbps. Japanese Journal Of Applied Physics Part 1-Regular Papers Short Notes & Review Papers, 41(3B):1664–1667, March 2002.
- [35] M. Shinotsuka, H. Iwasa, R. Furukawa, S. Murata, M. Abe, and Y. Kageyama. Semi transparent recording stack with fast-crystallization phase-change material for dual-layer optical disk. *Japanese Journal Of Applied Physics Part 1-Regular Papers Short Notes & Review Papers*, 41(3B):1693–1694, March 2002.
- [36] H. Iwasaki, M. Harigaya, O. Nonoyama, Y. Kageyama, M. Takahashi, K. Yamada, H. Deguchi, and Y. Ide. Completely Erasable Phase-Change Optical Disc. 2. Application Of Ag-In-Sb-Te Mixed-Phase System For Rewritable Compact Disc Compatible With Cd-Velocity And Double Cd-Velocity. Japanese Journal Of Applied Physics Part 1-Regular Papers Short Notes & Review Papers, 32(11B):5241–5247, November 1993.
- [37] C. N. Afonso, J. Solis, F. Catalina, and C. Kalpouzos. Ultrafast Reversible Phase-Change In Gesb Films For Erasable Optical Storage. Applied Physics Letters, 60(25):3123–3125, June 1992.
- [38] J. Solis, C. N. Afonso, J. F. Trull, and M. C. Morilla. Fast Crystallizing Gesb Alloys For Optical-Data Storage. *Journal Of Applied Physics*, 75(12):7788–7794, June 1994.
- [39] A. K. Petfordlong, R. C. Doole, C. N. Afonso, and J. Solis. In-Situ Studies Of The Crystallization Kinetics In Sb-Ge Films. *Journal Of Applied Physics*, 77(2):607–613, January 1995.

- [40] J. Solis, C. N. Afonso, S. C. W. Hyde, N. P. Barry, and P. M. W. French. Existence of electronic excitation enhanced crystallization in GeSb amorphous thin films upon ultrashort laser pulse irradiation. *Physical Review Letters*, 76(14):2519– 2522, April 1996.
- [41] M. C. Morilla, J. Solis, and C. N. Afonso. Phase change cycling for erasable optical storage driven by ultrashort laser pulses. *Japanese Journal Of Applied Physics Part 2-Letters*, 36(8A):L1015–L1018, August 1997.
- [42] K. Sokolowski-Tinten, J. Solis, J. Bialkowski, J. Siegel, C. N. Afonso, and D. von der Linde. Dynamics of ultrafast phase changes in amorphous GeSb films. *Physical Review Letters*, 81(17):3679–3682, October 1998.
- [43] J. Siegel, C. N. Afonso, and J. Solis. Dynamics of ultrafast reversible phase transitions in GeSb films triggered by picosecond laser pulses. *Applied Physics Letters*, 75(20):3102–3104, November 1999.
- [44] J. P. Callan, A. M. T. Kim, C. A. D. Roeser, E. Mazur, J. Solis, J. Siegel, C. N. Afonso, and J. C. G. de Sande. Ultrafast laser-induced phase transitions in amorphous GeSb firms. *Physical Review Letters*, 86(16):3650–3653, April 2001.
- [45] J. Solis and C. N. Afonso. Ultrashort-laser-pulse-driven rewritable phase-change optical recording in Sb-based films. *Applied Physics A-Materials Science & Processing*, 76(3):331–338, March 2003.
- [46] S. M. Wiggins, J. Solis, and C. N. Afonso. Influence of pulse duration on the amorphization of GeSb thin films under ultrashort laser pulses. *Applied Physics Letters*, 84(22):4445–4447, May 2004.
- [47] S. M. Wiggins, J. Bonse, J. Solis, C. N. Afonso, K. Sokolowski-Tinten, V. V. Temnov, P. Zhou, and D. von der Linde. The influence of wavelength on phase transformations induced by picosecond and femtosecond laser pulses in GeSb thin films. *Journal Of Applied Physics*, 98(11):113518, December 2005.
- [48] Y.C. Chen, C.T. Rettner, S. Raoux, G.W. Burr, S.H. Chen, R.M. Shelby, M. Salinga, W.P. Risk, T.D. Happ, G.M. McClelland, M. Breitwisch, A. Schrott, J.B. Philipp, M.H. Lee, R. Cheek, T. Nirschl, M. Lamorey, C.F. Chen, E. Joseph, S. Zaidi, B. Yee, H.L. Lung, R. Bergmann, and C. Lam. Ultra-Thin Phase-Change Bridge Memory Device Using GeSb. Electron Devices Meeting, 2006. IEDM '06. International, pages 1–4, 2006.

- [49] J. Tominaga, H. Fuji, A. Sato, T. Nakano, T. Fukaya, and N. Atoda. The near-field super-resolution properties of an antimony thin film. *Japanese Journal Of Applied Physics Part 2-Letters*, 37(11A):L1323–L1325, November 1998.
- [50] J. Tominaga, T. Nakano, and N. Atoda. An approach for recording and readout beyond the diffraction limit with an Sb thin film. Applied Physics Letters, 73(15):2078–2080, October 1998.
- [51] T. Fukaya, J. Tominaga, T. Nakano, and N. Atoda. Optical switching property of a light-induced pinhole in antimony thin film. *Applied Physics Letters*, 75(20):3114–3116, November 1999.
- [52] J. Ashley, M. P. Bernal, G. W. Burr, H. Coufal, H. Guenther, J. A. Hoffnagle, C. M. Jefferson, B. Marcus, R. M. Macfarlane, R. M. Shelby, and G. T. Sincerbox. Holographic data storage. *Ibm Journal Of Research And Development*, 44(3):341–368, May 2000.
- [53] S. R. Ovshinsky, E. J. Evans, D. L. Nelson, and H. Fritzsche. Radiation Hardness Of Ovonic Devices. *Ieee Transactions On Nuclear Science*, NS15(6):311–&, 1968.
- [54] D. Ielmini, D. Mantegazza, A. L. Lacaita, A. Pirovano, and F. Pellizzer. Switching and programming dynamics in phase-change memory cells. *Solid-State Electron*ics, 49(11):1826–1832, November 2005.
- [55] D. Ielmini, A. L. Lacaita, A. Pirovano, F. Pellizzer, and R. Bez. Analysis of phase distribution in phase-change nonvolatile memories. *Ieee Electron Device Letters*, 25(7):507–509, July 2004.
- [56] A. Pirovano, A. L. Lacaita, F. Pellizzer, S. A. Kostylev, A. Benvenuti, and R. Bez. Low-field amorphous state resistance and threshold voltage drift in chalcogenide materials. *Ieee Transactions On Electron Devices*, 51(5):714–719, May 2004.
- [57] M. H. R. Lankhorst, B. W. S. M. M. Ketelaars, and R. A. M. Wolters. Low-cost and nanoscale non-volatile memory concept for future silicon chips. *Nature Materials*, 4(4):347–352, April 2005.
- [58] J. Schnakenberg. Thermodynamik und Statistische Physik. Carl Grossmann Tübingen, 2000.
- [59] E. A. Di Marzio and A. J. M. Yang. Configurational entropy approach to the kinetics of glasses. *Journal Of Research Of The National Institute Of Standards* And Technology, 102(2):135–157, March 1997.

- [60] F. Spaepen and D. Turnbull. Metallic Glasses. Annual Review Of Physical Chemistry, 35:241–263, 1984.
- [61] M. P. Rosenblum, F. Spaepen, and D. Turnbull. Diffusion And Structural Relaxation In Compositionally Modulated Amorphous Metal-Films. Applied Physics Letters, 37(2):184–186, 1980.
- [62] H. S. Chen, L. C. Kimerling, J. M. Poate, and W. L. Brown. Diffusion In A Pd-Cu-Si Metallic Glass. Applied Physics Letters, 32(8):461–463, 1978.
- [63] S. R. Elliott. Physics of amorphous materials. Longman, 1984.
- [64] M. H. Cohen and D. Turnbull. Molecular Transport In Liquids And Glasses. Journal Of Chemical Physics, 31(5):1164–1169, 1959.
- [65] C. A. Angell, K. L. Ngai, G. B. McKenna, P. F. McMillan, and S. W. Martin. Relaxation in glassforming liquids and amorphous solids. *Journal Of Applied Physics*, 88(6):3113–3157, September 2000.
- [66] L. M. Martinez and C. A. Angell. A thermodynamic connection to the fragility of glass-forming liquids. *Nature*, 410(6829):663–667, April 2001.
- [67] L. M. Wang, C. A. Angell, and R. Richert. Fragility and thermodynamics in nonpolymeric glass-forming liquids. *Journal Of Chemical Physics*, 125(7):074505– 1, August 2006.
- [68] S. Sastry. The relationship between fragility, configurational entropy and the potential energy landscape of glass-forming liquids. *Nature*, 409(6817):164–167, January 2001.
- [69] J. A. Kalb. Crystallization kinetics in antimony and tellurium alloys used for phase change recording. PhD thesis, Rheinisch-Westflalischen Technischen Hochschule Aachen, 2006.
- [70] M. L. Williams, R. F. Landel, and J. D. Ferry. Mechanical Properties Of Substances Of High Molecular Weight .19. The Temperature Dependence Of Relaxation Mechanisms In Amorphous Polymers And Other Glass-Forming Liquids. Journal Of The American Chemical Society, 77(14):3701–3707, 1955.
- [71] G. Adam and J. H. Gibbs. On Temperature Dependence Of Cooperative Relaxation Properties In Glass-Forming Liquids. *Journal Of Chemical Physics*, 43(1):139–&, 1965.

- [72] M. Goldstein. Viscous Liquids And Glass Transition A Potential Energy Barrier Picture. *Journal Of Chemical Physics*, 51(9):3728–&, 1969.
- [73] S. Sastry, P. G. Debenedetti, and F. H. Stillinger. Signatures of distinct dynamical regimes in the energy landscape of a glass-forming liquid. *Nature*, 393(6685):554– 557, June 1998.
- [74] C. A. Angell, B. E. Richards, and V. Velikov. Simple glass-forming liquids: their definition, fragilities, and landscape excitation profiles. *Journal Of Physics-Condensed Matter*, 11(10A):A75–A94, March 1999.
- [75] I. Saika-Voivod, P. H. Poole, and F. Sciortino. Fragile-to-strong transition and polyamorphism in the energy landscape of liquid silica. *Nature*, 412(6846):514– 517, August 2001.
- [76] C. A. Angell and S. Borick. Specific heats C-p, C-v, C-conf and energy land-scapes of glassforming liquids. *Journal Of Non-Crystalline Solids*, 307:393–406, September 2002.
- [77] J. C. Dyre and N. B. Olsen. Landscape equivalent of the shoving model. *Physical Review E*, 69(4):042501, April 2004.
- [78] G. Ruocco, F. Sciortino, F. Zamponi, C. De Michele, and T. Scopigno. Land-scapes and fragilities. *Journal Of Chemical Physics*, 120(22):10666–10680, June 2004.
- [79] C. A. Angell. Energy landscapes for cooperative processes: nearly ideal glass transitions, liquid-liquid transitions and folding transitions. *Philosophical Transactions Of The Royal Society Of London Series A-Mathematical Physical And Engineering Sciences*, 363(1827):415–430, February 2005.
- [80] C. A. Angell. Entropy and fragility in supercooling liquids. *Journal Of Research Of The National Institute Of Standards And Technology*, 102(2):171–185, March 1997.
- [81] W. Kauzmann. The Nature Of The Glassy State And The Behavior Of Liquids At Low Temperatures. *Chemical Reviews*, 43(2):219–256, 1948.
- [82] J. H. Gibbs and E. A. DiMarzio. Nature Of The Glass Transition And The Glassy State. *Journal Of Chemical Physics*, 28(3):373–383, 1958.

- [83] F. H. Stillinger, P. G. Debenedetti, and T. M. Truskett. The Kauzmann paradox revisited. *Journal Of Physical Chemistry B*, 105(47):11809–11816, November 2001.
- [84] R. Richert and C. A. Angell. Dynamics of glass-forming liquids. V. On the link between molecular dynamics and configurational entropy. *Journal Of Chemical Physics*, 108(21):9016–9026, June 1998.
- [85] H. Tanaka. Relation between thermodynamics and kinetics of glass-forming liquids. *Physical Review Letters*, 90(5):055701, February 2003.
- [86] J. P. Sethna. Statistical Mechanics: Entropy, Order Parameters, and Complexity. Oxford University Press, 2006.
- [87] P. S. Gill, S. R. Sauerbrunn, and M. Reading. Modulated Differential Scanning Calorimetry. *Journal Of Thermal Analysis*, 40(3):931–939, 1993.
- [88] A. Boller, Y. Jin, and B. Wunderlich. Heat-Capacity Measurement By Modulated Dsc At Constant-Temperature. *Journal Of Thermal Analysis*, 42(2-3):307–330, August 1994.
- [89] B. Wunderlich, Y. M. Jin, and A. Boller. Mathematical-Description Of Differential Scanning Calorimetry Based On Periodic Temperature Modulation. Thermochimica Acta, 238:277–293, June 1994.
- [90] C. V. Thompson and F. Spaepen. Approximation Of The Free-Energy Change On Crystallization. Acta Metallurgica, 27(12):1855–1859, 1979.
- [91] D. Turnbull. Formation Of Crystal Nuclei In Liquid Metals. Journal Of Applied Physics, 21(10):1022–1028, 1950.
- [92] J. D. Hoffman. Thermodynamic Driving Force In Nucleation And Growth Processes. *Journal Of Chemical Physics*, 29(5):1192–1193, 1958.
- [93] K. F. Kelton. Crystal Nucleation In Liquids And Glasses. Solid State Physics-Advances In Research And Applications, 45:75–177, 1991.
- [94] J. W. Christian. *The Theory of Transformations in Metals and Alloys*. Pergamon Press Oxford, 2nd edition, 1975.
- [95] D. Turnbull and J. C. Fisher. Rate Of Nucleation In Condensed Systems. *Journal Of Chemical Physics*, 17(1):71–73, 1949.

- [96] R. Becker. On The Formation Of Nuclei During Precipitation. *Proceedings of the Physical Society*, 52:71, 1940.
- [97] D. Bonn and W. K. Kegel. Stokes-Einstein relations and the fluctuationdissipation theorem in a supercooled colloidal fluid. *Journal Of Chemical Physics*, 118(4):2005–2009, January 2003.
- [98] F. H. Stillinger. A Topographic View Of Supercooled Liquids And Glass-Formation. Science, 267(5206):1935–1939, March 1995.
- [99] P. G. Debenedetti and F. H. Stillinger. Supercooled liquids and the glass transition. *Nature*, 410(6825):259–267, March 2001.
- [100] J. A. Hodgdon and F. H. Stillinger. Stokes-Einstein Violation In Glass-Forming Liquids. *Physical Review E*, 48(1):207–213, July 1993.
- [101] K. F. Kelton, A. L. Greer, and C. V. Thompson. Transient Nucleation In Condensed Systems. *Journal of Chemical Physics*, 79(12):6261–6276, 1983.
- [102] D. Reguera, J. M. Rubi, and A. Perez-Madrid. Fokker-Planck equations for nucleation processes revisited. *Physica A-Statistical Mechanics And Its Applications*, 259(1-2):10–23, October 1998.
- [103] D. Kashchiev. Solution Of Non-Steady State Problem In Nucleation Kinetics. Surface Science, 14(1):209–&, 1969.
- [104] K. F. Kelton and A. L. Greer. Transient Nucleation Effects In Glass-Formation. Journal Of Non-Crystalline Solids, 79(3):295–309, February 1986.
- [105] K. F. Kelton. Transient Nucleation In Glasses. Materials Science And Engineering B-Solid State Materials For Advanced Technology, 32(3):145–151, July 1995.
- [106] K. F. Kelton and M. C. Weinberg. Calculation Of Macroscopic Growth-Rates From Nucleation Data. *Journal Of Non-Crystalline Solids*, 180(1):17–24, December 1994.
- [107] J. W. Cahn and J. E. Hilliard. Free Energy Of A Nonuniform System .1. Interfacial Free Energy. *Journal Of Chemical Physics*, 28(2):258–267, 1958.
- [108] J. W. Cahn and J. E. Hilliard. Free Energy Of A Nonuniform System .3. Nucleation In A 2-Component Incompressible Fluid. *Journal Of Chemical Physics*, 31(3):688–699, 1959.

- [109] J. S. Langer. Theory Of Condensation Point. Annals Of Physics, 41(1):108–&, 1967.
- [110] J. S. Langer. Statistical Theory Of Decay Of Metastable States. *Annals Of Physics*, 54(2):258–&, 1969.
- [111] J. S. Langer and L. A. Turski. Hydrodynamic Model Of Condensation Of Vapor Near Its Critical-Point. *Physical Review A*, 8(6):3230–3243, 1973.
- [112] L. A. Turski and J. S. Langer. Dynamics Of A Diffuse Liquid-Vapor Interface. *Physical Review A*, 22(5):2189–2195, 1980.
- [113] J. D. Gunton. Homogeneous nucleation. *Journal Of Statistical Physics*, 95(5-6):903–923, June 1999.
- [114] H. E. Kissinger. Reaction Kinetics In Differential Thermal Analysis. *Analytical Chemistry*, 29(11):1702–1706, 1957.
- [115] K. F. Kelton. Analysis of crystallization kinetics. Materials Science And Engineering A-Structural Materials Properties Microstructure And Processing, 226:142–150, June 1997.
- [116] Melvin Avrami. Kinetics of Phase Change. I General Theory. *The Journal of Chemical Physics*, 7(12):1103–1112, 1939.
- [117] Melvin Avrami. Kinetics of Phase Change. II Transformation-Time Relations for Random Distribution of Nuclei. *The Journal of Chemical Physics*, 8(2):212–224, 1940.
- [118] Melvin Avrami. Granulation, Phase Change, and Microstructure: Kinetics of Phase Change. III. *The Journal of Chemical Physics*, 9(2):177–184, 1941.
- [119] H. J. Lee, H. Ni, D. T. Wu, and A. G. Ramirez. Experimental determination of kinetic parameters for crystallizing amorphous NiTi thin films. *Applied Physics Letters*, 87(11):114102, September 2005.
- [120] H. J. Lee, H. Ni, D. T. Wu, and A. G. Ramirez. Grain size estimations from the direct measurement of nucleation and growth. Applied Physics Letters, 87(12):124102, September 2005.
- [121] Y. C. Her, H. Chen, and Y. S. Hsu. Effects of Ag and In addition on the optical properties and crystallization kinetics of eutectic Sb70Te30 phase-change recording film. *Journal Of Applied Physics*, 93(12):10097–10103, June 2003.

- [122] Y. M. Chen and P. C. Kuo. Effect of Ag or Cu doping on erasable phase-change Sb-Te thin films. *Ieee Transactions On Magnetics*, 34(2):432–434, March 1998.
- [123] Y. C. Her and Y. S. Hsu. Optical properties and crystallization characteristics of Ge-doped Sb70Te30 phase change recording film. *Japanese Journal Of Applied Physics Part 1-Regular Papers Short Notes & Review Papers*, 42(2B):804–808, February 2003.
- [124] B. W. Qiao, J. Feng, Y. F. Lai, Y. F. Cai, Y. Y. Lin, T. A. Tang, B. C. Cai, and B. M. Chen. Si-Sb-Te films for phase-change random access memory. Semiconductor Science And Technology, 21(8):1073–1076, August 2006.
- [125] D. Z. Hu, J. S. Zhu, and J. K. Lee. The crystallization of Cu-doped Ge2Sb2Te5. Integrated Ferroelectrics, 84:233–238, 2006.
- [126] W. D. Song, L. P. Shi, X. S. Miao, and T. C. Chong. Phase change behaviors of Sn-doped Ge-Sb-Te material. *Applied Physics Letters*, 90(9):091904, February 2007.
- [127] B. W. Qiao, J. Feng, Y. F. Lai, Y. Ling, Y. Y. Lin, T. Tang, B. C. Cai, and B. Chen. Effects of Si doping on the structural and electrical properties of Ge2Sb2Te5 films for phase change random access memory. *Applied Surface Sci*ence, 252(24):8404–8409, October 2006.
- [128] B. Liu, Z. T. Song, S. L. Feng, and B. Chen. Structure and sheet resistance of boron-implanted Ge2Sb2Te5 phase change film. Materials Science And Engineering B-Solid State Materials For Advanced Technology, 119(2):125–130, May 2005.
- [129] S. Privitera, E. Rimini, C. Bongiorno, A. Pirovano, and R. Bez. Effects of dopants on the amorphous-to-fcc transition in Ge2Sb2Te5 thin films. *Nuclear Instruments & Methods In Physics Research Section B-Beam Interactions With Materials And Atoms*, 257:352–354, April 2007.
- [130] S. P. Gu and L. S. Hou. Crystallization kinetics of Ge-Sb-Te-O phase-change thin films. *Journal Of Inorganic Materials*, 17(6):1258–1262, November 2002.
- [131] D. Dimitrov and H. P. D. Shieh. The influence of oxygen and nitrogen doping on GeSbTe phase-change optical recording media properties. *Materials Science And Engineering B-Solid State Materials For Advanced Technology*, 107(2):107–112, March 2004.

- [132] K. F. Kao, H. Y. Cheng, C. A. Jong, C. J. Tan, and T. S. Chin. Tungsten added Sb80Te20 for phase-change RAM. *Ieee Transactions On Magnetics*, 43(2):930– 932, February 2007.
- [133] J. C. Phillips. Topology Of Covalent Non-Crystalline Solids .1. Short-Range Order In Chalcogenide Alloys. *Journal Of Non-Crystalline Solids*, 34(2):153– 181, 1979.
- [134] J. C. Phillips and M. F. Thorpe. Constraint Theory, Vector Percolation And Glass-Formation. *Solid State Communications*, 53(8):699–702, 1985.
- [135] M. F. Thorpe, D. J. Jacobs, M. V. Chubynsky, and J. C. Phillips. Self-organization in network glasses. *Journal Of Non-Crystalline Solids*, 266:859–866, May 2000.
- [136] D. Selvanathan, W. J. Bresser, and P. Boolchand. Stiffness transitions in SixSe1-x glasses from Raman scattering and temperature-modulated differential scanning calorimetry. *Physical Review B*, 61(22):15061–15076, June 2000.
- [137] K. Tanaka. Structural Phase-Transitions In Chalcogenide Glasses. *Physical Review B*, 39(2):1270–1279, January 1989.
- [138] P. Boolchand, D. G. Georgiev, T. Qu, F. Wang, L. C. Cai, and S. Chakravarty. Nanoscale phase separation effects near r=2.4 and 2.67, and rigidity transitions in chalcogenide glasses. *Comptes Rendus Chimie*, 5(11):713–724, November 2002.
- [139] K. Tanaka. Glass-Transition Of Covalent Glasses. *Solid State Communications*, 54(10):867–869, 1985.
- [140] E. A. DiMarzio. On Second-Order Transition Of Rubber. Journal Of Research Of The National Bureau Of Standards Section A-Physics And Chemistry, A 68(6):611-&, 1964.
- [141] A. K. Varshneya, A. N. Sreeram, and D. R. Swiler. A Review Of The Average Coordination-Number Concept In Multicomponent Chalcogenide Glass Systems. *Physics And Chemistry Of Glasses*, 34(5):179–193, October 1993.
- [142] R. Kerner and M. Micoulaut. On the glass transition temperature in covalent glasses. *Journal Of Non-Crystalline Solids*, 210(2-3):298–305, March 1997.
- [143] M. Micoulaut. The slope equations: A universal relationship between local structure and glass transition temperature. *European Physical Journal B*, 1(3):277–294, February 1998.

- [144] M. Micoulaut. Network entropy and connectivity: the underlying factors determining compositional trends in the glass-transition temperature. *Comptes Rendus Chimie*, 5(12):825–830, December 2002.
- [145] G. Lucovsky, F. L. Galeener, R. C. Keezer, R. H. Geils, and H. A. Six. Structural Interpretation Of Infrared And Raman-Spectra Of Glasses In Alloy System Gel-Xsx. *Physical Review B*, 10(12):5134–5146, 1974.
- [146] L. Tichy and H. Ticha. On The Chemical-Threshold In Chalcogenide Glasses. Materials Letters, 21(3-4):313–319, November 1994.
- [147] L. Tichy and H. Ticha. Covalent Bond Approach To The Glass-Transition Temperature Of Chalcogenide Glasses. *Journal Of Non-Crystalline Solids*, 189(1-2):141–146, August 1995.
- [148] J. Z. Liu and P. C. Taylor. A General Structural Model For Semiconducting Glasses. *Solid State Communications*, 70(1):81–85, April 1989.
- [149] M. Lasocka. Semi-Empirical Correlations Between Group Number, Atomization Enthalpy And Glass-Transition Temperature. Zeitschrift Fur Physikalische Chemie Neue Folge, 156:123–127, 1988.
- [150] M. H. R. Lankhorst. Modelling glass transition temperatures of chalcogenide glasses. Applied to phase-change optical recording materials. *Journal Of Non-Crystalline Solids*, 297(2-3):210–219, February 2002.
- [151] J. Bicerano and S. R. Ovshinsky. Chemical-Bond Approach To The Structures Of Chalcogenide Glasses With Reversible Switching Properties. *Journal Of Non-Crystalline Solids*, 74(1):75–84, 1985.
- [152] W. H. Zachariasen. The Atomic Arrangement In Glass. *Journal of the American Chemical Society*, 54(10):3841–3851, 1932.
- [153] Linus Pauling. The Nature of the Chemical Bond. Cornell University Press, third edition, 1960.
- [154] P. Lebaudy, J. M. Saiter, J. Grenet, M. Belhadii, and C. Vautier. Identification Of Amorphous Zones In The Getesb System. *Materials Science And Engineering* A-Structural Materials Properties Microstructure And Processing, 132:273–276, February 1991.

- [155] U. Vempati and P. Boolchand. The thermally reversing window in ternary GexPxS1-2x glasses. *Journal Of Physics-Condensed Matter*, 16(44):S5121–S5138, November 2004.
- [156] P. Boolchand, D. G. Georgiev, and M. Micoulaut. Nature of glass transition in chalcogenides. *Journal Of Optoelectronics And Advanced Materials*, 4(4):823– 836, December 2002.
- [157] J. A. Kalb, M. Wuttig, and F. Spaepen. Calorimetric measurements of structural relaxation and glass transition temperatures in sputtered films of amorphous Te alloys used for phase change recording. *Journal Of Materials Research*, 22(3):748–754, March 2007.
- [158] C. Bichara, J. Y. Raty, and J. P. Gaspard. Structure and bonding in liquid tellurium. *Physical Review B*, 53(1):206–211, January 1996.
- [159] S. Raoux, M. Salinga, J. L. Jordan-Sweet, and A. Kellock. Effect of Al and Cu doping on the crystallization properties of the phase change materials SbTe and GeSb. *Journal Of Applied Physics*, 101(4):044909, February 2007.
- [160] I. Friedrich, V. Weidenhof, W. Njoroge, P. Franz, and M. Wuttig. Structural transformations of Ge2Sb2Te5 films studied by electrical resistance measurements. *Journal Of Applied Physics*, 87(9):4130–4134, May 2000.
- [161] D. H. Kim, F. Merget, M. Laurenzis, P. H. Bolivar, and H. Kurz. Electrical percolation characteristics of Ge2Sb2Te5 and Sn doped Ge2Sb2Te5 thin films during the amorphous to crystalline phase transition. *Journal Of Applied Physics*, 97(8):083538, April 2005.
- [162] J. Kalb, F. Spaepen, and M. Wuttig. Atomic force microscopy measurements of crystal nucleation and growth rates in thin films of amorphous Te alloys. Applied Physics Letters, 84(25):5240–5242, June 2004.
- [163] G. Ruitenberg, A. K. Petford-Long, and R. C. Doole. Determination of the isothermal nucleation and growth parameters for the crystallization of thin Ge2Sb2Te5 films. *Journal Of Applied Physics*, 92(6):3116–3123, September 2002.
- [164] R. Pandian, B. J. Kooi, J. T. M. De Hosson, and A. Pauza. Influence of capping layers on the crystallization of doped SbxTe fast-growth phase-change films. *Journal Of Applied Physics*, 100(12):123511, December 2006.

- [165] S. Privitera, S. Lombardo, C. Bongiorno, E. Rimini, and A. Pirovano. Phase change mechanisms in Ge2Sb2Te5. *Journal Of Applied Physics*, 102(1):013516, July 2007.
- [166] M. R. Armstrong, B. W. Reed, B. R. Torralva, and N. D. Browning. Prospects for electron imaging with ultrafast time resolution. *Applied Physics Letters*, 90(11):114101, March 2007.
- [167] B. J. Kooi, W. M. G. Groot, and J. T. M. De Hosson. In situ transmission electron microscopy study of the crystallization of Ge2Sb2Te5. *Journal Of Applied Physics*, 95(3):924–932, February 2004.
- [168] B. J. Kooi and J. T. M. De Hosson. On the crystallization of thin films composed of Sb3.6Te with Ge for rewritable data storage. *Journal Of Applied Physics*, 95(9):4714–4721, May 2004.
- [169] R. Pandian, B. J. Kooi, J. T. M. De Hosson, and A. Pauza. Influence of electron beam exposure on crystallization of phase-change materials. *Journal Of Applied Physics*, 101(5):053529, March 2007.
- [170] J. A. Kalb, F. Spaepen, and M. Wuttig. Kinetics of crystal nucleation in undercooled droplets of Sb- and Te-based alloys used for phase change recording. *Jour*nal Of Applied Physics, 98(5):054910, September 2005.
- [171] E. R. Meinders and C. Peng. Melt-threshold method to determine the thermal conductivity of thin films in phase-change optical recording stacks. *Journal Of Applied Physics*, 93(6):3207–3213, March 2003.
- [172] V. Weidenhof, I. Friedrich, S. Ziegler, and M. Wuttig. Atomic force microscopy study of laser induced phase transitions in Ge2Sb2Te5. *Journal Of Applied Physics*, 86(10):5879–5887, November 1999.
- [173] V. Weidenhof, N. Pirch, I. Friedrich, S. Ziegler, and M. Wuttig. Minimum time for laser induced amorphization of Ge2Sb2Te5 films. *Journal Of Applied Physics*, 88(2):657–664, July 2000.
- [174] I. Friedrich, V. Weidenhof, S. Lenk, and M. Wuttig. Morphology and structure of laser-modified Ge2Sb2Te5 films studied by transmission electron microscopy. *Thin Solid Films*, 389(1-2):239–244, June 2001.
- [175] V. Weidenhof, I. Friedrich, S. Ziegler, and M. Wuttig. Laser induced crystallization of amorphous Ge2Sb2Te5 films. *Journal Of Applied Physics*, 89(6):3168–3176, March 2001.

- [176] M. Laurenzis, A. Heinrici, P. H. Bolivar, H. Kurz, S. Krysta, and J. M. Schneider. Composition spread analysis of phase-change dynamics in GexSbyTe1-x-y films embedded in an optical multilayer stack. *Iee Proceedings-Science Measurement* And Technology, 151(6):394–397, November 2004.
- [177] D. H. Kim, F. Merget, M. Forst, and H. Kurz. Three-dimensional simulation model of switching dynamics in phase change random access memory cells. *Jour*nal Of Applied Physics, 101(6):064512, March 2007.
- [178] M. Mansuripur, J. K. Erwin, W. Bletscher, P. Khulbe, K. Sadeghi, X. D. Xun, A. Gupta, and S. B. Mendes. Static tester for characterization of phase-change, dye-polymer, and magneto-optical media for optical data storage. *Applied Optics*, 38(34):7095–7104, December 1999.
- [179] E. M. Wright, P. K. Khulbe, and M. Mansuripur. Dynamic theory of crystallization in Ge2Sb2.3Te5 phase-change optical recording media. *Applied Optics*, 39(35):6695–6701, December 2000.
- [180] P. K. Khulbe, X. D. Xun, and M. Mansuripur. Crystallization and amorphization studies of a Ge2Sb2.3Te5 thin-film sample under pulsed laser irradiation. *Applied Optics*, 39(14):2359–2366, May 2000.
- [181] G. W. Burr, M. Salinga, S. Raoux, R. M. Shelby, and M. Wuttig. Quantifying the Crystallization Speed of GeSb by Matching Optical Characterization to Numerical Simulation. In *Materials Research Society Spring Meeting 2008, San Francisco, CA, USA*, 2008.
- [182] F. J. Jedema, M. A. A. in Śt Zandt, R. A.M. Wolters, R. Delhougne, D. J. Gravesteijn, D. T. Castro, G.A.M. Hurkx, and K. Attenborough. Program window of doped Sb2Te phase change line cells. In *European Phase Change and Ovonics Symposium (EPCOS)*, 2007.

### BIBLIOGRAPHY

## Curriculum Vitae

### Angaben zur Person:

Name: Salinga

Vornamen: Martin Stefan
Geburtsdatum: 19. März 1979
Geburtsort: Herten (Westfalen)

Staatsangehörigkeit: deutsch Familienstand: ledig Kinder: keine

Schulbildung:

08/1985 - 07/1989 Bodelschwinghschule Gladbeck 08/1989 - 05/1998 Ratsgymnasium Gladbeck

Abschluss: Abitur (Gesamtnote: 1,3)

Zivildienst:

08/1998 - 08/1999 Malteser-Hilfsdienst-Gladbeck

Studium:

10/1999 - 12/2004 Physikstudium an der

Rheinisch-Westfälischen Technischen Hochschule (RWTH) Aachen

Vordiplom (Physik);

Datum: 10/2001

Gesamtnote: sehr gut

Diplom (Physik);

Datum: 12/2004

Gesamtnote: sehr gut (1,1)

Titel der Diplomarbeit: "Kinetik schneller Nukleations-

und Wachstumsprozesse in Te-Legierungen", angefertigt am I. Physikalischen Institut

der RWTH Aachen bei Prof. Dr. Matthias Wuttig;

10/2001 – 12/2004 Stipendiat des Evangelischen Studienwerkes Villigst e.V.

#### **Promotion:**

02/2005 – 03/2008 Arbeit an der Promotion in Physik am I. Physikalischen Institut

der RWTH Aachen bei Prof. Dr. Matthias Wuttig

#### Studien- und Forschungsaufenthalte im Ausland:

04/2004 – 08/2004 Forschungsaufenthalt im Rahmen der Diplomarbeit an

der Division of Engineering and Applied Sciences, Harvard University, Cambridge, Massachusetts, USA,

bei Prof. Dr. Frans Spaepen

02/2005 – 09/2006 Forschungsaufenthalt im Rahmen der Promotion in

dem IBM Almaden Research Center,

San Jose, California, USA

#### Veröffentlichungen:

1. M. Salinga, S. Ziegler, A. Schropp, J. Kalb und M. Wuttig

Viskositätsmessung an dünnen Schichten des Phasenwechselmediums AgIn-Sb2Te mit einem bulge-tester

Deutsche Physikalische Gesellschaft Frühjahrstagung 2004, Regensburg, Deutschland

2. S. Raoux, C. T. Rettner, J. L. Jordan-Sweet, M. Salinga und M. F. Toney
Crystallization behavior of phase change nanostructures

Engage of Company of Phase Change and Openia Science 2005. Combaid as a company of the company of t

European Symposium on Phase Change and Ovonic Science 2005, Cambridge, UK

3. R. M. Shelby, M. Salinga, F. A. Houle und S. Raoux

Phase-Change Dynamics of Eutectic GeSb Alloy

Materials Research Society Spring Meeting 2006, San Francisco, CA, USA

4. S. Raoux, M. Salinga, J. L. Jordan-Sweet und Q. Wang

Effect of Doping on the Properties of the Phase Change Materials SbTe and GeSb Materials Research Society Spring Meeting 2006, San Francisco, CA, USA

r Mar an IIII a (Mem amp), note

 M. Salinga, S. Raoux, J. L. Jordan-Sweet, M. F. Toney, C. T. Rettner, R. M. Shelby, G. W. Burr und C. M. Jefferson

Scaling and doping effects on grain size and switching properties of phase-change materials Materials Research Society Spring Meeting 2006, San Francisco, CA, USA

- 6. C. T. Rettner, L. Bozano, G. W. Burr, Y.-C. Chen, M. Hayashi, K. Gopalakrishnan, J. Hou,
  - X. Jiang, J. Jordan-Sweet, R. King, R. Miller, R. Moriya, S. Parkin, S. Raoux, M. Salinga,
  - J. Samuel, C. Scott, R. Shelby, R. Shenoy und L. Thomas

Application of Electron Beam Lithography to the Fabrication of Prototype Memory Devices Materials Research Society Fall Meeting 2007, Boston, MA, USA

- 7. Y.-C. Chen, C. T. Rettner, S. Raoux, G. W. Burr, S. H. Chen, R. M. Shelby, M. Salinga,
  - W. P. Risk, T. D. Happ, G. M. McClelland, M. Breitwisch, A. Schrott, J. B. Philipp, M. H. Lee, R. Cheek, T. Nirschl, M. Lamorey, C. F. Chen, E. Joseph, S. Zaidi, B. Yee, H. L. Lung,
  - R. Bergmann und C. Lam

Ultra-Thin Phase-Change Bridge Memory Device Using GeSb

IEEE International Electron Devices Meeting 2006, San Francisco, CA, USA

- 8. S. Raoux, M. Salinga, J. L. Jordan-Sweet und A. Kellock Effect of Al and Cu doping on the crystallization properties of the phase change materials SbTe and GeSb
- Y.-C. Chen, C. T. Rettner, S. Raoux, G. W. Burr, R. Shelby und M. Salinga Crystallization Kinetics of As-Deposited and Melt-Quenched Phase-Change Materials Materials Research Society Spring Meeting 2007, San Francisco, CA, USA

Journal of Applied Physics 101 (4): Art. No. 044909 FEB 15 2007

- M. Salinga, J. Kalb, M. Klein, T. Sontheimer, F. Spaepen und M. Wuttig Glass Transition and Crystallization in Phase Change Materials European Symposium on Phase Change and Ovonic Science 2007, Zermatt, Schweiz
- 11. G. W. Burr, M. Salinga, S. Raoux, R. M. Shelby und M. Wuttig Quantifying the Crystallization Speed of GeSb by Matching Optical Characterization to Numerical Simulation Materials Research Society Spring Meeting 2008, San Francisco, CA, USA